UNIVERSITÉ DU LUXEMBOURG

PhD-FSTC-2019-50
The Faculty of Sciences, Technology and Communication

DISSERTATION

Presented on 15/07/2019 in Esch-sur-Alzette, Luxembourg

to obtain the degree of

DOCTEUR DE L'UNIVERSITÉ DU LUXEMBOURG

EN *CHIMIE*

by

François LOYER
Born on 25 September 1989 in Rennes, France

STUDY OF NANOPULSED DISCHARGES FOR PLASMA-POLYMERIZATION: EXPERIMENTAL CHARACTERIZATION AND THEORETICAL UNDERSTANDING OF GROWTH MECHANISMS IN THE DEPOSITION OF FUNCTIONAL POLYMER THIN FILMS

Dissertation defence committee

Dr Choquet Patrick, dissertation supervisor
Doctor, Luxembourg Institute of Science and Technology

Dr Nicolas Boscher
Doctor, Luxembourg Institute of Science and Technology

Dr Jens Kreisel, Chairman
Professor, Université du Luxembourg

Dr Dirk Hegemann
Doctor, Gruppenleiter Plasma & Coating, EMPA, St. Gallen, Switzerland

Dr François Reniers, Vice Chairman
Professor, Université libre de Bruxelles

Table of contents

Abstract

Plasma processes are highly versatile methods able to promote the formation of thin films from a vast variety of compounds thanks to the numerous energetic species they generate. Notably, plasma-enhanced chemical vapor deposition (PECVD) processes have already led to the simultaneous synthesis and deposition of a wide variety of organic functional materials. Reciprocally, the many reactive species composing the plasma induce a non-negligible number of side reactions, yielding altered chemistry compared to conventional polymerization processes. Therefore, there is a strong need for controlled methods promoting conventional polymerization pathway in plasma-based processes to increase their range of application.

To this end, the atmospheric-pressure plasma-initiated chemical vapor deposition (AP-PiCVD) process was developed, differing from classical PECVD by its initiation source. AP-PiCVD relies on square-wave nanopulsed discharges with single ultra-short plasma on times (t_{on} ≈ 100 ns) and long plasma off-times (t_{off} = 0.1 – 100 ms) rather than alternative current sources yielding long and repeated discharges (t_{on} = 10 µs).

Methacrylate monomers initiated by nanopulsed discharges highlighted a shift of growth mechanisms from classical PECVD pathways (plasma-polymerization) to conventional free-radical polymerization. Notably, the growth of polymer layers with an extremely high retention of the monomer's chemistry and unprecedented molecular weights for an atmospheric-pressure plasma process is demonstrated at long plasma off-times. Moreover, a transition from gas phase to surface growth mechanisms is observed, allowing the deposition of conformal coatings similarly to low-pressure alternative chemical vapor deposition processes.

A thorough investigation of the thin films' chemistry confirms the conventional nature of the layers grown by AP-PiCVD and shed light upon the growth mechanisms in low-frequency nanosecond pulsed plasmas. While the on-time induces the formation of free radicals from the monomers' fragmentation which are able to initiate and terminate the chain addition process, conventional polymerization mechanisms are strongly promoted during the off-time yielding linear polymer core. Interestingly, new insights on selective initiation mechanisms based on sacrificial functions for an enhanced control of the molecular fragmentation are put forward and discussed.

The development of a model describing the kinetic of pulsed plasma was carried out and correlated with experimental observations, providing deeper understanding of the interaction between the gas phase and the surface. The extraction of important physical parameters for the description of the growth kinetics in AP-PiCVD is demonstrated and their significance discussed.

Using the fundamental knowledge developed on nanosecond pulsed plasma-initiated polymerization mechanisms, thermoresponsive copolymer layers grown by AP-PiCVD are reported for the first time. The properties of the layers are evaluated and related to their chemistry, allowing the determination of an optimal co-monomers ratio to integrate both of their individual properties as a unique functional thin film.

Acknowledgments

I thank the Luxembourg National Research Fund (FNR) for funding the “Nanopolypulse” project which was the basis for my thesis research.

I wish to thank Professor Jens Kreisel from the University of Luxembourg (UL) for being the president of the jury, but also for following my progress and his extremely useful advices through all these years as a member of my CET.

I thank Professor François Reniers from the Free University of Bruxelles (ULB) and Doctor Dirk Hegemann from EMPA in Switzerland for accepting to be the external jury members at my doctoral defense as well as for the discussions and interest they showed for my work.

I particularly thank Doctor Patrick Choquet and Doctor Nicolas Boscher from LIST for supervising my research work in a day to day basis and over the entirety of my work. Patrick’s constant support to make our daily life easier as PhD students, both from a scientific and administrative aspect, were highly valuable for the completion of my PhD thesis. The daily discussions and brainstorming with Nicolas allowed me improve personally and scientifically on many aspects thanks to high broad knowledge and experience, which he always shared happily and with an extreme patience.

I want to thank all the members from the SIPT unit as well as the analysis platform for all our discussions and the help they provided at all points during this thesis work.

I also am deeply thankful to my colleagues and friends I met during my time at LIST, those that left and all those that arrived since. I will always treasure our time spent together.

Finally, I wish to thanks all those I might have forgotten and those that didn’t recognize themselves in this acknowledgement, as well as my family and my friends from Bretagne who supported me since a long time ago.

Work done in conjunction with others

All of the experiment and analytical works presented in this thesis were carried out by the author, with the following exceptions:

- The X-ray photoelectron spectroscopy measurements were performed by Dr. Jérome Guillot at LIST.

- The Matrix-Assisted Laser Desorption/Ionization high-resolution mass spectrometry measurements were performed by Dr. Gilles Frache and Dana El Assad at LIST.

- The Size Exclusion Chromatography measurements were performed by Dr. Gilles Frache and Dr. Jessica Desport at LIST.

- The Scanning Electron Microscopy imaging and Energy-dispersive X-ray spectroscopy measurements presented in chapter 5 were performed by Jean-Luc Biagi at LIST.

- The Atomic Force Microscopy imaging in chapter 5 was performed by Dr. Patrick Grysan at LIST.

- The water contact angles measurements performed for the surface-free energies calculations presented in chapter 5 were performed by Dr. Nicolas D. Boscher and Dr. Maryline Moreno-Couranjou at LIST.

- The water contact angles measurements for the determination of the LCST in chapter 5 were performed by Dr. Maryline Moreno-Couranjou at LIST.

CHAPTER I – Introduction

This chapter aims at summarizing the existing descriptions of the growth mechanisms driving the formation of organic layers in chemical vapor deposition processes. The growth mechanisms and current theoretical models for plasma polymerization and alternative chemical vapor deposition processes are discussed. The relationship between the polymerization reactions and the growth mechanisms are highlighted in order to promote control over the polymer thin films' properties.

Content

1. Plasma

1.1. Classification of plasmas

Plasmas are composed of energetic particles, interacting with each other through elastic and inelastic collisions, transfer, or diffusion mechanisms.[1,2] While having a behavior close to neutral gases at the macroscopic level, they are considered as a distinct state of matter due to their unique micro- and macro-physical properties.

Plasmas are composed of neutral atoms and radicals, positive and negative ions, electrons and photons, constituting a very rich phase that can affect and be affected by their environment.[2–4] The electrons and ions – which are the main energy propagators in plasmas along with photons – are strongly influenced by direct collision (zero range), Coulomb collisions (short range), local charges (moderate range) and magnetic fields (long range).[4–7] As such, even if plasmas are macroscopically neutral, they behave microscopically as an ionized gas, making them highly reactive and versatile depending on their composition.[1,2] Notably, the degree of ionization α, determined from the densities of ionized species n_i (m^{-3}) and neutral species n_n (m^{-3}), gives information on the interactions within the plasma (eq. 1.1).[4,5]

For instance, the lower the degree of ionization the more likely a charged particle is to collide with a neutral particle as the Coulomb interactions between charged particles being negligible. When the degree of ionization increases, the charge particles interact more through Coulomb interaction, affecting their kinetic and the energy transfer mechanism, hence the overall properties of the plasmas.

$$\alpha = \frac{n_i}{n_i + n_n} \tag{1.1}$$

There are numerous variations of plasma depending on the properties of their energy carriers (*i.e.* electrons and ions) and on the energy transfer mechanisms (*i.e.* collision and radiation). Overall, plasmas are separated in two categories: non-thermal and thermal plasmas.

1.1.1. Non-thermal plasmas

Non-thermal plasmas are weakly ionized, conferring milder and more readily tunable energetic environments, as most of the energy transfers mechanisms in non-thermal plasma come from inelastic collision of the electrons and from the UV radiations. For this reason, electrons can reach very high temperature (*ca.* T_e = 10,000 K – 100,000 K) compared to the ions, neutrals and metastables (*ca.* T_h = 300 K – 1,000 K), hence having a much greater kinetic momentum.[2,7,8] Yet, the contribution of the heavy species is important, as they will determine the chemical reactions and physical interactions in the plasma phase, *e.g.* the overall gas temperature.[4,6,7]

Non-thermal plasmas can exist in multiple states covering a wide range of electron temperature and density, deeply affecting their electric property. Indeed, unlike common electronic devices, the voltage-current plots of plasmas are highly irregular and their current (*i.e.* flow of electric charges) may range over several orders of magnitude (Figure 1.1).[2] This behavior indicates the existence of different electric modes as the current increase.

At low current (*i.e.* between points A and C), the plasma is in a state of dark discharge as the gas becomes weakly conductive but is not visible. Especially at very low electric field (*i.e.* point A), the electrons do not have enough energy to propagate and ionize the gas. As the electric field increases and reaches a sufficient potential (*i.e.* point B), the plasma enters in the Townsend regime where electrons propagate and multiply through an avalanche mechanism, ionizing the gas phase and inducing VUV radiations. Corona discharges may be observed when both, the electric field and the electron density are high, notably on metallic edges of a surface electrode.

Inside the dark discharge regime, the current can increase gradually until the potential reaches a breakdown voltage (*i.e.* point C) where the plasma enters into the glow discharge regime. In this glow discharge regime (*i.e.* between points C and E), the current increases abruptly along with the electron density and the emission of VUV photons. In this regime, the plasma phase becomes completely apparent in the visible spectrum.

As the potential continue to rise exponentially with the current, the electrodes are heated up to the point where they start to thermally emit charged species (*i.e.* between points E and G). This regime, called the Arc regime, is characterized by a very high electronic current and electron density with low potential, marking the transition to thermal plasmas.

Variations of the I-V curve may be observed for different geometries and sources.[2]

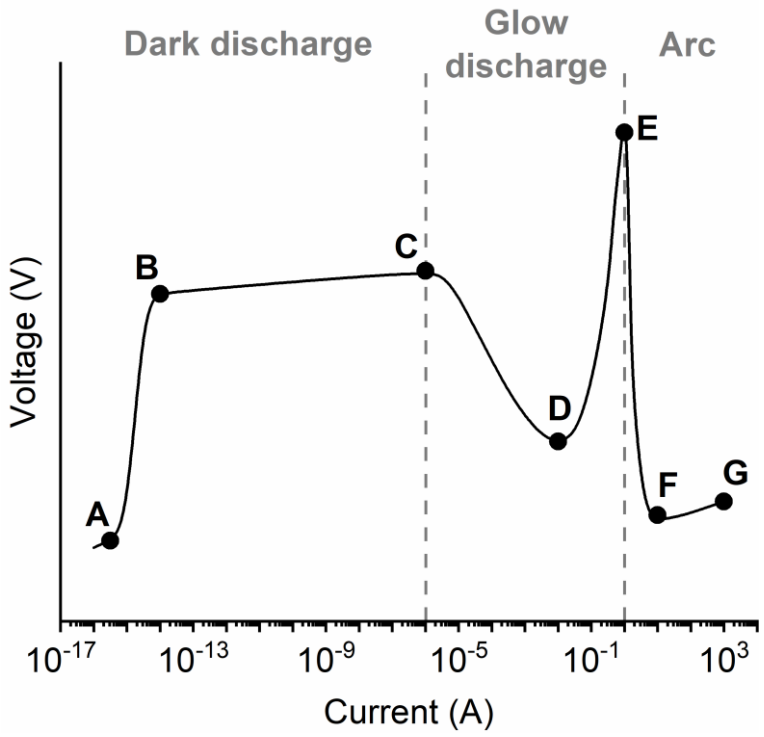

Figure 1.1. Evolution of a current-voltage plot in direct-current plasmas. [2]

1.1.2. Thermal plasmas

Thermal plasmas – or hot plasmas – are strongly or fully ionized phases driven by Coulomb interactions and having a very high electron density.[4,6,8,9] They are extremely energetic environment as, unlike non-thermal plasmas, the electrons and heavy species have the same temperature (*ca.* T_e = T_h = 10,000 K), greatly increasing the kinetic momentum of the ions, neutrals and metastable species.[4,6,8,9] The collision mechanisms in thermal plasmas can

either be inelastic (i.e. generation of active species) or elastic (i.e. transfer of heat from electrons to ions).[9]

1.2. Plasma-induced species

1.2.1. Electrons

Electrons are present in every plasma as negative charge carriers, maintaining the global neutrality of the plasma. They are generated using high-voltage sources, allowing the creations of positive and negative charges either by capacitive accumulation or by electromagnetic induction.[1,7,8,10–12]

Electrons play a major role in both non-thermal and thermal plasmas due to their high velocity (*ca.* T_e = 10,000 K – 100,000 K), able to either react with heavy species via inelastic collision or to partially transfer their energy via elastic collision.[1,2,7,8,13,14] Their energies are distributed over a broad range (*ca.* ε_e = 1 eV – 10 eV) typically following a Boltzmann distribution – *i.e.* electrons energy distribution function ($EEDF$) – with most electrons having an energy below 5 eV (Figure 1.2).[2,7,10,12,13]

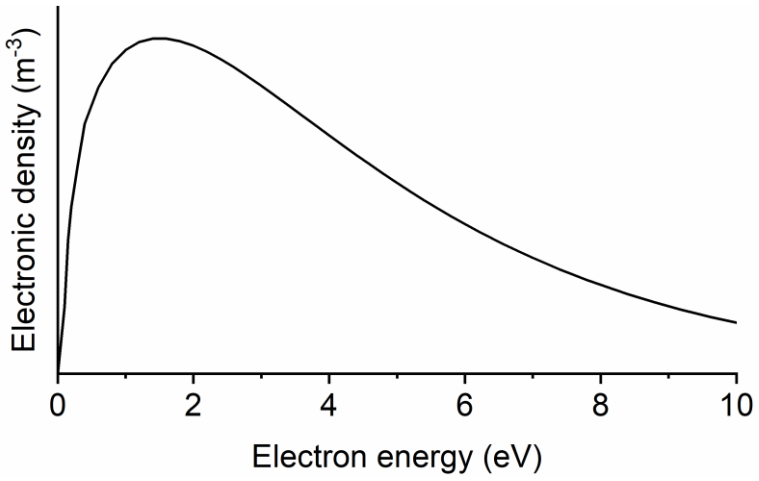

Figure 1.2. Typical electrons energy distribution function of a non-thermal plasma.

1.2.2. Ions

Most ions generated in a plasma are cations to counterbalance the electrons' negative charges, as the plasma must remain globally neutral. Typically, the ionization of the system is favored when using a plasmageneous gas (*e.g.* argon), as it will be ionized easily by electrons (eq. 1.2) or excited species through Penning ionization (eq. 1.3) and, in turn, can ionize other species (eq. 1.4).[1,2,7,11,12,14,15]

$$Ar + e^- \rightarrow Ar\bullet^+ + e^- + e^- \quad (1.2)$$

$$Ar^* + Ar \rightarrow Ar\bullet^+ + e^- + Ar \quad (1.3)$$

$$Ar^+ + O_2 \rightarrow Ar + O_2^+ \quad (1.4)$$

Ions are far more energetic than electron (*ca.* ε_i = 10 eV – 500 eV) – due to their higher mass – and their ion energy distribution (IED) is a bimodal distribution (Figure 1.3). In non-

thermal plasmas they do not have enough kinetic momentum to transfer their energy through translation collisions, and simply deactivate (eq. 1.5).[15–17]

$$Ar^+ + e^- \rightarrow Ar \quad (1.5)$$

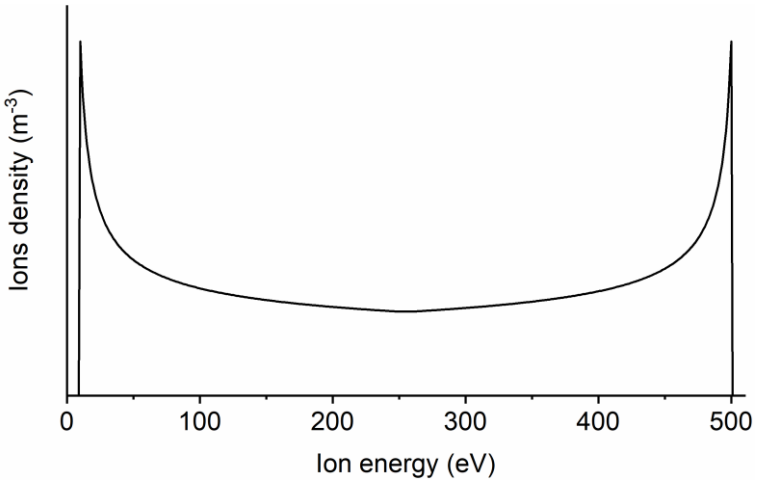

Figure 1.3. Typical ion energy distribution function of ions in non-thermal plasmas.

1.2.3. Excited species

From the numerous collisions in plasmas, an important part of this energy is transferred to the core level electrons of the atoms or molecules, converting from their stable ground-state to a metastable excited state (eq. 1.6).[1,11,12,14] When the excited electron goes back to its ground state a high energy photon is released (eq. 1.7), which can often be observed in the visible range as a glowing discharge.[1,11,12,14]

$$Ar + e^- \rightarrow Ar^* + e^- \quad (1.6)$$

$$Ar^* \rightarrow Ar + h\upsilon \quad (1.7)$$

These radiations are highly contributing to the plasma-polymerization mechanisms as they are able to transfer their energy even for non-thermal plasmas. Moreover, they can reach energies beyond the ones of the electrons (*ca.* $\varepsilon_{h\upsilon}$ = 3 eV – 100 eV).[1,2]

1.2.4. Free radicals

Free radicals are formed from inelastic collisions of electrons or photons with atoms and molecules. The transferred energy induces a homolytic breakdown of a chemical bond into two well-defined radicals (eq. 1.8). This fragmentation mechanism is highly dominant in low energy plasma, as the bond dissociation energy of organic molecules is typically lower than their ionization energy.[1,2,14,18]

$$H_2 + e^- \rightarrow 2H\bullet + e^- \quad (1.8)$$

While they have a low kinetic energy due the inelastic collision, the free radical species are highly reactive and they will try to stabilize themselves with their surrounding environment. Therefore, they have a strong effect on the chemical reactions and growth mechanisms in PECVD.

1.3. Initiation of plasmas

While plasmas are rare and unstable on earth, they naturally compose more than 99% of the known universe and can be generated from various sources of energy. Those plasmas can have extremely different properties and behaviors depending on their electrons' temperature (*i.e.* energy) and density (Figure 1.4).[2,8,9,19]

Stars are fully ionized plasmas – meaning they are constituted almost exclusively of ions and electrons – due to the extreme temperatures in their core and on their surface. In order to artificially reproduce sufficient temperatures to partially or fully ionize a gas, it requires the use of magnetic fields, inductively heating the plasma. Another instance of naturally generated plasmas can be observed from lightning discharges, originating from the accumulation of charges in clouds.

If plasmas are rare occurrences on Earth, they are vastly predominant in space. This is mostly due to the crucial differences in pressure, since plasmas are easier to be ignited under vacuum. Consequently, vacuum systems can be used to compensate for the Earth's natural atmosphere. Furthermore, a common approach is to use gases that are relatively easy to ionize in order to lower the energy required to initiate the plasma, such as noble gases (*i.e.* helium and argon) or common inert gases (*i.e.* nitrogen).[1,2]

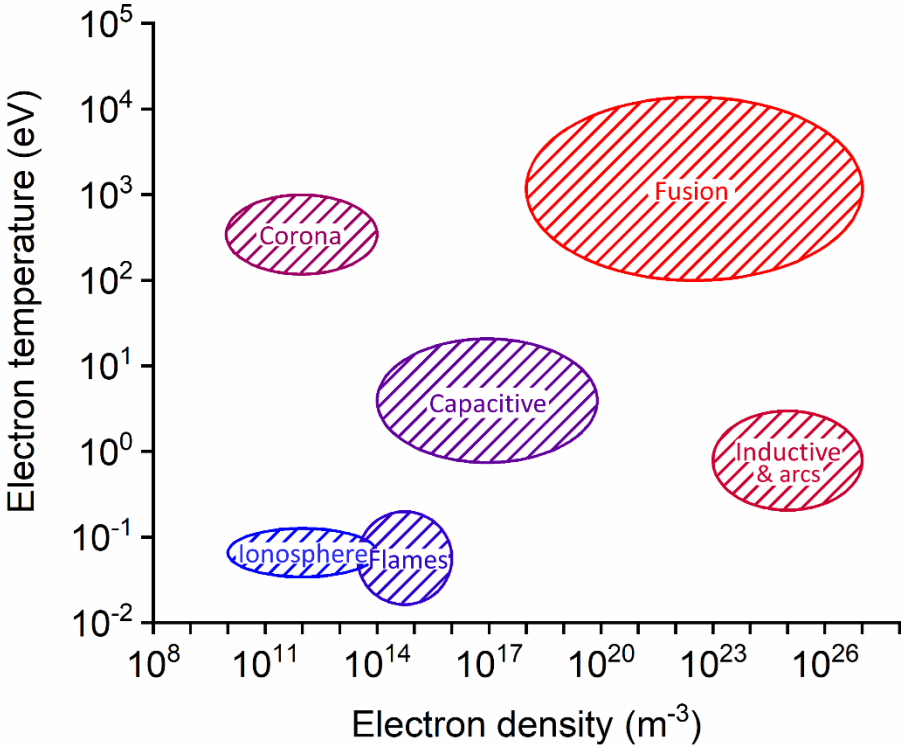

Figure 1.4. Classification of plasmas according to their electrons' properties.

Plasmas can be produced experimentally using high voltage sources to deliver the highly accelerated electrons required to initiate the discharge (Figure 1.5). The electrical parameters of the source (*i.e.* the electric potential, the frequency used, the application of pulses) have a strong influence on the plasma properties, namely the electron temperature and density as well as the gas temperature. Furthermore, depending on the frequency, the electric field generated from the potential will influence or not the electrons and ions.[1,2]

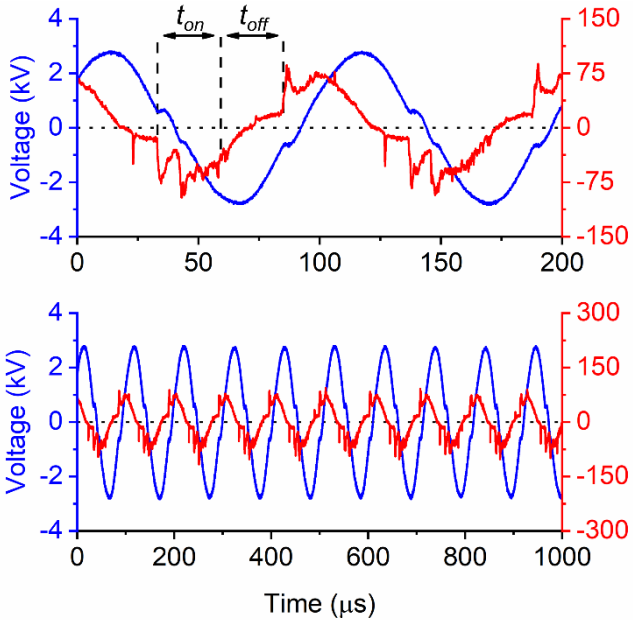

Figure 1.5. Traces of the applied voltage and the corresponding current discharges of an AC high-voltage source.

1.3.1. Microwave sources

Microwave plasmas are generated using the electron cyclotron resonance effect in a magnetron processes with a frequency superior to 1 GHz.[2,8,20–23] These plasmas have extremely high electron density (*ca.* n_e = 10^{20} m^{-3}), moderate electron temperature (*ca.* T_e = 15,000 K) and high gas temperature (*ca.* T_h = 5,000 K).[8]

Since $T_e \neq T_h$, microwave plasmas are non-thermal, however the very high electron density and gas temperature show that they are close to thermal plasmas and therefore highly energetics.[8] In order to obtain a large and homogeneous discharge, microwave plasma reactors can be operated under vacuum (*ca.* 0.1 mbar), but atmospheric microwave plasma processes were also developed.[2,8,24] Moreover, due to very high frequencies applied, only the electrons and not the ions follow the oscillation of the electric field.[7,8]

For this reason, microwave plasmas are useful tools for surface etching, the generation of ions (*e.g.* H^+, Ar^+ …), the synthesis of metals and oxides or the plasma-polymerization of non-polymerizable molecule (*e.g.* methane, silanes, siloxanes, …) through fragmentation and recombination mechanisms.[12,20–23,25–27]

1.3.2. Radio frequency

Radio frequency plasmas can be generated from either capacitive or inductive AC sources working in the radiofrequency range, between 1 MHz and 1 GHz.[2,8,28]

A capacitive discharge drastically reduces the electron density (*ca.* n_e = 10^{18} m^{-3}) and the gas temperature (*i.e.* T_h < 700 K) while the electron temperature remains sensibly the same (*ca.* T_e = 15,000 K).[8] Therefore, capacitive radio frequency plasmas are non-thermal and less energetic than microwave plasmas, allowing milder discharge conditions. They can also find different applications in the field of surface treatments (*i.e.* etching, generation of ions, syntheses of metals, oxides and non-polymerizable plasma-polymers). The alternating

electric field generated by radiofrequency plasmas do not influence the ion movements at these frequencies of oscillation.[7,8,28]

Capacitive radio frequency plasmas are actively used in plasma-polymerization processes for surface functionalization. Indeed, the fragmentation/recombination mechanisms are less dominant than in microwave plasmas, allowing the retention of some chemical functionalities which can safely attach on the surface (*e.g.* oxygen, hydroxyl, halogen …).[1,2,12,14,19,23,25]

An inductive discharge, on the other hand, generate a thermal plasma (*ca.* $T_e = T_h$ = 8000 K) and high electron density (*ca.* 10^{23} m^{-3}). In this operating mode, their plasma's properties are often sought to build ion sources for analysis or etching processes[1,2,12,23,28]

1.3.3. Low-frequency

Low-frequency plasmas are generated solely by capacitive AC sources, with working frequencies from a few kHz to 1 MHz.[1,8] The plasmas are all non-thermal, with moderate to high electron temperature (*ca.* T_e = 10,000 K – 100,000 K), low gas temperature (*ca.* T_h = 300 K – 1,000 K) and low electron density (*ca.* $n_e = 10^{18}$ m^{-3}).[8] Due to the very low operated frequencies, both electrons and ions follow the oscillation of the electric field, lowering the effect of ion bombardment.[7] Those plasmas can be operated either under vacuum or atmospheric conditions.

For those reasons, low-frequency plasmas are less energetic than microwave and radiofrequency plasmas, and therefore more suitable for a maximal retention of the chemistry. As such, at the atmospheric pressure, low-energy processes such as corona discharges and especially dielectric barrier discharges (DBD) have been thoroughly studied for plasma-polymerization.[1,2,8,23,29]

2. Plasma-polymerization CVD

2.1. Overview of previous research

The plasma-polymerization process is a subset of the plasma-enhanced chemical vapor deposition (PECVD) process, which takes advantage of the energetic plasma discharge to assist the growth of thin films on various substrates from volatile monomers. Therefore, plasma processes are able to operate in dry environment (*i.e.* solvent free) without the addition of chemical initiator, making them extremely attractive for ecological and practical purposes. Indeed, the highly energetic species in the plasma are able to activate and cross-link the organic precursors, even without conventional polymerizable functions (*e.g.* vinyl), allowing the deposition of a broad range of monomers.[1,2,8,23]

The term "plasma-polymer" was introduced in the early 1960s by Goodman, which highlighted the unique properties of these coatings and their differences compared to conventional polymers.[30] Further, in the 1980s, Yasuda worked on unifying the multi-disciplinary aspects of plasma-polymerization (*i.e.* chemistry, physic, interfaces …) in its reference book "Plasma-polymerization".[12] From this time, many different approaches of plasma-polymerization were developed, making the process an appealing alternative at both laboratory and industrial scale, pushing further the understanding of the many mechanisms that altogether form a plasma-polymer.

Therefore, the plasma-polymerization of many organic compounds have demonstrated the efficiency of the process for the growth of organic layers in flexible systems operating in various geometry (*e.g.* electrode, injection system) and under diverse experimental conditions (*e.g.* energy of the plasma, temperature, pressure). From the early 80s, Wertheimer *et al.* reported the successful plasma-polymerization of corrosion-resistant SiO_x organic layers with high cohesive strength from the non-polymerizable Hexamethyldisiloxane (HMDSO) using microwave plasmas.[22,23] The growth of robust and element-rich layers (*i.e.* doped in nitrogen, oxygen, phosphor, halogen …) have found many applications for industrial processes, from barrier layers to low-k dielectric layers.[22,25,31–37] The plasma-polymerization of molecules based solely on fragmentation and recombination mechanisms remain a highly attractive research subject to this day, being applied to silicone-based and carbon-based molecules (*e.g.* the synthesis of diamond from methane).[22,23,38,39]

Lowering the energy of the plasma promotes the retention of chemical moieties (*e.g.* NH_2, OH, SH) rather than just promoting atomic enrichment.[32,33,40] Therefore, a global approach for controlling the properties of the plasma-polymer is to use softer discharge power and lower frequency of discharge, such as radiofrequency or low frequency sources.[1,8,25] Notably, low-pressure plasma systems displayed great flexibility for the control of the properties of the plasma-polymer thin films. Indeed, from the 70s Kobayashi *et al.* studied the influence of different parameters as the discharge power, the flux of monomer, the pressure of the system and the chemistry of the monomer on the coating chemistry.[41,42] Further retention of the chemistry was obtained by decreasing the global power of the plasma discharges, either by lowering the power dissipated in the discharge, by pulsing the plasma or working in post-discharge.[23,34,40,43] Furthermore, low-pressure plasmas have been applied for the functionalization of complex surfaces, such as fibers or scaffolds, by taking advantage of the expansion of the plasma in the reactor's volume.[23,43–47] The ability to tune the physical state, robustness and chemistry of the grown plasma-polymer thin films is still of high interest in today's research and industry.

Atmospheric-pressure plasmas have more recently gained interest as an interesting solution for industrial upscaling. Therefore, the plasma-polymerization of organic monomers in atmospheric conditions have been performed for the functionalization of surfaces with element-rich (*e.g.* SiN_x, SiO_x, CPx …)[32–34,40,48,49] or moiety-rich (*e.g.* NH_2, OH, COOH, SH …).[50–57] However, in this environment, the surrounding atmosphere has a strong influence on the growth mechanisms as these reactive species are initiated into a $N_2/O_2/H_2O$ environment, which can induce additional secondary mechanisms. Indeed, those "polluted" species are also able to inhibit and/or contaminate the active plasma-polymer chains, behaving as a reactive solvent by comparison with wet chemistry.

The description of the growth mechanisms in plasma-polymerization is a key challenge in plasma processes due to the multi-disciplinary aspects of plasmas.[1,8,12,23] Therefore, theoretical models are generally focused on specific aspects of the physico-chemical mechanisms in plasma-polymerization and their application are usually limited to the associated experimental system.[58–60] A commonly accepted description of the chemical reactivity in plasma-polymerization was proposed by Yasuda and Lamaze, suggesting the prevalence of homolytic fragmentation of the organic monomer as an initial step for the growth mechanisms.[11,12] Tibbit *et al.* further confirmed this hypothesis by correlating a theoretical model – based on molecular fragmentation and reactivation mechanisms – with experimental kinetic data reported by Kobayashi *et al*..[41,42,61,62] Then, Yasuda has proposed a bicyclic free radical plasma-polymerization mechanism – named rapid step-growth polymerization – to take into account the reactivity of difunctional radical species (Figure 1.6), notably from the

opening of unsaturation link (*e.g.* C=C, C=O …).[12] This description of the interactions between plasma and organic molecules remain very simplified and requires additional information to better describe the growth mechanisms in plasma-polymerization.

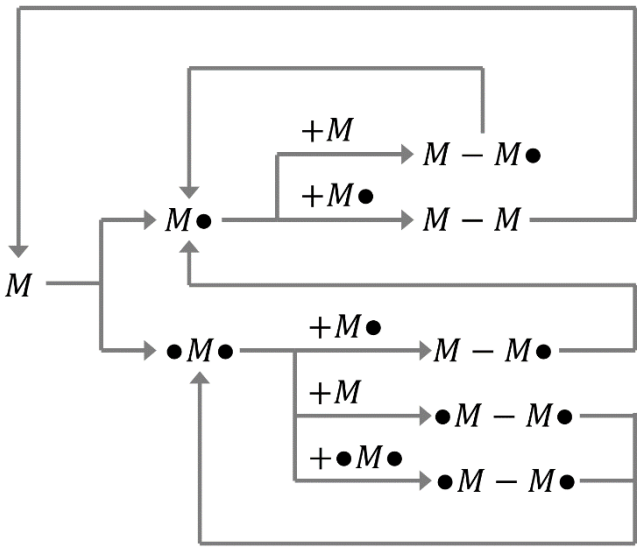

Figure 1.6. Bicyclic plasma-polymerization mechanisms of polymerizable monomers.[12]

Now, it has to be notified that most of the plasma "like polymer" film are most of time achieved by pulsing the discharge. Consequently, in order to offer a more efficient description of the growth mechanisms plasma-polymerization, the reactivity must be studied during these 2 parts: the mechanisms occurring while the plasma is active (*i.e.* during the discharge's on-time t_{on}), and the mechanisms occurring after the plasma deactivate (*i.e.* during the discharge's off-time t_{off}).

2.2. Growth mechanisms during the discharge

The exact role of each of the many different secondary species created during the discharge is extremely difficult, if not impossible, to determine without making approximation and generalization. In order to offer a global description of the ongoing mechanisms during the on time, it is usually more efficient to describe the effect of each mechanisms on the monomer, therefore, on the resulting plasma-polymer itself. Indeed, considering the vastly energetic and chemically reactive environment, each of these mechanisms should be seen as a statistical occurrence as they are bound to happen.

2.2.1. Fragmentation

The fragmentation of the monomer is the most dominant and essential mechanism to initiate the growth mechanisms, as determined by Yasuda and Lamaze.[12,63] It may occur from inelastic collision between the reactive species (*i.e.* electrons, photons, ion and excited species) and the monomer, yielding various free radical species from the non-specific breakdown of the molecule (Figure 1.7). Indeed, organic monomers are particularly sensitive to fragmentation mechanisms due to their rather low bond dissociation energies (BDE) (*ca.* ε_{BDE} = 2 eV – 5 eV) compared to the kinetic energy of the electrons and of the photons into the discharge.[18] This mechanism is the main process for the growth of plasma-polymers from non-polymerizable monomer, as they are unable to react with each other without this initial fragmentation process.

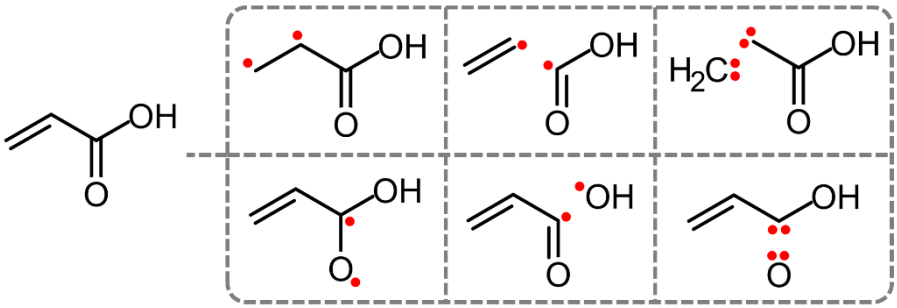

Figure 1.7. Possible σ-bond and π-bond homolytic breakdown of acrylic acid.

Different models have been proposed to describe the fragmentation mechanisms. Due to the variety of possible mechanisms leading to homolytic breakdown, each of them following its own frequency of occurrence, macroscopic approaches are required.

Notably, Hegemann et al. suggested an Arrhenius-like model for the calculation of the apparent activation energy E_a based on the Becker parameter ($B = W/F$), the mass deposition rate R_m and a geometrical factor of the reactor G (eq. 1.9).[64–67] This activation energy can be correlated to the bond dissociation energies from the injected molecules, yielding information on the type of fragmentation occurring during the plasma-polymerization.[66] Using Becker's composite parameters, this model aims at unifying the vast diversity of plasma-polymerization processes. Additionally, Hegemann *et al.* have introduced parameters to take into account the width d_{act} of the active plasma zone to describe the fragmentation mechanisms into the plasma (eq. 1.10); with the residence time of the molecular species τ_{act} and the conversion ratio of monomer x_{dep}, F the total gas flow, M the molecular weight of the monomer, T the standard temperature, P the standard pressure and R the gas constant.[65]

$$\frac{R_m}{F} = G * \exp(-\frac{E_a}{B}) \quad (1.9)$$

$$d_{act} = G \frac{\tau_{act} F}{x_{dep}} \frac{RT}{MP} \quad (1.10)$$

A slightly different form of Arrhenius equation based on the Yasuda parameter ($Y = W/FM$) have been suggested and applied by Scheltjens *et al.* for the description of the growth kinetic in atmospheric pressure plasmas (eq. 1.11), highlighting the relevance of the monomer's chemistry in the growth kinetic.[68–70]

$$\frac{R_m}{F*M} = G * \exp(-\frac{E_a}{Y}) \quad (1.11)$$

Wertheimer *et al.* suggested a different approach for the determination of the energy transferred to the monomers for initiating the reaction ΔE_g by integrating the plasma's power (*i.e.* the plasma potential V_{gap} multiplied by the dissipated current I_d) over a discharge cycle, with and without the monomer (eq. 12).[71,72] Notably, Wertheimer et al. have determined the average energy transferred per molecule E_m by normalizing the transferred energy ΔE_g with the monomer's flow rate F_d (eq. 13), which yields direct information on the potential fragmentation mechanisms initiating the plasma-polymerization.[71,72] Interestingly, the maximum of the measured transferred energy per molecule $E_{m,max}$ from Wertheimer et al. matches well with the activation energy E_a calculated by Hegemann et al., supporting the

validity of both approaches.[66,72] Furthermore, Wertheimer et al. have extended their calculation to different chemical families.[71–77]

$$\Delta E_g = E_{g,monomer} - E_{g,plasma} = \int^{monomer} V_{gap}\, I_d dt - \int^{plasma} V_{gap}\, I_d dt \quad (1.12)$$

$$E_m = \frac{\Delta E_g}{F_d} \quad (1.13)$$

2.2.2. Hydrogens' abstraction

An important form of fragmentation is the abstraction of hydrogen atoms from the monomer (Figure 1.8). If the C-H bond is not particularly weak (*ca.* ε_{C-H} = 4 eV), the hydrogen are usually located on the outer parts of the molecule, making them primary targets for inelastic collisions with the electrons and photons.[12,18,61] While the abstraction of hydrogens may not necessarily alter the core of the monomer, it creates local anchoring points that induces a cross-linking of the plasma-polymer chains and have, therefore, a strong impact on the properties of the plasma-polymer thin films.

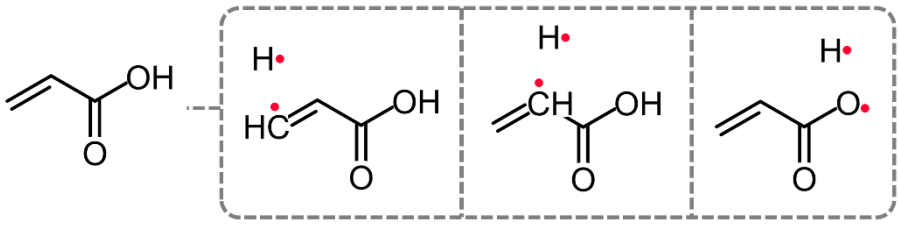

Figure 1.8. Possible homolytic hydrogen's abstraction of acrylic acid.

This abstraction of hydrogen atoms has brought to light highly critical mechanisms in the plasma-polymerization processes, which remain an important research subject to this day.

Indeed, Kobayashi *et al.* noted an important dependence between the chemistry of the monomer itself and the rate of deposition with identical experimental deposition conditions.[61] By investigating the possible degree of hydrogen abstraction of various monomers (hydrogen yield), they noted that monomer without unsaturation (i.e. alkanes) has lower deposition rate (high hydrogen yield), while monomer having more than one unsaturation (*i.e.* alkenes, alkynes, aromatics …) strongly increased their reactivity (and low hydrogen yield).[61]

From patterns observed during experimental measurements of the deposition rate and the hydrogen yield, Yasuda suggested a classification to differentiate those molecules: group I: contains a triple bond or aromatic structure; group II: contains a double bond or cyclic structure; group III: contains no unsaturation; group IV: contains one or more oxygen (Figure 1.9).[11,12]

Reniers *et al.* further confirmed the trend observed by Kobayashi et Yasuda, highlighting a strong influence of the number of unsaturation on the kinetic layer growth, the retention of the monomer's chemistry and, consequently, the abstraction of hydrogens in monomers from the group I to III.[69,78–80] Moreover, Reniers *et al.*, have recently reported new aspect related to the strong impact of the vinylic bonds on the plasma-polymerization mechanisms and the resulting chemistry, featuring preferential fragmentation of the monomer depending on the number and position of vinyl functions.[80,81] Furthermore, an alteration of the discharge itself depending on the number and position of vinyl bonds was reported by Reniers *et al.*, transitioning from a filamentary regime to a semi-homogeneous discharge.[80]

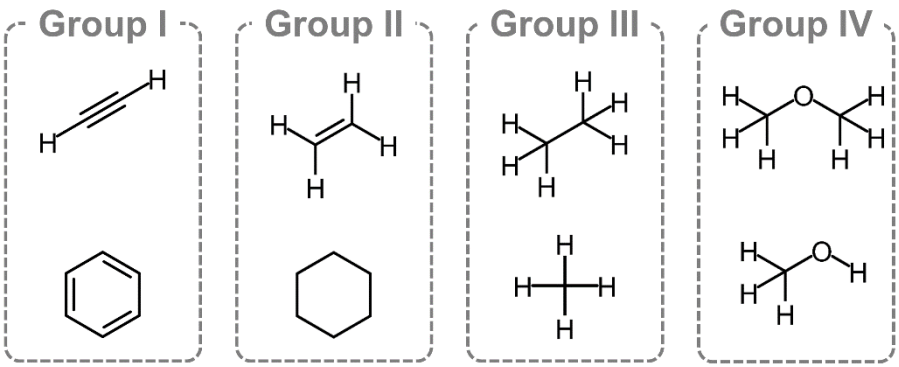

Figure 1.9. Classification of the families of monomers by Yasuda.

2.2.3. Reactive oxygen and nitrogen species

Among the possible fragments generated by the plasma discharge, reactive oxygen species (ROS) and reactive nitrogen species (RNS) are particularly reactive species (*e.g.* O_2^-, O^-, OH●, NO●, NO_2● or H_2O_2●), that may arise from the monomer itself or from its environment (N_2, O_2, H_2O …).[82–84] When they are in sufficient amount, those reactive oxygen species (ROS) and reactive nitrogen species (RNS) may deeply alter the growth mechanisms and the discharge itself due to an excess of anions and reactive species that quench the plasma, leading to oxidation reactions and to the introduction of contaminations.[83,85]

For these reasons, an open reactor can have a strong influence on the chemistry and the growth mechanisms in atmospheric-pressure plasma-polymerization processes. Yet, O_2 and N_2 can be intentionally injected in the plasma to generate ROS and RNS in order to modify the surface with oxygen-rich and nitrogen-rich elements.[83]

2.2.4. Etching

Etching mechanisms arise from collisions of highly energetic (*i.e.* VUV photon, thermal electrons and ions) and chemically reactive species (*e.g.* O_2^-, F^-) with the surface[23,85–88]. Indeed, organic compounds are particularly sensitive to surface etching, as their cohesive bonds are easily broken and the fragments sputtered, gradually altering the surface topography.[23,87,88]

Therefore, surface etching may be either beneficial or detrimental depending on the required properties and will be highly dependent of the properties of the plasma itself. Typically, working with low-energy and low-density plasmas (e.g. low frequency plasmas) in neutral environment represses the etching mechanisms to promote the deposition of homogeneous and smooth plasma-polymer thin films. Reciprocally, highly energetic and dense plasmas (*e.g.* microwave plasmas) in reactive environment will promote the etching mechanisms in order to promote the formation of patterned and nanostructured surfaces.[23,88]

2.3. Growth mechanisms following the discharge

The important variety of reactive species generated by the plasma are thereafter able to react following their chemical affinities and reactivity. The most reactive species (*i.e.* electrons and photons) and the heavy species (ions and metastables) quickly deactivate after the plasma discharge by simple recombination or by radiative emission.

Indeed, Kobayashi *et al.* observed a strong influence of the experimental parameters (*i.e.* the monomer's injection rate and the electrodes' gap) on the kinetic of plasma-polymerization.[41,42] Those variations of deposition rate were notably accompanied by changes in the films' conformation (*i.e.* oily, dense or powdery), hinting on different growth mechanisms with their own kinetic of reaction.[41,42]

During the off time, the growth mechanisms are largely dictated by the neutral and free radical molecules present in the gas phase and on the substrate's surface.[1,14] Therefore, monomers with polymerizable functions are able to grow conventionally following the plasma discharge, which can be promoted using pulsed high-voltage sources to extend the off-time.

2.3.1. Recombination

Recombination mechanisms of the free radical moieties quickly follow their fragmentations due to the high reactivity of these free radical species.[1,12,14] The way two fragmented plasma-polymers recombine is vastly dependent of their direct environment, and their possible stabilization mechanisms. Three scenarios can be anticipated: the formation of a σ-bond or coupling (Figure 1.10a), the reorganization of two free radicals in a neutral form by transfer mechanisms or dispropornation (Figure 1.10b) and the recombination of a radical with a neutral molecule by chain transfer (Figure 1.10c).[1,14,89] Both coupling and dispropornation mechanisms may occur intramolecularly or intermolecularly.

Non-polymerizable monomers are only able to grow by recombination mechanisms, leading to a loss of the initial monomer pattern as these molecules are continuously fragmented and chemical fragments are added (*i.e.* either element or moieties).

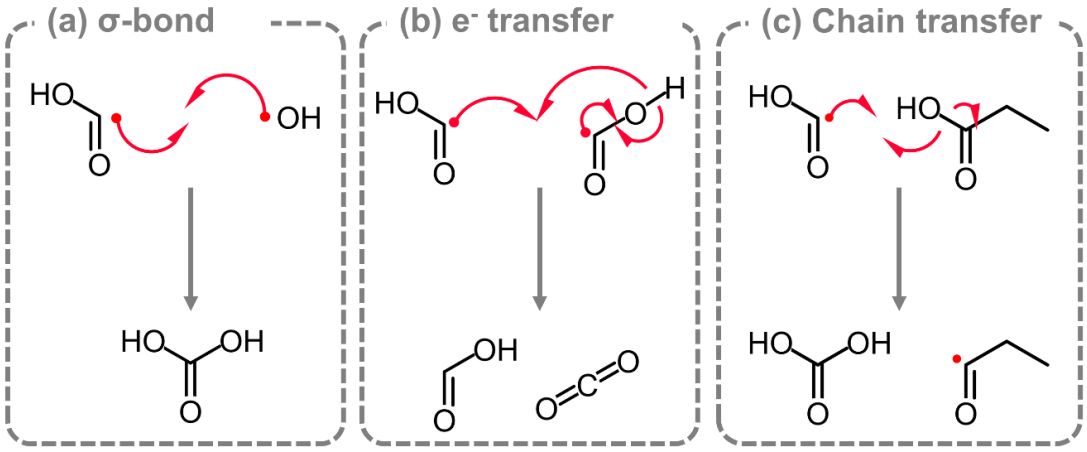

Figure 1.10. Free radical recombination mechanisms by (a) σ-bond formation or coupling and (b) transfer or dispropornation.

Monomers that possess chemical functionalities able to polymerize conventionally are able to grow without being fragmented, hence maintaining their original chemical pattern. Considering the important variety of species generated in the plasma, many conventional polymerization mechanisms are possible following the discharge.

2.3.2. Free radical polymerization

Free radical polymerization is a self-sustained reaction, taking advantage of the plasma free radical species to initiate and propagate conventionally the polymer chain from monomers with a vinyl function (Figure 1.11).[1,14,89]

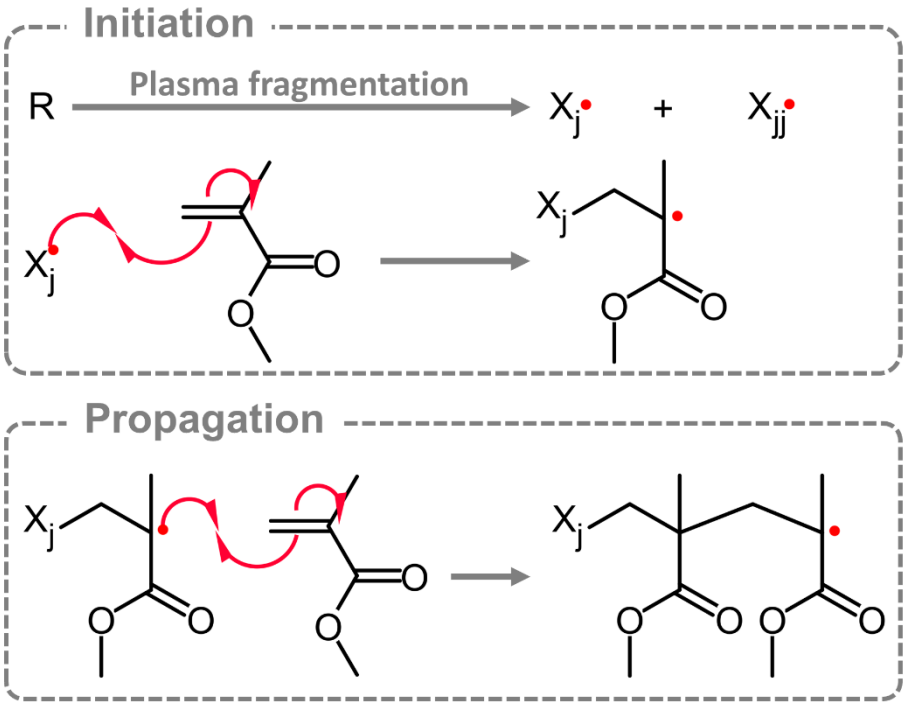

Figure 1.11. Conventional free radical polymerization of methyl methacrylate initiated by a free radical initiator.

While an initial fragmentation is required to start the polymerization process, conventional polymer can be grown as long as free radical plasma-polymer chains remain actives during the plasma off time.[89] Accordingly, using pulsed high-voltage sources to extend the off time promotes the free-radical polymerization mechanisms, strongly improving the chemistry of the plasma-polymer thin films (Figure 1.12).[1,14,50]

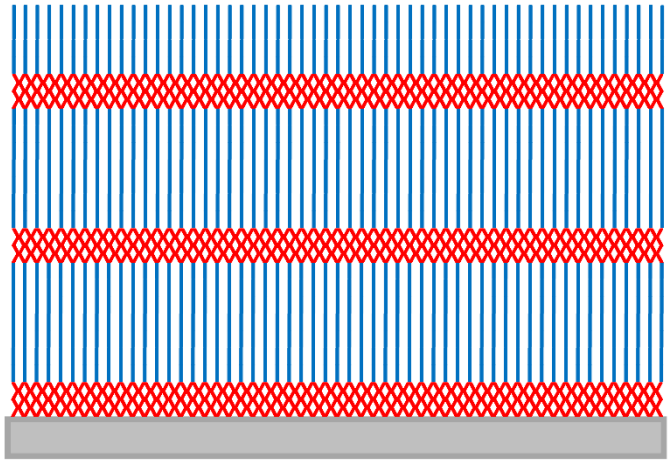

Figure 1.12. Scheme of plasma-polymer thin films grown by an AC-pulsed high-voltage sources. The altered plasma-polymer layers formed during the on time by fragmentation/recombination mechanisms are displayed in red, while the conventional

polymer formed by free-radical polymerization mechanisms during the off time are displayed in blue.

2.3.3. Oxidative polymerization

Oxidative plasma-polymerization relies on the ROS produced by the plasma to initiate the step-addition of the monomers, by electrophile addition and substitution mechanisms (Figure 1.13).[89] Unlike the free radical plasma-polymerization, oxidative plasma-polymerization is not self-sustained as each step-addition do not propagate the oxidized species, which need to be re-initiated to resume the growth of the chain.[89]

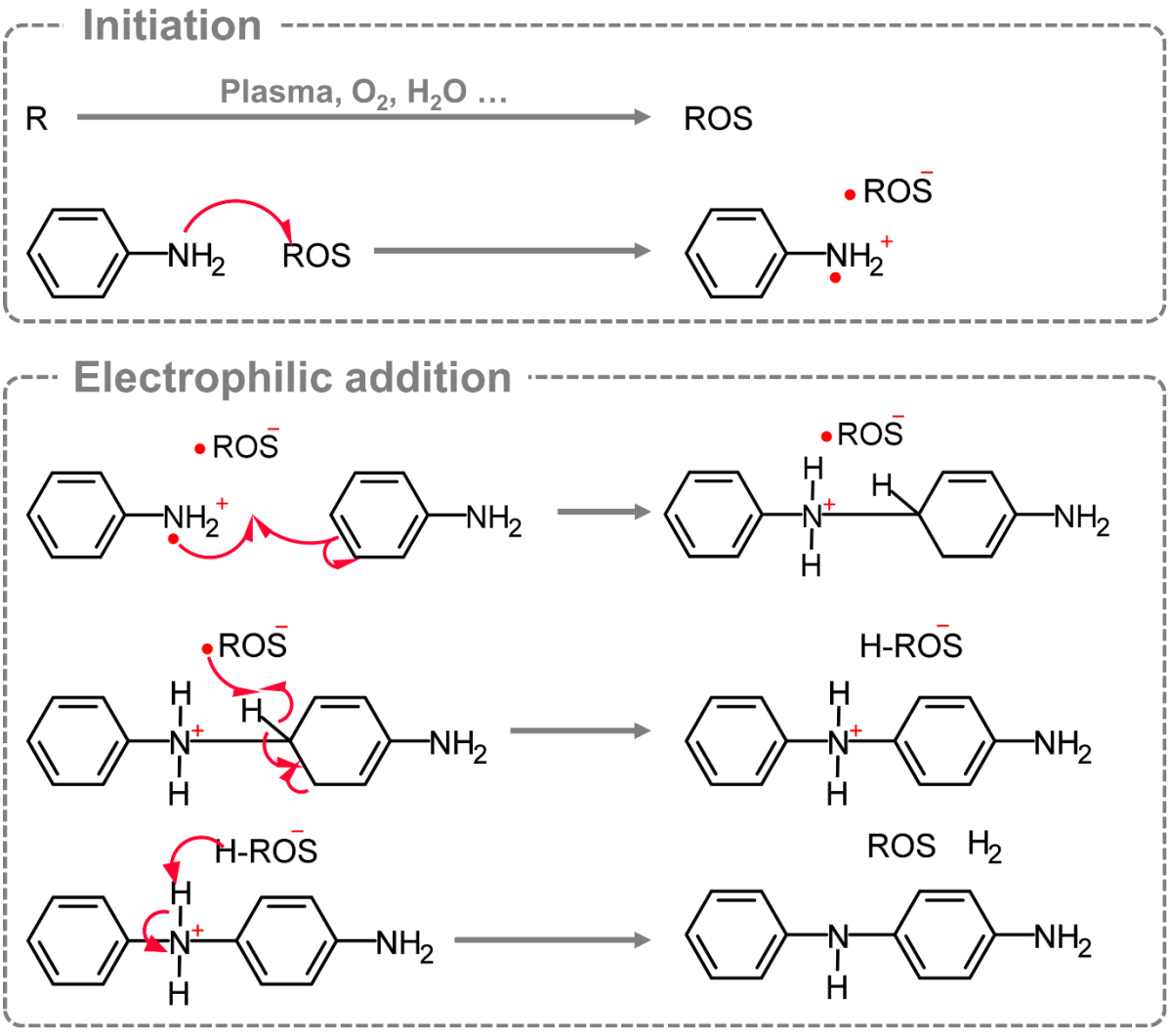

Figure 1.13. Oxidative polymerization mechanisms of aniline initiated by reactive oxygen species from the plasma.

Few studies on true oxidative plasma-polymerization processes are reported.[90,91] As each electrophilic addition deactivate the polymer chains, high discharge frequencies are required to promote the formation of oxidative species able to re-initiate the reaction. Therefore, oxidative polymerization in PECVD processes are highly subjected to fragmentation and recombination side-mechanisms, which are detrimental for the retention of the thin films' properties.

2.3.4. Ionic polymerization

Ionic chain polymerization requires the formation of terminal ions pair as propagating functions. The active site, usually a carbonium C^+ or carbanion C^-, is stabilized by a counter ion and is able to freely propagate in a self-sustained way (Figure 1.14).[89] Ionic polymerization is highly selective and do not terminate by recombination, as the terminal ions repel each other, requiring the introduction of terminating compounds (*e.g.* water).[89]

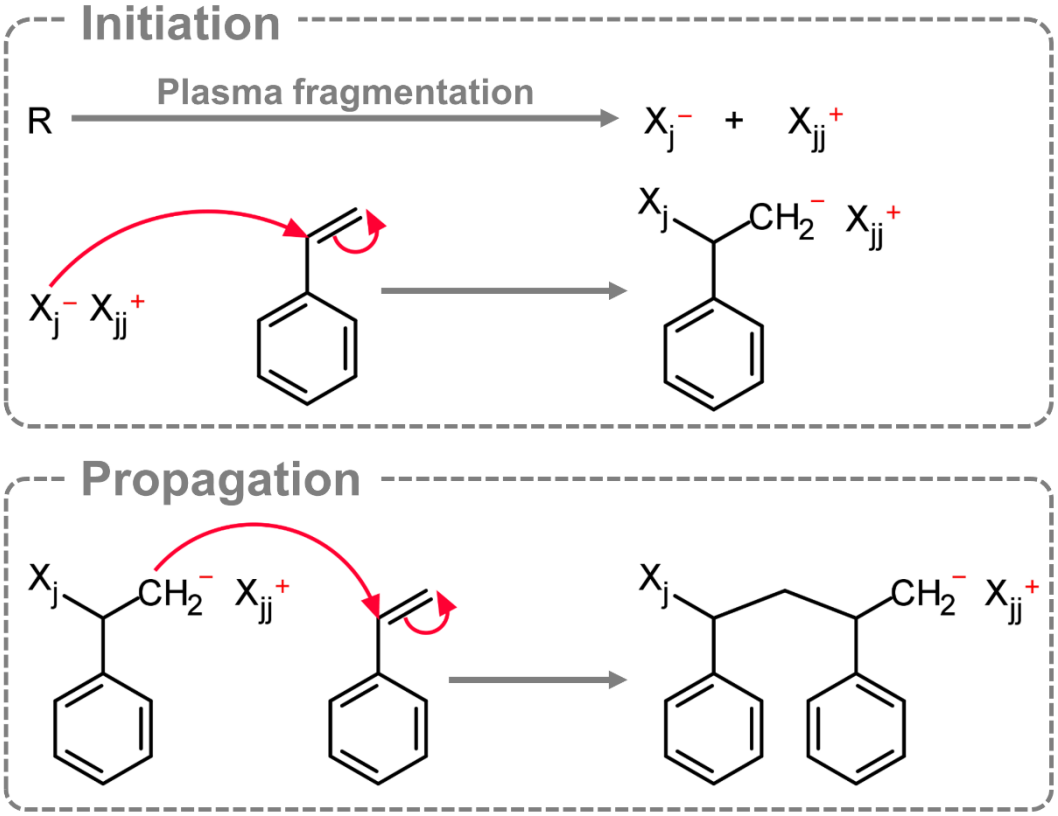

Figure 1.14. Ionic chain polymerization of styrene initiated by an anion X_j^-.

Ionic chain polymerization is a very difficult process to achieve with plasmas and it has never been reported as such due to non-specificity of the energetic species in plasmas and to the short lifetime of ions. Indeed, the formation of a high density of ionic species also promote fragmentation and etching mechanisms, which are detrimental for the retention of the monomer structure and the control of the thin film's topography. Moreover, while this type of polymerization is able to occur, it would be more efficiently promoted by the electron and free-radical species formed in the plasma phase and is therefore unsuited for this type of process.

2.4. Limitations of plasma-polymerization CVD

The numerous energetic species and mechanisms occurring during the plasma-polymerization of an organic molecule suggest a high potential for the simple synthesis of extremely diverse functional layers, but they also induce a lack of control of the ongoing mechanisms.[1,12] Indeed, all the previously described mechanisms are statistically bound to happen, each leading to formation of new species with their own reactivity that implies an intrinsic non-selectivity during the growth of the plasma-polymer layers.

Therefore, the existing description of plasma-polymerization mechanisms are often very generalized or restricted to a set of experimental systems, impeding a better understanding of the key parameters to optimize the existing processes. Indeed, even well accepted descriptions of the growth kinetic – such as the one developed by Hegemann *et al.* (eq. 1.9) – are still under debate to understand the real meaning of the equation's term and their global significance in various plasma-polymerization processes.[66,92]

Notably, the characteristic fragmentation/recombination mechanisms have a strong occurrence compared to conventional mechanisms, which are limited by the lifetime of the active species, strongly affecting the chemistry of the resulting plasma-polymer (Figure 1.15). Indeed, the loss of the original chemical pattern of the monomer prevents potential applications that require a retention of the monomer's chemistry over long polymeric chain.

Ultimately, this difficulty to produce conventional-like polymer layers using plasma-based processes highlight one of the most important limitation and objective in plasma-polymerization: the lack of control and understanding of the initiation mechanisms compared to other CVD methods.

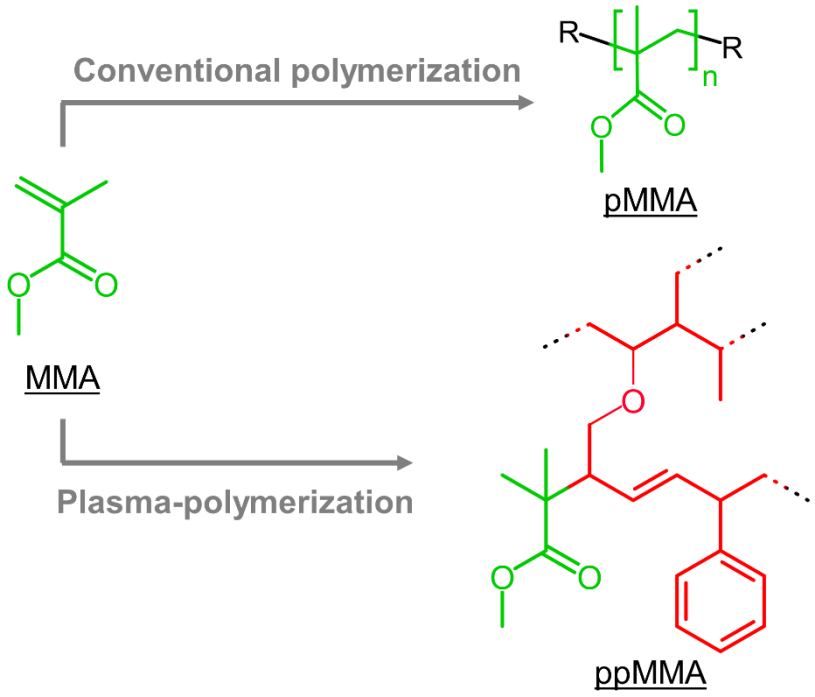

Figure 1.15. Scheme of the chemistry of methyl methacrylate polymerized conventionally and plasma-polymerized, the retention of the monomer's chemistry is highlighted in green and the alterations in red.

3. Conventional polymerization CVD

3.1. Overview of previous research

Conventional polymerization CVD processes have been an attractive alternative to solution-based approaches for the dry deposition of polymer thin films. To reproduce conventional

polymerization mechanisms in the gas phase, the CVD processes rely on alternative initiation methods and means to control the gas environment to replace the wet solvent. Conventional polymerization CVD processes operate under controlled vacuum (*i.e.* ranging from 10^{-3} to 1 Torr) to lower the environmental contamination and extend the lifetime of the volatile reactive species (*i.e.* free radicals, ions …), which are intrinsically shorter compared to liquid ones.

Interestingly, these highly controlled environment and increased lifetimes promote surface mechanisms yielding pinhole-free and conformal thin films.[93] Accordingly, conventional polymerization CVD processes are particularly suitable for the growth of multi-layers and the functionalization of highly textured surface (Figure 1.16), a feature hardly achievable from conventional solution-based approaches and plasma-polymerization CVD.[94]

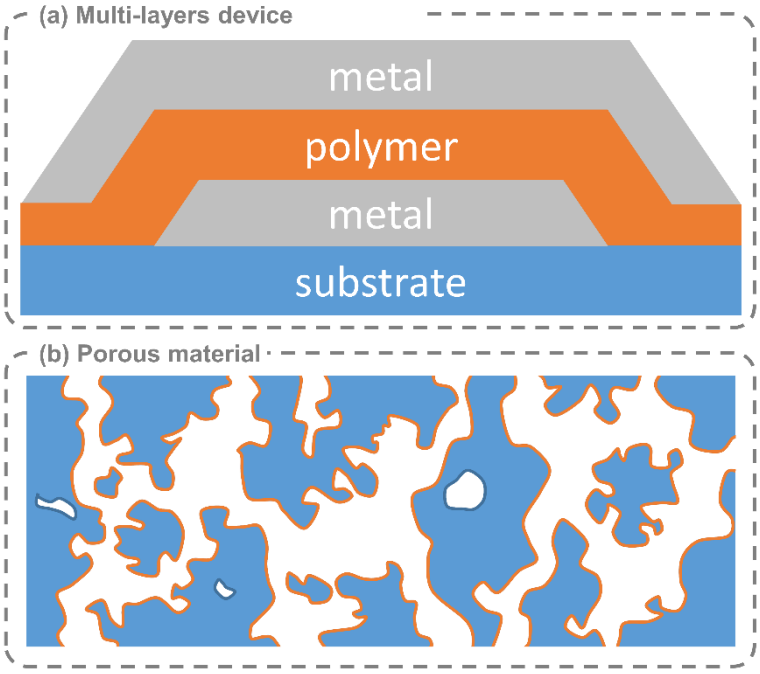

Figure 1.16. Scheme of (a) a multi-layers device and (b) a porous material coated by a conformal layer in orange.

The kinetic in conventional CVD processes are highly dependent of adsorption mechanisms, hence the P_M/P_{sat} coefficient as described by the Brunauer–Emmett–Teller (BET) equation (eq. 1.10); with P_M the monomer's partial pressure, P_{sat} its vapor pressure, c the coverage coefficient, V_{ad} the adsorbed volume and V_{ml} the volume of a monolayer.[95]

$$V_{ad} = \frac{V_{ml} \times c \times (P_m/P_{sat})}{(1-P_M/P_{sat})[1-(1-c)(P_M/P_{sat})]} \quad (1.10)$$

The growth mechanisms leading to conformal properties are highly dependent of the type of interaction on the substrate's surface. Two interactions based on adsorption and diffusion mechanisms are known: the Langmuir-Hinshelwood mechanism when both molecules are adsorbed on the surface and the Eley-Rideal mechanism when a molecule from the gas phase collides with an adsorbed molecule (Figure 1.17).[94]

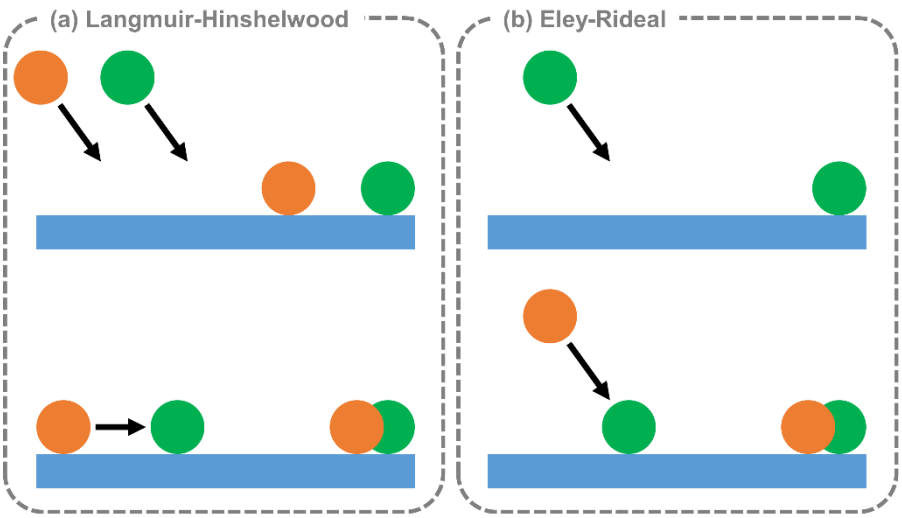

Figure 1.17. (a) Langmuir-Hinshelwood and (b) Eley-Rideal mechanisms describing surface reactions between two molecules.

Historically, CVD by thermal heating under vacuum have been employed to provide the energy for initiating the polymerization mechanisms by thermal cracking (*i.e.* homolytic opening of a saturated, unsaturated or cyclic C-C bond).[96–98] These cracking mechanisms require high energies and are very costly while suffering from the same lack of selectivity as plasma-polymerization. Therefore, alternative CVD processes have been investigated for the initiation of conventional polymerization mechanisms, using radical initiators (initiated CVD), photons (photoinitiated CVD), oxidants (oxidative CVD), catalysts (catalytic CVD) or saturated chemicals (molecular layer deposition).

3.2. Free radical polymerization via iCVD and piCVD

The free-radical polymerization is initiated by the generation of a free radical that is able to propagate through the vinyl bonds of the monomer (Figure 1.11). To generate free-radical initiators while preserving their integrity of the monomer's chemical structure by CVD, chemical initiators (*e.g.* Di-tert-butyl peroxide, azobisisobutyronitrile …) are activated with gentle energy sources below the BDE of the monomer.

Specifically, the labile initiators are decomposed either thermally (*ca.* 200°C) in initiated CVD (iCVD), or by UV light (*ca.* 350 nm) in photoinitiated CVD (piCVD).[94,97,99–101] The precise control over the wavelength in piCVD even allowed tuning of the energy to activate directly the monomer while preserving its structure, yet iCVD became the most flexible and researched conventional CVD process for free-radical polymerization.[102] The free radical species and monomers adsorb on the surface and propagate conventionally through the monomers' π-bonds, perfectly reproducing the self-sustained conventional free radical polymerization mechanisms (Figure 1.18).[89] Free radical species are able to terminate following classical pathways, either by coupling or by disproportionation (Figure 1.10).[89]

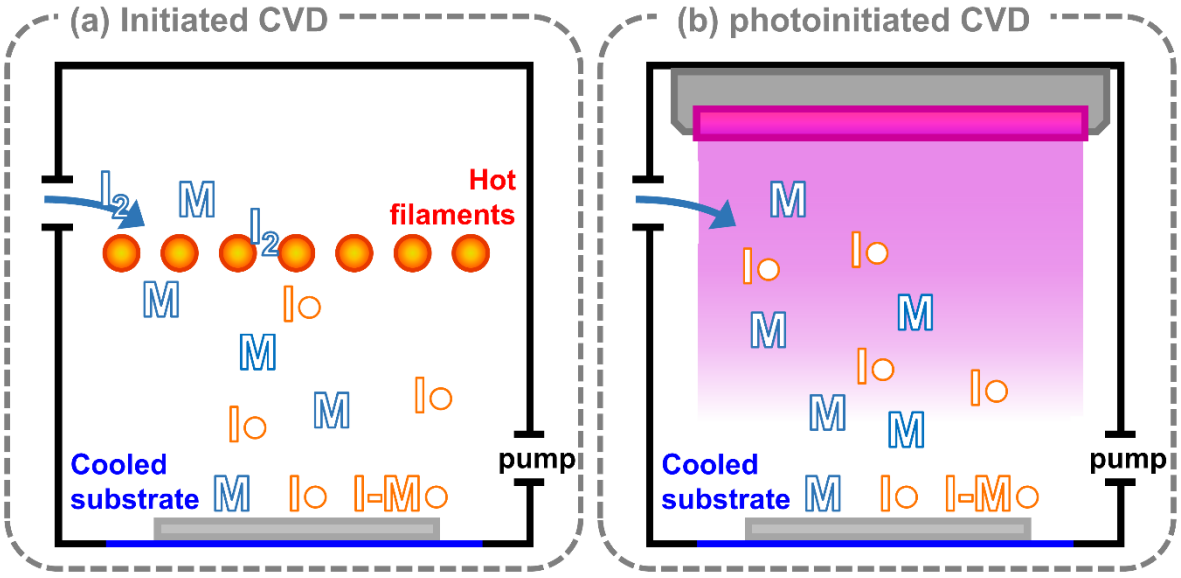

Figure 1.18. Schemes of (a) an iCVD reactor and (b) a piCVD reactor for conventional free radical polymerization.

Lau *et al.* described the relationship between the polymerization kinetic and the vapor pressure as predominant in iCVD processes.[103,104] Indeed, the adsorbed volume V_{ad} during the deposition was related to the P_M/P_{sat} ratio through the BET equation (eq. 1.10), highlighting the formation of multilayers with a coverage c of 2.536.[95] Notably, an adsorption-limited reactivity was demonstrated as the deposition rate (Figure 1.19a) and the molecular weight (Figure 1.19b) of monomers of the same family grown in identical conditions followed a linear trend according to their respective vapor pressure.[104]

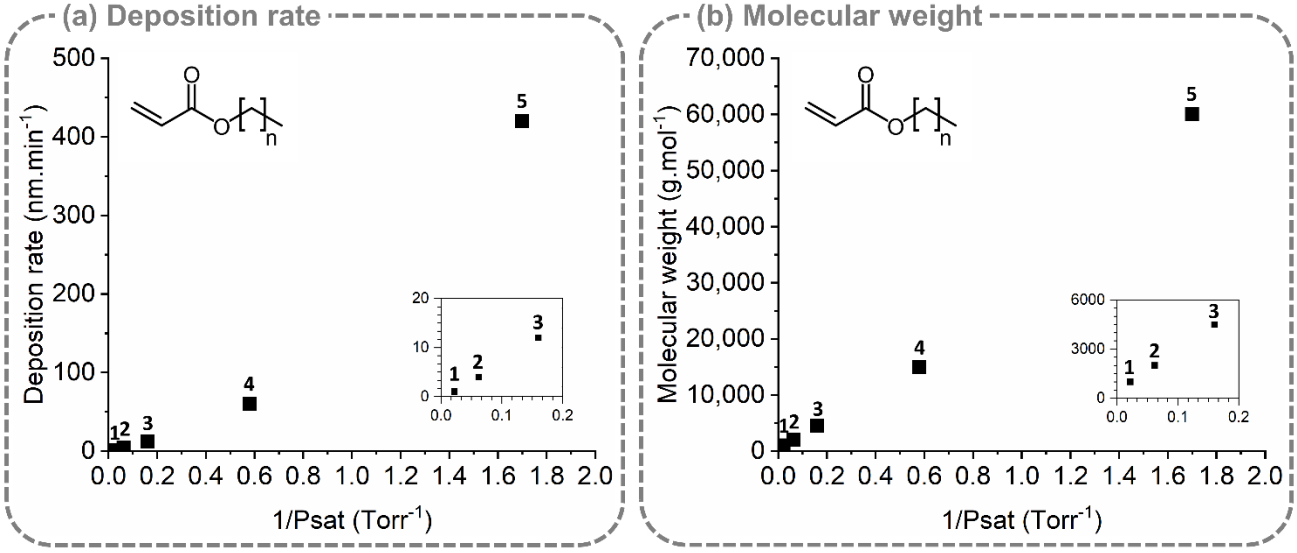

Figure 1.19. Evolution of the (a) deposition rate and (b) molecular weight of alkyl acrylates grown by iCVD according to their vapor pressure. The number of CH_2 units n on the acrylate chains are indicated on top of each point.[104]

In order to describe the relationship between the adsorption mechanisms in iCVD and the polymerization kinetic, Lau *et al.* proposed a chemical model based on theoretical mechanisms and experimental data (Figure 1.20a).[103] By expressing the concentration of

monomer to the adsorption kinetic through the BET equation (eq. 1.11) and to the experimental data through the deposition rate (eq. 1.12), Lau *et al.* were able to calculate the kinetic constant of polymerization. Specifically, the reaction rate (Figure 1.20b) and radical concentration of initiators and monomers (Figure 1.20c) could be expressed according to the concentration of monomer.[103]

$$[M] = \frac{\rho_M \times V_{ad}}{M_{W,M} \times V_{ml}} \tag{1.11}$$

$$R_p = \frac{DR \times \rho_p \times [M]}{h_{ml} \times \rho_{ad}} \tag{1.12}$$

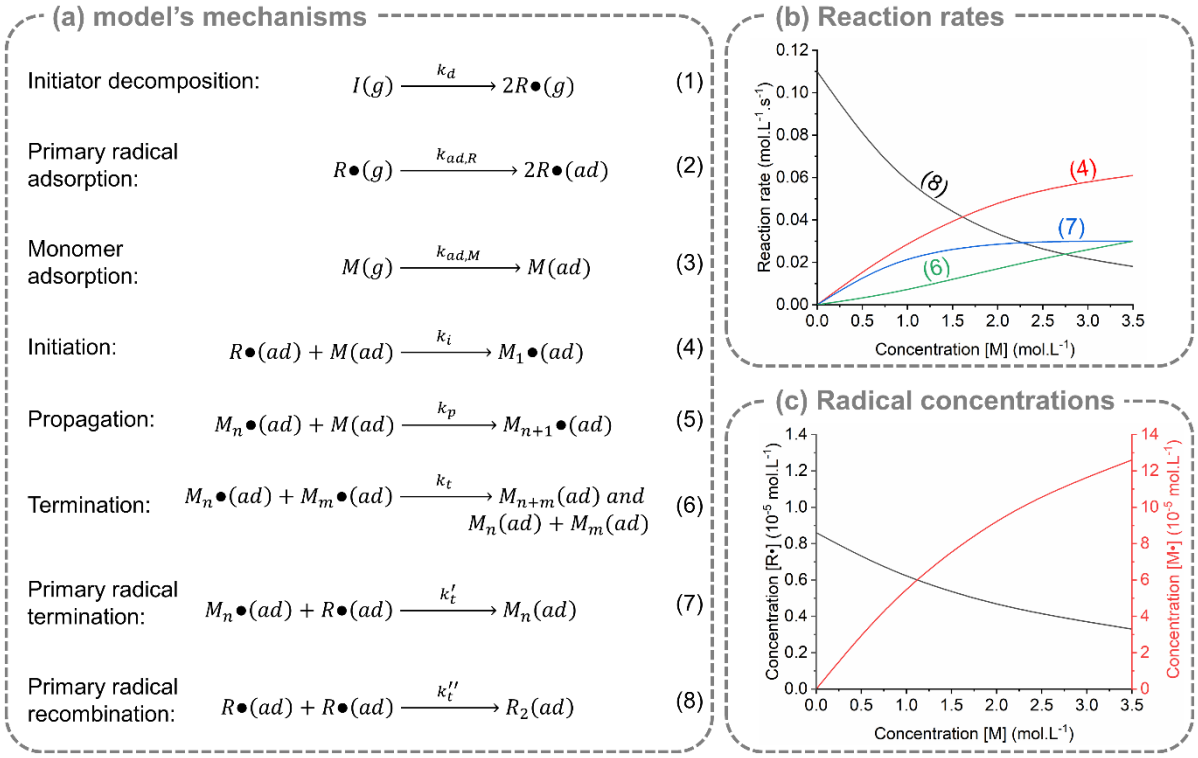

Figure 1.20. (a) Mechanisms used by Lau et al. in their kinetic model. Influence of the concentration of monomer $[M]$ on (b) the reaction rates of some of the model's mechanisms and (c) the free radicals' concentration of initatior $[R\bullet]$ and monomer $[M\bullet]$.[103]

In free radical polymerization, the kinetic reaction rates of initiation (eq. 1.13), propagation (eq. 1.14) and termination (eq. 1.15) are usually considered, but more reactions can be evaluated depending on the expected mechanism.[89]

$$R_i = k_i[R\bullet][M] \tag{1.13}$$

$$R_p = k_p[M\bullet][M] \tag{1.14}$$

$$R_t = k_t[M\bullet]^2 \tag{1.15}$$

In these studies, Lau *et al.* were therefore able to bring a description of the surface growth mechanisms supported by a chemical model of the polymerization kinetic. The accordance between experimental and calculated data further confirms the importance of adsorption mechanisms in the iCVD process, expressed as the strong dependence of the kinetic rates of polymerization to the P_M/P_{sat} ratio.[95,103,104]

As assumed in Lau et al.'s model, and following experimental observations, the propagation and terminations reactions (*i.e.* (5) and (6) in Figure 1.20a) are occurring as Langmuir-Hinshelwood mechanisms.[93,103] However, an increase of the free radical initiators' sticking coefficient (*i.e.* the probability a molecule will adsorb on the substrate) with the concentration of monomer (*i.e.* P_M/P_{sat}) indicates that they interact in an Eley-Rideal mechanism.[93,103]

At low P_M/P_{sat} (*i.e.* < 0.1), the free-radical initiators have lower sticking coefficient and are able to collide down the rough substrate's topography before initiating a monomer (*i.e.* (4) in Figure 1.20a).[93] This mechanism notably allows a homogeneous spread of free-radical growing species, even on textured substrates, hence promoting the growth of conformal thin films (Figure 1.21a).[93]

At high P_M/P_{sat}, the free-radical initiators have higher sticking coefficient and tend to react as soon as they reach the substrate without colliding.[93] Therefore, the polymerization will occur predominantly on the upper surface of a rough or textured substrate yielding non-conformal thin films comparable to low pressure plasma-polymerization (Figure 1.21b).[93]

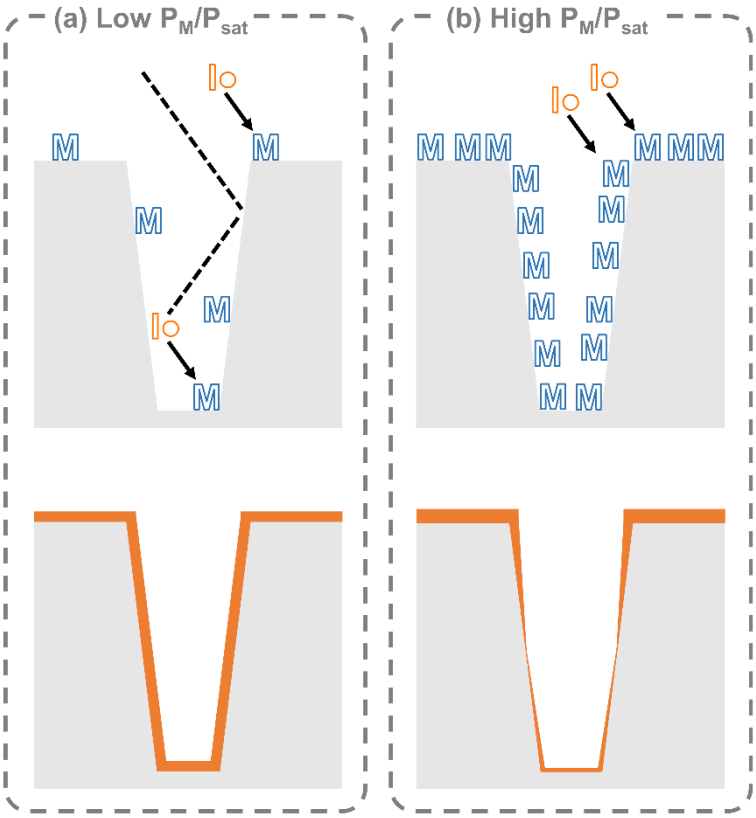

Figure 1.21. Scheme of the growth mechanisms in iCVD with (a) low P_M/P_{sat} values yielding conformal coatings and (b) high P_M/P_{sat} values yielding non-conformal coating.

Overall, the chemical and topographical growth mechanisms in iCVD are governed by adsorption mechanism. Interestingly, low vapor pressures P_{sat} tend to promote higher deposition rates and molecular weights, but increase the P_M/P_{sat} ratio, which could lead to non-conformal deposition.[93] In order to obtain an optimal deposition, a fine tuning of the monomer's partial pressure P_M is necessary, notably by injecting lower concentration of monomer $[M]$ if the P_{sat} is low. This requirement prevents the use of monomers with very low vapor pressure, as they would become increasingly difficult to inject in the system as their P_{sat} decrease.

Therefore, iCVD proved to be a highly reliable method for the growth of conventional polymer thin films by free radical polymerization, allowing the simultaneous deposition and synthesis of vinyl-bearing monomers. The vast number of vinyl-bearing monomers available, along iCVD's ability to grow conformal layers, presents a particular interest for applications requiring a complete coverage of the surface, such as barrier layers, water-repellent coatings, insulating layers in microelectronic or sensors (Figure 1.22).[93,94,99] Various types of conformal polymers thin films grown by iCVD have been reported, from acrylates to fluoromonomers, demonstrating the adaptability of the process.

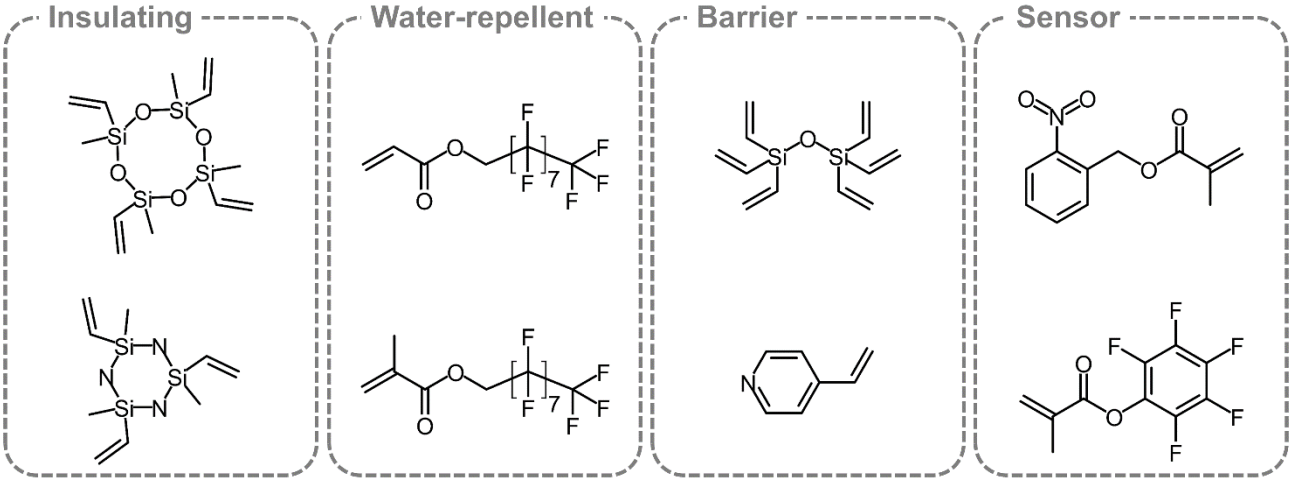

Figure 1.22. Example of monomers reported in iCVD and their applications.

3.3. Oxidative polymerization via oCVD

The oxidative polymerization is initiated by the monomer losing one electron from oxidizing species, forming a radical cation able to react with another monomer by electrophilic addition (Figure 1.13).[89] The growth mechanisms are not entirely specific as the initiation may occur on several position of the molecule, depending on the oxidation's and electrophilic addition's chemical affinities with the monomer's chemical functionalities. Moreover, the growth mechanisms are not self-sustained but it will require new oxidant species to reinitiate the polymerization process.[89]

The oxidative CVD (oCVD) processes rely on very similar mechanism as solution-based chemistry, taking into account adsorption and diffusion mechanisms. The oxidants (*e.g.* Lewis acids such as $AlCl_3$ or $FeCl_3$) are sublimed in a heated crucible (*ca.* 200°C) towards the substrate where they adsorb and react with the monomers (Figure 1.23).[93] Depending on its physical state, the monomer may either be injected from the gas phase or sublimed.[93,105,106]

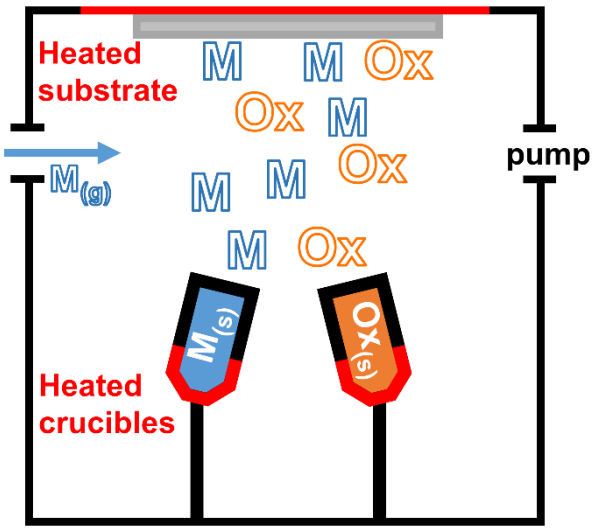

Figure 1.23. Scheme of an oCVD reactor showing both injections of the monomers through the gas phase or in a crucible.

While the kinetic of oxidative step-growth polymerization is thoroughly described in the literature, only few descriptions of the growth mechanisms in oCVD process exist.[89,105,107–109] Yet, the kinetic of oCVD should be similar to conventional polymerization methods, at least in their reactivity.

Expressing the kinetic rate of oxidative polymerization similarly to the free radical polymerization (eq. 1.16) shows a linear dependence of the observed kinetic constant k_{obs} with the concentration of formed polymer $[P]$ (Figure 1.24a).[89,110] Therefore, the growth kinetic of oxidative polymerization is driven by two rate-limiting states (Figure 1.24b), which can be described as a slow conversion from the oxidant and a catalyzed acceleration from the synthesis of polymer chains (eq. 1.17).[89,110]

$$R_{ox} = k_{obs}[M][Ox] \quad (1.16)$$

$$R_{ox} = k_1[M][Ox] + k_2[M][P] \quad (1.17)$$

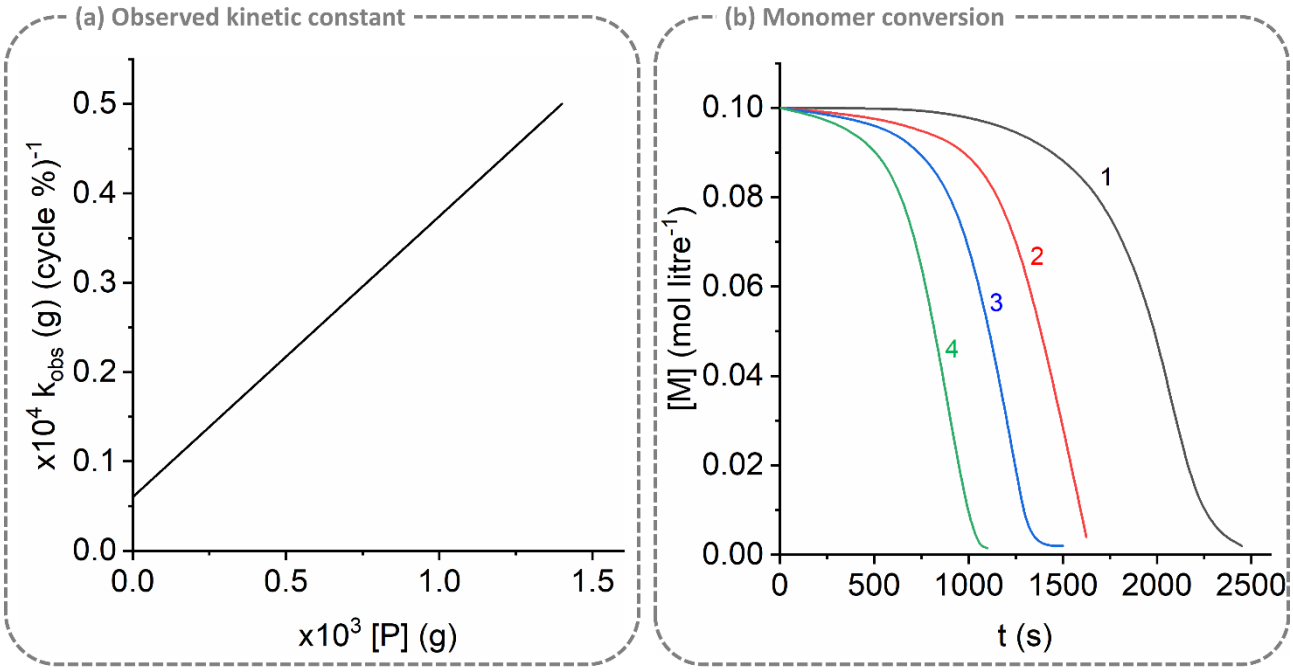

Figure 1.24. (a) Observed rate constant k_{obs} vs. the amount of polymer $[P]$ formed. (b) Kinetic curves of oxidative polymerization of a monomer (0.1 mol·L^{-1}) in the presence of an oxidant ($[Ox]_0$:$[M]_0$ = 1.25) measured at (1) 15°C, (2) 25°C, (3) 30°C and (4) 35°C.[110]

Similar mechanisms are globally expected in the oCVD process, but they do not account for the role of the adsorption mechanisms, which were shown to be process limiting in iCVD. Indeed, Lau *et al.* reported a correlation between the conjugation of the polymers grown by oCVD and the P_M/P_{sat} ratio.[111] However, no model has been developed linking the kinetic of oxidative polymerization in oCVD to the adsorption mechanisms. Yet, the ability to grow conformal thin films hints on prominent diffusion mechanisms on the surface, suggesting the prevalence of surface growth mechanisms and a strong dependence on the P_M/P_{sat} ratio.[93]

Since the electrophilic addition of monomers is performed at the loss of a hydrogen and an electron from each monomer, the unsaturation degree of the polymer increases by 1 for each addition.[89] Therefore, the oCVD polymerization is particularly attractive for the growth of polymer chains with high electronic couplings, hence electrons delocalization (Figure 1.25).[105–109,112] The long-range order conjugation of polymer thin films allows the growth of transparent conductive materials.[94,106,107,112,113] In particular, pEDOT was polymerized by oCVD on numerous occasions due to its coupling and electron-rich nature from its dioxyalkylene, forming flexible and transparent thin films with high conductivity up to 100 S·cm^{-1}.[112,114] The conductivity and work function of polymer conductors can be enhanced and controlled using dopant (*e.g.* Cl$^-$), making them attractive alternatives to current electronic systems.[114]

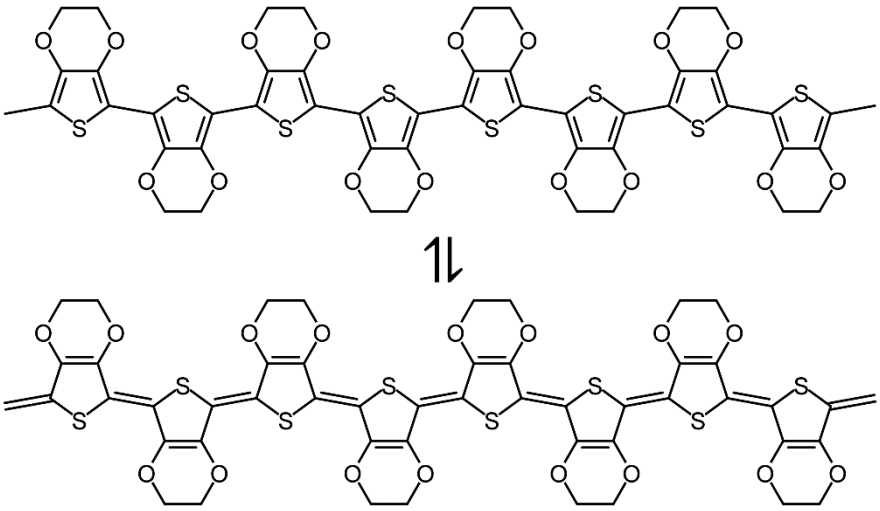

Figure 1.25. Electron delocalization in the conjugated pEDOT polymer.

3.4. Free-radical polymerization via PiCVD

Nanopulsed discharges represent a field of plasmas that was developed only during the last two decades. Based on square wave high-voltage sources with extremely fast rising and falling times (*ca.* 0.1 – 10 kV per ns) in order to generate the ultra-short discharges (*ca.* 100 – 1 ns), they offer new possibilities in the control of plasma processes due to their unique properties.

Indeed, the use of nanopulsed high voltage sources induce strong variations in the plasma properties and in the control of the reactive environment compared to AC sources. Since nanopulsed plasmas have no memory effect when they are associated to long off-times, each pulse discharge is completely independent and allow a unique control of the initiation mechanisms. Indeed, an ultra-short discharge implies different mobility and propagation of the charge carriers, as the electric field become instantaneous and unidirectional rather than maintained and oscillating. Therefore, the electron and the ion densities as well as their temperatures are expected to differ from a conventional AC discharge because of the discharge duration and its polarity.[115,116] Starikovskaia *et al.* notably reported different spatial distributions and decay times of the electric field and plasma species based on the gas density (*i.e.* the pressure), the polarity and the pulse's peak potential.[115,116]

Boscher *et al.* conjectured that nanopulsed sources show a significant potential for the plasma-initiated free radical polymerization of monomers bearing polymerizable bonds. Indeed, the combination of nanosecond pulsed plasma discharges with long time off allows to drastically lower the fragmentation mechanisms inherent to plasma-based processes, while the self-sustained free radical polymerization mechanisms become dominant during the off time. Using a 100 ns plasma (Figure 1.26a) and low frequencies of discharge they were able to confirm an extremely high retention of the vinyl-bearing glycidyl methacrylate's chemistry (Figure 1.26b), hinting on a prevalence of free radical polymerization mechanisms.[117]

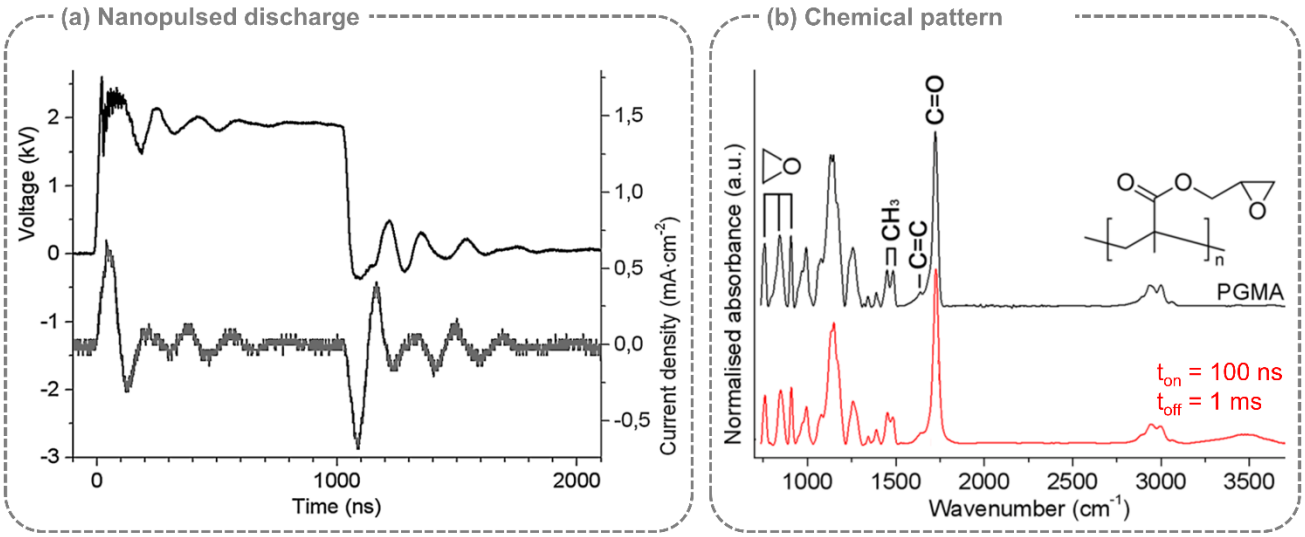

Figure 1.26. (a) Traces of 100 ns nanopulsed voltage and current discharges. (b) FTIR spectra of a conventionally polymerized poly(glycidyl methacrylate) and of a glycidyl methacrylate-based thin film formed using a 100 ns nanopulsed discharge and 1 ms off time.[117]

On that account, they also demonstrated the ability to treat large surface in an atmospheric-pressure DBD setup with mechanically stable epoxy-rich layers from glycidyl methacrylate monomers, allowing the immobilization of enzymes and the saturation of surfactant chemicals for the functionalization of bioactive materials (Figure 1.27a).[118]

Moreover, the plasma-polymer layers grown by nanopulsed discharges displayed a high degree of conformality compared to traditional plasma-polymerization processes, even under atmospheric condition (Figure 1.27b).[117] This shift of growth mechanisms hints on the promotion of surface reactions, comparable to conventional vacuum CVD, and was applied for the homogeneous functionalization of cotton fibers by a fire-retardant organophosphorus plasma-polymer coating (Figure 1.27c).[119] The conformality of the process was further highlighted by the retention of the fabric fibers after a burn test (Figure 1.27d).[119]

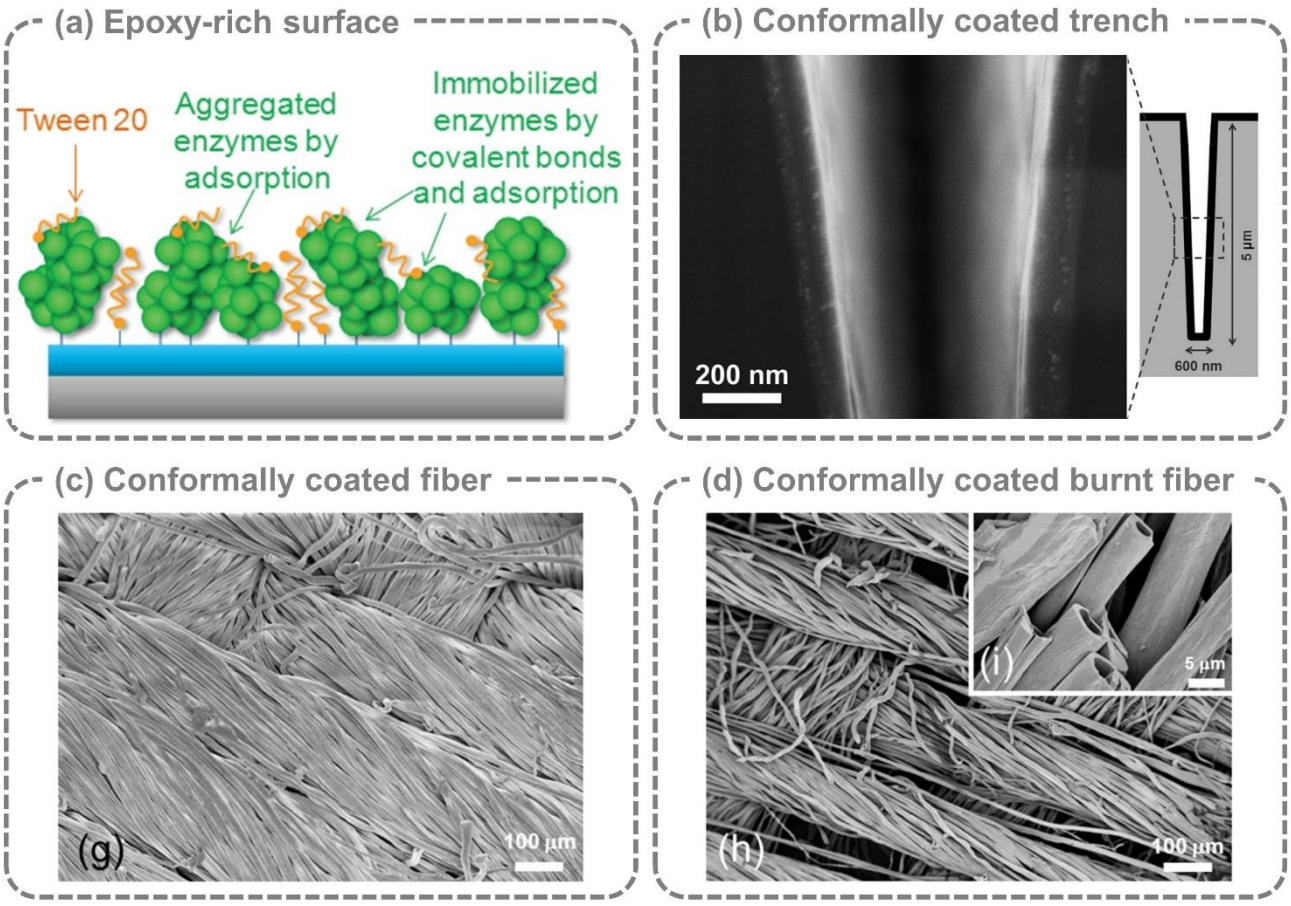

Figure 1.27 (a) Scheme of a nanopulsed epoxy-rich coating for enzyme immobilization and tween 20 surfactant saturation.[118] (b) Cross-sectional SEM image of a conformally coated by nanopulsed glycidyl methacrylate.[117] SEM images of cotton fibers conformally coated by nanopulsed diethylallylphosphate (c) before and (d) after a burn test.[119]

These overall results confirmed the strong potential of nanopulsed discharges for the promotion of free-radical polymerization surface mechanisms in an open-atmosphere setup. This novel approach towards the synthesis of conformal and conventional-like polymer layers was therefore name atmospheric-pressure plasma-initiated CVD (AP-PiCVD). However, there is still little understandings of the real growth mechanisms and the chemistry of these thin films, as well as the key parameters to promote the formation of those layers with high potential for entirely new fields of application.

4. References

1. Friedrich, J. (2006) *The Plasma Chemistry of Polymer Surfaces*, Wiley-VCH.

2. Friedman, A. (2008) *Plasma Chemistry*, Cambridge University Press.

3. Jörg Friedrich (2012) *The Plasma Chemistry of Polymer Surfaces: Advanced Techniques for Surface Design*.

4. Griem, H.R. (1997) *Principles of Plasma Spectroscopy*, Cambridge University Press.

5. Smirnov, B. (2011) *Fundamentals of Ionized Gases: Basic Topics in Plasma Physics*, Wiley-VCH.

6. Lieberman, M.A., and Lichtenberg, A.J. (2005) *Principles of Plasma Discharges and Materials Processing*, Wiley-VCH.

7. Umran, I., and Golkowski, M. (2011) *Principles of Plasma Physics for Engineers and Scientists*, Cambridge University Press.

8. Tendero, C., Tixier, C., Tristant, P., Desmaison, J., and Leprince, P. (2006) Atmospheric pressure plasmas: A review. *Spectrochim. Acta - Part B At. Spectrosc.*, **61** (1), 2–30.

9. Boulos, M.I. (1994) *Thermal Plasmas*, Springer-Verlag New York Inc.

10. Christophorou, L.G., and Olthoff, J.K. (2004) *Fundamental Electron Interactions with Plasma Processing Gases*, Springer.

11. Yasuda, H. (1981) Glow discharge polymerization. *J. Polym. Sci. Macromol. Rev.*, **16** (1), 199–293.

12. Yasuda, H. (1985) *Plasma Polymerization*, Academic Press.

13. Gahan, D., Daniels, S., Hayden, C., Scullin, P., O'Sullivan, D., Pei, Y.T., and Hopkins, M.B. (2012) Ion energy distribution measurements in rf and pulsed dc plasma discharges. *Plasma Sources Sci. Technol.*, **21** (2), 024004.

14. Friedrich, J. (2011) Mechanisms of plasma polymerization - Reviewed from a chemical point of view. *Plasma Process. Polym.*, **8** (9), 783–802.

15. Evdokimov, K.E., Konischev, M.E., Pichugin, V.F., and Sun, Z. (2017) Study of argon ions density and electron temperature and density in magnetron plasma by optical emission spectroscopy and collisional-radiative model. *Resour. Technol.*, **3** (2), 187–193.

16. Panagopoulos, T., and Economou, D.J. (1999) Plasma sheath model and ion energy distribution for all radio frequencies. *J. Appl. Phys.*, **85** (7), 3435–3443.

17. Kawamura, E., Vahedi, V., Lieberman, M.A., and Birdsall, C.K. (1999) Ion energy distributions in rf sheaths; review, analysis and simulation. *Plasma Sources Sci. Technol.*, **8** (3), R45–R64.

18. Luo, Y.-R. (2003) *Handbook of Bond Dissociation Energies in Organic Compounds*,

CRS Press LLC.

19. Khelifa, F., Ershov, S., Habibi, Y., Snyders, R., and Dubois, P. (2016) Free-Radical-Induced Grafting from Plasma Polymer Surfaces. *Chem. Rev.*, **116** (6), 3975–4005.

20. Musil, J. (1986) Microwave plasma: its characteristics and applications in thin film technology. *Vacuum*, **36** (1–3), 161–169.

21. Kaiser, M., Baumgärtner, K.M., and Mattheus, A. (2012) Microwave Plasma Sources - Applications in Industry. *Contrib. to Plasma Phys.*, **52** (7), 629–635.

22. Wertheimer, M.R., and Klemberg-Sapieha, J.A. (1984) Advances in Basic and Applied Aspects of Microwave Plasma Polymerization. *Thin Solid Films*, **115**, 109–124.

23. D'Agostino, R. (1990) *Plasma Deposition, Treatment, and Etching of Polymers*, Academic Press.

24. Suzuki, H., Nakano, S., Itoh, H., Sekine, M., Hori, M., and Toyoda, H. (2015) New line plasma source excited by 2.45 GHz microwave at atmospheric pressure. *Appl. Phys. Express*, **8** (3), 036001.

25. Wertheimer, M.R., and Moisan, M. (1985) Comparison of microwave and lower frequency plasmas for thin film deposition and etching. *J. Vac. Sci. Technol. A Vacuum, Surfaces, Film.*, **3** (6), 2643–2649.

26. Khachan, J., Pigott, J.R., Brand, G.F., Falconer, I.S., and James, B.W. (1993) A simple microwave plasma source for diamond deposition. *Rev. Sci. Instrum.*, **64** (10), 2971–2973.

27. Kim, J.H., Hong, Y.C., and Uhm, H.S. (2007) Synthesis of oxide nanoparticles via microwave plasma decomposition of initial materials. *Surf. Coatings Technol.*, **201**, 5114–5120.

28. Okumura, T. (2010) Inductively coupled plasma sources and applications. *Phys. Res. Int.*, **2010** (1), 164249.

29. Herbert, P.A.F., O'Neill, L., and Jaroszýnska-Wolínska, J. (2009) Soft Plasma polymerization of gas state precursors from an atmospheric pressure corona plasma discharge. *Chem. Mater.*, **21** (19), 4401–4407.

30. Goodman, J. (1960) The Formation of Thin Polymer Films in the Gas Discharge. *J. Polym. Sci.*, **44** (144), 551–552.

31. D'Agostino, R., Favia, P., Oehr, C., and Wertheimer, M.R. (2005) Low-temperature plasma processing of materials: Past, present, and future. *Plasma Process. Polym.*, **2** (1), 7–15.

32. Thiry, D., Francq, R., Cossement, D., Guillaume, M., Cornil, J., and Snyders, R. (2014) A detailed description of the chemistry of thiol supporting plasma polymer films. *Plasma Process. Polym.*, **11** (6), 606–615.

33. Thiry, D., Pouyanne, M., Cossement, D., Hemberg, A., and Snyders, R. (2018) Surface Engineering of Bromine-Based Plasma Polymer Films: A Step toward High Thiol Density Containing Organic Coatings. *Langmuir*, **34** (26), 7655–7662.

34. Lecoq, E., Duday, D., Bulou, S., Frache, G., Hilt, F., Maurau, R., and Choquet, P. (2013) Plasma polymerization of APTEs to elaborate nitrogen containing organosilicon thin films: Influence of process parameters and discussion about the growing mechanisms. *Plasma Process. Polym.*, **10** (3), 250–261.

35. Bulou, S., Le Brizoual, L., Hugon, R., De Poucques, L., Belmahi, M., Migeon, H.N., and Bougdira, J. (2009) Characterization of a N2/CH4 microwave plasma with a solid additive Si source used for SiCN deposition. *Plasma Process. Polym.*, **6**, 576–581.

36. Bulou, S., Le Brizoual, L., Miska, P., De Poucques, L., Hugon, R., Belmahi, M., and Bougdira, J. (2011) The influence of CH4 addition on composition, structure and optical characteristics of SiCN thin films deposited in a CH4/N 2/Ar/hexamethyldisilazane microwave plasma. *Thin Solid Films*, **520** (1), 245–250.

37. Struzzi, C., Scardamaglia, M., Hemberg, A., Petaccia, L., Colomer, J.F., Snyders, R., and Bittencourt, C. (2015) Plasma fluorination of vertically aligned carbon nanotubes: Functionalization and thermal stability. *Beilstein J. Nanotechnol.*, **6**, 2263–2271.

38. Ershov, S., Khelifa, F., Druart, M.E., Habibi, Y., Olivier, M.G., Snyders, R., and Dubois, P. (2015) Free radical-induced grafting from plasma polymers for the synthesis of thin barrier coatings. *RSC Adv.*, **5** (19), 14256–14265.

39. Shing, Y.H., Pool, F.S., and Rich, D.H. (1992) Low-pressure microwave plasma nucleation and deposition of diamond films. *Thin Solid Films*, **212** (1–2), 150–155.

40. Bulou, S., Lecoq, E., Loyer, F., Frache, G., Fouquet, T., Gueye, M., Belmonte, T., and Choquet, P. (2019) Study of a pulsed post-discharge plasma deposition process of APTES: synthesis of highly organic pp-APTES thin films with NH 2 functionalized polysilsesquioxane evidences. *Plasma Process. Polym.*, **16** (4), e1800177.

41. Kobayashi, H., Shen, M., and Bell, A.T. (1974) Effects Of Reaction Conditions On The Plasma Polymerization Of Ethylene. *J. Macromol. Sci. Part A - Chem.*, **8** (2), 373–391.

42. Kobayashi, H., Bell, A.T., and Shen, M. (1976) Effects of Monomer Flow Rate, Flow Configuration, and Reactor Geometry on the Rate of Plasma Polymerization. *J. Macromol. Sci. Part A - Chem.*, **10** (3), 491–500.

43. Oehr, C., Müller, M., Elkin, B., Hegemann, D., and Vohrer, U. (1999) Plasma grafting - A method to obtain monofunctional surfaces. *Surf. Coatings Technol.*, **116**–**119**, 25–35.

44. Hegemann, D., Indutnyi, I., Zajíčková, L., Makhneva, E., Farka, Z., Ushenin, Y., and Vandenbossche, M. (2018) Stable, nanometer-thick oxygen-containing plasma polymer films suited for enhanced biosensing. *Plasma Process. Polym.*, **15** (11), e1800090.

45. Vandenbossche, M., Gunkel-Grabole, G., Car, A., Bernard, L., Rupper, P., Maniura-Weber, K., Heuberger, M., Faccio, G., and Hegemann, D. (2018) Near-Surface Structure of Plasma Polymer Films Affects Surface Behavior in Water and its Interaction with Proteins. *Plasma Chem. Plasma Process.*, **38** (4), 851–870.

46. Vandenbossche, M., Dorst, J., Amberg, M., Schütz, U., Rupper, P., Heuberger, M., and Hegemann, D. (2018) Functionality and chemical stability of plasma polymer films

exhibiting a vertical cross-linking gradient in their subsurface. *Polym. Degrad. Stab.*, **156**, 259–268.

47. Savoji, H., Hadjizadeh, A., Maire, M., Ajji, A., Wertheimer, M.R., and Lerouge, S. (2014) Electrospun nanofiber scaffolds and plasma polymerization: A promising combination towards complete, stable endothelial lining for vascular grafts. *Macromol. Biosci.*, **14** (8), 1084–1095.

48. Bardon, J., Apaydin, K., Laachachi, A., Jimenez, M., Fouquet, T., Hilt, F., Bourbigot, S., and Ruch, D. (2015) Characterization of a plasma polymer coating from an organophosphorus silane deposited at atmospheric pressure for fire-retardant purposes. *Prog. Org. Coatings*, **88**, 39–47.

49. Hilt, F., Gherardi, N., Duday, D., Berné, A., and Choquet, P. (2016) Efficient Flame Retardant Thin Films Synthesized by Atmospheric Pressure PECVD through the High Co-deposition Rate of Hexamethyldisiloxane and Triethylphosphate on Polycarbonate and Polyamide-6 Substrates. *ACS Appl. Mater. Interfaces*, **8** (19), 12422–12433.

50. Klages, C., Katrin, H., and Kl, N. (2000) Surface Functionalization at Atmospheric Pressure by DBD-Based Pulsed Plasma Polymerization 1. *Plasmas Polym.*, **5** (2), 79–89.

51. Maurau, R., Boscher, N.D., Guillot, J., and Choquet, P. (2012) Nitrogen introduction in pp-HMDSO thin films deposited by atmospheric pressure dielectric barrier discharge: An XPS study. *Plasma Process. Polym.*, **9** (3), 316–323.

52. Manakhov, A., Moreno-Couranjou, M., Choquet, P., Boscher, N.D., and Pireaux, J.J. (2011) Diene functionalisation of atmospheric plasma copolymer thin films. *Surf. Coatings Technol.*, **205**, S466–S469.

53. Camporeale, G., Moreno-Couranjou, M., Bonot, S., Mauchauffé, R., Boscher, N.D., Bebrone, C., Van de Weerdt, C., Cauchie, H.M., Favia, P., and Choquet, P. (2015) Atmospheric-Pressure Plasma Deposited Epoxy-Rich Thin Films as Platforms for Biomolecule Immobilization-Application for Anti-Biofouling and Xenobiotic-Degrading Surfaces. *Plasma Process. Polym.*, 1–12.

54. Mauchauffé, R., Moreno-Couranjou, M., Boscher, N.D., Van De Weerdt, C., Duwez, A.-S., and Choquet, P. (2014) Robust bio-inspired antibacterial surfaces based on the covalent binding of peptides on functional atmospheric plasma thin films. *J. Mater. Chem. B*, **2** (32), 5168.

55. Mauchauffé, R., Bonot, S., Moreno-Couranjou, M., Detrembleur, C., Boscher, N.D., Van De Weerdt, C., Duwez, A.S., and Choquet, P. (2016) Fast Atmospheric Plasma Deposition of Bio-Inspired Catechol/Quinone-Rich Nanolayers to Immobilize NDM-1 Enzymes for Water Treatment. *Adv. Mater. Interfaces*, **3** (8), 1500520.

56. Mauchauffé, R., Moreno-Couranjou, M., Boscher, N.D., Duwez, A.S., and Choquet, P. (2016) Liquid-Assisted Plasma-Enhanced Chemical Vapor Deposition of Catechol and Quinone-Functionalized Coatings: Insights into the Surface Chemistry and Morphology. *Plasma Process. Polym.*, **13** (8), 843–856.

57. Moreno-Couranjou, M., Mauchauffé, R., Bonot, S., Detrembleur, C., and Choquet, P. (2018) Anti-biofouling and antibacterial surfaces: Via a multicomponent coating

deposited from an up-scalable atmospheric-pressure plasma-assisted CVD process. *J. Mater. Chem. B*, **6** (4), 614–623.

58. Yasuda, H., and Hirotsu, T. (1978) Distribution of polymer deposition in plasma polymerization. I. Acetylene, Ethylene, and the effect of carrier gas. *J. Polym. Sci. Polym. Chem. Ed.*, **16** (2), 313–326.

59. Yasuda, H., and Hirotsu, T. (1978) Distribution of polymer deposition in plasma polymerization. II. Effect of reactor design. *J. Polym. Sci. Polym. Chem. Ed.*, **16** (2), 313–326.

60. Yasuda, H., and Hirotsu, T. (1978) Distribution of polymer deposition in plasma polymerization. III. Effect of discharge power. *J. Polym. Sci. Polym. Chem. Ed.*, **16** (2), 313–326.

61. Kobayashi, H., Bell, A.T., and Shen, M. (1974) Plasma Polymerization of Saturated and Unsaturated Hydrocarbons. *Macromolecules*, **7** (3), 277–283.

62. Tibbitt, J.M., Jensen, R., Bell, A.T., and Shen, M. (1977) A Model for the Kinetics of Plasma Polymerization. *Macromolecules*, **10** (3), 647–653.

63. Yasuda, H., and Lamaze, C.E. (1973) Polymerization in an electrodeless glow discharge. III. Organic compounds without olefinic doublebond. *J. Appl. Polym. Sci.*, **17** (5), 1533–1544.

64. Becker, H. (1923) *Wissenschaftliche Veröffentlichungen aus dem Siemens-Konzern*, Springer.

65. Hegemann, D., Oehr, C., and Fischer, A. (2005) Design of functional coatings. *J. Vac. Sci. Technol. A Vacuum, Surfaces, Film.*, **23** (1), 5–11.

66. Hegemann, D., Hossain, M.M., Körner, E., and Balazs, D.J. (2007) Macroscopic description of plasma polymerization. *Plasma Process. Polym.*, **4** (3), 229–238.

67. Hegemann, D., Körner, E., and Guimond, S. (2009) Plasma polymerization of acrylic acid revisited. *Plasma Process. Polym.*, **6** (4), 246–254.

68. Sharma, A.K., and Yasuda, H. (1983) Plasma Polymerization of Tetramethyldisiloxane by a Magnetron Glow Discharge. *Thin Solid Films*, **110**, 171–184.

69. Scheltjens, G., Da Ponte, G., Paulussen, S., De Graeve, I., Terryn, H., Reniers, F., Van Assche, G., and Van Mele, B. (2016) Deposition Kinetics and Thermal Properties of Atmospheric Plasma Deposited Methacrylate-Like Films. *Plasma Process. Polym.*, **13** (5), 521–533.

70. Scheltjens, G., Van Assche, G., and Van Mele, B. (2016) Effect of Substrate Temperature on Thermal Properties and Deposition Kinetics of Atmospheric Plasma Deposited Methyl(methacrylate) Films. *Plasma Process. Polym.*, **14** (3), 1500213.

71. Watson, S., Nisol, B., Lerouge, S., and Wertheimer, M.R. (2015) Energetics of Molecular Excitation, Fragmentation, and Polymerization in a Dielectric Barrier Discharge with Argon Carrier Gas. *Langmuir*, **31** (37), 10125–10129.

72. Nisol, B., Gagnon, H., Lerouge, S., and Wertheimer, M.R. (2016) Energy of Reactions

in Atmospheric-Pressure Plasma Polymerization with Inert Carrier Gas. *Plasma Process. Polym.*, **13** (3), 366–374.

73. Nisol, B., Watson, S., Lerouge, S., and Wertheimer, M.R. (2016) Energetics of reactions in a dielectric barrier discharge with argon carrier gas: III Esters. *Plasma Process. Polym.*, **13** (10), 965–969.

74. Nisol, B., Watson, S., Lerouge, S., and Wertheimer, M.R. (2016) Energetics of Reactions in a Dielectric Barrier Discharge with Argon Carrier Gas: II Mixtures with Different Molecules. *Plasma Process. Polym.*, **13** (5), 557–564.

75. Nisol, B., Watson, S., Lerouge, S., and Wertheimer, M.R. (2017) Energetics of reactions in a dielectric barrier discharge with argon carrier gas: V hydrocarbons. *Plasma Process. Polym.*, **14** (8), 1600191.

76. Nisol, B., Watson, S., Meunier, A., Juncker, D., Lerouge, S., and Wertheimer, M.R. (2018) Energetics of reactions in a dielectric barrier discharge with argon carrier gas: VI PEG-like coatings. *Plasma Process. Polym.*, **15** (3), 1–10.

77. Mertens, J., Watson, S., Nisol, B., Wertheimer, M.R., and Reniers, F. (2019) Energetics of reactions in a dielectric barrier discharge with argon carrier gas: VII anhydrides. *Plasma Process. Polym.*, **16** (5), 1–7.

78. Kakaroglou, A., Scheltjens, G., Nisol, B., De Graeve, I., Van Assche, G., Van Mele, B., Willem, R., Biesemans, M., Reniers, F., and Terryn, H. (2012) Deposition and characterisation of plasma polymerised allyl methacrylate based coatings. *Plasma Process. Polym.*, **9** (8), 799–807.

79. Batan, A., Nisol, B., Kakaroglou, A., De Graeve, I., Van Assche, G., Van Mele, B., Terryn, H., and Reniers, F. (2013) The impact of double bonds in the APPECVD of acrylate-like precursors. *Plasma Process. Polym.*, **10** (10), 857–863.

80. Mertens, J., Baneton, J., Ozkan, A., Pospisilova, E., Nysten, B., Delcorte, A., and Reniers, F. (2019) Atmospheric pressure plasma polymerization of organics: effect of the presence and position of double bonds on polymerization mechanisms, plasma stability and coating chemistry. *Thin Solid Films*, **671**, 64–76.

81. Nisol, B., Arnoult, G., Bieber, T., Kakaroglou, A., De Graeve, I., Van Assche, G., Terryn, H., and Reniers, F. (2014) About the influence of double bonds in the APPECVD of acrylate-like precursors: A mass spectrometry study of the plasma phase. *Plasma Process. Polym.*, **11** (4), 335–344.

82. Di Meo, S., Reed, T.T., Venditti, P., and Victor, V.M. (2016) Role of ROS and RNS Sources in Physiological and Pathological Conditions. *Oxid. Med. Cell. Longev.*, **2016**, 1245049.

83. Fang, Z., Shao, T., Wang, R., Yang, J., and Zhang, C. (2016) Influences of oxygen content on characteristics of atmospheric pressure dielectric barrier discharge in argon/oxygen mixtures. *Eur. Phys. J. D*, **70**, https://doi.org/10.1140/epjd/e2016-60438-9.

84. Dvořák, P., Mrkvičková, M., Obrusník, A., Kratzer, J., Dědina, J., and Procházka, V. (2017) Fluorescence measurement of atomic oxygen concentration in a dielectric

barrier discharge. *Plasma Sources Sci. Technol.*, **26** (6), 065020.

85. Reuter, S., Niemi, K., Schulz-Von Der Gathen, V., and Döbele, H.F. (2009) Generation of atomic oxygen in the effluent of an atmospheric pressure plasma jet. *Plasma Sources Sci. Technol.*, **18** (1), 015006.

86. Kontziampasis, D., Constantoudis, V., and Gogolides, E. (2012) Plasma directed organization of nanodots on polymers: Effects of polymer type and etching time on morphology and order. *Plasma Process. Polym.*, **9** (9), 866–872.

87. Phan, L.T., Yoon, S.M., and Moon, M.W. (2017) Plasma-based nanostructuring of polymers: A review. *Polymers (Basel).*, **9** (9), 417–441.

88. Boscher, N.D., Vaché, V., Carminati, P., Grysan, P., and Choquet, P. (2014) A simple and scalable approach towards the preparation of superhydrophobic surfaces – importance of the surface roughness skewness. *J. Mater. Chem. A*, **2** (16), 5744.

89. Odian, G. (2013) *Principles of Polymerization*, Wiley-VCH.

90. Dams, R., Vangeneugden, D., and Vanderzande, D. (2006) Plasma deposition of thiophene derivatives under atmospheric pressure. *Chem. Vap. Depos.*, **12** (12), 719–727.

91. Liu, C., Goeckner, M.J., and Walker, A. V. (2017) Plasma polymerization of poly(3,4-ethylenedioxyethene) films: The influence of plasma gas phase chemistry. *J. Vac. Sci. Technol. A Vacuum, Surfaces, Film.*, **35** (2), 21302.

92. D'Agostino, R., Favia, P., Förch, R., Oehr, C., and Wertheimer, M.R. (2010) Editorial: Views on macroscopic kinetics of plasma polymerisation. *Plasma Process. Polym.*, **7** (5), 363–364.

93. Gleason, K.K. (2015) *CVD Polymers Fabrication of Organic Surfaces and Devices*, Wiley-VCH.

94. Wang, M., Wang, X., Moni, P., Liu, A., Kim, D.H., Jo, W.J., Sojoudi, H., and Gleason, K.K. (2017) CVD Polymers for Devices and Device Fabrication. *Adv. Mater.*, **29** (11).

95. Atkins, P. (2006) *Physical chemistry*, Oxford University Press.

96. Soroush, M. (2019) *Computational Quantum Chemistry*, Elsevier Inc.

97. Dorval Dion, C.A., and Tavares, J.R. (2013) Photo-initiated chemical vapor deposition as a scalable particle functionalization technology (a practical review). *Powder Technol.*, **239**, 484–491.

98. Shi, K., Liu, Z., Yang, C., Li, X.Y., Sun, Y.M., Deng, Y., Wang, W., Ju, X.J., Xie, R., and Chu, L.Y. (2017) Novel Biocompatible Thermoresponsive Poly(N-vinyl Caprolactam)/Clay Nanocomposite Hydrogels with Macroporous Structure and Improved Mechanical Characteristics. *ACS Appl. Mater. Interfaces*, **9** (26), 21979–21990.

99. Chen, N., Kim, D.H., Kovacik, P., Sojoudi, H., Wang, M., and Gleason, K.K. (2016) Polymer Thin Films and Surface Modification by Chemical Vapor Deposition : Recent Progress. (iCVD).

100. Chan, K., and Gleason, K.K. (2005) Photoinitiated chemical vapor deposition of polymeric thin films using a volatile photoinitiator. *Langmuir*, **21** (25), 11773–11779.

101. McMahon, B.J., Pfluger, C.A., Sun, B., Ziemer, K.S., Burkey, D.D., and Carrier, R.L. (2014) Photoinitiated chemical vapor deposition of cytocompatible poly(2-hydroxyethyl methacrylate) films. *J. Biomed. Mater. Res. - Part A*, **102** (7), 2375–2382.

102. Baxamusa, S.H., Montero, L., Dubach, J.M., Clark, H.A., Borros, S., and Gleason, K.K. (2008) Protection of sensors for biological applications by photoinitiated chemical vapor deposition of hydrogel thin films. *Biomacromolecules*, **9** (10), 2857–2862.

103. Lau, K.K.S., and Gleason, K.K. (2006) Initiated Chemical Vapor Deposition (iCVD) of Poly(alkyl acrylates): A Kinetic Model. *Macromolecules*, **39** (10), 3695–3703.

104. Lau, K.K.S., and Gleason, K.K. (2006) Initiated chemical vapor deposition (iCVD) of poly(alkyl acrylates): An experimental study. *Macromolecules*, **39** (iCVD), 3688–3694.

105. Bengasi, G., Baba, K., Frache, G., Desport, J., Gratia, P., Heinze, K., and Boscher, N.D. (2019) Conductive Fused Porphyrin Tapes on Sensitive Substrates by a Chemical Vapor Deposition Approach. *Angew. Chemie - Int. Ed.*, **131** (7), 2125–2130.

106. Smolin, Y.Y., Soroush, M., and Lau, K.K.S. (2017) Oxidative chemical vapor deposition of polyaniline thin films. *Beilstein J. Nanotechnol.*, **8** (1), 1266–1276.

107. Smolin, Y.Y., Soroush, M., and Lau, K.K.S. (2017) Influence of oCVD Polyaniline Film Chemistry in Carbon-Based Supercapacitors. *Ind. Eng. Chem. Res.*, **56** (21), 6221–6228.

108. Bengasi, G., Baba, K., Back, O., Frache, G., Heinze, K., and Boscher, N.D. (2019) Reactivity of Nickel(II) Porphyrins in oCVD Processes – Polymerisation, Intramolecular Cyclisation and Chlorination. *Chem. – A Eur. J.*, https://doi.org/10.1002/chem.201900793.

109. Baba, K., Bengasi, G., El Assad, D., Grysan, P., Lentzen, E., Heinze, K., Frache, G., and Boscher, N.D. (2019) Conductive Directly Fused Poly(Porphyrin) Coatings by Oxidative Chemical Vapour Deposition – From Single- to Triple-Fused. *European J. Org. Chem.*, **2019** (13), 2368–2375.

110. Mezhuev, Y.O., Korshak, Y. V, and Shtilman, M.I. (2017) Oxidative polymerization of aromatic amines: kinetic features and possible mechanisms. *Russ. Chem. Rev.*, **86** (12), 1271–1285.

111. Nejati, S., and Lau, K.K.S. (2011) Chemical vapor deposition synthesis of tunable unsubstituted polythiophene. *Langmuir*, **27** (24), 15223–15229.

112. Lock, J.P., Im, S.G., and Gleason, K.K. (2006) Oxidative chemical vapor deposition of conducting poly (3,4-ethylenedioxy-thiophene) films. *Macromolecules*, **39**, 5326–5329.

113. Ho, P.K.H., Kim, J., Burroughes, J.H., Becker, H., Li, S.F.Y., Brown, T.M., Cacialli, F., and Friend, R.H. (2000) Molecular-scale interface engineering for polymer light-emitting diodes. *Nature*, **404**, 481–484.

114. Im, S.G., Gleason, K.K., and Olivetti, E.A. (2007) Doping level and work function control in oxidative chemical vapor deposited poly (3,4-ethylenedioxythiophene). *Appl. Phys.*

Lett., **90** (15), 88–91.

115. Stepanyan, S.A., Soloviev, V.R., and Starikovskaia, S.M. (2014) An electric field in nanosecond surface dielectric barrier discharge at different polarities of the high voltage pulse: Spectroscopy measurements and numerical modeling. *J. Phys. D. Appl. Phys.*, **47** (48), 485201.

116. Zhu, Y., Shcherbanev, S., Baron, B., and Starikovskaia, S. (2017) Nanosecond Surface Dielectric Barrier Discharge (nSDBD) in Atmospheric Pressure Air: I. Measurements and 2D modeling of Morphology, Propagation and Hydrodynamic Perturbations. *Plasma Sources Sci. Technol.*, **26**, 125004.

117. Boscher, N.D., Hilt, F., Duday, D., Frache, G., Fouquet, T., and Choquet, P. (2015) Atmospheric pressure plasma initiated chemical vapor deposition using ultra-short square pulse dielectric barrier discharge. *Plasma Process. Polym.*, **12** (1), 66–74.

118. Bonot, S., Mauchauffé, R., Boscher, N.D., Moreno-Couranjou, M., Cauchie, H.M., and Choquet, P. (2015) Self-Defensive Coating for Antibiotics Degradation - Atmospheric Pressure Chemical Vapor Deposition of Functional and Conformal Coatings for the Immobilization of Enzymes. *Adv. Mater. Interfaces*, **2** (14), 1500253.

119. Hilt, F., Boscher, N.D., Duday, D., Desbenoit, N., Levalois-Grützmacher, J., and Choquet, P. (2014) Atmospheric pressure plasma-initiated chemical vapor deposition (AP-PiCVD) of poly(diethylallylphosphate) coating: A char-forming protective coating for cellulosic textile. *ACS Appl. Mater. Interfaces*, **6** (21), 18418–18422.

CHAPTER II – Experimental processes and analyses

This chapter aims at providing all the necessary information about the experimental and analytical procedures used in this thesis. The specific data treatments and calculations developed where needed are described in details.

Content

1. AP-DBD Reactor

1.1. AP-DBD Reactors and Electrodes

All the plasma-enhanced chemical vapor deposition experiments described in this PhD thesis were performed at atmospheric-pressure in dielectric barrier discharge (DBD) configuration (Figure 2.1a). As mentioned in Chapter 1, AP-DBDs allow the generation of non-thermal discharges within the whole electrode's volume, allowing the coating of large surfaces.

The AP-DBD system, purchased from Fraunhofer IST (Braunschweig, Germany), is composed of two 15 mm wide and 300 mm long high-voltage electrodes, in red in Figure 2.1b. The carrier gas (*i.e.* argon) and the monomer pass through a 0.5 mm wide and 300 mm long slit located in between the 2 high-voltage electrodes, allowing a homogeneous and laminar supply in the discharge volume. On each outer sides of the high-voltage electrodes, two argon curtains are created through 0.5 mm wide and 300 mm long slits to passivate the atmosphere.

The bottom electrode, where the substrates to be coated are secured by Kapton tape, is a grounded stainless-steel table set to move back and forth at a speed of 1 $mm \cdot s^{-1}$. The discharge gap (*i.e.* distance between the high-voltage electrodes and the substrates) is fixed at 1 mm for all the deposition experiments.

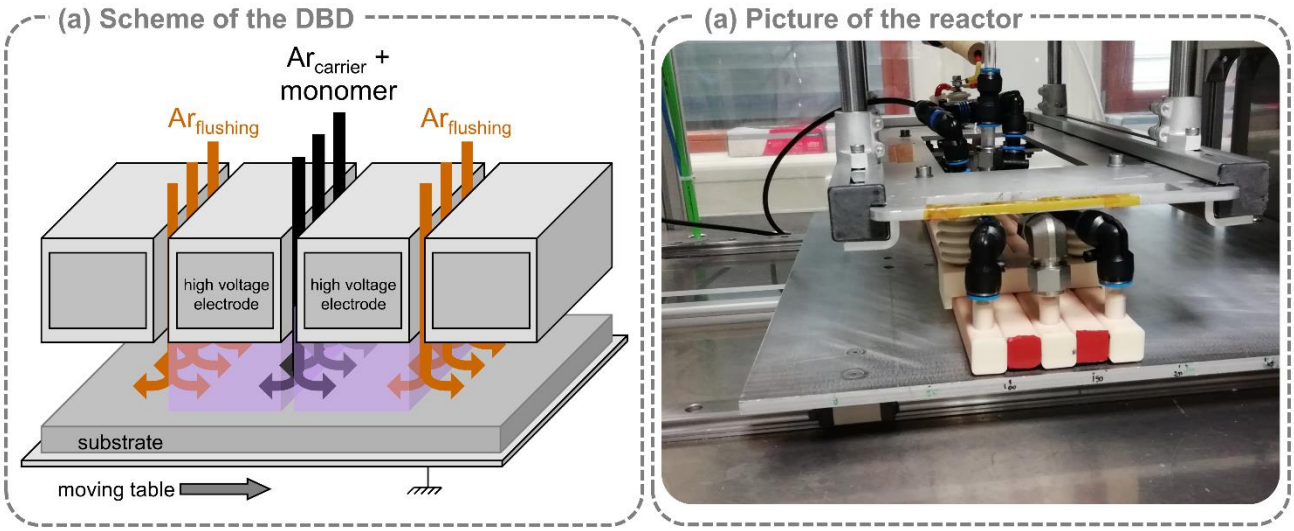

Figure 2.1. (a) Schematic representation and (b) photograph of the AP-DBD reactor.

1.2. High-voltage source

The atmospheric-pressure plasma-initiated chemical vapor deposition (AP-PiCVD) of polymer layers relies on the use of high-voltage square-wave pulses produces by one of the two generators acquired from the Effitech society (Gif-sur-Yvette, France, www.effitech.fr): EFFITECH1 (Figure 2.2a) and EFFITECH2 (Figure 2.2b). The high-voltage square-wave pulses produce two distinct current discharges (ca. 100 ns) at the voltage rising and falling edges. The duration and repetition frequency of the high voltage square-wave pulses determined the length of the plasma off-times.

Figure 2.2. Picture of the (a) AHTPB10F (called EFFITECH1) and (b) AHTPB20F (called EFFITECH2) generators.

1.2.1. Electric properties of the discharge

Both the high-voltage square-wave pulses and the current discharges were investigated using a Teledyne Lecroy HDO4054A oscilloscope, together with a Teledyne Lecroy PPE 20 kV high-voltage probe directly connected at the Effitech generators' exit and a Teledyne Lecroy CP030 current probe connected on the grounded electrode, respectively. A 1 cm thick glass plate covered by grounded aluminum tape was used as the bottom electrode for the current measurements, in order to collect all the electrons reaching its surface and avoid their dissipation in the reactor.

Both generators allow the production of perfectly reproducible ultrashort plasma discharges with a fixed on-time and adaptable pulse-times and off-times (Figure 2.3a). The ultrashort on-time discharge (*ca.* t_{on} = 100 ns) is selected to lower the exposure time of the molecules to the plasma discharge, effectively lowering the fragmentation by several orders compared to classical PECVD generators (*i.e.* AC or AC-pulsed). The off-time is entirely tunable, allowing frequencies of discharge from 1 Hz (*i.e.* t_{off} = 1 s) up to 10,000 Hz (*i.e.* t_{off} = 100 µs). Two approaches based on different high-voltage square-wave pulses are used in this work, either fixed to 15 µs or set equal to the desired plasma off-time.

The first electrical excitation mode (short high-voltage pulses) (Figure 2.3b) involves 15 µs high-voltage square-wave pulses producing two distinct current discharges (ca. 100 ns) at the voltage rising and falling edges. The high-voltage square-wave pulse duration was set to 15 µs to produce reproducible and stable current discharges in the range of frequencies studied, *i.e.* from 10 Hz to 10,000 Hz. Therefore, the short pulses methods imply a double discharge for each high voltage pulse with an innate frequency of 66,667 Hz. In order to simplify the descriptions of the effect of the off-time, the double nano-discharges during each pulse are considered as a single discharge in this work. This electrical excitation mode was applied for the synthesis of the compounds described in the Chapters 3 to 5.

The second method (long high-voltage pulses) (Figure 2.3c) set a different duration of the high-voltage square-wave pulses in function of the frequency applied in order to match the plasma off-time. Since there are no current discharge when capacitive electrodes are saturated, the duration of the high-voltage square-wave pulse is equivalent to the off-time, reducing the plasma occurrence to a single plasma discharge per cycle ($t_{on} + t_{off/pulse}$). This approach withdraws the drawback of the double plasma discharges when using 15 µs high-voltage square-wave pulses. However, further investigations are still required to understand the effect of a permanent electric field on the plasma properties. This approach was applied for the synthesis of the compounds described in the Chapter 6.

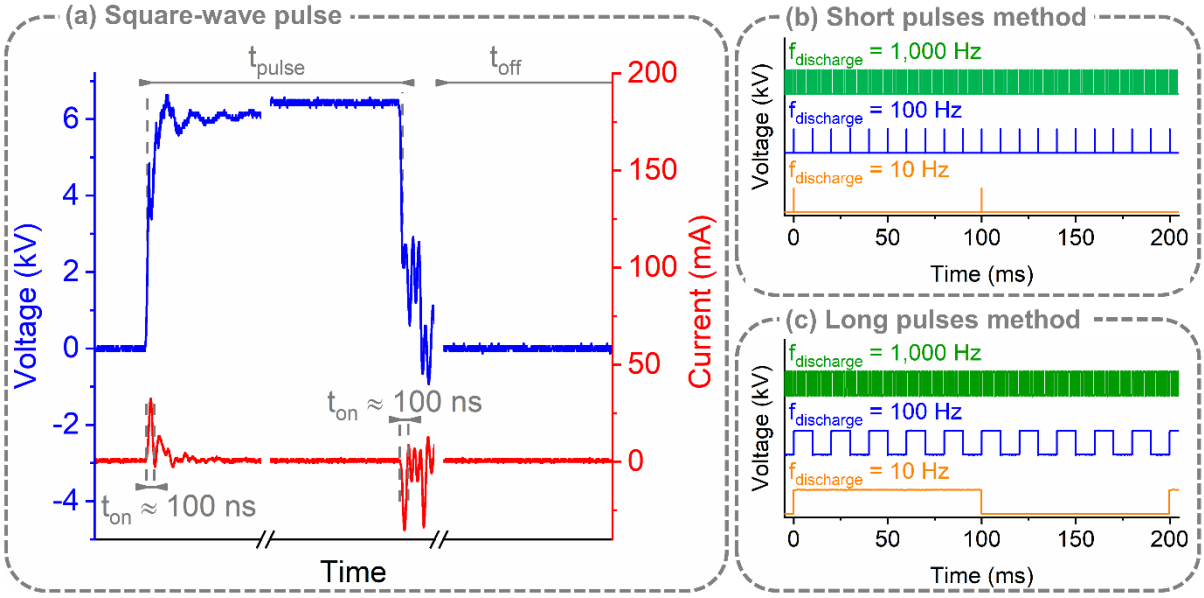

Figure 2.3. (a) Traces of the high-voltage square-wave pulse and current discharges. (b) Voltage trace for the short high-voltage pulses method for different frequencies. (c) Voltage trace of the long high-voltage pulses method for different frequencies.

1.2.2. Reproducibility and independence of the discharges

For all experiments reported in this work, no heating of the substrate or the electrodes was observed, with the only exception at 10,000 Hz when this frequency is maintained for a long time. To avoid a possible heating of the system, all the deposition performed above 3,160 Hz were performed with a resting time of 5 min after each pass.

Variations of the vibrational and rotational electron temperature were monitored for discharge frequencies between 10 Hz and 1,000 Hz by time-continuous optical emission spectroscopy (TC-OES) using a Princeton Instruments Acton SP2500i. Unfortunately, OES measurements

require to maintain the plasma on for a long time, making measurement for the 10,000 Hz frequency impossible without possibly damaging the electrode. No increase of the vibrational (Figure 2.4a) and rotational (Figure 2.4b) electron temperatures were observed for the investigated frequencies, as the Ar and OH emissions remain almost perfectly identical for all the investigated frequencies. Since the traces of the high voltage square-wave pulses and the current discharges do not change with the frequency either, the electronic density is expected to not increase significantly in the range of frequency studied. Therefore, the high voltage square-wave pulses investigated allow the production of electrically and chemically independent AP-DBD discharges.

In order to check for re-initiations of the plasma following to the current discharges, the argon species activated from the plasma discharge were monitored by time-resolved optical emission spectroscopy (TR-OES) using a Princeton Instruments Acton SP2750 spectrometer equipped with a Pi-Max 3 i-CCD and a grating of 150 lines·mm^{-1} blazed at 300 nm. The lifetime of the argon species matches with the current discharge's measurement, showing an initiation and deactivation of the argon excited species in the order of a hundred of nanoseconds at voltage rising and falling edges (Figure 2.4c).

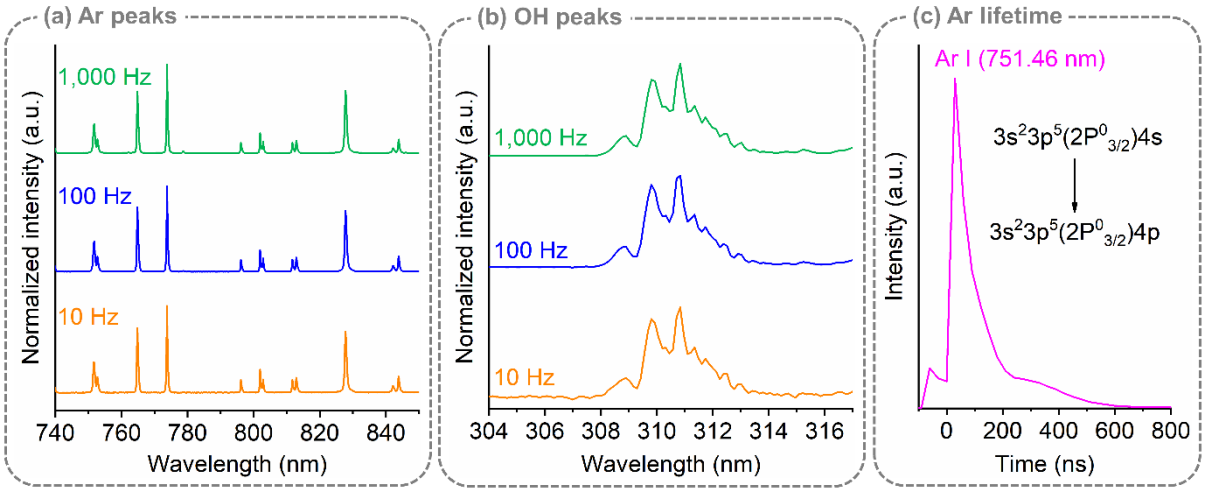

Figure 2.4. TC-OES measurements performed in open atmosphere with argon, zoomed in the range of (a) the Ar peak emissions between 740 and 850 nm and of (b) the OH emissions between 304 and 316 nm. (c) TR-OES measurements of the Ar I line at 751.46 nm's lifetime with a 30 ns gate species detected in a pure argon plasma discharge.

1.3. Injection systems

Almost all the monomers investigated in this work were injected as vapors using a double bubbler system to prevent a drawback of the monomer (Figure 2.5).

The gases flows were fixed using MKS gas flow-meters in the required range (*i.e.* from 1 to 20 SLM) and an MKS gas flow controller.

Argon (Air Liquid, 99.999%) was used as a carrier and process gas for all experiments. The flow of carrier gas $F_{carrier}$ in the bubbler was determined considering the vapor pressure of the monomers.

The total gas flow of argon was set to either 20 SLM or 30 SLM based on the electrodes' surfaces (*i.e.* 15 x 300 mm²) and the discharge gap (*i.e.* 1 mm) by adding an additional flux

of argon $F_{process}$, yielding residency times of the injected species of 13 ms and 9 ms, respectively.

In Chapter 6, the NVCL monomer was melted in a heated bubbler up to 50°C using a hot water bath, while the injection lines were heated up to 60°C using Watlow "stretch-to-length" heaters alimented by a Watlow temperature controller. A second bubbler system in parallel was used to inject both comonomers into the discharge.

The only exception to gas phase injection presented in this work is the EDOT in Chapter 4 from the study by Abessolo et al., which used nebulizers to spray liquid layers. In this case, the Ar/O_2 process flow composed the 20 SLM. However, the experimental synthesis was not done by the author and will not be detailed.

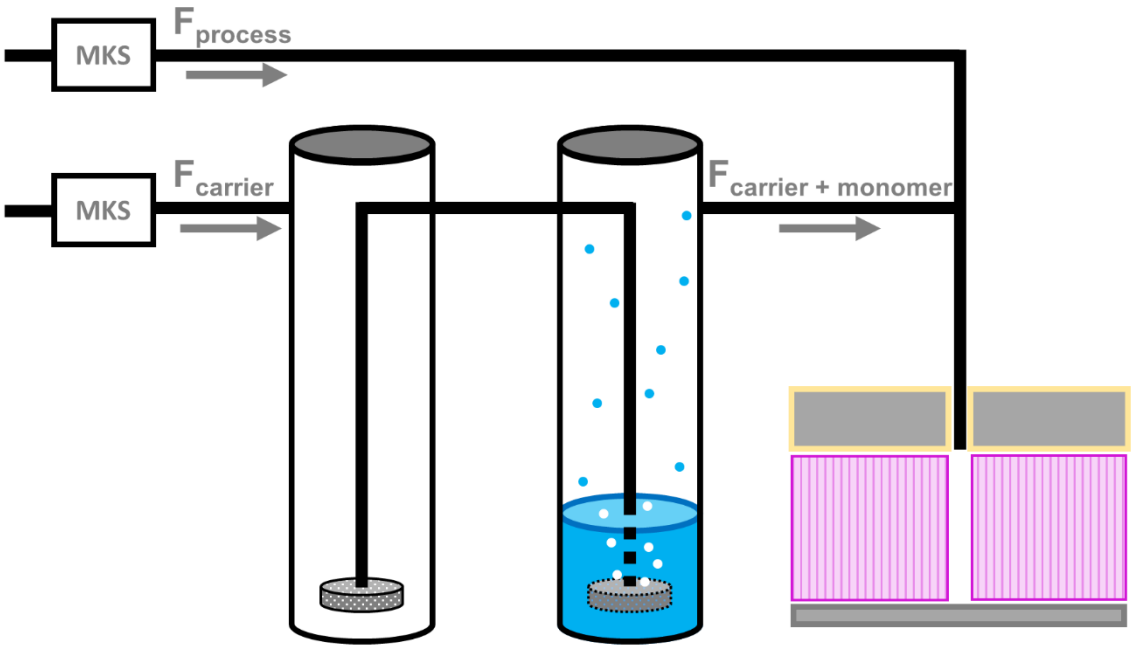

Figure 2.5. Scheme of the bubbler injection system.

1.4. Monomers

The monomers were purchased from Sigma Aldrich and used without purification step. Methyl methacrylate (MMA, 99%), butyl methacrylate (BMA, 99%) and glycidyl methacrylate (GMA, 97%) are studied in Chapters 3 to 5, while n-vinyl caprolactam (NVCL, 98%) and ethylene glycol dimethacrylate (EGDMA, 98%) in Chapter 6. The properties of the monomers used in this work and their chemistry are summed up in Table 2.1.

The conventionally polymerized references for pMMA and pGMA were bought from Sigma Aldrich, pBMA from Polymer Source. Conventional pNVCL was synthesized by Prof. Alexander Shaplov from LIST.

Table 2.1. Properties of the monomers, namely: M the molar weight, $k_{p,20°C}$ and $k_{p,50°C}$ the propagation constant at 20°C and 50°C, P_{sat} the vapour pressure, ρ_{mono} the liquid density and ρ_{vap} the vapour density.

	Chemistry	M g·mol^{-1}	$k_{p,20°C}$ L·mol^{-1}·s^{-1}	$k_{p,50°C}$ L·mol^{-1}·s^{-1}	P_{sat} Torr	ρ_{mono} kg·L^{-1}	ρ_{vap} g·L^{-1}
MMA	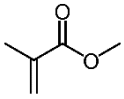	100.121	274	642	29	0.95	4.46
BMA	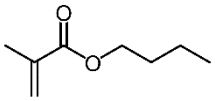	142.196	-	753	2	0.89	-
GMA	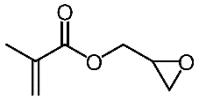	142.155	494	1220	0.3	1.08	6.25
NVCL	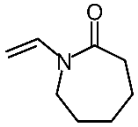	139.190	-	-	0.36*	1.03	-
EGDMA	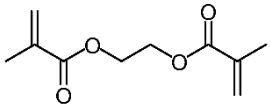	198.220	-	-	0.19	1.05	-

* Value obtained at 50°C.

1.5. Substrates

All depositions were carried on polished 4 in. silicon wafers (Siltronix, Archamps, France). Prior to each experiment they were cleaned using a 95%/5% argon/oxygen plasma for 40 s at a discharge frequency of 1,000 Hz.

2. Chemical analyses

2.1. Fourier transform infrared spectroscopy

2.1.1. Method

Fourier transform infrared (FTIR) transmission measurements were performed on a Bruker Vertex 70 spectrometer (Ettlingen, Germany) equipped with a MCT detector. The spectra are acquired after a 5 min purge in nitrogen, they average 150 scans obtained with a readout frequency of 5 kHz and a spectral resolution of 4 cm^{-1}.

The substrates were double polished silicon wafers to avoid a loss of signal intensity due to scattering effects in transmission mode.

2.1.2. Peaks analysis

FTIR transmission measurements give insight on the chemistry of the whole thin film bulk, as the infrared light is absorbed at a specific wavenumber (*i.e.* energy) by the moieties composing the molecule. Therefore, the obtained spectra is a fingerprint of the thin film's chemistry.

FTIR offers crucial insight in the fragmentation and recombination mechanisms in plasmas, as a change of chemical environment of the moieties will be reflected on the spectra. In order to compare the data obtained at different discharge frequencies and from different monomers, the carbonyl peak (C═O) will be chosen for normalization due to its expected high resilience to fragmentation.

2.1.3. Chemical quantification

FTIR gives quantitative information on the concentration of molecule in the thin film and it can be used to determine the molar concentration of copolymers. Especially in transmission mode in which the laser go through the whole thin film, the concentration c can be related to the absorbance intensity A_υ following the Beer-Lambert law (eq. 2.1), with h the film's thickness and ε_υ the molar absorptivity of the vibrational band υ.

$$A_\upsilon = \varepsilon_\upsilon \times h \times c \tag{2.1}$$

The molar concentration of monomer composing a homopolymer film may be determined from its experimental data (eq. 2.2): the monomer molar weight M and the density of the plasma-polymer thin film ρ_{film}, which can be calculated from weight, thickness and surface measurements.

$$c_{homopolymer} = \frac{\rho_{film}}{M_{monomer}} \tag{2.2}$$

Therefore, the molar absorptivity can be calculated for single vibrational band (eq. 2.3), typically a carbonyl C═O.

$$\varepsilon_{\upsilon,C=O} = \frac{A_{\upsilon,C=O}}{h_{film} \times M} \tag{2.3}$$

Knowing the molar absorptivity of one specific peak for two distinct homopolymers 1 and 2 allow the quantification of their copolymer's molar composition (eq 2.4).

$$\frac{c_{homopolymer,1}}{c_{homopolymer,1} + c_{homopolymer,2}} = \left(\frac{A_{\upsilon,2}}{A_{\upsilon,1}} \times \frac{\varepsilon_{\upsilon,1}}{\varepsilon_{\upsilon,2}} + 1\right)^{-1} \tag{2.4}$$

2.2. Ultraviolet-visible

2.2.1. Method

Ultraviolet-visible (UV-vis) measurements were performed on a Tecan Infinite M1000 Pro in transmittance mode.

2.2.2. Lower critical solution temperature

The lower critical solution temperatures (LCST) of thermoresponsive polymers dissolved in milliQ water were obtained by integrating their absorption spectra over the visible range (*i.e.* 300 to 800 nm) at temperatures ranging from 18°C to 80°C.

2.3. X-ray photoelectron spectroscopy

2.3.1. Method

X-ray photoelectron spectroscopy (XPS) measurements were performed on a Kratos Axis-Ultra DLD instrument, using an Al Kα source (1486.6 eV) with a pass energy of 20 eV and an energy resolution of 0.5 eV. A flooding gun was used to reduce charging effect on the samples surface.

The data treatments were performed using CasaXPS-2315.

2.3.2. Elementary composition

The X-ray beam allow the extraction of electrons on the film's surface, which are collected and have their kinetic energy measured. Therefore, the nature of the electron give insight in the chemical composition of the film, as their kinetic energy is specific to an atom's core level (*e.g.* C 1s)

By integrating the area of one core level per detected element, a quantitative determination of the elementary composition of the film's surface is possible (taking into account the relative sensitivity factor of each element).

2.3.3. Bonding composition

The kinetic energy of an electron will also be influenced by its environment, in particular the type of bond it was involved in. Therefore, the binding energy of a C 1s bonded to a carbon will be different to a C 1s bonded to an oxygen, allowing the determination of the bonding composition by deconvoluting the elementary peak.

As for FTIR, the elementary deconvolution may give information on the real chemistry of the film. However, the different bond detected in a core level are highly overlap making the fitting difficult without databases. This is particularly the case for plasma-polymer, where the chemistry might be highly altered and several components are impossible to detect due to their overlap. Yet, if the thin film bears a chemistry close to a conventional polymer, database may be used to gain insight in its real chemistry.

2.3.4. Chemical quantification

As XPS is a quantitative method, it can also be used to quantify the composition of a copolymer.

The elementary composition may be simply used to extract their composition if one of the comonomer contains an atom that the other doesn't. It might be particularly interesting in case of alteration of the chemistry preventing a reliable fitting.

The bonding composition might be used as well, provided that the chemistry is known, to extract the copolymer's composition. The same core level (typically C 1s) of each

homopolymer grown in identical experimental condition will be fitted independently. The bonding composition of both fits can be added to copolymer spectra, fixing the fit parameters of each homopolymer (*i.e.* the FWHM, the position and the relative ratios between the peaks). The copolymer spectra can then be fitted, only allowing one peak for each homopolymer to change in area (typically C-C/C-H) and quantifying its composition.

2.4. Size exclusion chromatography

2.4.1. Method

Size exclusion chromatography (SEC) analyses were performed using a Thermo Scientific (Sunnyvale, CA) Dionex UltiMate 3000 LC system. Each measurement corresponds to the soluble fraction of the polymer in THF and is not necessarily the entire distribution. The elution times were translated into molecular weights using reference standards ranging from 162 to 364 000 g mol−1 (Agilent EasiVial PS-M).

2.4.2. Integration of the polymer length distributions

The polymeric length of the plasma-polymers deposited by AP-PiCVD were evaluated by SEC measurements, yielding the distribution in molecular weights. To describe the polymer length of the plasma-polymers composing the thin films, the distribution of molecular weights are integrated to obtain the average molar mass in number M_n (eq. 2.5) and the average molar mass in weight M_w (eq. 2.6), with N_i the number of species i with a molar mass M_i.

$$M_n = \frac{\sum M_i N_i}{\sum N_i} \tag{2.5}$$

$$M_w = \frac{\sum M_i^2 N_i}{\sum M_i N_i} \tag{2.6}$$

While the average molar masses in number and weight yield information on the polymeric growth of the thin films, they have to be considered carefully as the reference standards might not be suitable for calibration of strongly crosslinked thin films, especially at high frequencies of discharge.

2.5. High-resolution mass-spectroscopy

2.5.1. Method

Matrix-assisted laser desorption/ionization high-resolution mass-spectroscopy (MALDI-HRMS) analyses were performed using AP-MALDI PDF+ ion source from MassTech Inc. (Columbia, MA) coupled to a LTQ/Orbitrap Elite from Thermo Scientific (San Jose, CA). Dithranol diluted in THF was used as a matrix to promote desorption and ionization by the laser. 0.1 µL of matrix was spotted on the thin films to form a co-crystal with the soluble part of the film when the THF evaporates.

2.5.2. Mass peak analyses

MALDI-Orbitrap have an extremely high resolution in mass in the order of the ppm, allowing the separation of the many species arising from the fragmentation/recombination mechanisms during the plasma on-time. The high resolution in mass is counterbalanced by

the low spatial resolution (*ca.* 100 µm) and the low mass range (*i.e.* 50 – 4000 m/z), making MALDI-Orbitrap an analysis method for the determination of growth mechanisms in homogeneous samples rather than the characterization of their molecular weights.

To avoid a confusion between plasma-induced fragmentation and laser-induced fragmentation, conventional pMMA references (PDI < 1.1) with molecular masses of 500 g•mol^{-1} and 4000 g•mol^{-1}, respectively, were spin-coated and analyzed by MALDI-Orbitrap spectrometry with the laser set at its maximum intensity (Figure 2.6). Both references exhibited quite exclusively pMMA $(MMA)_n$ oligomers with sodium adducts and terminal groups R related to its initiation $[R(MMA)_nR + Na]^+$, displaying only a few well-defined side-mechanisms. These results do not match with the observations made for any of the ppMMA MALDI-HRMS spectra grown by plasma. Indeed, all spectra presented in this work display numerous strong sets of distributions in-between the oligomer units, related to a plasma-induced fragmentation occurring during the synthesis/deposition steps and not to laser-induced mechanisms.

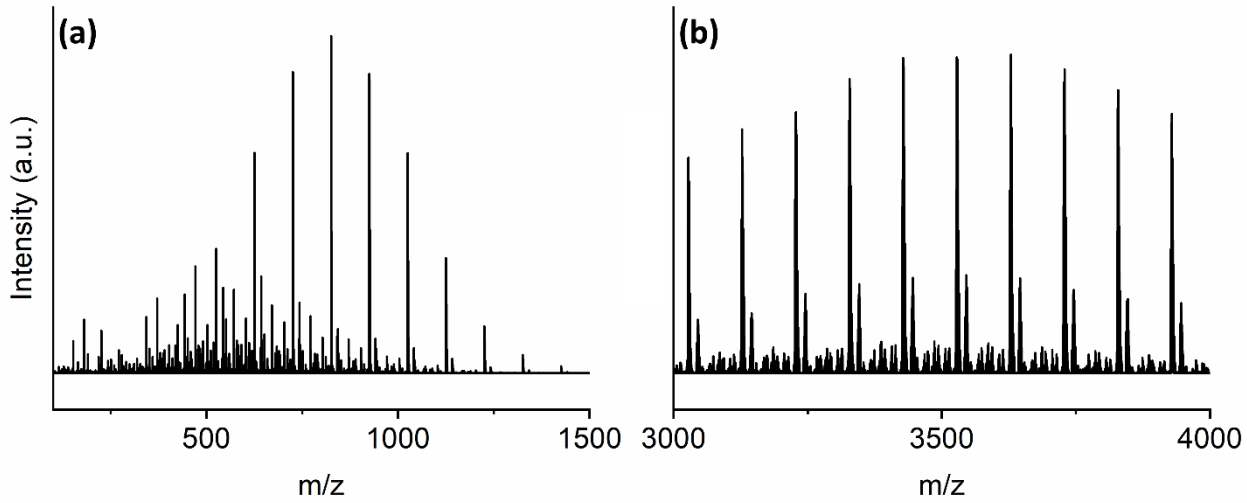

Figure 2.6. MALDI-HRMS spectra of spin-coated conventional pMMA references with molecular weights of (a) 500 g•mol-1 from Agilent in the mass range m/z = 100 − 1500 and (b) 4000 g•mol^{-1} from Sigma Aldrich in the mass range m/z = 3000−4000. The molecular weight of the pMMA 500 g•mol^{-1} from Agilent is actually observed around 800 g•mol^{-1}.

2.5.3. Mass deficiency calculations

The numerous side-species detected in the plasma-induced polymer spectra (ca. 200 – 1,000 per 100 m/z) makes the determination of growth mechanisms from solving the chemistry of the mass peak individually impossible. In order to address those spectra, the mass deficiency between the unknown mass peaks and a known reference – typically an oligomer – were calculated to look for patterns in fragmentation/recombination mechanisms rather than a unique solution per peak.

3. Thin film analyses

3.1. Secondary electron microscopy

3.1.1. Method

Secondary electron microscopy (SEM) were performed using a Hitachi SU-70 FE-SEM (Tokyo, Japan). In order to avoid distortions due to charge effect, the samples were coated with a 5 nm platinum film prior to the SEM observations. Both secondary electrons and backscattered electrons were collected for the images.

3.1.2. Surface imaging

Top-view imaging of the thin films were obtained by SEM to investigate the topography of the thin films at zoom levels ranging from 1,000 to 50,000 times.

3.1.3. Thickness and conformality

Cross-section imaging of the thin films were obtained by SEM to investigate their thickness and conformality. Following the deposition, clean cuts of the substrates were obtained using a tungsten pencil.

3.2. Atomic force microscopy

3.2.1. Method

Atomic force microscopy (AFM) was performed using a MFP 3D Infinity (Asylum Research, Santa Clara, CA) in tapping mode at a scanning rate of 1 Hz. AFM images were obtained for 2 µm by 2 µm surfaces and a median correction of the levelling was applied for each measurement using the software Gwyddion 2.52.

3.2.2. Topography

Imaging of the surface is obtained by AFM and plotted using the amplitude modulation of the cantilever.

3.2.3. Roughness

The root-mean-square height of the images Sq is calculated over the whole surfaces from the height modulation of the AFM tip.

3.3. Profilometry

3.3.1. Method

The surface and topography of the thin films were investigated using a KLA-Tencor P-17 Stylus profiler (Milpitas, CA). The stylus scanned the surface of the sample with a speed of 10 µm•s^{-1} and an applied force of 0.2 mg, the data were collected at a scan frequency of 100 Hz.

3.3.2. Thickness

Tweezers were used to scratch the thin films down to the substrate in order to investigate their thickness.

3.4. Ellipsometry

3.4.1. Method

Ellipsometry was performed using a FS-1 from Film Sense with 3 wavelengths.

3.4.2. Thickness

The thickness was obtained from a fitting using a Cauchy function (eq. 2.7) with A, B and C the Cauchy coefficient, n the refractive index and λ the wavelength.

$$n = A + \frac{B}{\lambda^2} + \frac{C}{\lambda^4} \quad (2.7)$$

3.5. Weight measurement

3.5.1. Method

Weight measurements were performed using a microscale from Sartorius ME36S (Goettingen, Germany) with a precision of 0.1 µg. The weights of the thin films were evaluated by weighting the substrate before and after the deposition. In every case, the weight was normalized by the coated surface in order to allow comparison between different conditions.

3.6. Water contact angle

3.6.1. Method

Water contact angle (WCA) measurement were performed using a DSA100 (Krüss, Hamburg, Germany) equipped with a TC30 (Krüss, Hamburg, Germany) chamber, allowing measurements at temperatures ranging from 10°C to 60°C. Each measurement is the average of 5 to 10 droplets deposited on the same thin film.

3.6.2. Surface free energy

The surface free energies (SFE) of the thermoresponsive thin films were determined at 22°C and 60°C by applying a linear fit to the extended Fowkes equations (eq. 2.8) using three liquids with distinct dispersions and polarizations energies (Table 2.2).

$$\frac{\gamma_1^{SFE}}{\sqrt{\gamma_1^{disp}}} \frac{1+\cos\theta_1}{2} = \sqrt{\gamma_2^{pola}} \sqrt{\frac{\gamma_1^{pola}}{\gamma_1^{disp}}} + \sqrt{\gamma_2^{disp}} \quad (2.8)$$

Table 2.2. Total SFE γ^{SFE} together with their Dispersive γ^{disp} and Polar γ^{polar} components of water, ethylene glycol, and diiodomethane

	γ^{SFE} mJ·m^{-2}	γ^{disp} mJ·m^{-2}	γ^{polar} mJ·m^{-2}
water	72.6	21.6	51.0
ethylene glycol	48.8	32.8	16.0
diiodomethane	50.8	49.5	1.3

4. Theoretical calculations

4.1. DFT

Density functional theoretical (DFT) calculations were achieved using the ORCA 4.0.1 program suite. All the calculations were carried out using the hybrid DFT functional B3LYP along with the numerical chain of sphere approximation RIJCOSX and the dispersion correction D3. Ahlrichs' basis set def2-SVP and Weighend's auxiliary basis set def2/J were used for every calculation. Numerical frequency analysis was performed for every calculation to ensure a local minimum of energy. Bond dissociation energies (BDEs) were determined using the standard enthalpy of formation of each homolytic fragment (eq. 2.9). Doublet intermediary species for single σ-bonds (Figure 2.6a) and triplet intermediaries localized by protons for unsaturated bonds (Figure 2.6b) were considered; with E_{el} the electron's energy, E_{ZPE} the zero point energy, E_{trans} the translational energy, E_{rot} the rotational energy, E_{vib} the vibrational energy and k_bT the kinetic energy.

$$\Delta H_f = E_{el} + E_{ZPE} + E_{trans} + E_{rot} + E_{vib} + k_bT \quad (2.9)$$

The resulting BDEs are not aimed for experimental accuracy as they are roughly 10% higher than the literature, but for self-comparison between each other in order to determine the weakest points of the monomers.

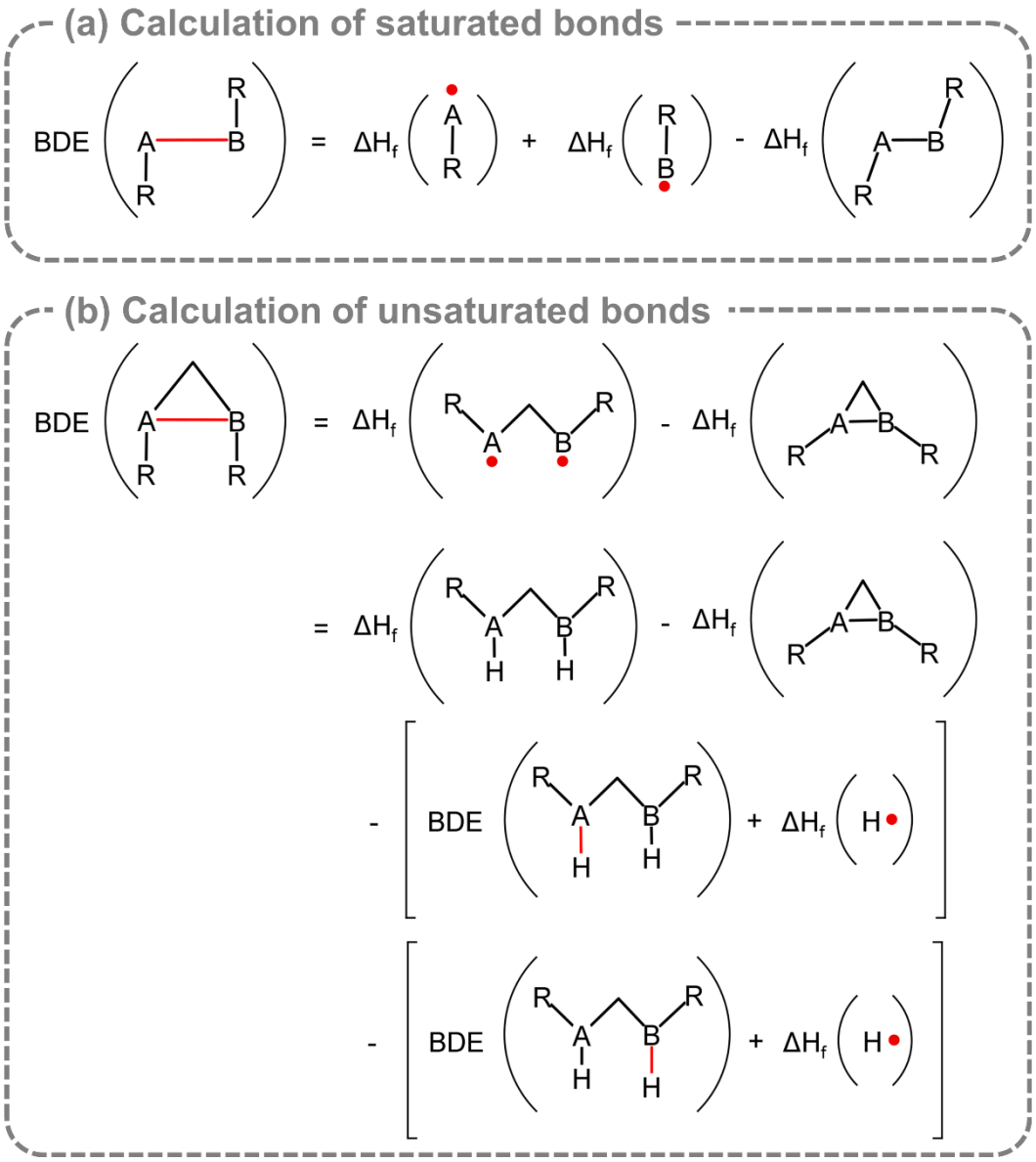

Figure 2.6. Calculation of bond dissociation energy using (a) doublet intermediaries for single σ-bonds and (b) a proton-localized triplet intermediary for unsaturated bonds.

CHAPTER III - Nanopulsed discharges for the AP-PiCVD of polymer layers: an experimental study

This chapter reports the chemical and morphological properties of the layers deposited from vinylic monomers using an ultrashort plasma pulsed dielectric barrier discharge operating at atmospheric pressure. A comparison between the prepared layers and conventional polymer layers is introduced. To this end, a set of three methacrylate monomers (methyl, butyl, and glycidyl methacrylate) are investigated using nanosecond pulsed plasma discharges (*ca.* 100 ns) at various discharge frequencies ranging from 31.6 Hz to 10,000 Hz. Polymeric layers with excellent retention of the monomers' chemical structure, high weight-average molar mass and an excellent thin film conformality are achieved for the lowest frequencies. Insights based on the nanosecond pulsed plasma experimental parameters and the monomer's intrinsic properties for the promotion of conventional polymerization mechanisms by AP-PiCVD are provided.

Article published from these results

Loyer, F., Frache, G., Choquet, P., and Boscher, N.D. (2017) Atmospheric Pressure Plasma-Initiated Chemical Vapor Deposition (AP-PiCVD) of Poly(alkyl acrylates): An Experimental Study. *Macromolecules*, **50** (11), 4351–4362.
Full contribution (experimental & analyses & redaction)

Content

1. Introduction

The initiation of the free-radical polymerization by low frequency nanosecond pulsed plasma discharges, called plasma initiated chemical vapor deposition (PiCVD), has displayed a high potential for the formation of polymeric layers with a high retention of the monomers' chemical structure compared to traditional PECVD approach[1,2] Notably, the ability to preserve sensitive chemical functionalities (*e.g.* epoxy function) while allowing the deposition of conformal layers using AP-DBD systems opens new possibilities for the functionalization of large surfaces with smart polymer thin films.[1–3]

Yet, the limitations and key parameters entailing such improved properties via different growth mechanisms are yet to be clearly determined. Towards this aim, the simultaneous polymerization and growth by AP-PiCVD of three methacrylate monomers – methyl, butyl and glycidyl methacrylate, further referred to as MMA, BMA and GMA, respectively – is investigated. Each monomer is selected for its intrinsic growth properties, namely their kinetic of polymerization (*i.e.* propagation constant k_p) and kinetic of adsorption (*i.e.* vapor pressure P_{sat}) (Table 2.1). Using an AP-DBD setup (Figure 2.1) and a square-wave pulsed generator from EFFITECH (Figure 2.2), nanopulsed discharges (t_{on} ≈ 100 ns) are generated from a 15 µs pulse with a peak voltage of 6.5 kV in order to initiate the self-sustained free-radical polymerization, which will maintain the growth during the off-time (Figure 3.1). The independent discharges – as evidenced by OES (Figure 2.4) – are investigated at different discharge frequencies ranging from 31.6 Hz (t_{off} = 31.6 ms) to 10,000 Hz (t_{off} = 100 µs).

From the thorough analyses of the methacrylate-based layers grown by AP-PiCVD, their chemistry, polymeric growth and topography are related to the transition from dominant free-radical polymerization mechanisms to dominant plasma mechanisms. Based on those observation, conclusions and insight for the promotion of free-radical polymerization pathways via surface mechanisms using nanopulsed discharges toward the deposition of conventional and conformal polymer thin films are provided.

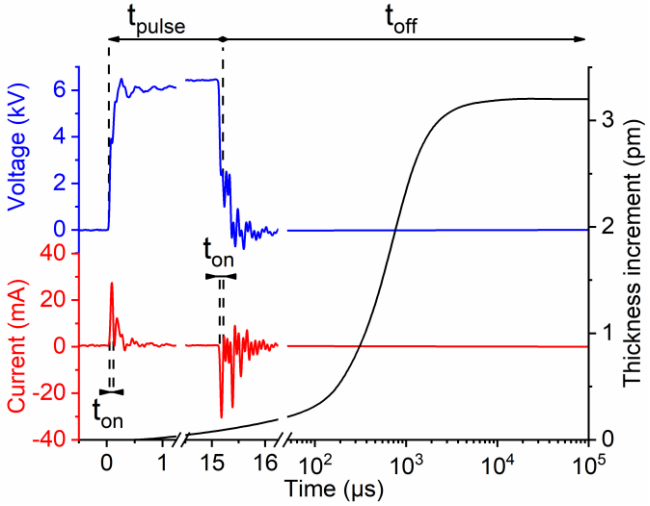

Figure 3.1. Traces of the 15 µs electrical potentials and 100 ns current discharges from the nanopulsed generators followed by an example of a self-sustained growth during the off-time.

2. Results and discussion

2.1. Effect of the discharge frequency on the growth rates

The weight and thickness growth rates of the methacrylate-based thin films deposited by nanosecond pulsed DBD were evaluated for all the investigated frequencies. A prominent self-sustained free-radical growth during the off-time was evidenced, as higher thickness and weight increments per cycle (*i.e.* $t_{on} + t_{off}$, with t_{on} kept constant) were observed for longer t_{off} (Figure 3.2a-c).While all 3 methacrylates exhibit a similar trend, they do not reach their plateau at the same time. As the plateau indicates the termination of the free-radical polymerization mechanism, the methacrylates demonstrate very different lifetimes despite their close chemistry.

Their distinct reactivity is also observed with the evolution of the growth rates in thickness and in weight according to the discharge frequency (Figure 3.2d-f), showing a transition of dominant mechanisms. This shift – visible as a sudden drop of the deposition rate – appears to also be strongly correlated to the monomer itself, as it occurs at different discharge frequency for each methacrylate. Indeed, this effect is observed for both BMA and GMA at $f_{transition,BMA}$ = 3,160 Hz and $f_{transition,GMA}$ = 1,000 Hz, respectively. MMA on the other hand does not appear to reach its frequency of transition even at discharge frequencies as high as 10,000 Hz.

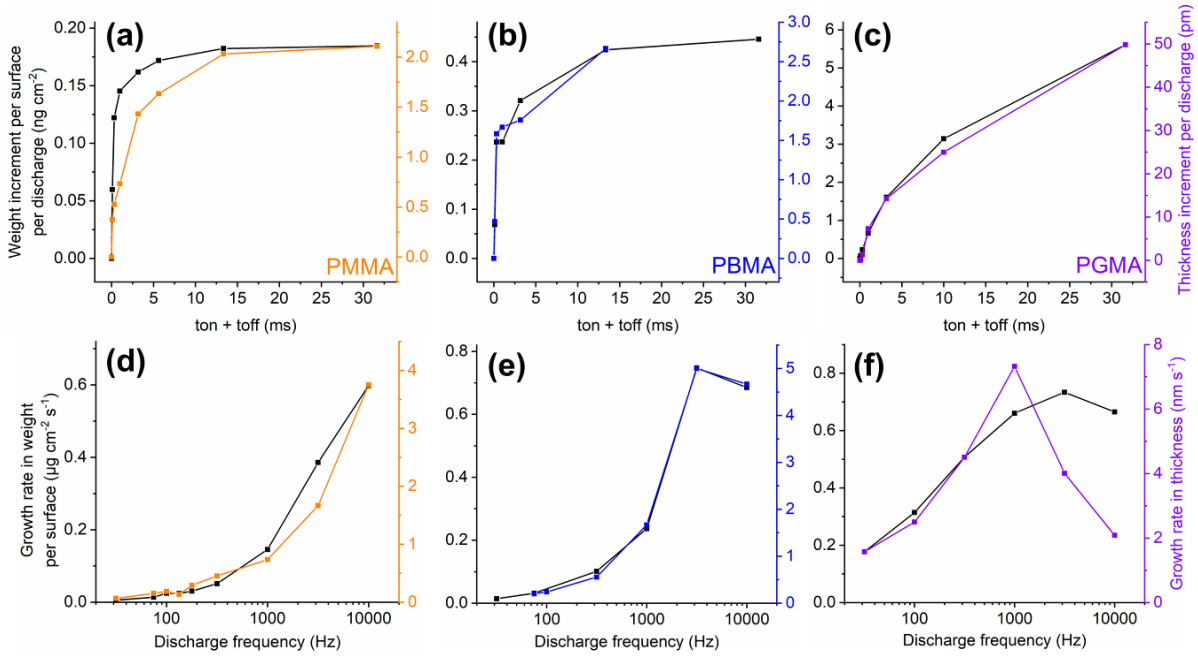

Figure 3.2. Weight and thickness increment per discharge according to the cycle time ($t_{on} + t_{off}$) and growth rates per second according to the duty cycle for the films grown from (a, d) MMA, (b, e) BMA and (c, f) GMA.

In Figures 3.2e and 3.2f, the decreased growth rate at discharge frequencies below the frequency threshold (*i.e.* long t_{off}) may simply be explained by a lower concentration of propagating species due to the use of fewer discharges per second, typically as the free-radicals reach their average lifetimes and deactivate. Over the frequency threshold (*i.e.* short

t_{off}), the plasma processes are anticipated to overcome the free-radical polymerization processes since each molecule will be exposed to a higher number of plasma discharges before reaching the substrate. Thus, the growth of short-chain oligomers at higher discharge frequencies is expected, as the fragmentation and dissociation of the monomer is more pronounced, inducing a high production of radicals and other species that are able to interrupt the growth of the polymeric chains. From those observations, it is clear that the films elaborated with AP-PECVD are the result of a highly monomer-dependent competition between the fragmentation and the conventional free-radical polymerization mechanisms. In any case, the free-radical polymerization pathway is expected to be greatly favored for the lowest discharge frequencies (*i.e.* the longest t_{off}).

As such, during these long plasma off-times, the occurring surface reactions are assumed to be close to the radical polymerization steps taking place in both the solution phase and in an iCVD process.[4–6] Thus, for very long t_{off}, the deposition rate should be strongly influenced by the concentration of initiating species and active growing chains ($[M\bullet]$), the concentration of monomer adsorbed on the surface ($[M]$) and the rate constant for propagation (k_p). The monomer surface concentration being directly related to the ratio of the monomer's vapor-phase concentration (P_M) and its saturated vapor pressure (P_{sat}), the studied methacrylate monomer surface concentrations can be ranked as: $[M_{MMA}]_{(ad)} < [M_{BMA}]_{(ad)} < [M_{GMA}]_{(ad)}$ as P_M is kept constant for all the deposition experiments.[7] Additionally, their respective propagation rate constants are ordered as follow: $k_p^{MMA} \sim k_p^{BMA} < k_p^{GMA}$ (Table 2.1). From those observations, it is interesting to note that the deposition rates (DR) for the low frequency experiments (100 Hz in the following comparison), which ranked as follow: DR_{MMA} (0.18 nm·s^{-1}) < DR_{BMA} (0.24 nm·s^{-1}) << DR_{GMA} (2.50 nm·s^{-1}), are in accordance with the $[M]$ and k_p ratings, supporting the assumption that the surface reactions taking place during the plasma off-times are analogous to the radical polymerization steps in the bulk phase.

In addition, while the densities of the MMA and BMA thin films, *ca.* 1.21 g·mL^{-1} and 1.59 g·mL^{-1} respectively, are pretty constant over the range of studied frequencies, the growth rates in weight and thickness of the GMA thin films do not follow the same trend. Such change of density (Figure 3.2f) may arise from the presence of the reactive epoxy ring of GMA, which is expected to be more sensitive towards plasma fragmentation for high discharge frequencies and would favor a cross-linking by creation of a radical anchor point through ring opening mechanisms.

2.2. Effect of the discharge frequency on the chemistry

Numerous mechanisms occur during the PECVD of methacrylate monomers (*e.g.* free radical polymerization, plasma-polymerization or random crosslinking, dissociation, ionization, etching.[8] In addition to influencing the growth rates, the combination of these mechanisms is well known to impact the chemical composition and structure of the resulting thin films.[8,9] Consequently, the effects of the different discharge frequencies on the monomers' chemistry need to be evaluated and compared to their conventional counterparts.

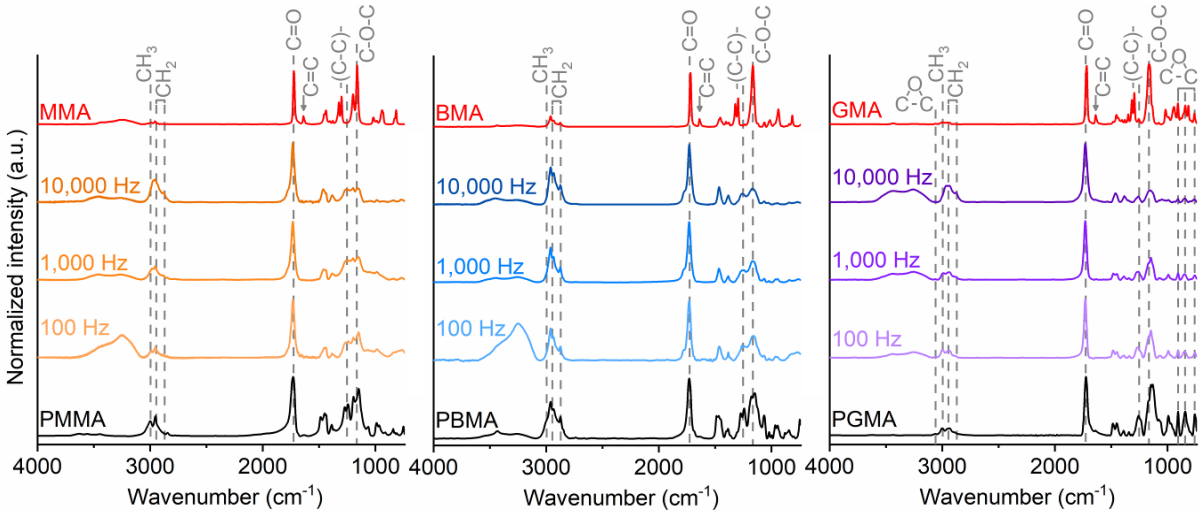

Figure 3.3. FTIR spectra of the thin films grown from MMA, BMA and GMA at different discharge frequencies. The spectra of both the liquid precursor (MMA, BMA and GMA) and the conventionally polymerized pMMA, pBMA and pGMA powder are shown as references on the corresponding figure. The C=O band[10] (1,723 cm^{-1}), presents in the methacrylate monomer, reference polymer and the prepared thin films is used to normalized all the spectra.

FTIR was used to investigate the different bonding arrangements in the films and to compare them to their precursor and to their corresponding reference polymer powder (Figure 3.3). Regardless of the pulse's frequency or thin films precursor, the vinyl bond vibrations[10] (1,635 and 1,310 cm^{-1}) disappeared for all the grown thin films, supporting the dominance of initiation mechanisms comparable to the free-radical polymerization pathways. Irrespective of the monomer investigated, the spectra of the films obtained for the lowest frequencies display a very close match in comparison to reference polymers, while a greater number of discrepancies is observed as the pulse's frequency gets higher. Typically, a rise is observed in the intensity of the vibrational bands corresponding to CH_2 bonding[10] (2,953, 2,875 and 1,447 cm^{-1}), opposed to a drop of the CH_3 vibrational bands domains[10] (2,995, 2,840, 1,483 and 1,391 cm^{-1}). An increase in the carbon bonds substitutions is indicative of a more pronounced reorganization of the monomer molecules toward a crosslinked structure. An interesting disparity appears among the polymers' vibrational energies between 3200 and 3,600 cm^{-1}, corresponding to hydrogen stretching vibrations. While the ppMMA and ppBMA FTIR spectra show a quick surge for hydroxyl bands vibrations[10,11] (3,252 and 3,427 cm^{-1}) as the pulse's frequency decrease, ppGMA exhibit the opposite behavior with an increase of the hydroxyl stretching vibrations for high pulse's frequencies. If the opening of the sensitive epoxy function of ppGMA at high discharge frequencies seems to be the obvious reason for the increase of OH vibration, the antagonist observation seemed more subtle to understand for the two other methacrylate monomers. The most probable explanation would be the integration of water from the atmosphere during the longer off-times at lower discharge frequencies, leading to an important broadening of the hydroxyl band toward lower energy levels (3,252 cm^{-1}). An alternative explanation to this effect could be the strong influence of intermolecular vibrations[10,11] due to the addition of proton acceptor groups,[12,13] The presence of proton acceptors originating from the surrounding atmosphere (despite the surrounding atmosphere passivation using Ar barrier fluxes) is a fair assumption, however it assuredly requires more investigations to draw any conclusion regarding its relationship with the frequency of nanosecond DBD pulses.

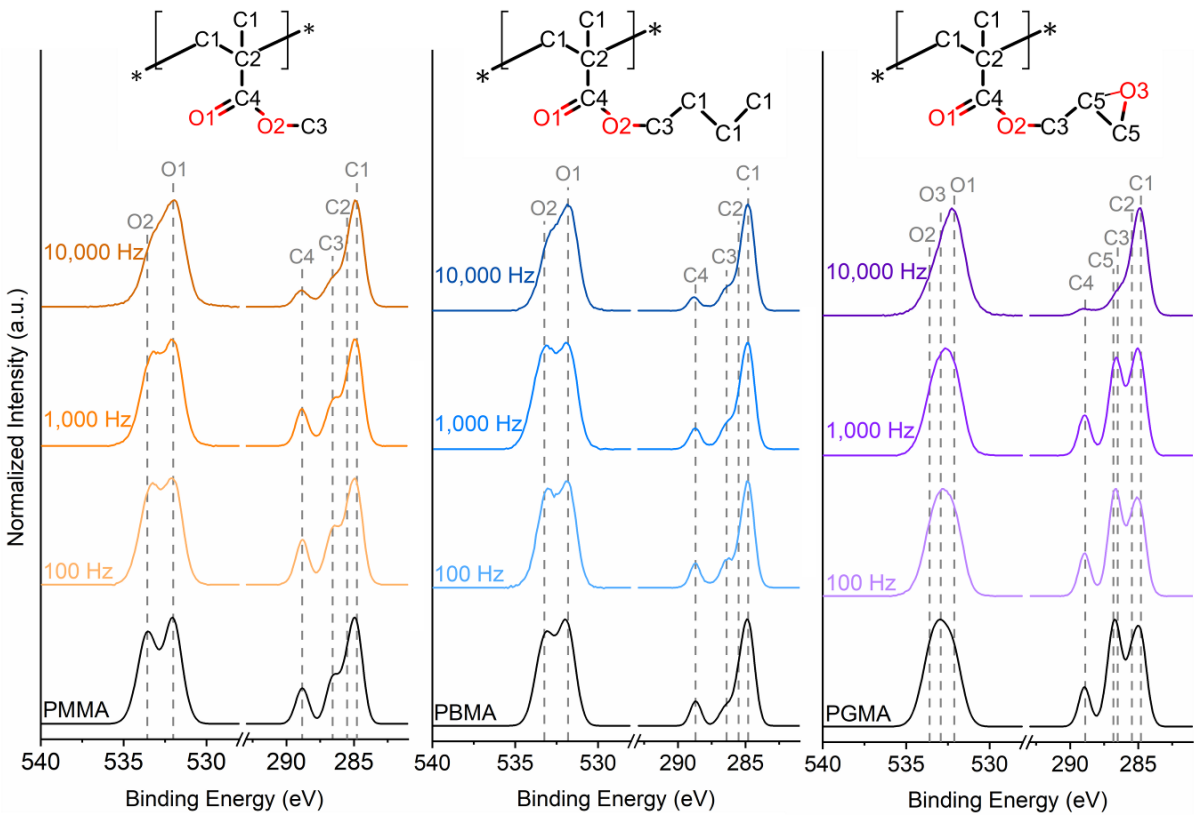

Figure 3.4. XPS spectrum of the O 1s and C 1s core levels for the ppMMA, ppBMA and ppGMA films deposited at different pulse's frequencies, with the C-H binding energy fixed at 284.8 eV. The O 1s and C 1s core level of the conventionally polymerized pMMA, pBMA and pGMA powders are shown as references.

XPS elemental analysis of the films elaborated using low pulse's frequencies display almost no difference with the theoretical values for their corresponding polymer (Table 3.2). In addition, no evidence of nitrogen contamination from the surrounding atmosphere was detected for these films. On the other hand, higher carbon concentrations and lower oxygen concentrations than the expected ones were measured for the films elaborated from higher discharge frequencies. Furthermore, trace level of nitrogen, integrated from excessive reaction of the monomers with the surrounding atmosphere, were detected. The C 1s and O 1s core levels envelopes for the thin films described in the present work were compared in order to highlight both the similarities and changes in chemistry (Figure 3.4). Similarly to the FTIR observations, the C 1s and O 1s core levels spectra for the films obtained for the lowest frequencies display a close match to the ones for the reference polymers. While increasing the discharge frequency, C-O simple bonds[14] (*i.e.* C3 & O2) appear as more prone to alteration. In particular, the GMA's C-O components,[14] including both the ether and the epoxy bonds (*i.e.* C3 & O2 and C5 & O3 respectively) were shown to almost completely disappear at 10,000 Hz.

Table 3.2. Atomic ratios of ppMMA, ppBMA and ppGMA thin films at different discharge frequencies in comparison to their theoretical values.

		O (%)	N (%)	C (%)
ppMMA	**Theory**	28.5	0.0	71.5
	100 Hz	27.3	0.1	72.6
	1,000 Hz	25.1	0.1	74.9
	10,000 Hz	19.0	0.2	80.8
ppBMA	**Theory**	20.0	0.0	80.0
	100 Hz	20.9	0.0	79.1
	1,000 Hz	17.6	0.0	82.5
	10,000 Hz	16.6	0.2	83.3
ppGMA	**Theory**	30.0	0.0	70.0
	100 Hz	26.6	0.0	73.4
	1,000 Hz	26.7	0.0	73.3
	10,000 Hz	13.8	0.8	85.4

2.3. Effect of the discharge frequency on the polymeric growth

From both the previous FTIR and XPS observations, the chemical functionalities appear to be very well preserved for low discharge frequencies (*i.e.* below 100 Hz). This contrasts with the usual cross-linking and reactive functions breakdown observed in plasma-polymers. The following section will aim at demonstrating the formation of conventional polymer layers from specific polymer characterization methods, *i.e.* matrix-assisted laser desorption/ionization high resolution mass spectrometry (MALDI-HRMS) and size exclusion chromatography (SEC). The mass spectra in the range m/z = 100−1,400 of the GMA-based thin films elaborated from the lowest frequency is dominated by ppGMA proton adduct with proton terminal groups $[H(GMA)_nH + H]^+$ up to n = 7 repetition units (Figure 3.5c). The most common alteration, with a mass difference of 0.0364 Da, corresponds to the substitution of a CH_4 unit (*i.e.* a terminal methyl bond) with an O unit (*i.e.* a ketone/aldehyde bond) hinting on an effect of the atmospheric environment (O_2 and H_2O) (Figure 3.5f). This reaction appears to be even more prominent for the films deposited from MMA (Figure 3.5d) and BMA (Figure 3.5e) at low discharge frequencies, correlating with an increase of hydroxyl function and the previous FTIR observations for the 3,252 and 3,427 cm^{-1} bands (Figure 3.3). As the pulse's frequency is increased, a greater number of structural modifications are observed, indicating a prevailing influence of the plasma polymerization processes, including their side reactions (Figure 3.5a-c). Thanks to the high mass resolution analyses and after zooming into one of the main oligomer unit (Figure 3.5d-f), it reveals that the variations from the plasma phase where numerous peaks coming from the plasma fragmentation are more found for the films elaborated from the highest frequency, resulting from one to several dissociation and recombination reactions. However, the number of species between the oligomer units appears to be extremely monomer dependent, with MMA films (Figure 3.5a) displaying a non-negligible amount in comparison to BMA (Figure 3.5b) and especially GMA (Figure 3.5c) films. Those observations would have an important consequence on the growth mechanism as it would suggest that MMA is more sensitive to side-reactions while BMA and GMA growing chains tend to quickly adsorb on the substrate and deactivate, relating to their vapor

pressure P_{sat}, before being reactivated by either the plasma or an incoming radical monomer, hence statistically lowering the addition of impurities.

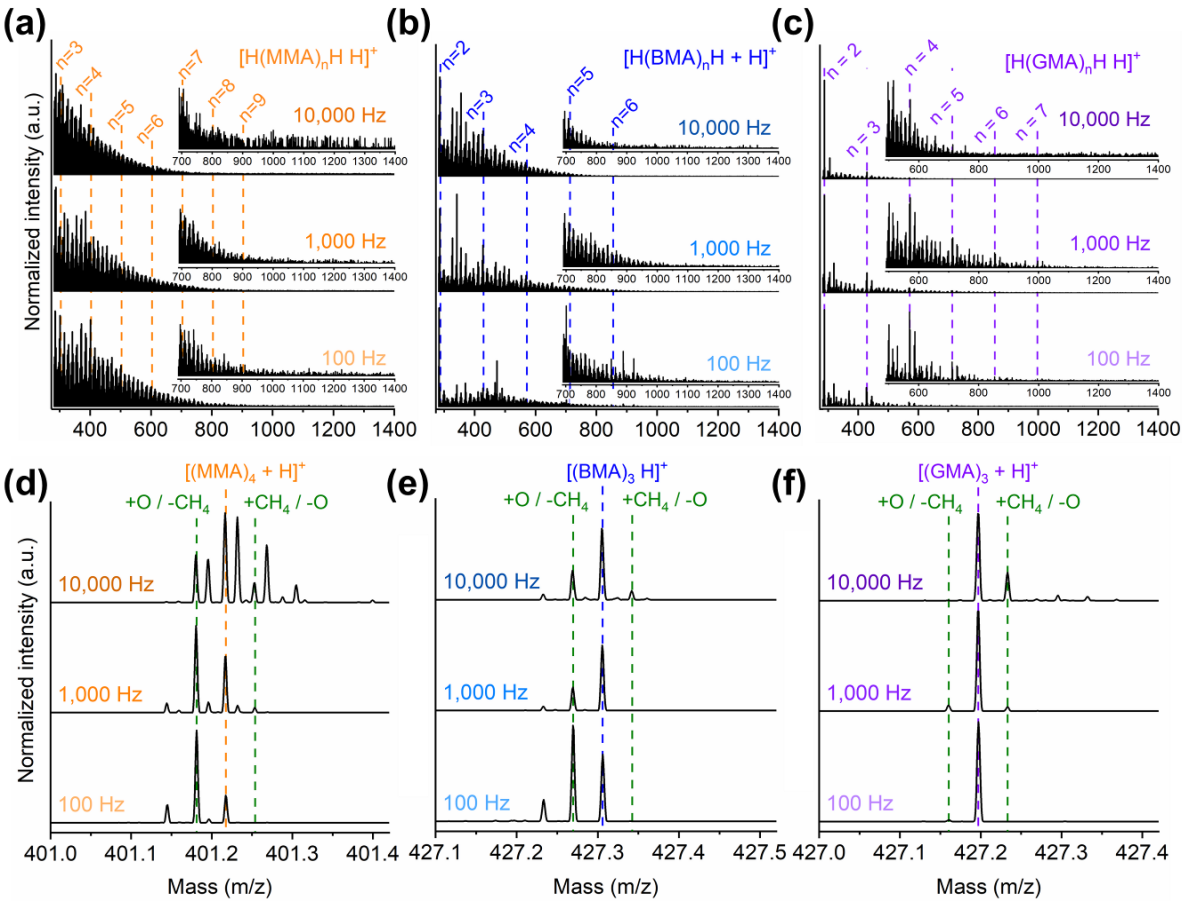

Figure 3.5. MALDI-HRMS spectra in the mass ranges (a, b & c) m/z = 280−1400 for thin films elaborated for various pulse's frequencies from MMA, BMA and GMA, respectively. Zoom on the (d) 4th oligomer at m/z = 401.0−401.42 (e) 3rd oligomer at m/z = 427.1−427.52 and (f) 3rd oligomer at m/z = 427.0−427.42 for thin films elaborated for various pulse's frequencies from MMA, BMA and GMA, respectively.

In order to further understand the effect of these plasma formed species on the polymeric chain growth, SEC measurements were performed on all the grown films. The measurements were plotted and compared to each other in elution time since the molar weight cannot be reliably assessed due to the chemistry discrepancies between the low and high pulse's frequency thin films. Indeed, The organic layers elaborated from low discharge frequencies display one main peak (*i.e.* 9 min for ppMMA and ppBMA and 6.5 min for ppGMA) (Figure 3.6), which can be seen as the – almost unique – contribution of a singular distribution, implying the existence of one predominant compound and suggesting a polymer-like growth. In addition, a low intensity peak or plateau appears at shorter retention times (*i.e.* higher molecular weights) for both MMA and BMA-based layers (Figure 3.6a,b), indicating the potential formation of polymer compounds up to several hundreds of thousands of grams per mole.

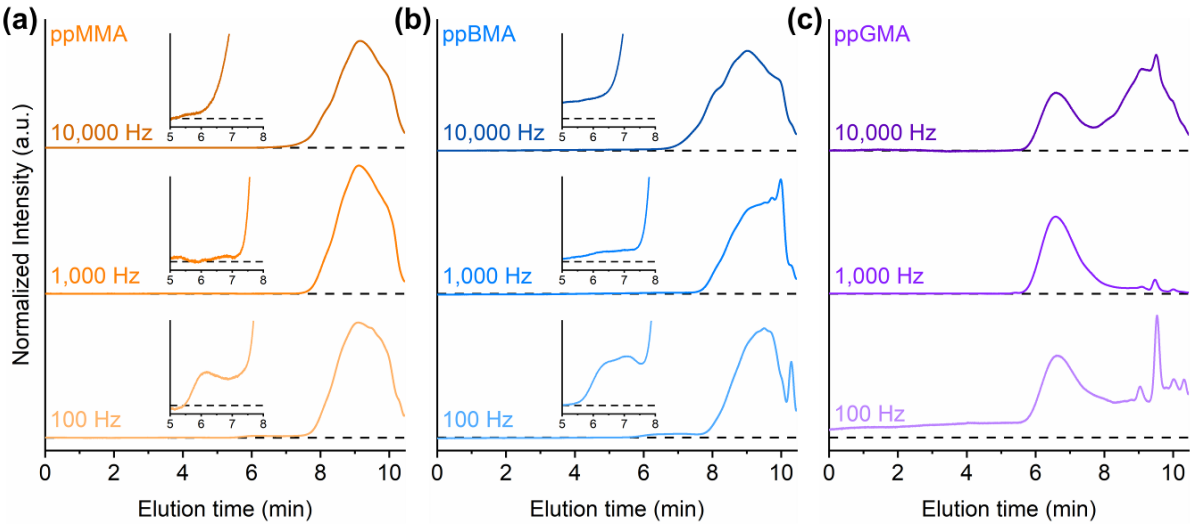

Figure 3.6. SEC measurement for the films elaborated from MMA, BMA and GMA for various pulse's frequencies. (a, b & c) over the whole range spectra. The high molecular weight tails in the 5 to 8 minutes range are displayed for MMA and BMA.

Assuming that polymeric chains of ppMMA, ppBMA and ppGMA are grown for the low discharge frequencies, average molar masses in weight (M_W) of 2,596 g·mol^{-1}, 4,761 g·mol^{-1} and 94,364 g·mol^{-1} respectively were estimated for the methacrylate films grown at 100 Hz, integrated around their polymer distribution peaks (*i.e.* between 5 min and 10.5 min for ppMMA and ppBMA, and narrowed around 5.6 min and 8 min for ppGMA). On the other hand, several overlapping peaks are observed for the high pulse's frequency plasma-polymer coatings, suggesting the presence of several compounds with different chemistries. Surprisingly, the elution times for these peaks are similar to the ones observed for the low discharge frequencies polymer layers grown from MMA and BMA. Thus, the arising distribution peaks (*ca.* 9 min) could easily be misinterpreted as long polymeric chains comparable to the ones observed for low discharge frequencies. However, based on our previous FTIR and XPS investigations, high DCs are proven to lead to the formation of altered chemistries with a high degree of cross-linking. These highly cross-linked structures obtained at higher discharge frequencies are expected to rapidly migrate through the chromatographic column due to their 3D conformation. Hence, the formed chemistries cannot be calibrated from any known compounds, as they would incorrectly appear as higher molecular weight species. In the case of GMA, several overlapping peaks are also observed for the plasma-polymer coating grown at 10,000 Hz at an elution time comparable to the ones observed for the films elaborated from MMA and BMA at 10,000 Hz (*ca.* 9 min), suggesting that for higher discharge frequencies, the deposition is more driven by the plasma condition rather than by the monomer's intrinsic kinetics properties. Interestingly, for the plasma-polymer coatings grown from GMA at 10,000 Hz, a distribution at an identical elution time as the polymer distribution of the 100 Hz polymer layers is observed (*ca.* 6.5 min), indicating the continuation of the free-radical polymerization path. Further, taking in consideration that the plasma residues elution time coincides with ppMMA and ppBMA polymeric distribution, we can relate the alterations of the low tail of the Gaussian distribution (Figure 3.6a,b) to the evolution of polymer favoring mechanisms (high molecular plateau) as well as the plasma-polymerization favoring mechanisms (expansion of the fragment distribution peaks) over the frequency. Therefore the competition between the "kinetic regime", prominent for the lowest frequencies, and the "plasma polymer regime", prominent for the highest frequencies, is readily observed from the SEC spectra of the GMA samples

with a greater fraction related to the Gaussian polymeric distribution at low frequency and the apparition of new distributions related to plasma-polymer-like compounds at higher frequencies (Figure 3.6c). Such transition could not be readily evidenced from the SEC spectra of the MMA and BMA samples due to the overlap of the polymeric and plasma-polymer distributions (Figure 3.6a,b). Thus, the apparent average molar mass in weight ($M_W{}^*$) was determined at all frequencies for MMA and BMA distributions, taken between 5 min and 10.5 min to remove the influence of the monomer and solvent contamination. For each of the investigated monomer, the apparent M_w* plotted versus the discharge frequency effectively exhibits the transition from one dominant mechanism to the other, displaying a bowl shape with a minimum around 1,000 Hz and an increase of the apparent $M_W{}^*$ for both low pulse's frequencies (*i.e.* long t_{off}) due to the promotion of a "kinetic regime" and at high pulse's frequencies (*i.e.* short t_{off}) as it converts toward a "plasma polymer regime" (Figure 3.7).

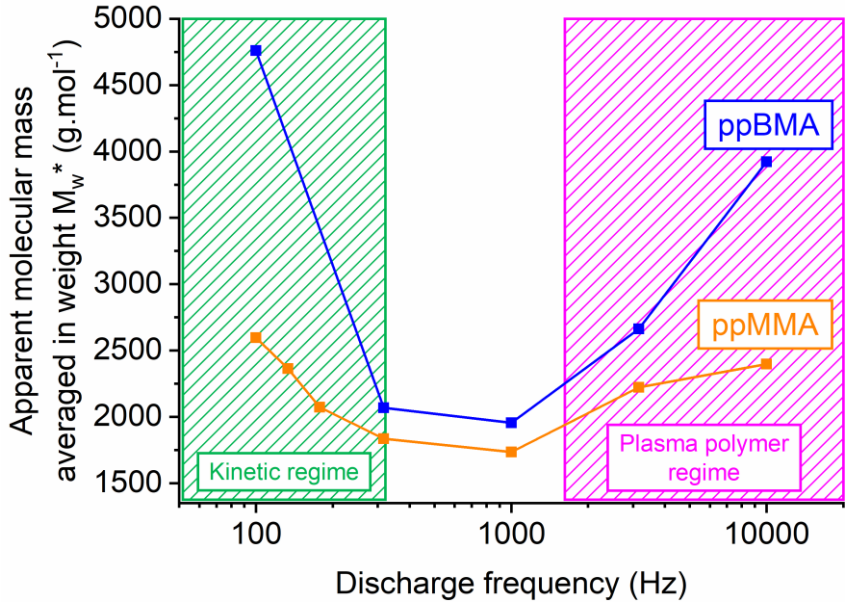

Figure 3.7. Apparent average molar mass in weight ($M_W{}^*$) for the films elaborated from MMA and BMA for various pulse frequencies. $M_W{}^*$ values are extracted from the respective SEC measurements and a polystyrene calibration. One should note that the $M_W{}^*$ are given for the need of the discussion and that these values do not constitute an accurate information for the high discharge frequency films. Due to the splitting of the polymeric and plasma-polymer distributions for the GMA samples, the integration of both Gaussians in a single $M_W{}^*$ is not required and not possible.

2.4. Effect of the discharge frequency on the morphology

The deposition rates (Figure 3.2) and the apparent average molar mass in weight (Figure 3.7) both highlighted the occurrence of a competition between the plasma-polymerization and the conventional free-radical polymerization mechanisms during the nanosecond pulsed DBD of methacrylates. The influence of the pulse's frequency and the methacrylate monomer on this competition can also be observed on the morphology of the films (Figure 3.8 & 3.9). While the top view SEM observations reveal the formation of smooth and particle-free films for the lowest pulse's frequencies, rough surfaces were formed for frequencies above 10,000 Hz for MMA and BMA and 1,000 Hz for GMA (Figure 3.8).

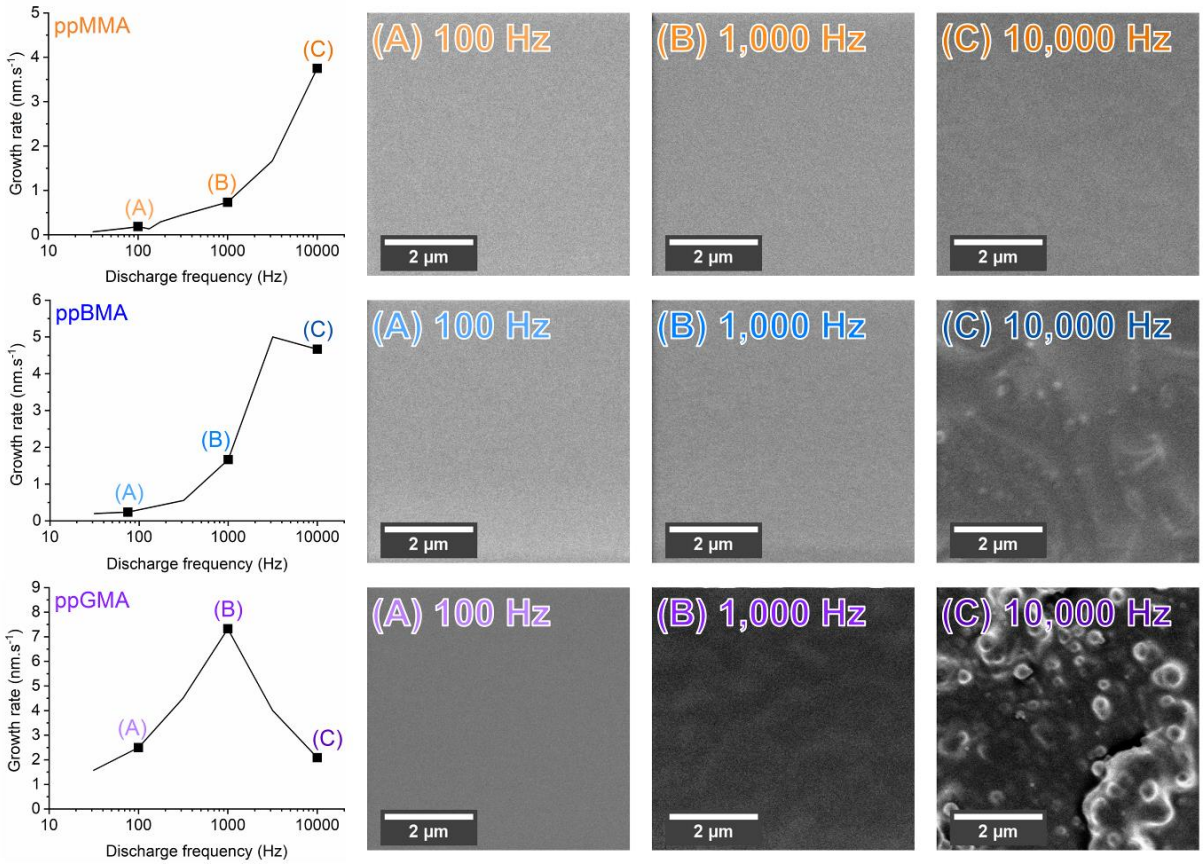

Figure 3.8. (left) Growth rates per second according to the duty cycle for the films grown from MMA, BMA and GMA. (right) Top-view SEM images of the ppMMA, ppBMA and ppGMA films at 100 Hz, 1,000 Hz and 10,000 Hz. The three different films are produced with comparable thickness so the microstructure changes cannot be associated to thickness dependent mechanisms.

Interestingly, the morphology was shown to be independent on the growth rate, implying that the film's roughening is not related to an excessive deposition rate but rather to excessive gas phase reactions induced by the highest pulse's frequency. A concrete example is the SEM images of the films elaborated from GMA at 100 Hz and 10,000 Hz, which exhibit strong discrepancies in their morphology in spite of identical growth rates. In a perfectly repeatable manner, the thin films realized at pulse's frequencies strictly inferior to the deposition rate transition display a smooth surface (Figure 3.8). At the transition frequency, several rough features start to emerge on the surface and above this transition, a greater number of particles is formed as the pulse's frequency increases, rapidly deteriorating the film morphology down to a highly granular surface. Such behavior is related to the gas phase reaction of the methacrylate monomers with the abundant reactive species generated by the plasma discharges that induce a high concentration of condensable vapors, increasing the nucleation and growth of numerous particles.

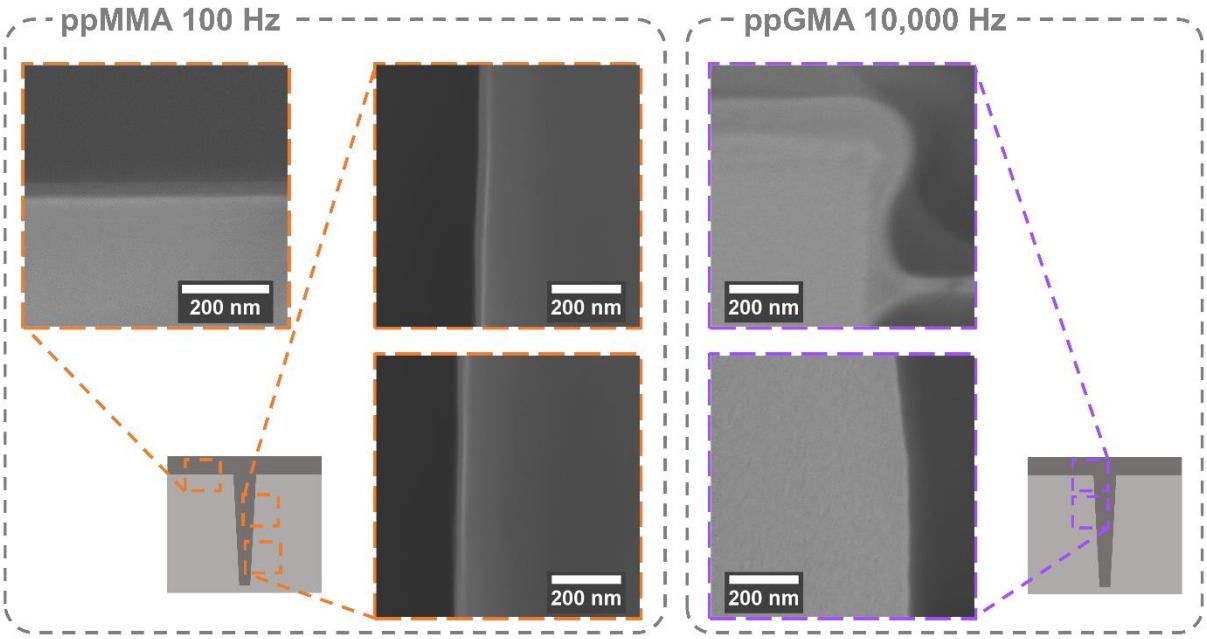

Figure 3.9. Cross-section SEM images of the thin films deposited from MMA at 100 Hz (left) and GMA at 10,000 Hz (right) on 5 µm deep and 600 nm wide trenches on silicon wafers. It is noteworthy to mention that the conformal or non-conformal behavior of the thin films is mainly related to the pulse's frequency and to a lesser extend to the P_M/P_{sat} ratio. Polymer layers grown from GMA at low pulse's frequency also displayed an excellent conformality.[1]

To confirm the above statements, a polymer layer elaborated at 100 Hz and a plasma-polymer coating at 10,000 Hz were deposited on 5 µm deep and 600 nm wide trenched silicon wafers. The SEM cross-section observation of the thin film deposited from GMA at 10,000 Hz reveals the non-conformality of the coating, with the absence of deposition after a few hundred nanometers down into the trench. A bridge between the two sides of the trench is even created. Such comportment is not surprising as PECVD processes are well known for their non-conformal behavior due to the high sticking coefficient of the formed reactants that readily condensate on the mouth of porosities. On the other hand, the smooth polymer layers elaborated from MMA and GMA[1] at 100 Hz exhibits an excellent conformality with a ratio between the thicknesses at the bottom and top of the trench higher than 85 %. Therefore, using low discharge frequencies, the methacrylate monomers adsorb onto the surface where they are consumed by the free-radical polymerization reaction with the previously adsorbed radicals generated by the ultrashort square-wave pulse plasma discharges.

2.5. Insights in the experimental conditions and growth mechanisms in AP-PiCVD

Although plasma-based processes, including AP-PiCVD, are unlikely to ever produce true homopolymers thin films such as iCVD does, the present investigations assuredly exhibit strong similarities with the iCVD method,[5,6,15] with respect to the growth mechanisms and the resulting thin films' characteristics. For low plasma pulse's frequencies, surface reaction mechanisms (*i.e.* adsorption and subsequent free-radical polymerization) are preponderant, leading to an unprecedented degree of polymerization for PECVD processes (Figure 3.6) coupled to the formation of thin films with a high level of conformality when using low P_M/P_{sat}

values (Figure 3.9). Such as for iCVD, the use of a vinyl monomer is a prerequisite and can allow the simultaneous synthesis and deposition of polymer with various functionalities.[2,3] While iCVD implies the use of an initiator (*e.g.* di-*tert-butyl peroxide)* broken down into radicals by hot filaments to begin the free-radical polymerization of vinyl monomers at the substrate surface, the AP-PiCVD approach involves the ultrashort plasma pulses to initiate the free-radical polymerization reaction. By replicating the free-radical polymerization in the vapor phase at atmospheric-pressure, the described method provides a simple one-step and up-scalable route towards the deposition of a wide range of polymer thin films.[3] Interestingly, the method can easily be adapted to existing AP-DBD surface treatment lines through the implementation of a nanosecond HV pulses generator. The present study highlighted several times the duality between two different modes (Figure 3.10), *i.e.* the plasma-enhanced CVD (PECVD) and the plasma-initiated CVD (PiCVD) of plasma-polymer and polymer-like thin films, respectively. Each of the two modes, both occurring while combining plasma and vinyl monomers, can be greatly favored under certain conditions. A quite obvious rule when performing the plasma-initiated chemical vapor deposition (PiCVD) of polymer thin films is to use a low repetition frequency of the ultrashort square-wave pulses, consistent with the lifetime of the free-radical polymerization lifetimes for the selected monomer. Indeed, the weight and thickness increment per discharge according to the cycle time ($t_{on} + t_{off}$) revealed that in the case of MMA monomer, no significant deposition occurs when t_{off} exceeds 10 ms (Figure 3.2a). Thus, there is no point using frequencies lower than 100 Hz under these conditions as it would only result in a decay of the growth rate with no significant enhancement of the chemistry. In contrast, the weight and thickness increment per discharge according to the cycle time demonstrated that the free-radical polymerization of the GMA monomer can perpetuate over 100 ms[1] (Figure 3.2c), suggesting that a 10 Hz discharge frequency would lead to an improvement of the film's chemistry.

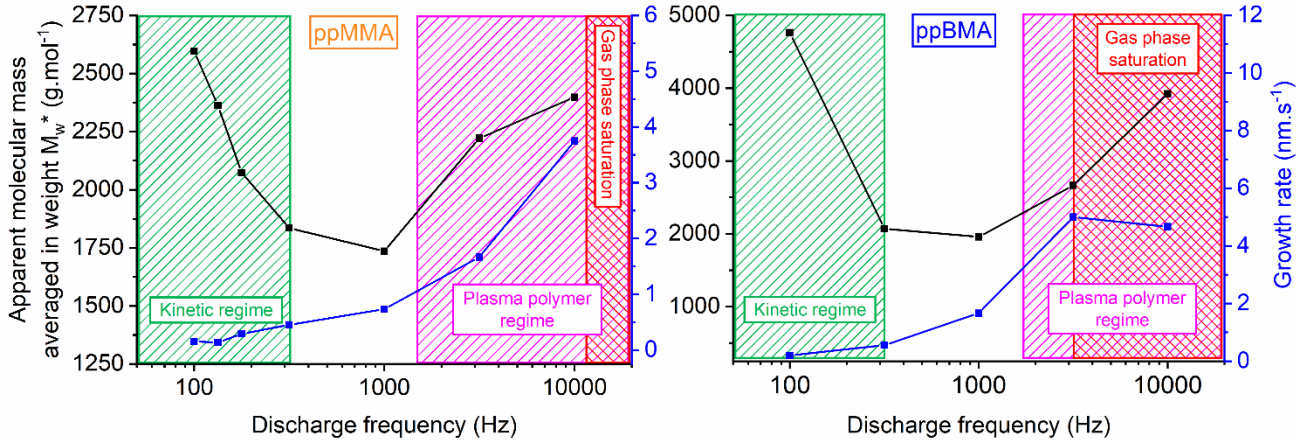

Figure 3.10. Apparent average molar mass in weight (M_w*) and Growth rates per second according to the duty cycle for the films grown from (left) MMA and (right) BMA.

Such as described previously, for low discharge frequencies, the deposition rate is shown to be directly related to the P_M/P_{sat} ratio. Notably, plotting the deposition rates in thickness versus the P_M/P_{sat} ratio for different input fluxes of GMA grown at a discharge frequency of 100 Hz shows that it follows a type III BET isotherm (Figure 3.11), with a monolayer value h_{ml} of 1.9183 nm and a coverage value c of 0.0101 indicating the formation of multilayers.[7] Thus, a monomer with a lower vapor pressure (P_{sat}), adsorption to the surface would be promoted and both the growth rate and the conventional polymerization pathway will be enhanced. Nevertheless, the vapor pressure should be sufficient enough to allow delivery of

the monomer at atmospheric-pressure. Aerosol-assisted CVD is a common practice at atmospheric-pressure when employing low P_{sat} precursors,[16] however, this is not recommended for the PiCVD of polymer-like thin films as this would result in many condensation or droplet spots and form irregular and non-conformal coatings. For monomer with high vapor pressure, one could consider increasing P_M (*i.e.* through the increase of the carrier gas flux), bearing in mind that plasma processes are strongly affected by the composition of the plasma gas.[17] An alternative option is to decrease the substrate temperature in order to enhance the adsorption rate and favor the polymeric growth.

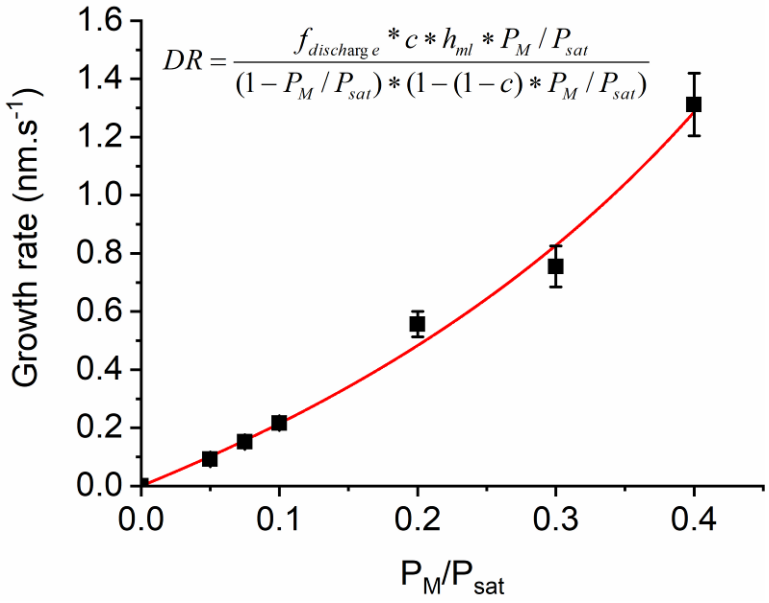

Figure 3.11. Evolution of the growth rates per second for GMA thin films grown with different carrier fluxes, at a fixed discharge frequency of 100 Hz, and plotted according to the P_M/P_{sat} ratio determined using the flux. The growth rate DR was mathematically related to a BET isotherm equation using the frequency in order to consider each side of the equation over 1 s of deposition.

It is worth noting here that, in contrast with several other PECVD processes,[18] the use of low frequency ultrashort square-wave pulse plasma DBD does not lead to an increase of the substrate temperature. Moreover, early trials of MMA and BMA films grown with low frequency modes all yielded highly viscous and non-regular coatings until inert gas curtain (*e.g.* argon) were added on each side of the deposition area, highlighting the importance of passivating the surrounding open-air atmosphere to avoid the non-negligible contamination and chain termination in accordance with our MS observations (Figure 5d-f). In addition to these few guidelines, the monomer chemical structure and intrinsic properties are expected to influence the PiCVD of polymer-like thin films. Notably, the propagation and termination rate constants (k_p and k_t) have been shown to influence the deposition kinetics.

3. Outlines

The side-mechanisms in plasma syntheses are unavoidable drawbacks of the process which require a careful consideration for the determination of the input parameters (i.e. power, on-time, off-time, pressure, atmospheric passivation, physical properties of the monomer …).

In this chapter, the application of nanopulsed plasmas (*ca.* 100 ns) for the deposition of 3 different methacrylates and the thorough study of the effect of different discharge frequencies (*i.e.* 31.6 – 10,000 Hz) on their properties highlighted different growth mechanisms compared to the sinusoidal source traditionally applied in plasma-polymerization.

The use of longer off-times (*ca.* t_{off} > 1 ms) strongly promotes a higher retention of the polymeric units' chemical functionalities, in exchange for lower deposition rates as the concentration of reactive species. Furthermore, the films' deposition were shown to be determined by surfaces mechanisms (*i.e.* adsorption, diffusion), allowing the growth of conformal polymer thin films, a feat unparalleled in atmospheric and plasma processes.

On the other hand, shorter off-times (*ca.* t_{off} < 1 ms) highlighted the existence of sudden transitions corresponding to shifts of predominant growth mechanism from surface free-radical polymerization (*i.e.* propagation and termination) to gas phase plasma polymerization mechanisms (*i.e.* fragmentation and recombination).

Finally, using 3 monomers from the same family, this study showed a deep influence of the chemical and physical properties on the resulting layers, especially visible by the strong discrepancies between ppMMA/ppBMA and ppGMA high-resolution mass spectrometry and size exclusion chromatography spectra.

In order to resolve those discrepancies, and to be able to further understand the growth mechanisms in the AP-PiCVD process, a deeper study of the high-resolution mass spectrometry data is necessary.

4. References

1. Boscher, N.D., Hilt, F., Duday, D., Frache, G., Fouquet, T., and Choquet, P. (2015) Atmospheric pressure plasma initiated chemical vapor deposition using ultra-short square pulse dielectric barrier discharge. *Plasma Process. Polym.*, **12** (1), 66–74.

2. Hilt, F., Boscher, N.D., Duday, D., Desbenoit, N., Levalois-Grützmacher, J., and Choquet, P. (2014) Atmospheric pressure plasma-initiated chemical vapor deposition (AP-PiCVD) of poly(diethylallylphosphate) coating: A char-forming protective coating for cellulosic textile. *ACS Appl. Mater. Interfaces*, **6** (21), 18418–18422.

3. Bonot, S., Mauchauffé, R., Boscher, N.D., Moreno-Couranjou, M., Cauchie, H.M., and Choquet, P. (2015) Self-Defensive Coating for Antibiotics Degradation - Atmospheric Pressure Chemical Vapor Deposition of Functional and Conformal Coatings for the Immobilization of Enzymes. *Adv. Mater. Interfaces*, **2** (14), 1500253.

4. Odian, G. (2013) *Principles of Polymerization*, Wiley-VCH.

5. Gleason, K.K. (2015) *CVD Polymers Fabrication of Organic Surfaces and Devices*, Wiley-VCH.

6. Lau, K.K.S., and Gleason, K.K. (2006) Initiated Chemical Vapor Deposition (iCVD) of Poly(alkyl acrylates): A Kinetic Model. *Macromolecules*, **39** (10), 3695–3703.

7. Atkins, P. (2006) *Physical chemistry*, Oxford University Press.

8. Friedrich, J. (2006) *The Plasma Chemistry of Polymer Surfaces*, Wiley-VCH.

9. Yasuda, H. (1985) *Plasma Polymerization*, Academic Press.

10. Socrates, G. (2004) *Infrared and Raman characteristic group frequencies*, Wiley-VCH.

11. Bellamy, L.J. (1980) *The Infrared Spectra of Complex Molecules*, Chapman and Hall.

12. Baitinger, W.F., Schleyer, P. vo. R., Murty, T.S.S.R., and Robinson, L. (1964) Nitro groups as proton acceptors in hydrogen bonding. *Tetrahedron*, **20** (7), 1635–1647.

13. Gordy, W. (1939) Spectroscopic evidence of hydrogen bonds: Aniline and some substituted phenols. *J. Chem. Phys.*, **7** (3), 167–171.

14. Beamson, G. Briggs, D. (1992) *High Resolution XPS of Organic Polymers*, Wiley-VCH.

15. Wang, M., Wang, X., Moni, P., Liu, A., Kim, D.H., Jo, W.J., Sojoudi, H., and Gleason, K.K. (2017) CVD Polymers for Devices and Device Fabrication. *Adv. Mater.*, **29** (11).

16. Knapp, C.E., Hyett, G., Parkin, I.P., and Carmalt, C.J. (2011) Aerosol-Assisted Chemical Vapor Deposition of Transparent Conductive Gallium - Indium - Oxide Films. **23** (7), 1719–1726.

17. Kobayashi, H., Bell, A.T., and Shen, M. (1974) Plasma Polymerization of Saturated and Unsaturated Hydrocarbons. *Macromolecules*, **7** (3), 277–283.

18. Boscher, N.D., Olivier, S., Maurau, R., Bulou, S., Sindzingre, T., Belmonte, T., and Choquet, P. (2014) Photocatalytic anatase titanium dioxide thin films deposition by an atmospheric pressure blown arc discharge. *Appl. Surf. Sci.*, **311**, 721–728.

CHAPTER IV – Nanopulsed discharges for the AP-PiCVD of polymer layers: a chemical study

This chapter aims at gaining a deeper understanding of the growth mechanisms and of the thin films' chemistry during the AP-PiCVD processes, when it is either predominant conventional polymerization pathways (*i.e.* low discharge frequencies) or predominant plasma-polymerization pathways (*i.e.* high discharge frequencies). A thorough study of the high-resolution mass spectrometry spectra obtained from MMA and GMA based layers grown at discharge frequencies of 100 and 10,000 Hz allows to extract the growth mechanisms behind the plasma-initiation polymerization during the discharge on-time and off-time. Ultimately, correlating those results with density functional theory (DFT) calculations yield key information on the relationship between the monomer's chemistry and the resulting fragmentation processes during the plasma discharges.

Article(s) published from these results

Loyer, F., Bengasi, G., Frache, G., Choquet, P., and Boscher, N.D. (2018) Insights in the initiation and termination of poly(alkyl acrylates) synthesized by atmospheric pressure plasma-initiated chemical vapor deposition (AP-PiCVD). *Plasma Process. Polym.*, **15** (5), 1800027.
Full contribution (experimental work on deposition, characterization and calculation, analysis and interpretation, redaction of the manuscript)

Abessolo Ondo, D., Loyer, F., Chemin, J.-B., Bulou, S., Choquet, P., and Boscher, N.D. (2018) Atmospheric plasma oxidative polymerization of ethylene dioxythiophene (EDOT) for the large-scale preparation of highly transparent conducting thin films. *Plasma Process. Polym.*, **15** (4), 1700172.
Partial contribution (analysis and interpretation of the HRMS data, calculation of EDOT's HOMO, redaction of the related section 3.2 that is presented in this thesis)

Content

1. Introduction

The combination of ultra-short (*i.e.* tens to hundreds of nanoseconds) plasma pulses together with long plasma off-time (*i.e.* up to hundreds of milliseconds) was demonstrated to efficiently initiate the free-radical polymerization of vinyl monomers while greatly reducing the detrimental plasma fragmentation (*cf.* Chapter 3).[1,2] By retaining the advantage of the regular PECVD systems (atmospheric, versatile, cheap) while promoting growth mechanisms comparable to vacuum CVD systems (conventional polymerisation, conformal deposition), the AP-PiCVD process appear as a promising alternative for the deposition of polymer thin films. Therefore, the methacrylate thin films grown in conditions promoting conventional polymerization, as determined in Chapter 3, will be denoted as conventional polymers (*i.e.* pMMA, pBMA, pGMA …) further on.

This first part of this Chapter provides an in-depth study of the high-resolution mass-spectra of the thin films elaborated from MMA and GMA at 100 Hz and 10,000 Hz. Indeed, the presence of numerous side-species on the high-resolution mass-spectra of the thin films grown at the lowest frequencies, typically below 100 Hz, remain unresolved. Notably, the $pMMA_{100Hz}$ (Figure 4.1a) and $pBMA_{100Hz}$ thin films displayed a very high chemical retention of their polymeric profile by FTIR and XPS. However, their high-resolution mass-spectrometry spectra obtained by MALDI-ORBITRAP showed numerous side-species hinting on dominant fragmentation/recombination mechanisms. Unlike the two other monomers studied along Chapter 3, the mass spectra of $pGMA_{100Hz}$ thin films grown under the same conditions (Figure 4.1b) is more consistent with the other chemical analyses (FTIR, XPS), being dominated by its pure oligomeric forms while the side-species appear with much lower intensities.

The second part of this Chapter will discuss the reactivity of monomers depending on their chemistry in order to relate the discrepancies between $pMMA_{100\ Hz}$'s and $pGMA_{100Hz}$'s spectra to plasma-induced growth mechanisms. Evidences of a strong influence of the monomer's chemistry on specific fragmentation pathways is evidenced from the methacrylates and further investigated by the study of a non-vinylic compound, *i.e.* 3,4-ethylenedioxythiophene (EDOT) in order to remove any conventional polymerization growth mechanism.

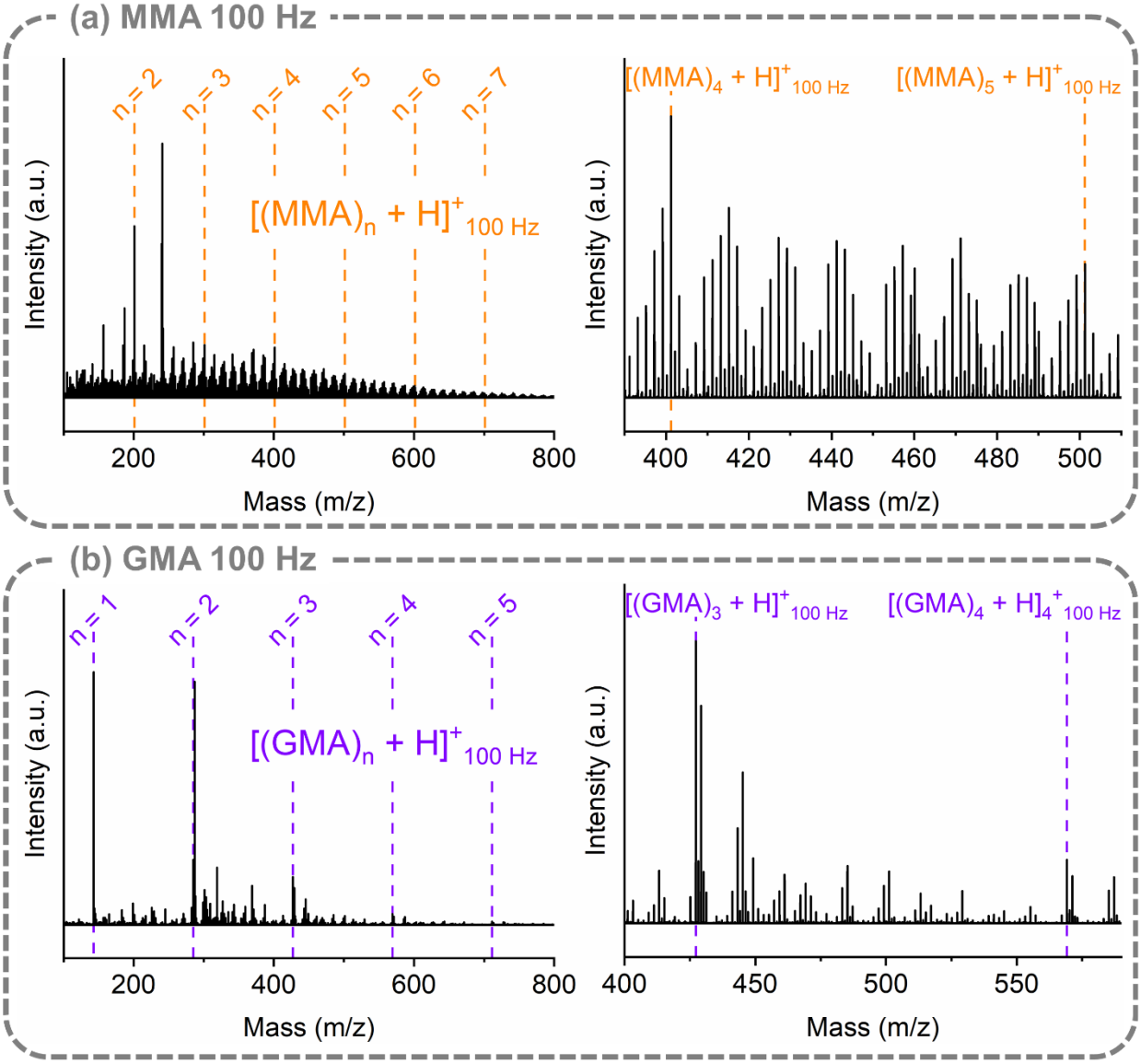

Figure 4.1. MALDI-HRMS spectra for thin films elaborated at a discharge frequency of 100 Hz from MMA in the mass range (a) m/z = 100-800 and m/z = 390-510, and (b) GMA in the mass range m/z = 100-800 and m/z = 400-590. Their respective oligomer units are indicated with dashed lines.

2. Results and discussion

2.1. Mechanisms during the plasma on time

While iCVD implies the use of an initiator with a labile bond (*e.g.* di-*tert*-butyl peroxide) cleaved into well-defined radicals by hot filaments to begin the free-radical polymerization of vinyl monomers,[3–5] AP-PiCVD relies on ultrashort plasma pulses to create radicals that further initiate the free-radical polymerization reaction. Since plasmas are composed of a wide variety of reactive species, including highly energetic species, a plurality of non-specific reactions (*i.e.* fragmentation or dissociation, ionization, recombination or integration) occurs

in PECVD processes.[6,7] The AP-PiCVD approach temporally isolate those discharges in order to lower the number of interactions between the plasma and the monomers, hence reducing the occurrence of those mechanisms over a full cycle ($t_{on} + t_{off}$). Still, in dielectric barrier discharge systems, the reactive species can reach high energies (*i.e.* tens of eV), [8–11] far above the bond dissociation energies of organic molecules (*i.e.* several eV).[12] Therefore, a sensible description of the role of temporally isolated discharges is a single fragmentation of the molecules per discharge, occurring on any bond of the molecule. From this assumption, a series of reactive radical fragments and their stabilized compounds can be proposed for each of the investigated monomers, *i.e.* MMA (Figure 4.2a) and GMA (Figure 4.3a). Thus, a quite simple hypothesis to interpret the high number of side-species observed by MALDI-HRMS (Figure 4.1) is that the radical species directly derived from the investigated monomer can freely play the role of initiating (R_i), terminating group (R_t) or simple adducts (vinyl) in the AP-PiCVD reaction. In addition, the formation of an unsaturation through intramolecular hydrogen transfer or simple disproportionation was also considered as a terminating process, yielding the oligomer form $[(M)_n + H]^+$ corresponding to the main mass peaks observed at low discharge frequency (Figure 4.1). Remarkably, the masses calculated for the $[R_i(M)_n R_t + H]^+$ oligomers, with R_i the initiating and R_t the terminating species selected from any of the fragments reported in Figure 4.2b (MMA) and Figure 4.3b (GMA), match with the main peaks detected via MALDI-HRMS. Quite visually, the experimental data and the calculated masses of the $[R_i(M)_n R_t + H]^+$ oligomers similarly arranged in sets of distributions spread between two successive conventional $[(M)_n + H]^+$ oligomer units (Figure 4.2c & 4.3c).

Such a peculiar distribution is arising from the single plasma-induced fragmentation of monomers composed of elements with close atomic masses (*i.e.* carbon and oxygen). Indeed, the proposed single plasma-induced fragmentation of the monomer considerably reduced the possible combinations between consecutive $[(M)_n + H]^+$oligomer units, giving rise to sets of $[R_i(M)_n R_t + H]^+$Gaussian shaped distributions roughly separated by 14 m/z. As a consequence, the number of sets observed between two successive $[(M)_n + H]^+$ oligomer units is directly related to the summed number of carbon and oxygen atoms composing the monomers (excluding the low atomic weight hydrogen atoms), respectively 7 atoms for MMA ($C_5H_8O_2$) and 10 atoms GMA ($C_7H_{10}O_3$).

Ultimately, using a simple assumption of a single breakdown of the monomer allowed to address the main side-species observed on the MALDI-HRMS spectra of the thin films synthesized at low plasma pulses frequency (f = 100 Hz). Accordingly, it can be assumed that the poly(methacrylates) thin films synthesized by AP-PiCVD mainly differ from their counterparts synthesized via conventional methods by the variety of their end-groups, *i.e.* $[R_i(M)_n R_t + H]^+$, clarifying the discrepancies between the chemical analyses and the mass spectrometry data reported in Chapter 3.

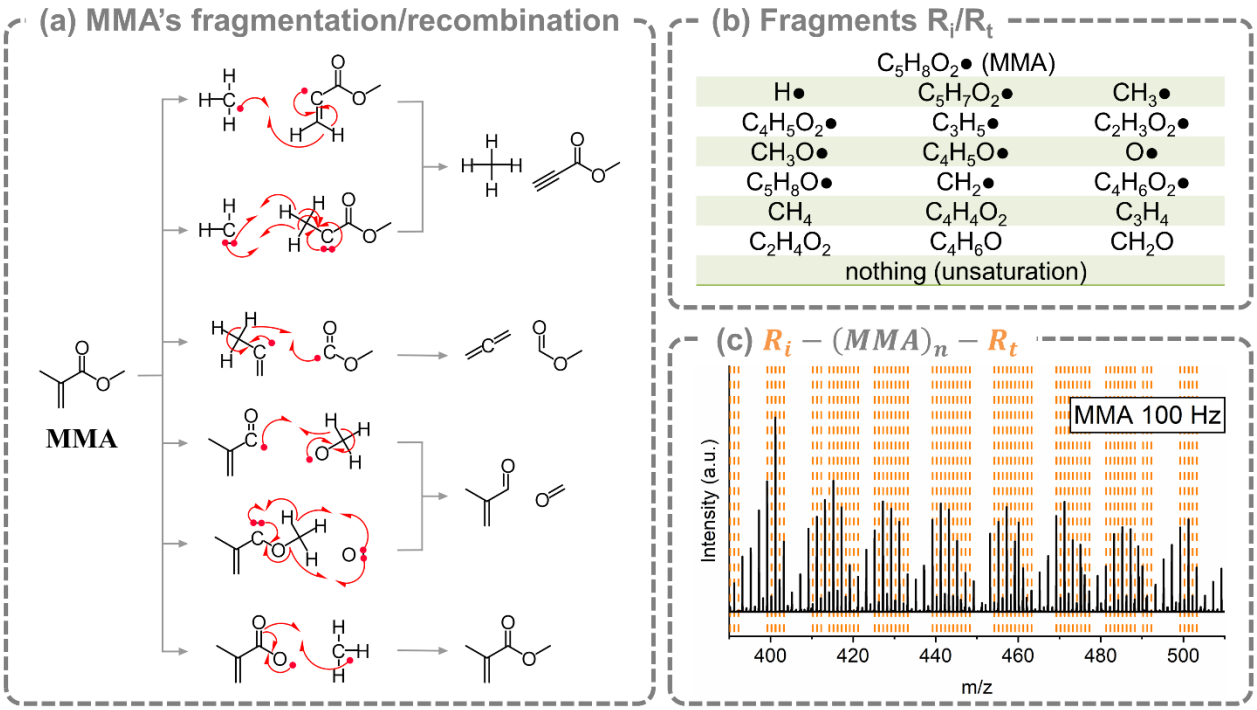

Figure 4.2. (a) Possible σ-bond breakdowns for a MMA molecule and proposed stabilization mechanisms via intramolecular electron flow and hydrogen abstraction. (b) Proposed list of resulting radical and neutral fragments. (c) MALDI-HRMS spectra in the mass range m/z = 390-510 of a thin film elaborated from MMA at 100 Hz. The mass peaks resulting from the possible $[R_i(MMA)_nR_t + H]^+$ combinations derived from table (b) are indicated in orange.

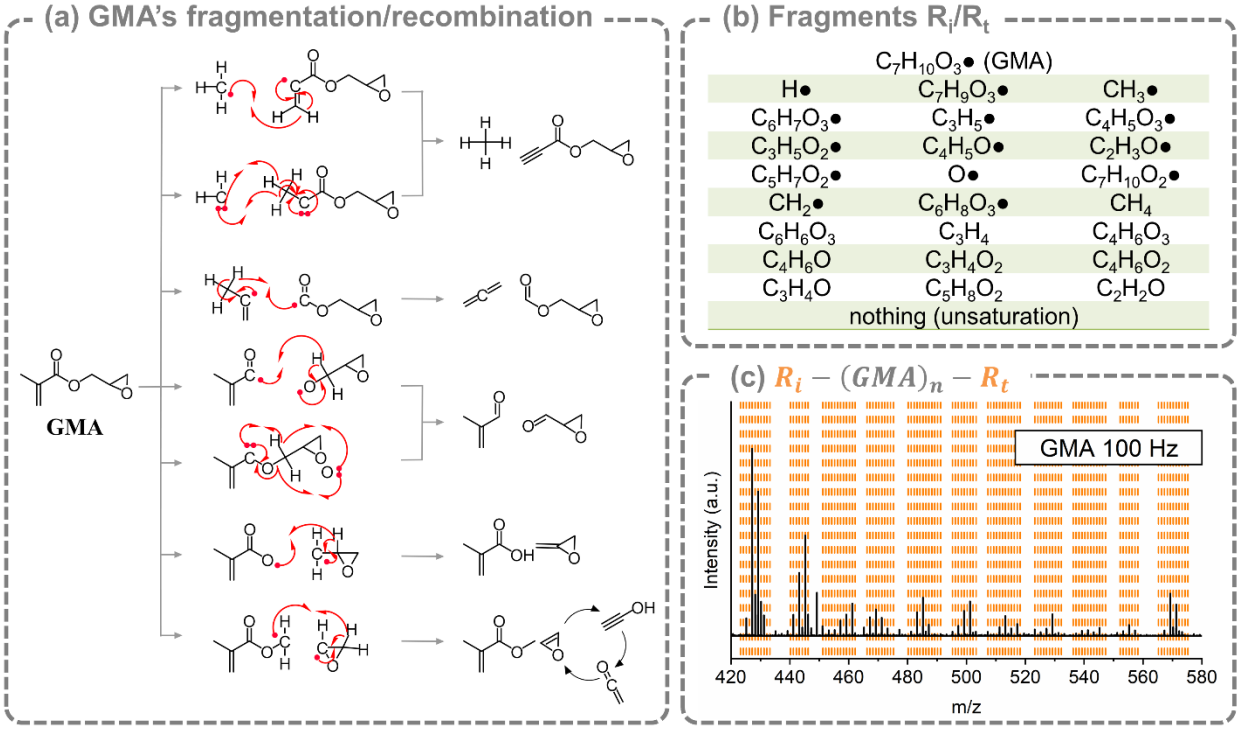

Figure 4.3 (a) Possible σ-bond breakdowns for a GMA molecule and proposed stabilization mechanisms via intramolecular electron flow and hydrogen abstraction. (b) Proposed list of the resulting radical and neutral radical fragments. (c) MALDI-HRMS spectra in the mass

range m/z = 420-520 of a thin film elaborated from GMA at 100 Hz. The mass peaks resulting from the possible $[R_i(GMA)_nR_t + H]^+$ combinations derived from table (b) are indicated in orange.

2.2. Mechanisms following the plasma on time

2.2.1. The reactivity of oxygen species versus the discharge frequency

The observations made above undoubtedly confirms that conventional polymers are grown during the AP-PiCVD of vinyl compounds and validates the hypothesis of a single plasma-induced fragmentation of the monomer as the main source of initiating and terminating radical species. Nevertheless, if a single plasma-induced fragmentation of the monomer allowed to allocate the main peaks recorded on the MALDI-HRMS (Figure 4.2c & 4.3c), even when taking into account the isotopic contribution, several peaks remained unaddressed. From these highly-resolved MS peaks, several side mechanisms have already been highlighted in Chapter 3. Notably mass transitions of m/z = ±0.0364, which can be extended to a higher set of transitions m/z = {±0.0364; ±0.0728; ±15.9266; ±15.963; ±15.9994; ±16.0358; ±16.0722; …} corresponding to different integration or subtraction mechanisms of oxygenated compounds. Interestingly, association of those oxygen-related masses – integration or subtraction – to the primary fragment's initiation/termination mechanism described above spreads the MS peaks over the whole mass range (Figure 4.4a). Ultimately, zooming in on the low-frequency MALDI-HRMS spectra of the thin films elaborated at 100 Hz demonstrates an almost complete assignation of the highly resolved mass peaks (Figure 4.4a).

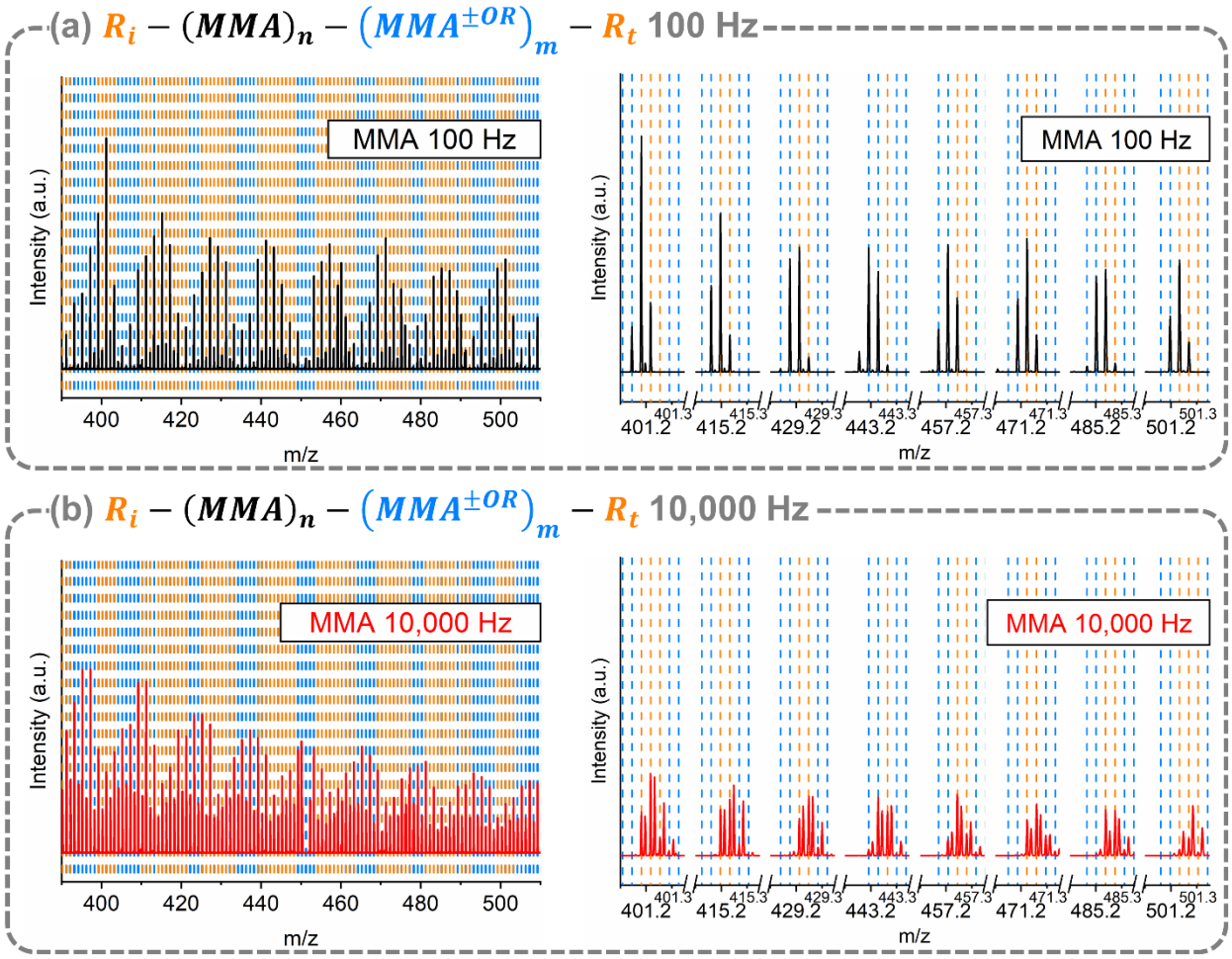

Figure 4.4. MALDI-HRMS spectra of MMA-based thin films grown at a discharge frequency of (a) 100 Hz and (b) 10,000 Hz in the mass range m/z = 390-510 and focused on the 100 Hz's maxima for each set of distribution between $[(MMA)_4 + H]^+$ (m/z = 401.2175) and $[(MMA)_5 + H]^+$ (m/z = 501.2699). The mass peaks resulting from the single plasma-induced fragmentation are indicated in dashed orange lines. The mass peaks arising from the integration or subtraction of oxygenated groups are depicted in dashed blue lines. For the ease of the readers, only the MMA's MALDI-HRMS spectra, selected for their more statistical distribution, are shown.

Both integration and subtraction of those oxygen-based compounds are both indiscriminately considered while they clearly are opposite mechanisms. Investigating how the oxygen integration or subtraction translate around the $[R_i(MMA)_nR_t + H]^+$ combinations shows that low frequency (f = 100 Hz) ultra-short plasma pulses engendered oxygenated groups integration (Figure 4.4a, 4.5). This is most likely originating from the steady reactivity of oxygen and water emanating from the surrounding atmosphere of the open-air reactor with the free-radicals still active on the substrate, clarifying the existence of strong hydroxyl vibration bands observed with FTIR (Figure 3.3) at long off-times (*i.e.* low discharge frequencies).

At high frequency (f = 10,000 Hz), the integration of oxygen becomes negligible and is replaced by the opposite mechanism, i.e. oxygen subtraction (Figure 4.4b, 4.5) in accordance with XPS results showing a decrease of the oxygen concentration when the pulse frequency increases (Figure 3.4). Unlike the integration of oxygen species which depended on the

lifetime and reactivity of the growing free-radical chains, the subtraction of oxygen is an instantaneous process induced by a molecular breakdown of the monomers.

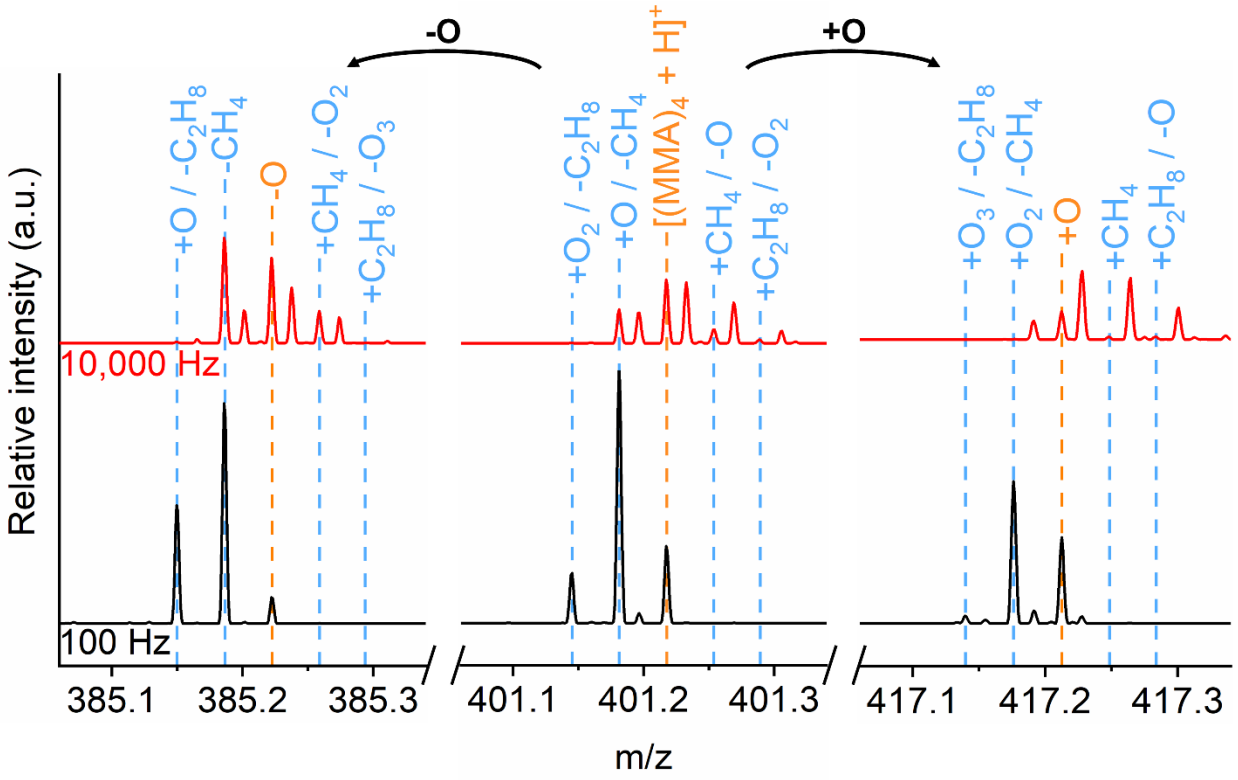

Figure 4.5. MALDI-HRMS spectra of MMA-based thin films at discharge frequencies of 100 Hz in black and 10,000 Hz in red focused on the n = 4 oligomer Gaussian distribution and the mass patterns resulting from one ±O translation. Both spectra are normalized according to the 4th oligomer (m/z = 401.2175). The mass peaks resulting from oxygen propagation $\pm OR$ are indicated in dashed blue lines

2.2.2. Carbon integration and crosslinking

Alongside the oxygen subtraction-related peaks observed for the high frequency (f = 10,000 Hz) discharges, some peaks remain undetermined, separated by a mass deficiency of m/z = +0.0164 from the mass peaks previously highlighted (Figures 4.5). Based on XPS (Figure 3.4) and FTIR (Figure 3.3) characterizations, it is known that increasing the plasma pulses frequency leads to a decrease in the oxygen content ($-O$ subtraction) and an increase of the carbon content ($+C$ addition) into the grown layers. Applying carbon $+CR_y$ repetitions to the mass distributions ensures a complete coverage of the mass spectra (Figure 4.6). Interestingly, unlike the integration and subtraction of oxygen-related mechanisms discussed above, the subtraction of carbon is not evidenced by any mass peaks and can be considered as an absent mechanism. As such, an increase in the carbon backbone structure, *i.e.* cross-linking, is consistent with a statistical fragmentation of the monomer. Essentially, while the carbon integration is completely absent from the dominant species for the films elaborated at the lowest frequency (Figure 4.6), carbon integration is preeminent for the films elaborated from the highest frequency, indicating a strong alteration of the chemistry at 10,000 Hz.

Ultimately, the switch between a chemistry defined by $[R_i(M)_nR_t + H]^+$ or $[R_i(M)_n(M^{+OR})_mR_t + H]^+$ for the films synthesized at low-frequency (100 Hz) to a chemistry

expressed by $[R_i(M)_n(M^{+OR})_m(M^{-OR})_o(M^{+CR})_lR_t + H]^+$ at high-frequency (10,000 Hz) is highly characteristic of the transition from conventional polymerization to plasma-polymerization where the dominant structures become heavily altered through $+C_y/-O_x$ mechanisms.

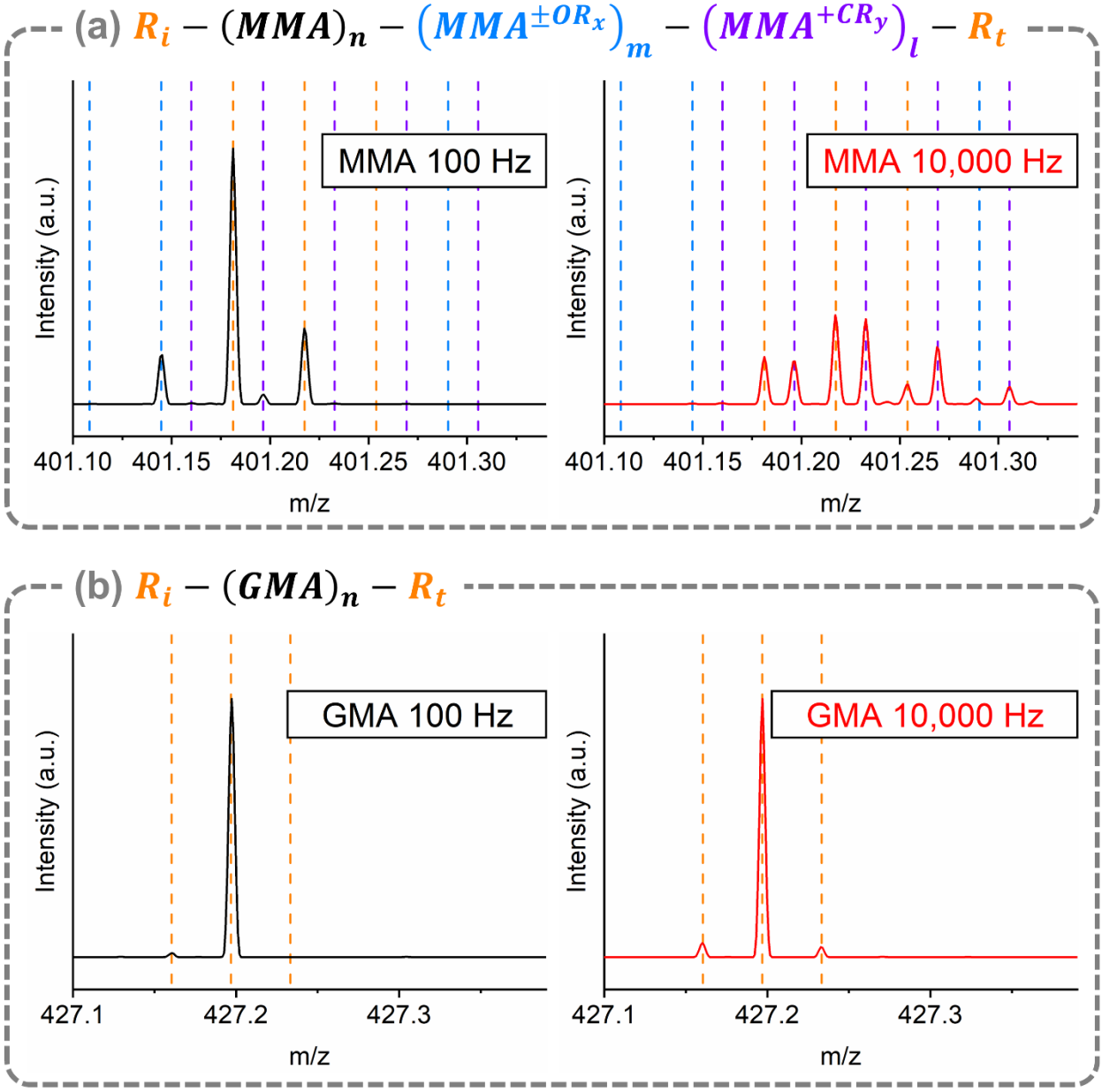

Figure 4.6. MALDI-HRMS spectra of (a) MMA and (b) GMA thin films in at discharge frequencies of 100 Hz and 10,000 Hz zoomed around MMA's 4th oligomer (m/z = 401.2175) and GMA's 3rd oligomer (m/z = 427.1968) respectively.

2.2.3. Specific and non-specific fragmentation mechanisms

Both of the mass spectra of the thin films elaborated from MMA and GMA at low plasma pulses frequencies (f = 100 Hz) almost exclusively result from the combination of the various $[R_i(M)_n(M^{+OR})_mR_t + H]^+$ possibilities. However, the discrepancies in the MS peaks distributions between $pMMA_{100\ Hz}$ and $pGMA_{100\ Hz}$ (Figure 4.2c, 4.3c) and the magnitude of

the side mechanisms (Figure 4.6) suggest a strong influence of the monomer itself on the plasma-initiated polymerization pathway.

Different frequency thresholds related to the coating properties were highlighted in the chapter 3, such as its polymeric growth, observed by SEC (Figure 3.6), as well as the film's surface morphology and conformality using SEM (Figure 3.8 & 3.9). The switch from conformal films to granular films was easily explained by an excess of reactive species as the discharge frequency intensify. The increased interactions between the plasma and the monomer inducing a change from surface to gas phase reactions, hinting on an intimate relation with the monomer's intrinsic ability to adsorb (*cf.* BET isotherm equation P_M/P_{sat}).[13]

On the other hand, SEC measurements of the films elaborated from different methacrylate monomers revealed a common plasma pulses frequency threshold from conventional polymers to plasma-polymers. This collective limit suggests a global energy maximum for this family of monomer, transitioning from low plasma pulses frequency mechanisms (*i.e.* plasma–induced initiation/termination from fragments and oxygen integration mechanisms) to high plasma pulses frequency mechanisms (*i.e.* oxygen subtraction and carbon integration and cross-linking mechanisms). However, important differences in the average molar masses in weight (Mw) were observed between the $pMMA_{100\ Hz}$ ($M_W \approx$ 2,600 g•mol^{-1}) and $pGMA_{100\ Hz}$ (M_W = 94,000 g•mol^{-1}) thin films (Figure 3.6). Such difference in polymeric length is indicative of termination mechanisms and readily correlates with the MMA's intense and GMA's very minor side-species on the MS spectra of the respective thin films elaborated at low plasma pulses frequency.

To understand the strong difference in average molar weight in mass between the pMMA and pGMA layers grown by AP-PiCVD, DFT calculations were performed and the stability of each bond was compared to the electron energy distribution of the plasma phase. Inspection of the calculated highest occupied molecular orbitals (HOMO) of both MMA and GMA (Figure 4.7) distinctly shows strong electron density on the vinyl function as well as the oxygens' nonbonding electrons and the methyl C-H bonds, highlighting the favored free radical polymerization pathway. The possible electron/hydrogen delocalizations within the molecule through the methyl/vinyl or carboxyl/vinyl are also observed.

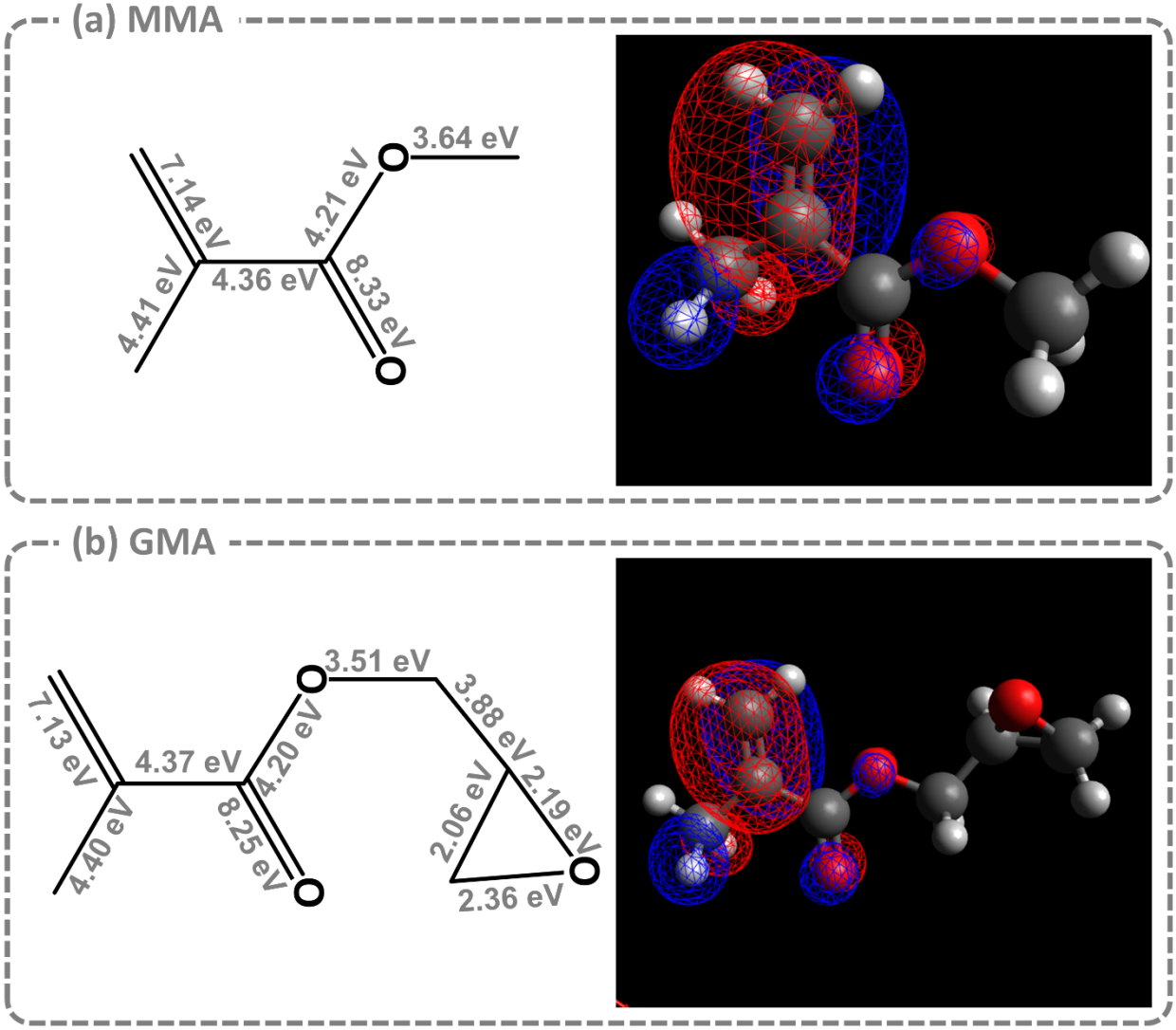

Figure 4.7. Bond dissociation energies (BDE) and highest occupied molecular orbitals' (HOMO) electron density of (a) MMA and (b) GMA calculated with DFT geometrical and frequency optimization

Moreover, calculation of the bond dissociation energies (BDE) of MMA (Figure 4.7a) points out the ether/methyl as the weakest bond (*e.g.* 3.64 eV). Yet, the differences in energy with the other single σ-bonds are globally quite low (ΔBDE < 0.5 eV), consistently with MMA's evident sensitivity to a non-specific molecular breakdown. On the other hand, the epoxy function in the GMA molecule (Figure 4.7b) appears considerably weaker than the other single σ-bonds ($\Delta BDE \approx$ 2 eV), suggesting a much greater sensitivity to specific plasma breakdown as its BDE would be in the lower part of the electron energy density. Indeed, a homolytic breakdown and hydrogenation of the epoxy ring $[(GMA)_n + H_2 + H]^+$ matches with previous FTIR analyses (Figure 3.3) and the mass value corresponding to the low frequency's second most and high frequency's most dominant compound in MALDI-HRMS (Figure 4.8). Still, the periodical distribution of the molecular breakdown remains observable for GMA, highlighting the competition between a non-specific breakdown due to the highly energetic species within the plasma phase (> 6 eV) and specific fragmentations due to the molecule chemical sensitivity itself.

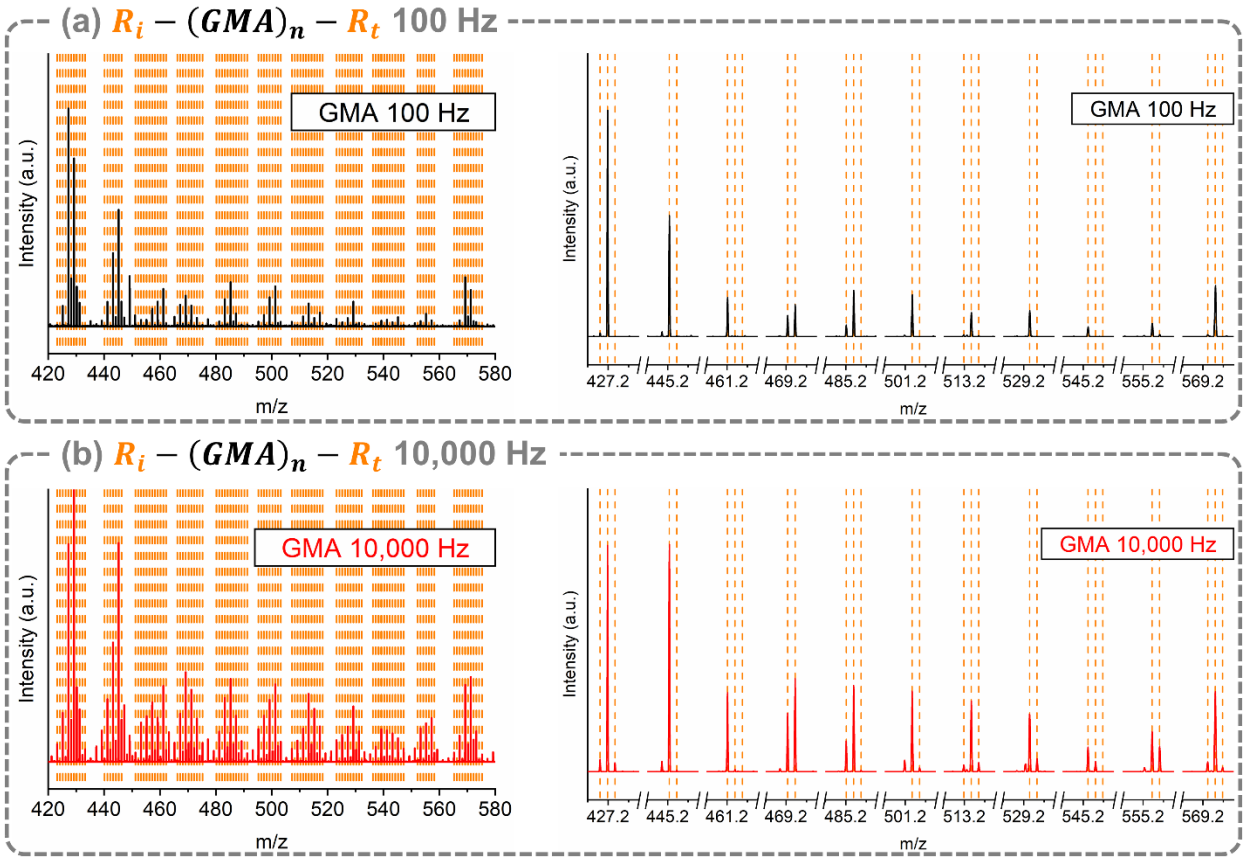

Figure 4.8. MALDI-HRMS spectra of GMA based thin films (a-b) in the mass range m/z = 420 580 at a discharge frequency of (a) 100 Hz and (b) 10,000 Hz. MALDI-HRMS spectra of GMA based thin films focused on the 100 Hz's maxima for each distribution between GMA's third (m/z = 427,1968) and fourth (m/z = 569,2598) oligomers are displayed. The mass peaks resulting from the 1st order mechanism are indicated in dashed orange.

2.2.4. Sacrificial functions for specific fragmentation: the oxidative plasma-polymerization of ppEDOT

The molecule functionalities' influence on PECVD processes have been studied several times over the last 3 decades, from Yasuda early works highlighting the impact of the molecule functionalities on the deposition rate[14] and the sensitivity to hydrogen abstraction[15] to very recent progresses in the understanding of the process kinetic[16–19] or the influence of double bonds on the growth mechanisms.[18–20] Altogether, those numerous studies point to the same direction, using the molecule's functionalities as a mean to circumvent the unavoidable molecular breakdown induced by plasma media. This observation also applies where the negative impact of plasma is strongly attenuated, such as in the PiCVD approach. Indeed, if the long off-time ensure conventional polymerization pathways, the intense non-specific plasma-induced fragmentation creates species able to entirely block the reactive end of the growing chains, yielding low molecular weight polymers (Figure 3.8).

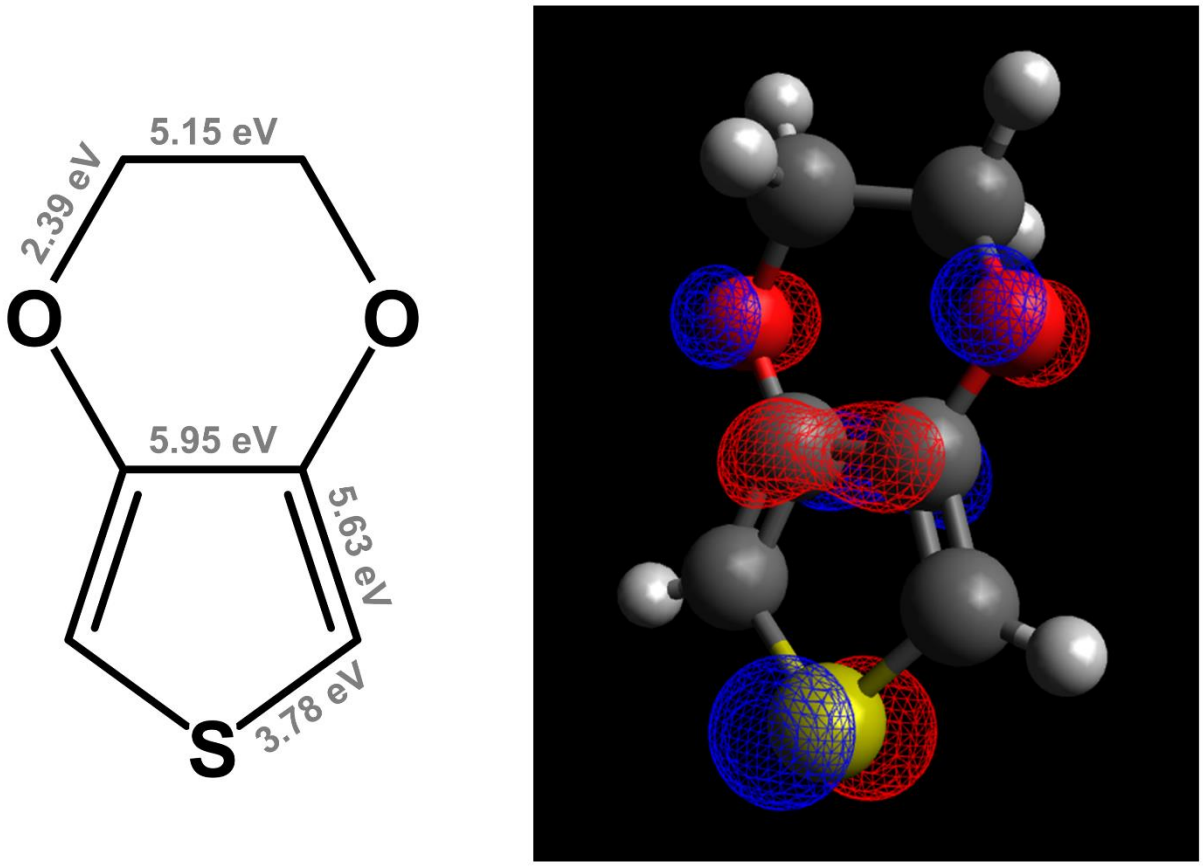

Figure 4.9. Bond dissociation energies (BDE) and highest occupied molecular orbitals' (HOMO) electron density of EDOT calculated with DFT geometrical and frequency optimization. Figure (a) reproduced from Liu, C., Goeckner, M.J., and Walker, A. V. (2017) Plasma polymerization of poly(3,4-ethylenedioxyethene) films: The influence of plasma gas phase chemistry. *J. Vac. Sci. Technol. A Vacuum, Surfaces, Film.*, **35** (2), 21302.[21]

Several approaches can be conceived to improve the efficiency of a targeted monomer such as using additional polymerization promoters (*e.g.* vinyl group) or sacrificial function (*e.g.* epoxy group). If the former is a well-known concept as per the forementioned studies, the latter opens new perspectives in plasma-polymers chemistry as correctly functionalizing the molecule will create a buffer effect globally reducing the plasma-induced breakdown, while promoting adhesion through a natural cross-linking in the case of the epoxy. This strategy is not specific to free-radical polymerization of vinyl compounds and may be implemented to promote a higher selectivity for the PECVD reaction of other compounds. In particular, the use of a sacrificial function is of the utmost importance when the growth mechanisms require harsher conditions. In contrast with the free-radical polymerization that can self-sustain for several tens of milliseconds at atmospheric-pressure, the oxidative polymerization of thiophene-based monomers requires two electrons per monomer unit. Thus, high ultrashort plasma pulse frequencies are needed to generate a sufficient amount of ROS over an appropriate duration. For instance, conductive and transparent thin films of ppEDOT were deposited by plasma-assisted oxidative polymerization using AP-DBD ignited with a 5,000 kHz ultrashort plasma pulse frequency and fed with an argon-oxygen mixture containing 5% of oxygen. In these extreme conditions, a complete fragmentation of the molecule could be expected, yet electrical measurements confirmed a conductivity of 10^{-2} S•cm^{-1} indicating a long-range order coupling.

Interestingly, Liu et al. have determined the bond dissociation energies of the EDOT molecule using DFT calculation (Figure 4.9).[21] Consistently, the weakest functions are the two rings composing EDOT, more specifically the C-O of the dioxyethylene ring (BDE = 2.39 eV) and the C-S of the thiophene (BDE = 3.78 eV) should go through specific fragmentation mechanisms. In order to gain insight on the growth mechanisms of this oxidative polymerization, the MALDI-HRMS spectrum of ppEDOT grown by ultrashort plasma pulsed AP-DBD was investigated (Figure 4.10). While the pure PEDOT oligomer units $[H(C_6H_4SO_2)_nH + H]^+$ were detected up to the trimer, demonstrating the ability to promote an oxidative polymerization pathway using atmospheric-pressure plasma. The mass spectra of all samples elaborated in the presence of oxygen appears to be dominated by a series of PEDOT oligomers terminated with hydrogen and carbonated groups $[H(C_6H_4SO_2)_nCH + H]^+$ detected up to the pentamer units (Figure 4.10). In between those prevailing species, as for the methacrylates, numerous side-species corresponding to non-specific mechanisms are divided in Gaussian-like distributions.

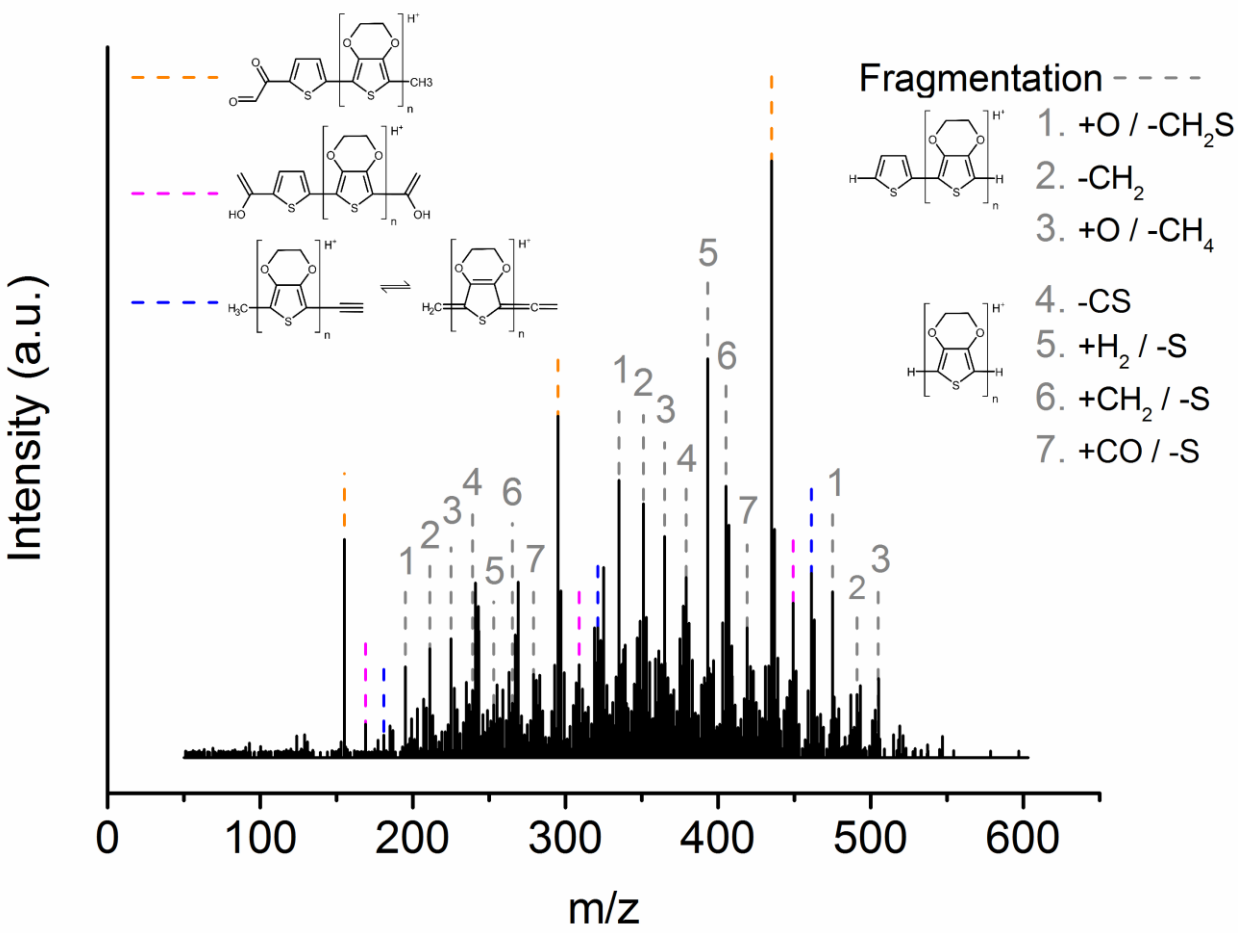

Figure 4.10. MALDI-HRMS spectra in the mass range m/z = 50–600 of the ppEDOT grown from a plasma gas containing 5% of oxygen and at a discharge frequency of 5,000 Hz.

Because the dioxyethylene ring is by far the weakest function, the potential cleavage orderings of the dioxyethylene ring as well as the resulting species were investigated, yielding pure EDOT and thiophene as the most probable monomer blocks along with several notable secondary species such as glyoxal (O=CH–HC=O), ketene (H_2C=C=O) and acetylene (HC≡CH) (Figure 4.11). As such, The previously reported dominant chemical states, $[H(C_6H_4SO_2)_nH + H]^+$, can be chemically expressed as a mix between at least one thiophene

and either no or several EDOT units, likely terminated by a methyl and a glyoxal group. Observing both the loss of the dioxyethylene ring (*i.e.* the breakdown from EDOT to thiophene) and the integration of the glyoxal as a recurrent and prevailing condition would suggest intramolecular one-pot ring-fragmentation/fragment-addition/thiophene-polymerization from the side species. Furthermore, while not as abundant, numerous other fragments and monomer associations are detected at various chain lengths suggesting a strong link between the terminal ends and the conductivity.

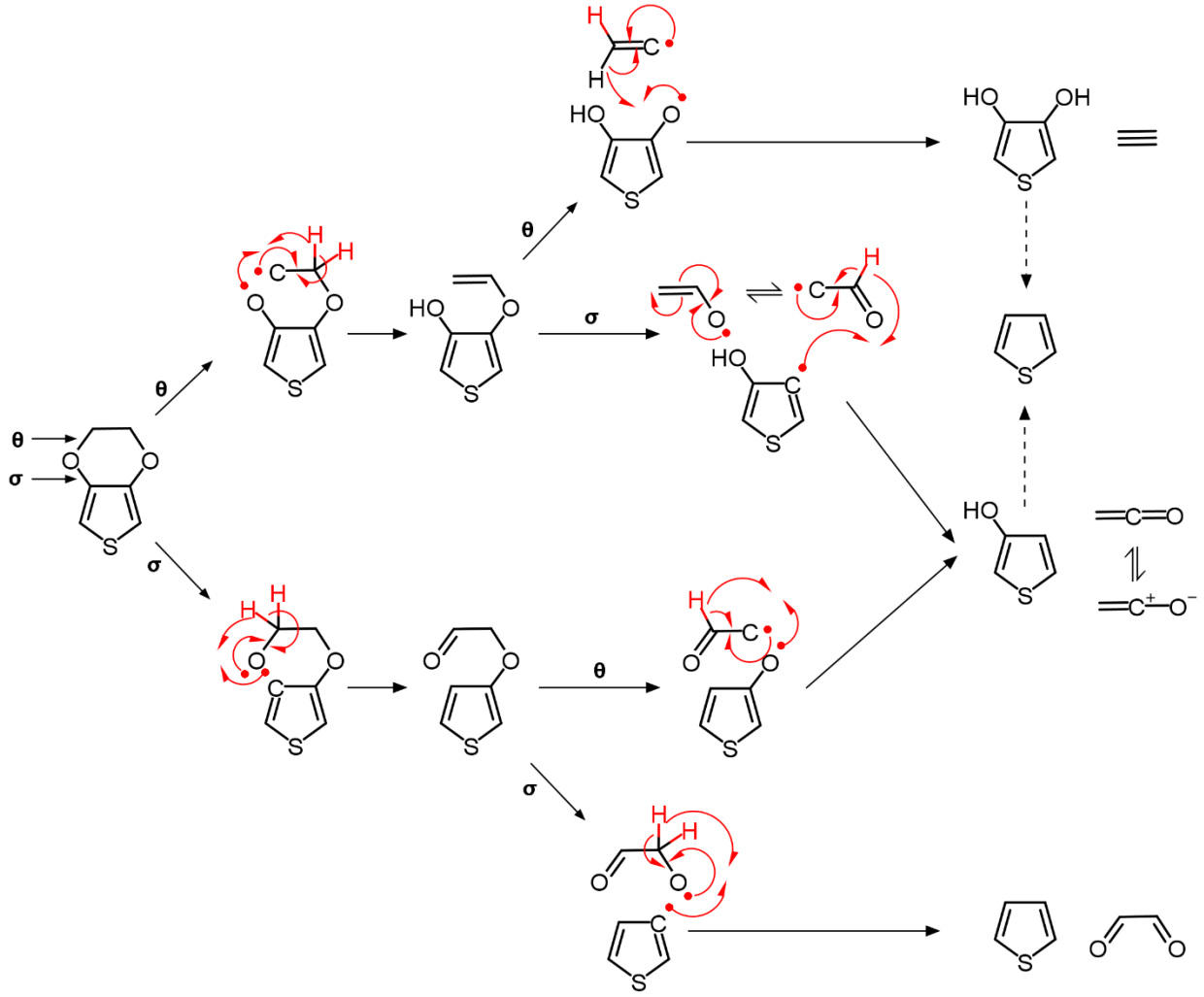

Figure 4.11. Proposed mechanisms for the dioxyethylene ring breakdown through inner (σ) or outer (θ) cleavages along with their respective resulting fragments

Indeed, almost all the possible EDOT/thiophene associations of oligomer units with the different terminal ends arising from the glyoxal formation were identified on the experimental mass spectrum of the ppEDOT thin film elaborated in the presence of oxygen (Figure 4.10). Considering their nature (*i.e.* dialdehydes, vinylic aldehyde, acetylene...) the dioxyethylene side-species appear able to promote oxidative polymerization, either through usual oxidation process yielding typical growing PEDOT or through a nucleophilic aromatic addition. As predicted from its bond dissociation energy, the fragmentation of the dioxyethylene function is the most dominant mechanisms during the plasma on-time, serving the role of sacrificial function for the rest of the molecule which is sufficiently preserved from non-specific fragmentation to be conductive. Unfortunately, the sub-species of the dioxyethylene

fragmentation are highly reactive species able to react with the EDOT species, blocking its terminal ends further preventing the growth of long coupled polymer chains.

Furthermore, as expected from its lower than average BDE, the thiophene ring also suffers from specific fragmentation as seen by the second most dominant EDOT-periodic series of peaks observed in the MALDI-HRMS spectrum, although at a much lower level than the dioxyethylene.

Ultimately, due to the high frequencies and strong ROS, the plasma-assisted oxidative polymerization of ppEDOT combined both strong specific and non-specific mechanisms. The dioxyethylene acting as a sacrificial function allowed for the deposition of EDOT/thiophene chains retaining their coupling, hence their macroscopic conductivity. A promising alternative to promote the growth of conventional pEDOT by ultrashort plasma pulsed AP-DBD would be to replace the dioxyethylene by another sacrificial function which do not fragment entirely under the plasma.

3. Outlines

The determination of the growth mechanisms is a key challenge for all PECVD processes. Unlike conventional chemistry-based techniques (wet, iCVD, oCVD, …), a complete resolution of the mechanisms and the polymer final structure is almost impossible due to the high energy species from the plasma yielding unavoidable non-specific reactions.

Rather than finding the exact chemistry of the structure, combining a global solution and a precise determination of the chemistry appeared more fitted for plasma polymers. Notably, the FTIR and XPS analyses of MMA and GMA both yielded an excellent retention of the chemistry, which correspond to the core of the polymer chain grown during the off-time. Yet, other key properties such as the molar weight required information to correlate them with their chemistry, notably on the growth mechanisms occurring during the on-time. To that aim, high-resolution mass spectrometry such as MALDI-ORBITRAP are absolutely required to separate the numerous species which would otherwise overlap. Calculating the mass deficiency around the known oligomer peaks yields many information in the form of patterns, not directly on the chemical structure but on the ongoing mechanisms.

Using this approach, more than 99% of the mass spectra were solved, giving information on the true chemistry and the form of the polymer for MMA and GMA grown by AP-PiCVD. Furthermore, their difference of properties could be related to the initial fragmentation during the on-time, during which MMA breaks down completely yielding fragments blocking its reactive ends and preventing further propagation. GMA, on the other hand, is protected by its epoxy function which act as sacrificial function due to its much lower BDE than the rest of the molecule.

These two kinds of behavior, which we referred to as non-specific and specific fragmentation, are crucial for the final properties of the plasma polymer thin film and can be predicted from the monomer itself using calculation methods such as DFT. Molecules with an overall low difference in BDE will fragment in an non-specific way since they have no preferential attack point other than the vinyl, yielding short polymer chains with an higher alteration of the chemistry. On the other hand, having more than one function with low to very low BDE, it will protect the rest of the molecule, as those function will be easily targeted by the energy species.

Therefore, choosing the sacrificial function is key for optimizing the properties of the resulting thin films. In the example of the ppEDOT synthesis, the thiophene ring was an easy target for specific fragmentation due to its slightly lower BDE. Yet, due to the presence of the dioxyethylene which had four breaking points with very low BDE, conductive ppEDOT was successfully synthesized.

If, from the experimental observations, the influence of the sacrificial function appears determinant in the resulting properties of the plasma-polymerized films, it is of high interest to couple experimental data with more theoretical studies going in-depth in the pulsed plasma-polymerization mechanisms.

4. References

1. Boscher, N.D., Hilt, F., Duday, D., Frache, G., Fouquet, T., and Choquet, P. (2015) Atmospheric pressure plasma initiated chemical vapor deposition using ultra-short square pulse dielectric barrier discharge. *Plasma Process. Polym.*, **12** (1), 66–74.

2. Hilt, F., Boscher, N.D., Duday, D., Desbenoit, N., Levalois-Grützmacher, J., and Choquet, P. (2014) Atmospheric pressure plasma-initiated chemical vapor deposition (AP-PiCVD) of poly(diethylallylphosphate) coating: A char-forming protective coating for cellulosic textile. *ACS Appl. Mater. Interfaces*, **6** (21), 18418–18422.

3. Gleason, K.K. (2015) *CVD Polymers Fabrication of Organic Surfaces and Devices*, Wiley-VCH.

4. Lau, K.K.S., and Gleason, K.K. (2006) Initiated Chemical Vapor Deposition (iCVD) of Poly(alkyl acrylates): A Kinetic Model. *Macromolecules*, **39** (10), 3695–3703.

5. Lau, K.K.S., and Gleason, K.K. (2006) Initiated chemical vapor deposition (iCVD) of poly(alkyl acrylates): An experimental study. *Macromolecules*, **39** (iCVD), 3688–3694.

6. Lu, X., Naidis, G. V., Laroussi, M., Reuter, S., Graves, D.B., and Ostrikov, K. (2016) Reactive species in non-equilibrium atmospheric-pressure plasmas: Generation, transport, and biological effects. *Phys. Rep.*, **630** (April), 1–84.

7. Friedrich, J. (2006) *The Plasma Chemistry of Polymer Surfaces*, Wiley-VCH.

8. Friedman, A. (2008) *Plasma Chemistry*, Cambridge University Press.

9. Umran, I., and Golkowski, M. (2011) *Principles of Plasma Physics for Engineers and Scientists*, Cambridge University Press.

10. Christophorou, L.G., and Olthoff, J.K. (2004) *Fundamental Electron Interactions with Plasma Processing Gases*, Springer.

11. Goldston, R.J., and Rutherford, P.H. (1995) *Introduction To Plasma Physics*, IOP Publishing.

12. Luo, Y.-R. (2003) *Handbook of Bond Dissociation Energies in Organic Compounds*, CRS Press LLC.

13. Atkins, P. (2006) *Physical chemistry*, Oxford University Press.

14. Yasuda, H. (1981) Glow discharge polymerization. *J. Polym. Sci. Macromol. Rev.*, **16** (1), 199–293.

15. Yasuda, H., Bumgarner, M.O., and Hillman, J.J. (1975) Polymerization of organic compounds in an electrodeless glow discharge. V. Amines and nitriles. *J. Appl. Polym. Sci.*, **19**, 1403–1408.

16. Hegemann, D., Hossain, M.M., Körner, E., and Balazs, D.J. (2007) Macroscopic description of plasma polymerization. *Plasma Process. Polym.*, **4** (3), 229–238.

17. Hegemann, D., Körner, E., and Guimond, S. (2009) Plasma polymerization of acrylic acid revisited. *Plasma Process. Polym.*, **6** (4), 246–254.

18. Scheltjens, G., Da Ponte, G., Paulussen, S., De Graeve, I., Terryn, H., Reniers, F., Van Assche, G., and Van Mele, B. (2016) Deposition Kinetics and Thermal Properties of Atmospheric Plasma Deposited Methacrylate-Like Films. *Plasma Process. Polym.*, **13** (5), 521–533.

19. Nisol, B., Watson, S., Lerouge, S., and Wertheimer, M.R. (2017) Energetics of reactions in a dielectric barrier discharge with argon carrier gas: V hydrocarbons. *Plasma Process. Polym.*, **14** (8), 1600191.

20. Nisol, B., Arnoult, G., Bieber, T., Kakaroglou, A., De Graeve, I., Van Assche, G., Terryn, H., and Reniers, F. (2014) About the influence of double bonds in the APPECVD of acrylate-like precursors: A mass spectrometry study of the plasma phase. *Plasma Process. Polym.*, **11** (4), 335–344.

21. Liu, C., Goeckner, M.J., and Walker, A. V. (2017) Plasma polymerization of poly(3,4-ethylenedioxyethene) films: The influence of plasma gas phase chemistry. *J. Vac. Sci. Technol. A Vacuum, Surfaces, Film.*, **35** (2), 21302.

CHAPTER V - Nanopulsed discharges for the AP-PiCVD of polymer layers: a kinetic study

This chapter aims at providing a model to give a qualitative description of the plasma-polymerization mechanisms that drive the synthesis and deposition of polymer layers in AP-PiCVD. As such, the development of a theoretical-experimental model named the pulsed plasma method (PPM) is detailed and applied to the cases of MMA and GMA. Important information on the growth mechanism are obtained, notably on the plasma-polymerization kinetic, the impact of the nanosecond discharge on the chemistry of the plasma-polymer and on the reactivity of free-radicals in the gas phase and at the surface.

Article(s) published from these results

Loyer, F., Frache, G., Choquet, P., and Boscher, N.D. (2017) Atmospheric Pressure Plasma-Initiated Chemical Vapor Deposition (AP-PiCVD) of Poly(alkyl acrylates): An Experimental Study. Macromolecules, 50 (11), 4351–4362.
Full contribution (experimental work on deposition, analyses and interpretation, development of the equations, redaction of the manuscript)

Content

1. Introduction

The experimental analyses of the methacrylate-based layers grown by AP-PiCVD and described in Chapter 3 and Chapter 4 highlighted the ability of nanopulsed discharges to strongly promote conventional free-radical polymerization pathways. Consecutive to the ultra-short discharge (*i.e.* t_{on} = 100 ns), the plasma produces radicals and the vinylic monomers adsorb on the substrate where the free-radical polymerization is occurring, ensuring an excellent retention of their chemical structure. Long plasma off-times, in accordance with the adsorbed free-radicals' lifetime, further reduce the fragmentation mechanisms while promoting surface mechanisms and the growth of conformal layers under atmospheric conditions (Figure 5.1a).

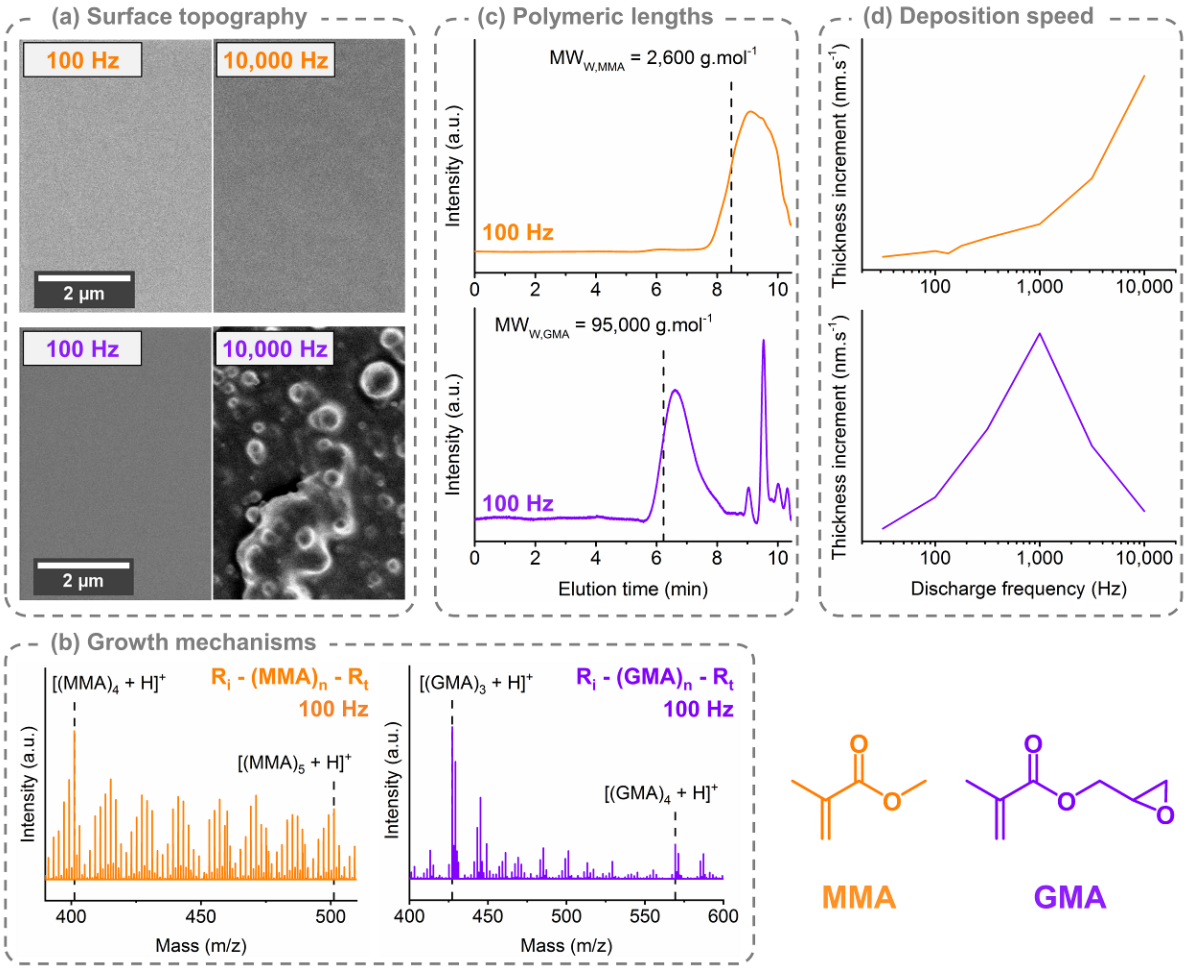

Figure 5.1. Summary of experimental data for MMA and GMA-based thin films grown by AP-PiCVD (presented in Chapters 3 and 4) on which the present kinetic study relies on, namely (a) the surface topography by scanning electron microscopy (SEM) of the thin films grown at 100 and 10,000 Hz, (b) the matrix-assisted laser desorption/ionization high-resolution mass spectra (MALDI-HRMS) of the thin films grown at 100 Hz, (c) the size distribution by size exclusion chromatography (SEC) of thin films grown at 100 Hz and (d) the deposition rate according to the discharge frequency.

Consequently, the chemical and physical properties of the thin films grown using ultra-short plasma pulses result from a competition between conventional polymerization reactions

(initiation, propagation and termination) and plasma-polymerization reactions (fragmentation and recombination). Such competition is notably expressed by the switch from oxygen integration at low plasma discharges frequencies to oxygen depletion and carbon integration when the frequency of plasma pulses increases. This transition is accompanied by variations in the morphology of the produced thin films, as a result of a shift from predominant gas phase mechanisms to predominant surface mechanisms (Figure 5.1a). The prevalence of those proposed reaction pathways is governed by the plasma discharge conditions and gas phase composition, revealing strong discrepancies between monomers of the same family (Figure 5.1b). In particular, previous works highlighted that the polymerization kinetics of AP-PiCVD are strongly related to the monomers' sensitivity to fragmentation during the nanopulsed discharge (Figure 5.1c) and the repetition frequency of the ultra-short plasma pulses (Figure 5.1d). The present chapter aims at providing a model to describe and understand the AP-PiCVD kinetic data. Since the polymerization does not take place under steady-state conditions in AP-PiCVD, a new model called the pulsed plasma method (PPM) is proposed. Unlike other models describing the kinetic of plasma polymerization, the PPM model integrates the non-steady plasma initiation, the polymerization propagation and termination, as well as chain transfer events, allowing an extraction and comparison of the kinetic parameters highlighting the key mechanisms undergone by the monomer under pulsed plasma discharges. Moreover, evidences from the PPM model provide chemical and physical descriptions for previously reported frequency-dependent transitions in AP-PiCVD and the dominant mechanisms for different deposition conditions.

2. Results and discussion

2.1. Model development

Such as depicted in Figure 5.2, the proposed mechanisms for the AP-PiCVD polymerization start with the monomer's ($M_{(g)}$) homolytic activation by the ultra-short plasma pulses leading to either (i) the creation of radical monomer species ($M\bullet_{(g)}$) out of the vinyl's π-bond opening or (ii) the statistical cleavage of the whole molecule forming radical fragments ($X\bullet_{(g)}$), resulting from low energy (ca. $\varepsilon_{(i)} \geq 2$ eV) and high energy (ca. $\varepsilon_{(ii)} \geq 4$ eV) electronic interactions.[1–4]

Subsequently, the primary radicals ($M\bullet_{(g)}$) and fragments ($X\bullet_{(g)}$) may either (iii) recombine ($M_{(g)}$ or $X_{(g)}$) or (iv) diffuse to the surface where they are adsorbed ($M\bullet_{(ad)}$ and $X\bullet_{(ad)}$) allowing (v) the polymerization to propagate freely.

Additionally, neutral fragments ($X_{(ad)}$, and contributions from the atmosphere) may also interact during the polymeric growth by chain transfer reactions (vi), consequently ending the growing chain by an X_j termination and producing a free-radical $X_j\bullet$.[5] While unlikely due to their higher reactivity in the vinyl-rich environment, the fragmented radical species ($X\bullet$ and $X_{jj}\bullet$.) are also able to activate a monomer or polymer chain (vi) by abstraction of an atom or group of atoms.[5]

Finally, the polymerization may also be conventionally terminated by disproportionation or coupling reactions with primary radicals or other growing chains (vii).

In light of the proposed mechanisms (Figure 5.2) and of the specific limitations arising from AP-DBD systems, the common methods used to solve the free-radical polymerization's kinetics cannot be applied to the AP-PiCVD process, as its overall setup and layer's growth mechanisms differ from wet chemistry or iCVD methods (Table 5.1). Notably, the generation of reactive species in a partially passivated open air system implies a different knowledge of the initial parameters such as the monomer concentration $[M]_{(g)}$, the concentration of radical species $[M\bullet]_{(g)}$ over time, the amount of radical species participating to the polymerization reaction $[M\bullet]_{reacted}/[M\bullet]_{reactive}$ the propagation rate and the actual reaction volume.

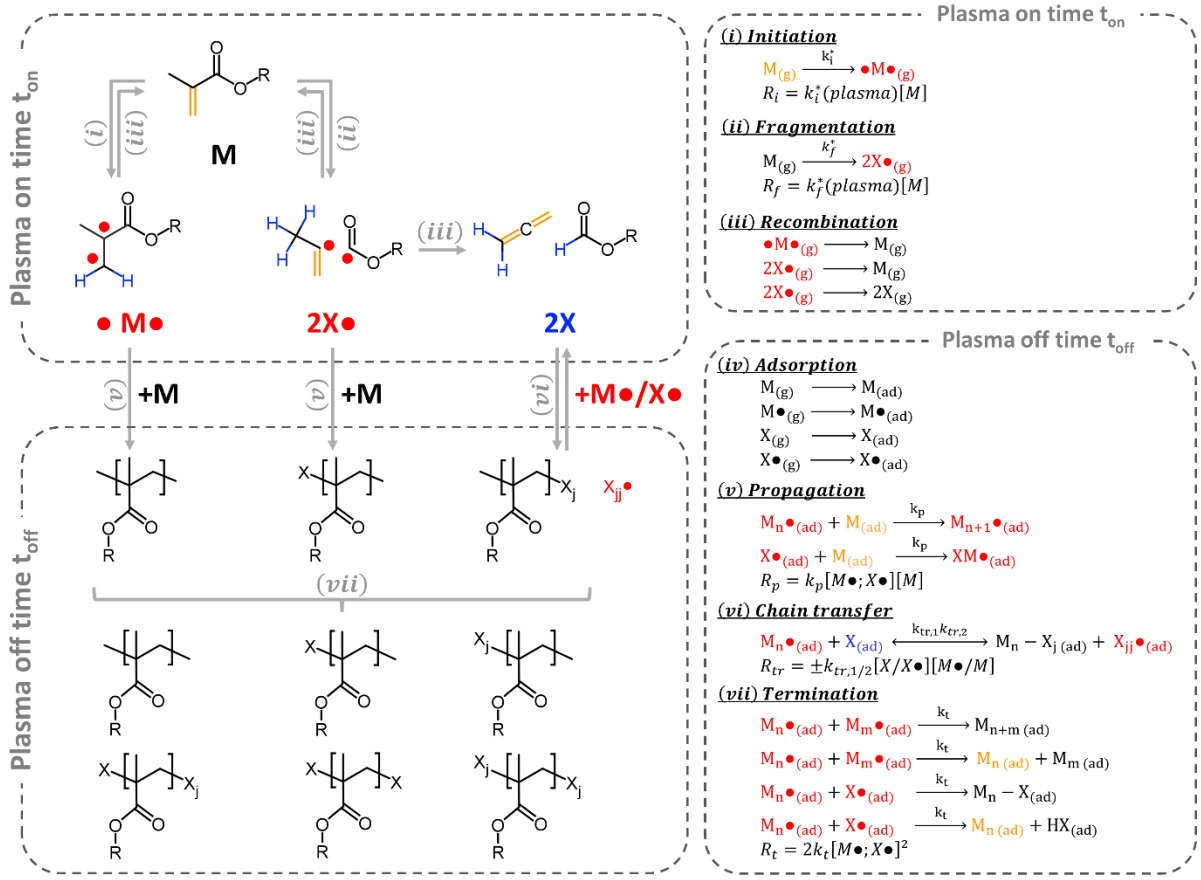

Figure 5.2. Example of the possible species resulting from the interactions between the plasma reactive species and the methacrylates (R = CH3 and CH2–CH(O)CH for MMA and GMA, respectively). The global reactions and the kinetic rate equations are provided, with the significant chemical functions for the considered polymerization mechanism(s) associated to a color. Namely, the vinyl's initiation in yellow, the free-radical polymerization in red and the neutral species (from recombined fragments or the atmosphere) in blue.

Consequently, the polymerization mechanisms need to be adapted to the medium, especially to take into account the chain transfer reactions which usually maintain the global concentration of radicals in closed systems, have to be reconsidered. Indeed, within AP-PiCVD's continuously renewed gas phase, the number of reacted transfer agents $X_{jj}\bullet$. – from neutral fragmented X reacting by chain transfer with free-radicals – that would normally be able to participate in the polymerization a second time can be considered as statistically low unless they are already adsorbed on the surface. As such, chain transfer mechanisms must be treated as a termination process resulting from the plasma fragmentation, therefore lowering the effective concentration of free-radicals as well as blocking the chains' terminal reactive ends in the operation.

Table 5.1. Comparison between different free-radical polymerization approach (i.e. wet chemistry, iCVD and AP-PiCVD) based on the system initial information and the resulting kinetic equations. The plasma-induced initiation R_i^* and fragmentation R_f^* equations are developed for the sake of coherence, however their plasma-kinetic constants (*i.e.* k_i^* and k_f^*) will not be addressed.

Parameters	Wet chemistry	iCVD	AP-PiCVD
$[M]$	Initially known, decrease over polymerization	Constant flux of monomer	Constant flux of monomer
$[M\bullet]$	Controlled through the amount of initiator [I] and the polymerisation conditions	Constant flux of initiator [I] activated by hot filaments	Renewed in a constant uncontrolled amount with each discharge, mixed with side-species from fragmentation
$\frac{[M\bullet]_{reacted}}{[M\bullet]_{reactive}}$	Almost all of the radical initiators react	Unknown number of radical initiators react	Unknown number of radical initiators react
Medium volume	Known closed volume	Closed chamber under renewed vacuum	Open air volume with gradients of reactivity partially passivated by argon barriers
Initiation	$R_i = k_i[I] = k_t[M\bullet]^2$	$R_i = k_i[I] = k_t[M\bullet]^2$	$R_i^* = k_i^*[M]_{(g)}$
Propagation	$R_p = k_p[M][M\bullet]$	$R_p = k_p[M][M\bullet]$	$R_p = k_p[M][M\bullet]$
Chain transfer	$R_{tr} = k_{tr}[X][M\bullet]$	$R_{tr} = k_{tr}[X][M\bullet]$	$R_{tr} = k_{tr}[X][M\bullet] = k_{tr}[X\bullet][M]$
Termination	$R_i = k_t[M\bullet]^2 = k_i[I]$	$R_i = k_t[M\bullet]^2 = k_i[I]$	$R_i = k_t[M\bullet]^2$
Fragmentation	-	-	$R_f^* = k_f^*[M]_{(g)}$

Moreover, due to their comparable reactivity and the lack of information on the plasma-dependent kinetic rate of fragmentation R_f^*, $M\bullet$ and $X\bullet$ cannot be individually discerned from each other and will be considered as a unique radical concentration $[M\bullet]$ resulting from the initiation mechanism, R_i^*. Specifically, while the ratio of fragmented reactive species $X\bullet$ compared to the conventional free-radicals $M\bullet$ would not change the initiation mechanisms, they would strongly affect the molecular chain length through non-propagating termination potentially inducing cross-linking phenomena, and therefore will be monitored through the chain transfer mechanisms.

Finally, the use of ultra-short plasma pulses prevent the application of the well-known steady-state approximation (*i.e.* $d[M\bullet]/dt$ = 0 at any time)[5] since the concentration of radicals cannot be considered constant during each plasma pulse, unlike low-pressure iCVD processes or conventional wet chemistry approaches.[6]

2.2. Pulsed plasma method – Mathematical model for non-steady-state conditions

Some AP-PiCVD parameters such as the constant concentration of monomer in the gas phase $[M]_{(g)}$ can easily be calculated using the plasma-monomers' intrinsic properties (Table 2.1) and the deposition parameters (Eq. 5.1). The parameters are the monomer's saturation pressure P_{sat}, its molecular weight $M_{W,M}$ and its vapor density $\rho_{vap,M}$, as well as the flux of carrier gas $F_{carrier}$, the total flux F_{tot}, the total pressure P_{tot}, the temperature T, and the gas constant R.

$$P_{sat}V = n_M RT \tag{5.1}$$

$$P_{sat}F_{carrier} = n_{M,F}RT$$

$$n_{M,F} = \frac{P_{sat}F_{carrier}}{RT} = F_M \frac{\rho_{vap,M}}{M_{W,M}}$$

$$F_M = F_{tot}\frac{P_M}{P_{tot}}$$

$$\frac{P_{sat}F_{carrier}}{RT} = F_{tot}\frac{P_M}{P_{tot}}\frac{\rho_{vap,M}}{M_{W,M}}$$

$$P_M = \frac{n_M RT}{V} = [M]_g RT$$

$$\frac{P_{sat}F_{carrier}}{RT} = F_{tot}\frac{[M]_g RT}{P_{tot}}\frac{\rho_{vap,M}}{M_{W,M}}$$

$$[M]_g = \frac{P_{tot}P_{sat}F_{carrier}}{F_{tot}R^2T^2}\frac{M_{W,M}}{\rho_{vap,M}}$$

The pulsed plasma method (PPM), is based on the same principle as the traditional non-steady models – rotating sector method (RSM)[7–9] and pulsed-laser polymerization (PLP)[10–12] – using light pulse energy sources with various illumination times (t_{on}) and dark times (t_{off}) (Figure 5.3a).

Unlike the more recent PLP model which requires low and highly resolved energy outputs,[5] the RSM model only needs the experimental growth parameters (Table 5.2) to mathematically describe the free-radicals' concentration in non-steady kinetics. Therefore, adapting the RSM equations to our nanopulsed plasma on-time (*i.e.* t_{on} = 100 ns) and adaptable plasma off-times (*i.e.* t_{off} = 31.6 – 0.1 ms) constructed the basis for the PPM model, allowing further data extraction of the kinetic parameters defining the surface/gas phase mechanisms of pulsed plasma polymerization. In the traditional RSM approach, one would simply plot the ratio between the propagation rate R_p and the propagation rate in steady-state conditions $R_{p,s}$ (*i.e.* under constant illumination, DC_s = 1), versus the logarithm of the on-time $log_{10}(t_{on})$ (Eq. 5.2).[5] Comparing the shift between the experimental plot and the model plot it is possible to estimate $log_{10}(\tau_s)$ and, subsequently, the kinetic ratio k_p/k_t (Eq. 5.3).[5]

$$\frac{R_p}{R_{p,s}} = \frac{[\overline{M\bullet}]}{[M\bullet]_s} = DC\left[1 + \frac{\tau_s}{t_{on}} ln\left(\frac{[M\bullet]_{max}/[M\bullet]_{min} + [M\bullet]_{max}/[M\bullet]_s}{1 + [M\bullet]_{max}/[M\bullet]_s}\right)\right] \tag{5.2}$$

$$\tau_s = \frac{[M\bullet]_s}{R_t} = \frac{1}{k_t[M\bullet]_s} = \frac{k_p[M]}{k_t R_{p,s}} \tag{5.3}$$

Unfortunately, this convenient determination of τ_s cannot be applied to our AP-PiCVD approach, since the RSM model requires the on-time (t_{on}) to be an independent variable and the off-time (t_{on}) a constant (Figure 5.3b), compelling a complete fitting of the function.

Table 5.2. Description of the significant parameters used in PPM calculations.

Parameters	Description	Parameters	Description
$\boldsymbol{t_{on}}$ $\boldsymbol{(s)}$	Plasma on-time, fixed around 100 ns	$\boldsymbol{[M\bullet]_{max}}$ $\boldsymbol{(mol \cdot L^{-1})}$	Radical concentration at the end of the plasma on-time (t_{on})
$\boldsymbol{t_{off}}$ $\boldsymbol{(s)}$	Plasma off-time, variable between 100 µs and 100 ms	$\boldsymbol{[M\bullet]_{min}}$ $\boldsymbol{(mol \cdot L^{-1})}$	Radical concentration at the end of the plasma off-time (t_{off})
$\boldsymbol{\tau_{qs}}$ $\boldsymbol{(s)}$	Average lifetime of a growing radical	$\boldsymbol{R_p}$ $\boldsymbol{(mol \cdot L^{-1} \cdot s^{-1})}$	Molecular propagation rate
$\boldsymbol{DC}$	Duty cycle of the pulse	$\boldsymbol{DR}$ $\boldsymbol{(m \cdot s^{-1})}$	Film's thickness deposition rate

Additionally, the RSM model is based on the experimental measurement of a steady-state mode (*i.e.* DC_s = 1), which is intrinsically incompatible with an AP-DBD set-up since the electrons need to accumulate on the surface before reaching a breakdown potential to generate the discharge. In order to be as close as possible to the steady-state, one can work with a sinewave plasma ignition source to determine the deposition rate that would correspond to quasi-steady-state conditions, denoted as "qs" further in the text (Figure 5.3c).

Simple electrical measurements give the ratio between the plasma on and off-times (*i.e.* DC_{qs}), approximately 50% in the present case (Figure 5.3c). The average ratio of radical conversion $[\overline{M\bullet}]/[M\bullet]_{qs}$ requires pre-calculations of its inner terms to fit this function with our plasma off-time-dependent experimental data.

Notably, solving the RSM equations describing the on-time and off-time (Eq. 5.4) as linear systems with two variables (Eq. 5.5), the radical ratios $[M\bullet]_{max}/[M\bullet]_{qs}$ and $[M\bullet]_{min}/[M\bullet]_{qs}$ are individually developed.

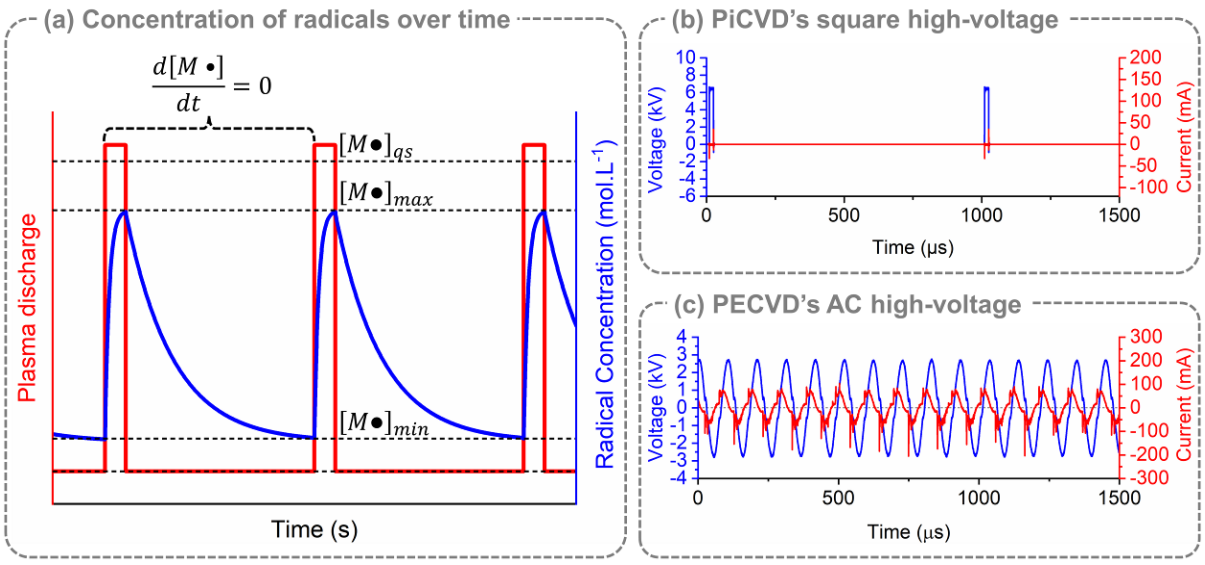

Figure 5.3. (a) Scheme of the concentration of radicals following the plasma discharge over time in a square-wave plasma discharge. For the sake of the discussion the two current discharges are approximated as a single one. Both the calculated initiated $[M\bullet]_{max}$ and the remaining $[M\bullet]_{min}$ radical concentration are displayed as well as the radical concentration $[M\bullet]_{qs}$ corresponding to a continuous discharge mode (*i.e.* quasi-steady-state mode). Traces of the applied voltage and the corresponding current discharges for (b) the ultra-short AP-DBD pulses at a frequency of 1000 Hz (*i.e.* t_{off} = 1 ms) and (c) the sine wave-excited AP-DBD (*i.e.* quasi-steady-state mode)

$$\frac{t_{on}}{\tau_s} = \tanh^{-1}\left(\frac{[M\bullet]_{max}}{[M\bullet]_s}\right) - \tanh^{-1}\left(\frac{[M\bullet]_{min}}{[M\bullet]_s}\right) \tag{5.4}$$

$$\frac{t_{off}}{\tau_s} = \frac{[M\bullet]_{qs}}{[M\bullet]_{min}} - \frac{[M\bullet]_{qs}}{[M\bullet]_{max}}$$

$$\tanh^{-1}(a) - \tanh^{-1}(b) = \frac{1}{2}\ln\left(\frac{1+a}{1-a}\right) - \frac{1}{2}\ln\left(\frac{1+b}{1-b}\right) \tag{5.5}$$

$$\frac{(1+a)(1-b)}{(1-a)(1+b)} = e^{2t_{on}/\tau_s} = c$$

$$(1+a)(1-b) = c[(1-a)(1+b)]$$

$$(1+a)\left(1-\frac{1}{1/a+d}\right) = c\left[(1-a)\left(1+\frac{1}{1/a+d}\right)\right]$$

$$a^2[(c-1)+d(c+1)] + a[d(1-c)] + [1-c] = 0$$

$$\frac{[M\bullet]_{max}}{[M\bullet]_{qs}} = \frac{-\left[\frac{t_{off}}{\tau_s}(1-e^{2t_{on}/\tau_s})\right] \pm \sqrt{\left[\frac{t_{off}}{\tau_s}(1-e^{2t_{on}/\tau_s})\right]^2 - 4\left(\left[(e^{2t_{on}/\tau_s}-1)+\frac{t_{off}}{\tau_s}(e^{2t_{on}/\tau_s}+1)\right]*[1-e^{2t_{on}/\tau_s}]\right)}}{2\left[(e^{2t_{on}/\tau_s}-1)+\frac{t_{off}}{\tau_s}(e^{2t_{on}/\tau_s}+1)\right]}$$

$$\frac{[M\bullet]_{min}}{[M\bullet]_{qs}} = \frac{-\left[\frac{t_{off}}{\tau_s}(e^{2t_{on}/\tau_s}-1)\right] \pm \sqrt{\left[\frac{t_{off}}{\tau_s}(e^{2t_{on}/\tau_s}-1)\right]^2 - 4\left(\left[(e^{2t_{on}/\tau_s}-1)-\frac{t_{off}}{\tau_s}(e^{2t_{on}/\tau_s}+1)\right]*[1-e^{2t_{on}/\tau_s}]\right)}}{2\left[(e^{2t_{on}/\tau_s}-1)-\frac{t_{off}}{\tau_s}(e^{2t_{on}/\tau_s}+1)\right]}$$

Assuming that the thin films' density does not change too significantly from low to high frequencies, the $R_p/R_{p,qs}$ ratio can be correlated to the deposition rate ratio DR/DR_{qs}. This

ratio is theoretically evaluated from Eq. 5.2 at a given τ_s, and experimentally from the measured thin film deposition rates according to the frequency.

Although, one has to be cautious before making any comparison, as the model ratio $\left(DR/DR_{qs}\right)_{PPM}$ needs to take into account the τ_s (Eq. 5.6), which is dependent on the conversion ratios, and the experimental ratio $\left(DR/DR_{qs}\right)_{exp}$ has to be reduced to one pulse for both terms of the division (Eq. 5.7).

$$\left(\frac{DR}{DR_{qs}}\right)_{PPM} = \frac{[M\bullet]_{max}-[M\bullet]_{min}}{[M\bullet]_{qs}} DC \left[1 + \frac{\tau_s}{t_{on}} ln\left(\frac{[M\bullet]_{max}/[M\bullet]_{min}+[M\bullet]_{max}/[M\bullet]_{qs}}{1+[M\bullet]_{max}/[M\bullet]_{qs}}\right)\right] \quad (5.6)$$

$$\left(\frac{DR}{DR_{qs}}\right)_{exp} = \frac{DC}{DC_{qs}} \frac{DR}{DR_{qs}} \quad (5.7)$$

Ultimately, the converted experimental data (Eq. 5.7) can be fitted with the proposed theoretical function (Eq. 5.6) by adjusting τ_s. Information on the radical lifetime, the radical conversion ratios for both MMA (Figure 5.4a) and GMA (Figure 5.4b) as well as the kinetic ratio k_p/k_t from Eq. 5.3 are extracted and summarized in Table 5.3.

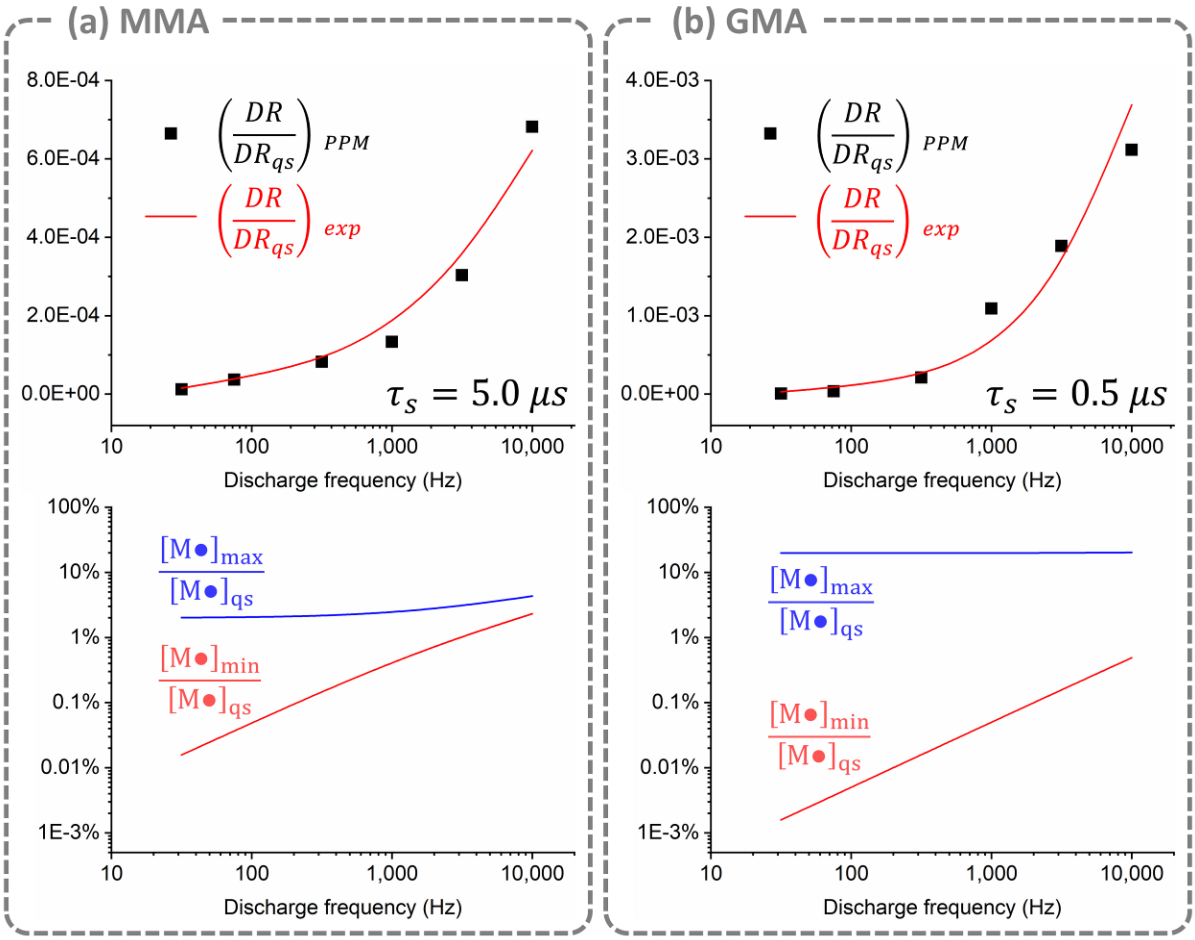

Figure 5.4. Experimental DR/DR_{qs} data for (a) MMA and (b) GMA thin films grown at various pulsed plasma frequencies (t_{on} ≈ 100 ns) and their fitting with the PPM model. The calculated steady-state radical lifetime τ_s is provided for each monomer for the conditions investigated,

along with their theoretical radical conversion ratios $[M\bullet]_{max}/[M\bullet]_{qs}$ and $[M\bullet]_{min}/[M\bullet]_{qs}$ following each plasma discharge and each pulse cycle, respectively.

As expected from the studied frequency range, the maximum conversion rates from monomer to radical with the ultra-short plasma discharge is quite high (*ca.* 5 and 20% for MMA and GMA, respectively, for t_{on} = 100 ns), highlighting the potential of ultrashort plasma pulses to effectively initiate a free-radical polymerization of vinyl monomer even for low DCs. When these data are normalized to the time, this range of value is comparable to PLP experiments (*ca.* 2 – 3% at t_{on} = 10 ns),[13] hinting on a linear influence of the activation-time on the conversion ratio. In addition, the strong effect of the plasma off-time on the radical species concentration after each cycle (Table 5.3) is coherent with the assumption that a suitable t_{off} is not only important but essential.

Table 5.3. Pulsed Plasma Model parameters extracted from the experimental fitting.

Parameters	**MMA**		**GMA**	
$[\boldsymbol{M}]_{(g)}$ $(\boldsymbol{mol \cdot L^{-1}})$	$1.95 \cdot 10^{-5}$		$1.31 \cdot 10^{-5}$	
$\boldsymbol{\tau_s}$ $(\mu \boldsymbol{s})$	5.00		0.50	
$\boldsymbol{k_p/k_t}$	$3.36 \cdot 10^{-6}$		$1.92 \cdot 10^{-7}$	
$[\boldsymbol{M}\bullet]_{\boldsymbol{max}}/[\boldsymbol{M}\bullet]_{\boldsymbol{qs}}$ (%)	f = 31.6 Hz	f = 10,000 Hz	f = 31.6 Hz	f = 10,000 Hz
	2.02 %	4.31 %	19.74 %	20.21%
$[\boldsymbol{M}\bullet]_{\boldsymbol{min}}/[\boldsymbol{M}\bullet]_{\boldsymbol{qs}}$ (%)	f = 31.6 Hz	f = 10,000 Hz	f = 31.6 Hz	f = 10,000 Hz
	$1.57 \cdot 10^{-4}$ %	2.32 %	$1.58 \cdot 10^{-5}$ %	0.49 %

Interestingly, expanding the range of the theoretical calculations for ultra-short pulses (t_{off} ≈ 100 ns) shows that both $[M\bullet]_{max}/[M\bullet]_{qs}$ and $[M\bullet]_{min}/[M\bullet]_{qs}$ steadily increase with the discharge frequency, until they reach a quasi-steady-state at 10 MHz when DC_{qs} tends toward 1 (Figure 5.5a). On the other hand, the discharges' duration in AP-DBD ignited using a sinusoidal excitation (t_{on} ≈ 10 µs per sinusoid) yields a constant amount of initiation $[M\bullet]_{max}$, independently of the plasma off-time, suggesting a complete conversion of the gas phase for each plasma discharge (Figure 5.5b). This correlates with the ratios of conversion being highly affected by the time of discharge, hence the necessity to reduce the plasma on-time to prevent the excessive and detrimental alteration and depletion of the monomer.

Following that assumption, the radical ratios become conversion percentages and may be used to describe our system's non-steady kinetic at any frequency.

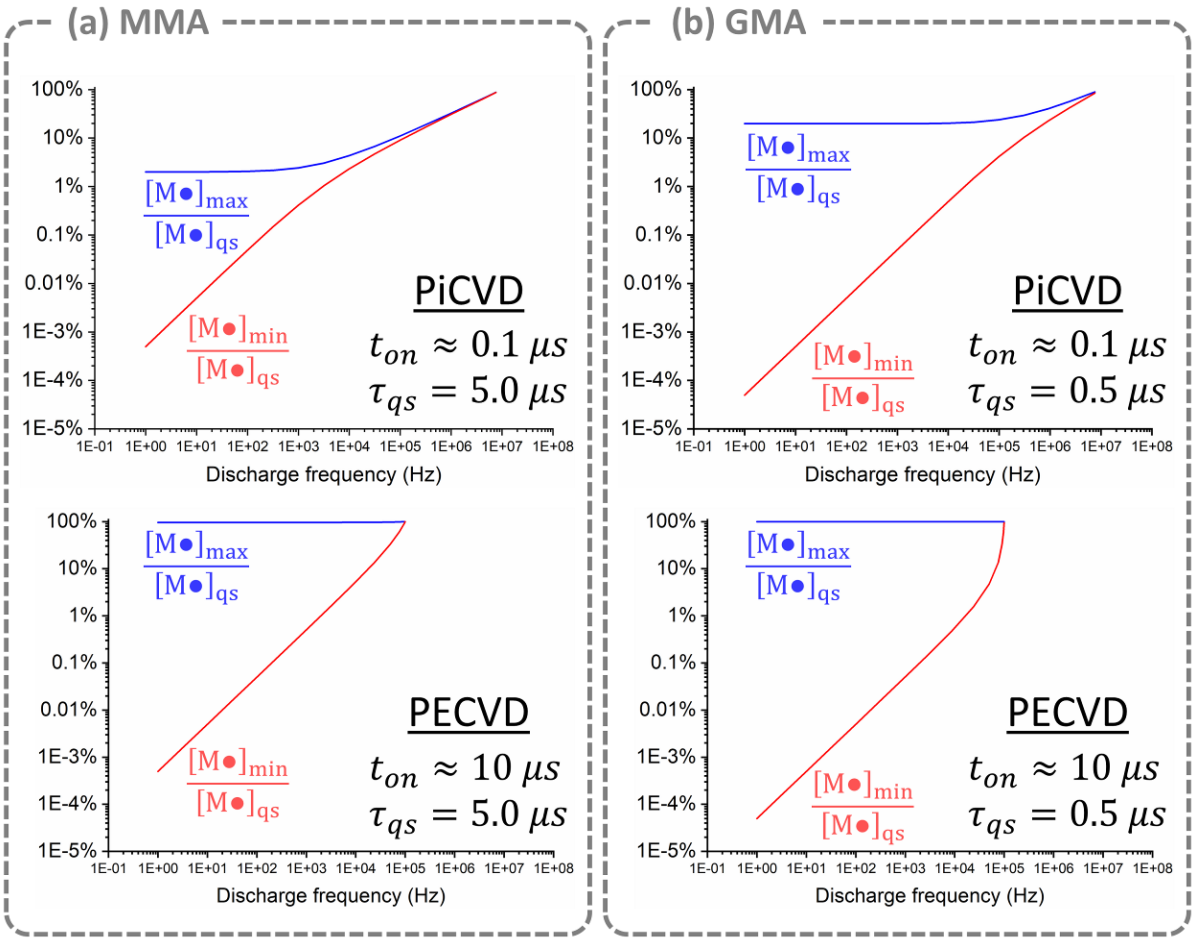

Figure 5.5. Theoretical radical conversion ratios $[M\bullet]_{max}/[M\bullet]_{qs}$ and $[M\bullet]_{min}/[M\bullet]_{qs}$ following each discharge initiation and each pulse cycle, calculated from (a) MMA's and (b) GMA's τ_s. Both initiation time of PiCVD (t_{on} ≈ 100 ns) and PECVD (t_{on} ≈. 10 µs) are considered.

2.3. Non-steady kinetic of open-volume pulsed plasma discharges

If the steady-state assumption cannot be verified at any given time for pulsed plasmas, it is still valid when the mechanisms are considered over a full discharge cycle (Figure 5.3a). As such, taking in consideration the contribution of each mechanism to the total amount of radicals (Table 5.1), the kinetic rates over the time span of one cycle can be related to each other (Eq. 5.8).

Using the propagation rate equation (*i.e.* $R_p = k_p[M]_{(g)}[M\bullet]_{(g)}$), Eq. 5.8 can be expressed as a second order polynomial function of the propagation rate R_p versus the plasma-initiation rate R_i^* (Eq. 5.9), independently of the radical concentration $[M\bullet]$. As such, based on the PPM model, it is possible to mathematically express the theoretical rate of initiation during one discharge $R_{i,gas}$ (Eq. 5.10) as well as the converted experimental radical consumption per discharge $R_{p,surface}$ (Eq. 5.11), relating the gas phase mechanisms to the surface reactivity. From Eq. 5.9, the plot of $R_{i,gas}$ versus $R_{p,surface}$ can be fitted with a simple quadratic function (Figure 5.5) and the kinetic constants (*i.e.* ${k_t}/{k_p}^2$ and $k_{tr}[AX]/k_p$) extracted from the fitting.

$$\frac{d[M\bullet]}{dt} = R_i^* - R_t \pm R_{tr} \quad (5.8)$$
$$\frac{d[M\bullet]}{dt} = R_i^* - k_t[M\bullet]^2 \pm k_{tr}[AX][M\bullet]$$

$$R_i^* = \frac{k_t}{{k_p}^2}\frac{1}{{[M]_{(g)}}^2}{R_p}^2 \pm \frac{k_{tr}}{k_p}\frac{[AX]_{(g)}}{[M]_{(g)}}R_p \quad (5.9)$$

$$R_{i,gas} = \frac{DC}{t_{on}}\frac{[M\bullet]_{max}-[M\bullet]_{min}}{[M\bullet]_{qs}}[M]_{(g)} \quad (5.10)$$

$$R_{p,surface} = DC\frac{DR\rho_{poly,M}}{h_{medium}\rho_{vap,M}}[M]_{(g)} \quad (5.11)$$

Although, one should be careful of the working frequency range, as fitting the kinetic rates below the transition frequency from predominant gas phase mechanisms to predominant surface mechanisms (Figure 5.1a) yielded for both monomers a negative value for the second-degree parameter of the polynomial (Figure 5.6). This global deviation of the curve tendency arises from preponderant surface mechanisms below this threshold, while the PPM model describes the gas-phase polymerization mechanisms. However, the effect on the kinetic parameters' absolute values is globally quite low (*ca.* two times higher or lower) compared to the orders of magnitude considered, as confirmed by a third methacrylate monomer (butyl methacrylate BMA). Therefore, MMA's second-degree fit parameter will be considered as positive in further discussions. No assumption is made on the sign of the polynomial's first-degree parameter since both initiation and termination are possible by chain transfer depending on who is acting as the transfer agent.

Using the k_t/k_p values obtained from the PPM calculations and the quadratic fit parameters, all kinetic constants can be calculated for both MMA and GMA, aside from the fragmentation and initiation constants k_f and ${k_i}^*$, which depend on the plasma power output and species' properties.

Interestingly, when the electrode gap is considered as the reaction medium (*i.e.* h_{medium} = 1 mm), the constant of propagation k_p is much lower than the ones known in wet chemistry (Table 2.1), 0.015 and 0.052 $L \cdot mol^{-1} \cdot s^{-1}$ for MMA and GMA respectively. This is coherent with the fact that not all the radicals formed within the discharge gap will contribute to the thin film growth, as most of the formed reactive species will deactivate into the gas phase and be flushed away. Moreover, rather short radical lifetimes (*ca.* τ_s = 1 µs) were calculated for steady-state conditions, in range with the lifetime of the argon species as determined by time-resolved optical emission spectroscopy (TR-OES) measurements (Figure 2.4c).[14]

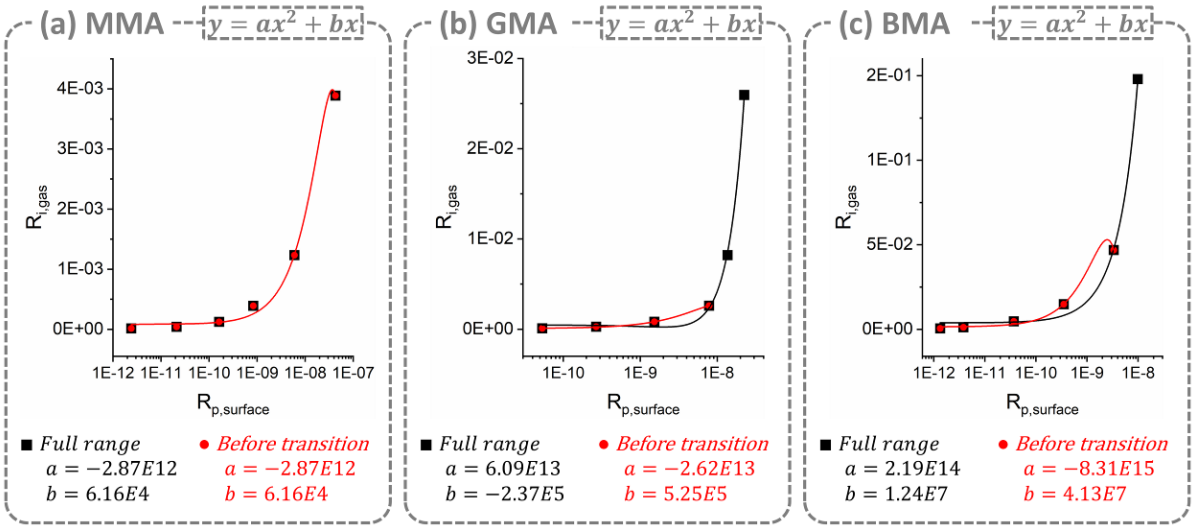

Figure 5.6. Fit of the theoretical initiation rate $R_{i,gas}$ according to the experimental propagation rate $R_{p,surface}$ for (a) MMA, (b) GMA and (c) BMA by a second order polynomial function. The black solid curves are fits over the complete range of frequency, while the red solid curves are fits realized before the frequency transition (*i.e.* f ≤ 10,000 Hz for MMA, f ≤ 1,000 Hz for GMA and f ≤ 3,160 Hz for BMA). The quadratic fit parameters are given in every case. BMA's fits parameters are displayed for the sake of the argument, but should not be considered exact due to missing constants (*e.g.* monomer's vapour density) which were assumed based on MMA's and GMA's values.

In order to estimate the effective volume contributing to the thin film's growth, one can reverse the calculation using the theoretical value of the kinetic constant of propagation $k_{p,theo}$ reported in the literature (Table 2.1). This reactive volume $h_{reactive}$ was rather similar between MMA and GMA, yielding distances in the range of several hundreds of nanometers (*i.e.* 0.5 and 0.2 µm, respectively). Interestingly, these distances do not match with obvious physical constants related to the plasma discharge, such as the mean free path of the molecules (≤0.05 µm) or the plasma sheath (≥100 µm).

Still, the transport time necessary for a molecule to diffuse through this reactive volume is approximately 60 µs for MMA and GMA, which matches with the investigated range of plasma off-times. More interestingly, it can also be correlated with the frequency threshold corresponding to the transition from conventional polymer to plasma-polymer determined from the evolution of the apparent molecular mass in weight obtained by size exclusion chromatography (Figure 5.7) determined in Chapter 3.

Very reasonably with plasma physic considerations, and in accordance with mass spectrometry study in Chapter 4, the PPM model suggests that the shift from conventional free-radical polymerization growth to plasma-polymerization mechanisms is largely dependent of the monomer's exposure to several discharges (*i.e.* fragmentation) within the volume defined by $h_{reactive}$. Indeed, the amount of monomer species suffering several plasma-induced fragmentations during their traveling time increase exponentially with the discharge frequency (Figure 5.7), stressing the requirement to temporally isolate the discharge and use appropriate plasma off-times.

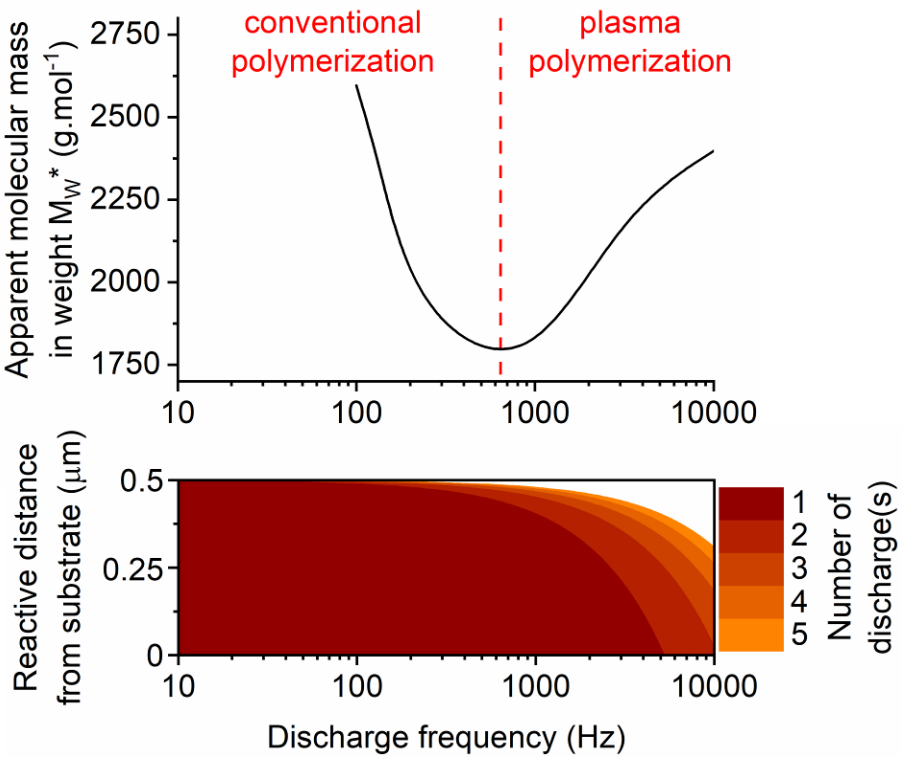

Figure 5.7. MMA's apparent molecular mass in weight M_W* from SEC measurements and the spatial distribution of the number of discharge(s) per molecule depending on its position within the reactive volume $h_{reactive}$ and the discharge frequency. The substrate is located a 0 µm.

While a quantitative solution of the kinetic parameters is possible based on the SEC measurements, this method is not applicable to all monomers and requires a very high number of points to find the exact transition frequency. Yet, the correlation between the experimental and theory suggests that qualitative information can be obtained on the different polymerization mechanisms.

Therefore, every kinetic constant was calculated according to the exact reaction volume $h_{reactive}$ previously determined from the theoretical propagation constant, $k_{p,theo}$ (Table 5.4). Consequently, the corresponding kinetic parameters give access to the complete kinetic rates R_i, R_p, R_t, and R_{tr} and to the reactive concentration of species participating to each of the polymerization mechanisms during one discharge cycle (Figure 5.8). Each of the calculated concentrations is associated to its respective mechanism's lifetime: t_{on} for the initiation R_i; τ_s for the fragment's transfer R_{tr}; $t_{on} + t_{off}$ for the conventional propagation R_p and termination R_t. The deactivation of MMA's and GMA's growing chains after 10 ms (Figure 3.2a) and 100 ms,[15] respectively, are taken into account in the calculations.

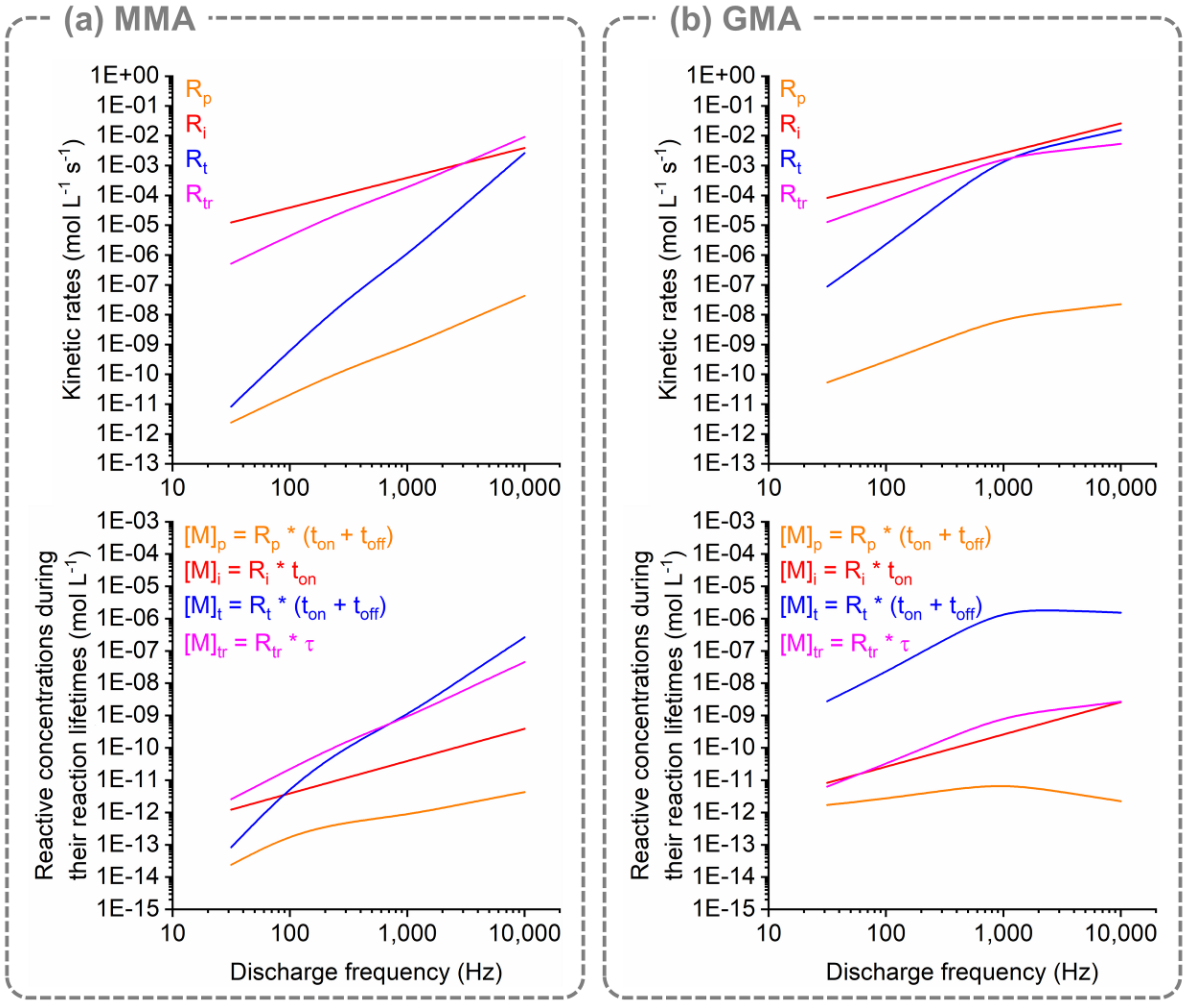

Figure 5.8. Calculated kinetic rates R_X and reactive concentrations $[M]_X$ for each of the polymerization mechanisms (*i.e.* propagation, initiation, termination and chain-transfer) for (a) MMA and (b) GMA.

The prevalence of transfer mechanisms for MMA (Figure 5.8a) and conventional terminations for GMA (Figure 5.8b) is strongly linked to the monomer fragmentation upon plasma exposure. The mass-spectrometry study in Chapter 4 showed that the MMA molecule was statistically broken down by the high energy species (Figure 5.1d), generating numerous compounds able to initiate or terminate the polymerization reaction. On the other hand, GMA was effectively protected from this non-specific fragmentation by the low energy epoxy function acting as a sacrificial function (Figure 5.1d). As a result, their difference in chain transfer reactions is certainly related to the amount of chain transfer agents resulting from the molecular breakdown (*i.e.* $[AX]_{MMA} \gg [AX]_{GMA}$), affecting in inverse proportion both methacrylates' conventional terminations.

Moreover, as one would expect, the concentrations of conventional initiators are increasing with the duty cycle, consistently with the amount of species remaining at the end of each pulse $[M\bullet]_{min}$ (Figure 5.4). Ultimately, both the initiation rate derived from the PPM model and the propagation rate extracted from the experimental deposition rate relate to the reactions occurring in the gas phase and on the surface (*i.e.* in the $h_{reactive}$volume).

Table 5.4. Kinetic parameters calculated from the PPM model and experimental data using a reaction medium distance $h_{reactive}$ (0.5 µm and 0.2 µm for MMA and GMA respectively) corrected by the theoretical kinetic constant of propagation k_p (Table 2.1).

Parameters	MMA	GMA
$\boldsymbol{k_{p,theo}}$ $(\boldsymbol{L \cdot mol^{-1} \cdot s^{-1}})$	$2.74 \cdot 10^2$	$4.94 \cdot 10^2$
$\boldsymbol{k_t}$ $(\boldsymbol{L \cdot mol^{-1} \cdot s^{-1}})$	$4.08 \cdot 10^7$	$1.29 \cdot 10^9$
$\boldsymbol{k_{tr}[AX]}$ $(\boldsymbol{s^{-1}})$	$1.13 \cdot 10^3$	$1.54 \cdot 10^3$

In order to compare the two, it is possible to calculate the radical concentrations in the reactive volume $[M\bullet]_{reactive}$ from the theoretical-experimental model (Eq. 5.12) and the radical concentrations in the thin film $[M\bullet]_{reacted}$ from experimental values (Eq. 5.13), corresponding to the amount of radical species available in the reactive volume and the amount of radical species having reacted, respectively.

$$[M\bullet]_{reactive} = \sqrt{\frac{R_t}{k_t}} \tag{5.12}$$

$$[M\bullet]_{reacted} = \frac{R_p}{k_p[M]_g} \tag{5.13}$$

GMA's percentage of radical reactivity steadily increases with the frequency until it saturates at 1,000 Hz, while MMA is reaching saturation at 10,000 Hz. Those behaviors perfectly correlate with the deposition rates tendencies and the topographic observations done by SEM (Figure 5.1a,c), highlighting the transition from preponderant surface mechanisms to preponderant gas phase mechanisms. This additional information based on both experimental and theoretical data confirms the nature of this transition as a saturation of the reactive species on the surface when the radicals cannot adsorb anymore and the reactivity reaches 100% (Figure 5.9a). Indeed, GMA's low vapor pressure implies that the surface would be more prone to saturate from an excess of reactive species from the gas phase. On the other hand, MMA does not reach its saturation level for the investigated deposition conditions, since it has low adsorption due to its high vapor pressure. Ultimately, due to the apparent linear evolution of the reactivity percentage compared to the discharge frequency plotted in $\log_{10}$ in both axes (Figure 5.9b), one does not need to reach or even get close to the saturation threshold to extract this information by a simple linear extrapolation.

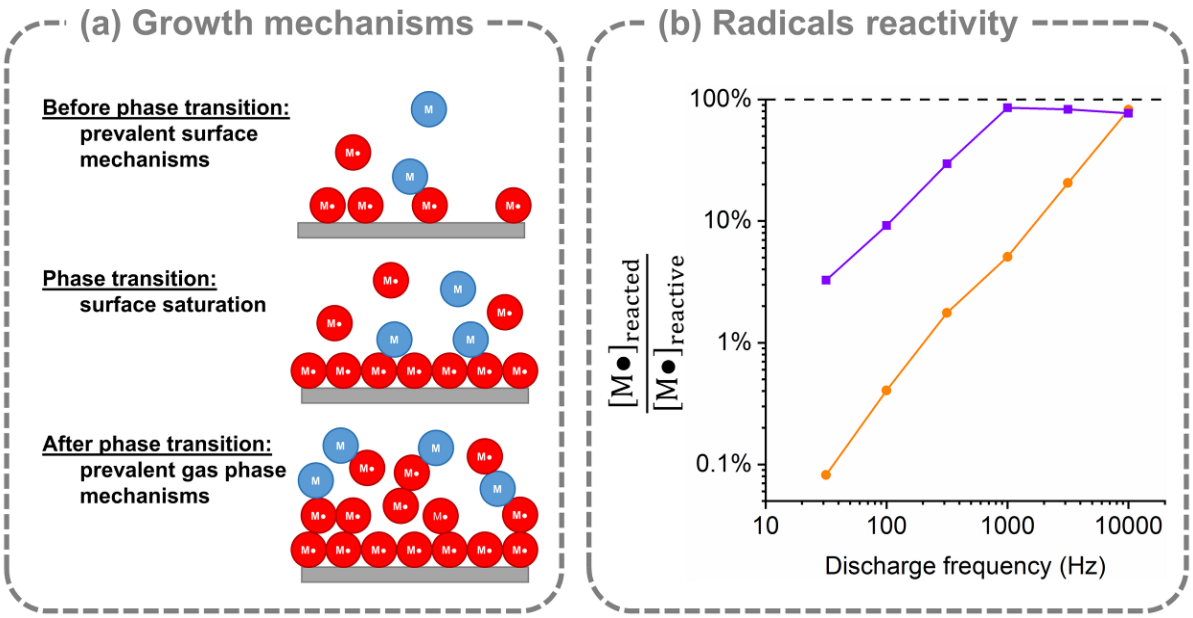

Figure 5.9. (a) Scheme of the transition between surface and gas phase mechanisms due to an excess of reactive species adsorbed on the substrate. (b) Ratio between the concentration of radicals reacted $[M\bullet]_{reacted}$ over the concentration of radicals created $[M\bullet]_{reactive}$ according to the frequency for MMA and GMA.

3. Outlines

The development of models for plasma-polymerization processes is difficult due to the multiphysics aspects of the interactions and mechanisms occurring. Therefore, most models focus on a few of those aspects (e.g. chemical reactivity, fragmentation, gas propagation, plasma parameters …) to describe one or a group of systems.

The PPM model propose an original description of the plasma-polymerization mechanisms in pulsed-plasmas based on the experimental parameters and the monomer's growth rate. The mixed theoretical-experimental approach improves the understanding of different mechanisms occurring and their dependency on the monomer and process properties. Notably, applying the PPM model to the MMA and GMA cases allowed to evidence very different behaviors during and following the discharge, consistently with the previous high-resolution mass-spectrometry analyses highlighting their strong discrepancies upon exposure to nanopulsed plasmas.

MMA appeared to have an inferior amount of free-radical being available following the nanopulsed discharge (*i.e.* t_{on}) and a superior amount remaining after the cycle (*i.e.* $t_{on} + t_{off}$) compared to GMA. This behavior hints on either less fragmentation from MMA or faster termination mechanisms preventing the growth of the layer. The extraction of the kinetic parameters of the polymerization mechanisms (*i.e.* initiation, propagation, termination and chain-transfer) highlighted the extremely low propagation rate of MMA, which correlates with the high chain-transfer indicating chain-blocking mechanisms. GMA, on the hand, display higher propagation rate and conventional termination mechanisms during the whole cycle $t_{on} + t_{off}$. This difference of termination, arising from the initial fragmentation, appear as a

key mechanism to control the properties of plasma-polymer thin films comforting the finding from the mass-spectrometry study in Chapter 4.

Further, the PPM model allowed for a deeper understanding of the growth mechanisms between the gas phase and the surface as the equations are solved by combining data from the gas phase (theoretical + experimental) and the surface (experimental). Notably, the effective reactive volume in the gas phase was determined from this study. This key information highlights a direct relationship between the number of nanosecond discharges to which a monomer molecule is exposed and the degree of alteration of the thin film's chemistry. Precisely, to be comparable with conventional polymers, one discharge appears as the maximum threshold above which altered plasma-polymers are formed. Finally, the reactivity of the plasma-induced free-radicals from the gas phase to the surface could be determined from the PPM model, shedding light on the mechanisms behind the transition from surface-based to gas phase-based growth mechanisms, as a saturation of the surface from radical and active species.

The PPM model appears as a strong tool for the description of growth mechanisms in pulsed plasma deposition processes, hindered only by the required data on the monomer properties to perform the calculations. On the other hand, the range of applications for this model extends beyond the study of the nanopulsed plasmas frequency presented in this Chapter, but may be applied to the study of other variables (*e.g.* monomer partial pressure).

Ultimately, the outcomes of this theoretical study match with our experimental observations and the analyses of the different chemical mechanisms occurring during the PECVD reaction of vinylic monomers using nanosecond plasma pulses.

4. References

1. Yasuda, H. (1985) *Plasma Polymerization*, Academic Press.

2. Friedrich, J. (2006) *The Plasma Chemistry of Polymer Surfaces*, Wiley-VCH.

3. Umran, I., and Golkowski, M. (2011) *Principles of Plasma Physics for Engineers and Scientists*, Cambridge University Press.

4. Goldston, R.J., and Rutherford, P.H. (1995) *Introduction To Plasma Physics*, IOP Publishing.

5. Odian, G. (2013) *Principles of Polymerization*, Wiley-VCH.

6. Lau, K.K.S., and Gleason, K.K. (2006) Initiated Chemical Vapor Deposition (iCVD) of Poly(alkyl acrylates): A Kinetic Model. *Macromolecules*, **39** (10), 3695–3703.

7. Briers, B.F., and Leonard, D. (1926) The Influence of the Intensity of Illumination on the Velocity of Photochemical Changes. The Determination of the Hean Life of a Hypothetical Catalyst. *J. Chem. Soc.*, **129**, 562–569.

8. Moss, S.J., and Moore, J.W. (1982) Free-radical polymerization using the rotating-sector method: A computer-based study. **59** (12), 1021–1024.

9. Antunes, F., Barclay, L.R.C., Vinqvist, M.R., and Pinto, R.E. (1998) Determination of

propagation and termination rate constants by using an extension to the rotating-sector method: Application to PLPC and DLPC bilayers. *Int. J. Chem. Kinet.*, **30** (10), 753–767.

10. Olaj, O.F., and Bitai, I. (1987) The laser flash-initiated polymerization as a tool of evaluating (individual) kinetic constants of free radical polymerization. *Die Angew. Makromol. Chemie*, **155**, 177–190.

11. Lyons, R.A., Hutovic, J., Piton, M.C., Christie, D.I., Clay, P.A., Manders, B.G., Kable, S.H., and Gilbert, R.G. (1996) Pulsed-laser polymerization measurements of the propagation rate coefficient for butyl acrylate. *Macromolecules*, **29** (6), 1918–1927.

12. Seabrook, S.A., Tonge, M.P., and Gilbert, R.G. (2005) Pulsed laser polymerization study of the propagation kinetics of acrylamide in water. *J. Polym. Sci. Part A Polym. Chem.*, **43** (7), 1357–1368.

13. Beuermann, S. (2002) Propagation Kinetics in Free-Radical Polymerizations. *Macromol. Symp.*, **182**, 31–42.

14. Gordeev, I., Choukourov, A., Šimek, M., Prukner, V., and Biederman, H. (2012) PEO-like plasma polymers prepared by atmospheric pressure surface dielectric barrier discharge. *Plasma Process. Polym.*, **9** (8), 782–791.

15. Boscher, N.D., Hilt, F., Duday, D., Frache, G., Fouquet, T., and Choquet, P. (2015) Atmospheric pressure plasma initiated chemical vapor deposition using ultra-short square pulse dielectric barrier discharge. *Plasma Process. Polym.*, **12** (1), 66–74.

CHAPTER VI – Nanopulsed discharges for the AP-PiCVD of polymer layers: an applicative study

This chapter aims at bringing to fruition the understanding gained along the preceding Chapters through the preparation of functional polymer layers using the proposed AP-PiCVD method. N-vinyl caprolactam (NVCL), a monomer whose thermoresponsive functional property is highly sensitive to fragmentation, is successfully homopolymerized and copolymerized with ethylene glycol dimethacrylate (EGDMA), yielding water-soluble and water-stable thermoresponsive thin films, respectively. Strong chemical retention and high thermoresponsiveness are achieved, highlighting the ability of AP-PiCVD to grow functional homopolymers and copolymers layers with properties matching the ones of the homo/copolymer synthesized from conventional solution-based and CVD approaches.

Article(s) published from these results

Loyer, F., Frache, G., Choquet, P., and Boscher, N.D. (2017) Atmospheric Pressure Plasma-Initiated Chemical Vapor Deposition (AP-PiCVD) of Poly(alkyl acrylates): An Experimental Study. Macromolecules, 50 (11), 4351–4362.
Full contribution (experimental work on deposition, analyses and interpretation, redaction of the manuscript)

Content

1. Introduction

The growth mechanisms driving the AP-PiCVD of polymer layers have been thoroughly investigated in the previous Chapters using different methacrylate monomers. The combination of experimental and theoretical studies highlighted the key parameters to promote the growth of high molecular weight conventional polymers. Notably, the association of ultra-short plasma discharge on-times with long off-times is essential to statistically limit fragmentation and recombination mechanisms while promoting the free-radical polymerization pathway. The use of monomers bearing chemical buffer functions was also shown to yield a strong improvement of the molecular weight. Unfortunately, there are only few commercially available monomers that fit this description, especially when considering monomers suitable for the growth of functional polymers. Therefore, unless monomers specifically designed to regulate orienting the fragmentation mechanisms (possessing sacrificial functions such as epoxy) are synthesized, the use of conventional monomers remains the best compromise for the AP-PiCVD of conventional polymers.

To demonstrate the ability of the AP-PiCVD method to grow functional polymer layers, n-vinyl caprolactam (NVCL) was deposited using low plasma pulse frequencies. In light of the knowledge developed along the preceding chapters, the high-voltage square wave pulses were modified to further lower the number of plasma pulses affecting the monomers. Precisely, the length of the high-voltage square wave pulses was extended to half of the period (Figure 2.2c), creating two distinct plasma discharges at the rising and falling edge of the high-voltage square wave pulses. This allows to further lower the number of plasma discharges seen by the monomers exposed to a single plasma discharge per cycle.

Poly n-vinyl caprolactam (pNVCL), a thermoresponsive polymer (TRP), undergoes a reversible collapse or expansion of its polymer chains expressed by a shift from hydrophilic to hydrophobic at a specific temperature.[1,2] This transition temperature – *i.e.* lower critical solution temperature (LCST) – when the polymer switch from hydrophilic to hydrophobic as the temperature increases is strongly dependent on the monomer chemistry, the polymeric chain length and the presence of comonomers.[2–4]

Therefore, the first section of this chapter aims at isolating conditions that favor the growth of TRP layers. In a second part, NVCL will be copolymerized with ethylene glycol dimethacrylate (EGDMA) n order to improve the mechanical properties of the plasma-polymer layers, and possibly tune the LCST. EGDMA is a cross-linking agent able to expand the polymer chains in 3 dimensions due to its two vinyl functions (Table 2.1). Indeed, TRPs are known for their poor adhesion and high solubility in solvent, making them difficult to meet practical applications as functional layers.[5]

2. Results and discussion

2.1. AP-PiCVD of water-soluble TRP layers

pNVCL's thermoresponsivity is known to follow a Flory-Huggins behavior, implying that the intensity of its thermoresponse is dependent of its molecular weight. Hence, the adjustment of the PNVCL polymer chain length offers a unique way for the tuning of the LCST value without any comonomer.[2–4]

Therefore, two different approaches are available towards the synthesis of stable thermoresponsive pNVCL layers: promoting the chemistry or the cross-linking. Using lower plasma pulses frequencies would allow a better retention of the chemistry, most probably improving the coiling effect and thus the thermal response of these NVCL-based thin films. On the other hand, using higher plasma pulses frequencies may induce an innate cross-linking of the NVCL-based thin films, affecting its molecular weight and consequently its LCST.

Hence, discharge frequencies from 10 Hz to 3,160 Hz were investigated to determine the kinetics of the free-radical polymerization of NVCL and the frequency threshold where the surface reactions, that is, adsorption and free-radical polymerization, become preponderant over the gas phase mechanisms, as determined in Chapter 3 (Figure 6.1a). From the growth rates, deduced from the thickness and the weight measurements, a maximum deposition rate is obtained for an ultrashort plasma pulses frequency of 316 Hz. The importance of gas phase reactions above 316 Hz is evidenced by the rough morphology of the NVCL-based thin films, such as observed by SEM (Figure 6.1b). On the other hand, all the NVCL-based thin films elaborated at frequencies below 316 Hz exhibited a smooth morphology driven by the preponderant adsorption of plasma-formed radicals and monomers at the substrate's surface and their subsequent polymerization (Figure 6.1b).

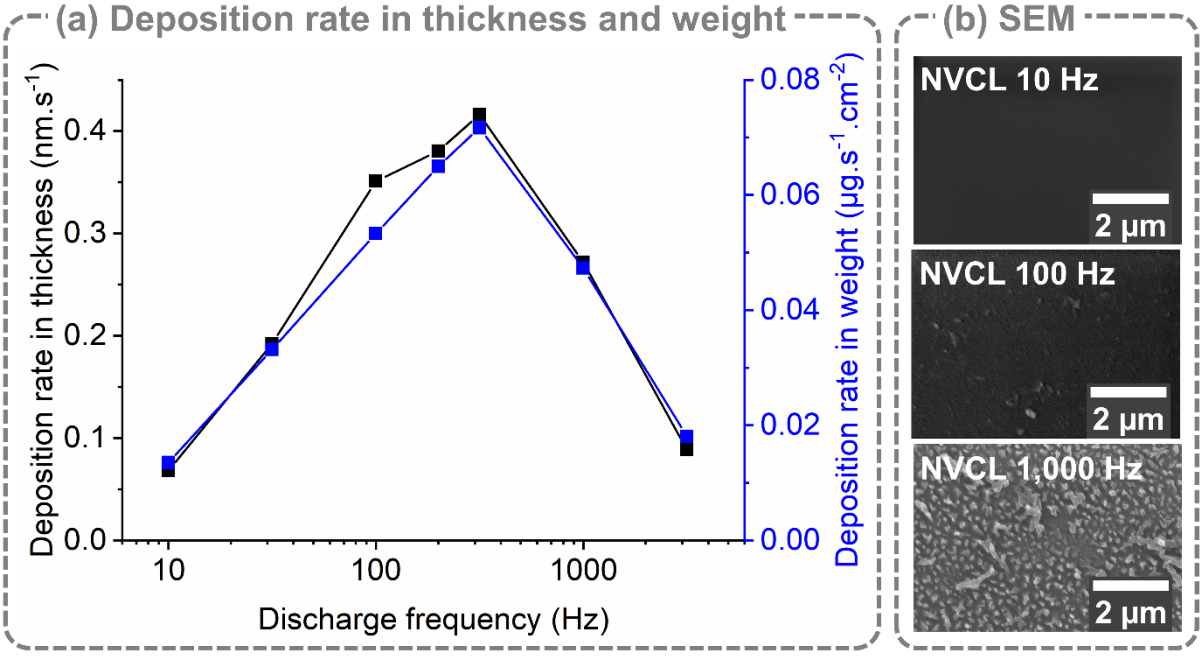

Figure 6.1. (a) Deposition rate per second of NVCL according to the discharge frequency. (b) SEM top-view images of NVCL-based thin films grown by AP-PiCVD at different discharge frequencies.

In an identical manner as for the methacrylates, size exclusion chromatography (SEC) analyses of the NVCL-based thin films display an important shift in average molecular mass in weight M_W (Figure 6.2a) as the discharge frequency increases. The plasma-polymers' distribution display different elution times, ranging from 4,100 g·mol^{-1} for the 10 Hz layer displaying a high molecular number plateau (Figure 6.2b) down to 950 g·mol^{-1} for the 1,000 Hz layer (Figure 6.2c).

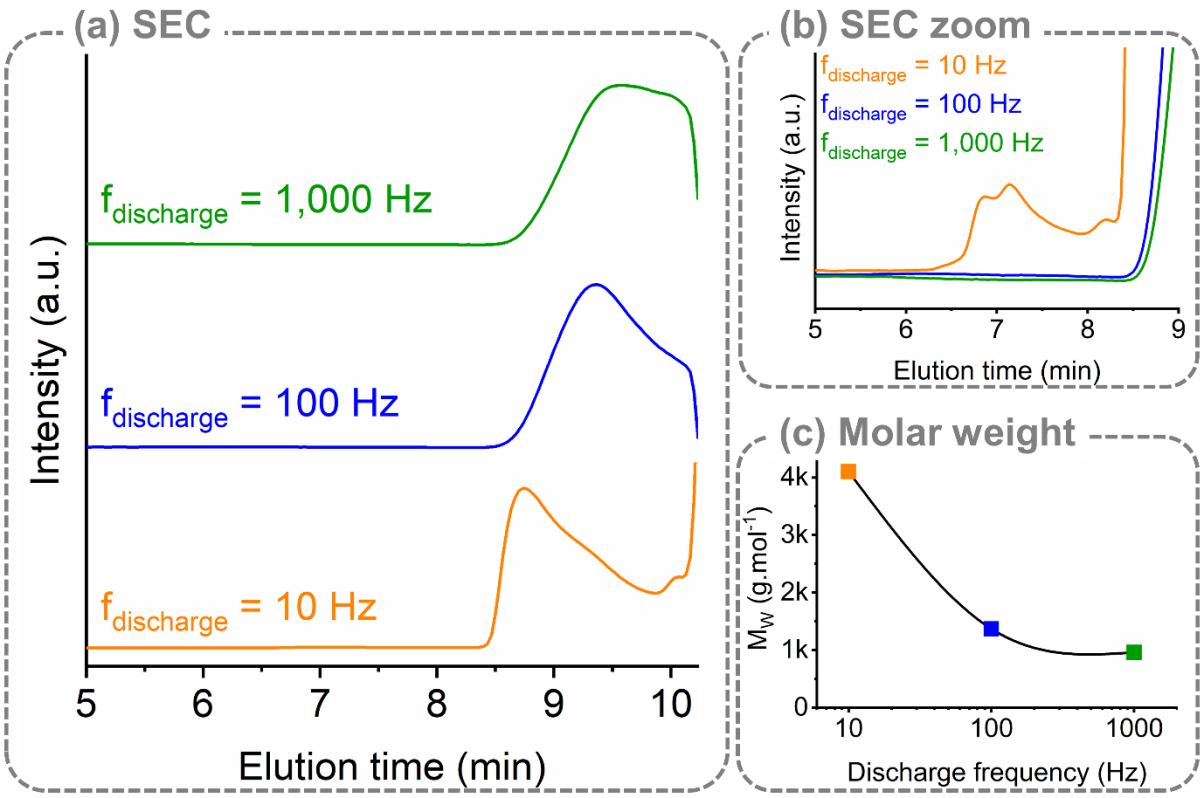

Figure 6.2. Size exclusion chromatography (SEC) of NVCL-based thin films grown by AP-PiCVD at discharge frequencies of 10 Hz, 100 Hz, and 1000 Hz plotted (a) over the whole range of elution time and (b) zoomed on the short elution time of the Gaussian tails. (c) Average molar masses in weight (M_W) of the NVCL-based thin films grown at different discharges frequencies.

The strong effect of the discharge frequency on the size exclusion chromatogram suggests the formation of shorter and/or cross-linked structures at higher plasma pulses frequencies due to an excess of reactive species. To elucidate the impact of the plasma pulses frequency on the solubility/stability of NVCL-based thin films, immersion tests in Milli-Q water for 30 min were carried out. For each of the investigated plasma pulses frequency, the thin films were completely washed-off by water, such as evidenced by FTIR analyses, which only displayed the OH vibration from lingering water and Si−O vibration from the silicon wafer (Figure 6.3a). This observation is not surprising since PNVCL is entirely dissolved in water. However, by reference to other PECVD works, it can be reported that no sufficient cross-linking of the NVCL-based thin films can be achieved with these plasma process conditions.

In order to check their thermoresponsivity, and despite their solubility in water, the films' surface energies were investigated by instantaneous water contact angle (WCA) measurements at 25 and 60°C. Interestingly, the NVCL-based thin films elaborated at the lowest plasma pulses frequencies exhibited a thermoresponse (Figure 6.3b), with a maximum water contact angle variation for the thin film deposited using a plasma pulse frequency of 10 Hz (ΔWCA_{10Hz} = 20°). This range of variation is coherent with WCA values obtained for water-soluble PNVCL homopolymer layer obtained by iCVD.[6] On the other hand, the NVCL-based thin films elaborated at the highest plasma pulses frequency (f = 1000 Hz) did not show any thermoresponsive properties ($\Delta WCA_{1,000Hz}$ = 0°).

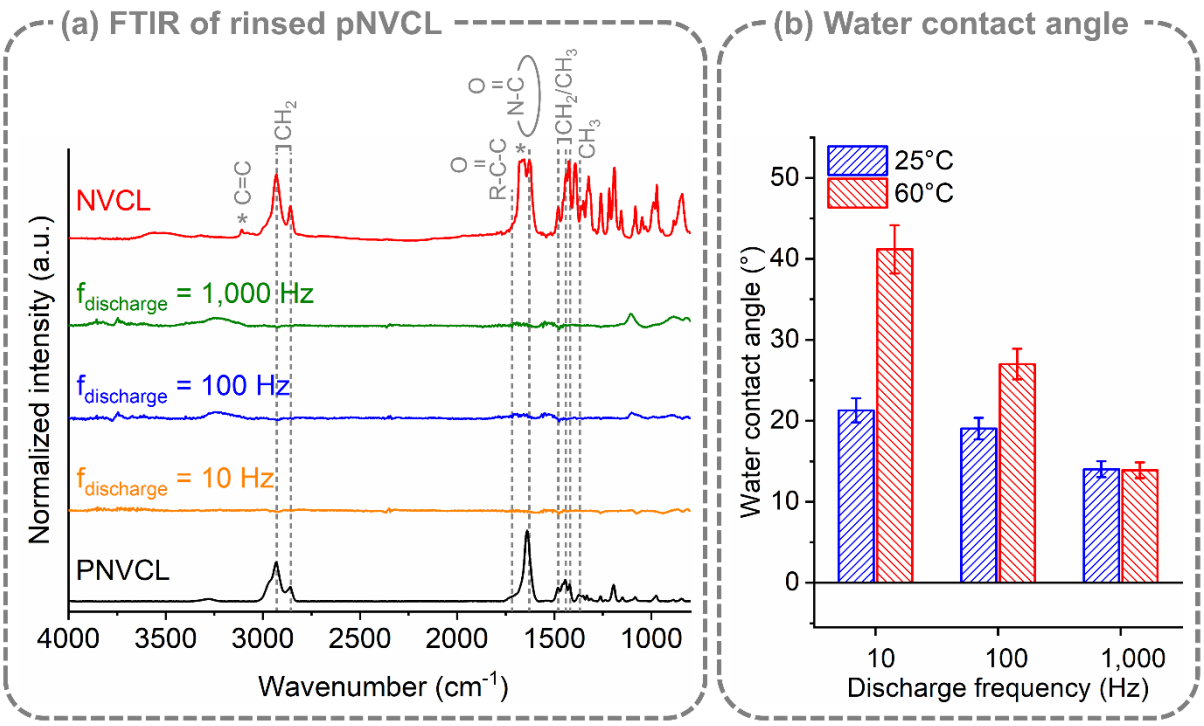

Figure 6.3. (a) FTIR spectra of PNVCL homopolymer layers grown by AP-PiCVD at different discharge frequencies measured after being immersed for 30 min in milliQ water. The monomer NVCL and conventionally polymerized PNVCL are showed as references. (b) Water contact angle measurements performed at 25 and 60°C for NVCL-based thin films grown by AP-PiCVD at different discharge frequencies

Such as observed from the SEC and WCA measurements, the plasma pulses frequency has a strong influence on the resulting chemical retention of the synthesized thin films, actively impacting their properties. Indeed, while significant alterations of the chemistry can be identified by FTIR spectroscopy as the plasma pulses frequency increase, the free-radical polymerization pathway is evidenced for all the NVCL-based thin films by the disappearance of the vinyl vibrational bands (3108 cm^{-1} and 1665 cm^{-1}) (Figure 6.4a). Moreover, the retention of the caprolactam function is ascertained through the carbonyl vibrational peak in the lactam $(N–C{=}O)_{ring}$ group at 1620 cm^{-1} and, to a lesser extent, the peak ratios conservation between the CH_2 vibrational bands (2927, 2859, 1479, 1445, and 1424 cm^{-1}) pointing to the preservation of the lactam ring structure.[6,7]

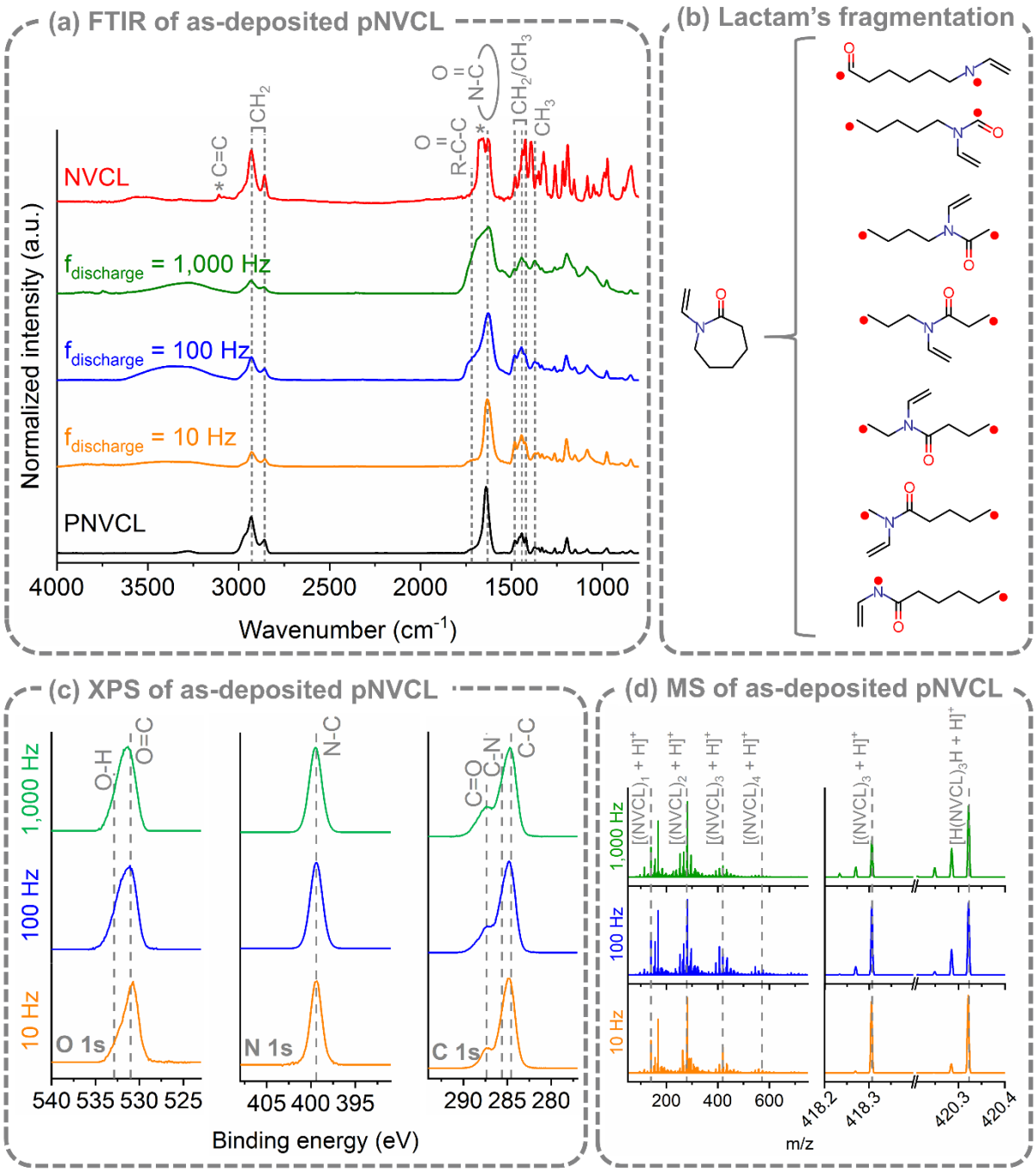

Figure 6.4. (a) FTIR spectra of NVCL-based thin films grown by AP-PiCVD at different discharge frequencies. The monomer NVCL and conventionally polymerized PNVCL are showed as references. (b) Potential 7 fragments resulting from a single caprolactam ring-opening through a plasma-induced homolytic cleavage. (c) O 1s, N 1s and C 1s XPS core level spectra of NVCL-based thin films grown at 10 Hz, 100 Hz, 1,000 Hz by AP-PiCVD. The binding energy of the NVCL bonds along with hydroxyl bonds is indicated in grey lines. (d) MALDI-HRMS spectra of films elaborated from NVCL at different discharge frequencies in the mass ranges m/z = 50−750, m/z = 418.2−418.4 and m/z = 420.2−420.4.

Nevertheless, as the frequency of plasma pulses is increased, a broad band centered at 3300 cm^{-1} appears due to the formation of hydroxyl group.[7] In addition, a broadening of the band located around 1730 cm^{-1} corresponding to a series of different carbonyl C═O

vibrational bands is observed, hinting on the lactam ring opening while increasing the plasma pulses frequency.[7]

The fragmentation of the NVCL-based thin films at higher ultrashort plasma pulse frequencies is also highlighted by XPS measurements (Figure 6.4c). Such a deviation from the monomer chemistry is notably observed from the O 1s XPS spectra that reveal a broadening and shifting of the main peak as the ultrashort plasma pulse frequency increases. This is further corroborated by the increase of the single CH_3 band at 1370 cm^{-1} for higher discharge frequencies, suggesting a transition from $CH_{2,ring}$ functions to terminal CH_3, supporting the possibility to tune to some extent the film's structure and thus its thermoresponsive properties using plasma-induced fragmentation.

To confirm the suggested chemistry, matrix-assisted laser desorption/ionization high resolution mass spectrometry measurements (MALDI-HRMS) were performed on our NVCL-based thin films. In accordance with FTIR analyses and for every discharge frequency considered, a small amount of side-species and the strong retention of conventional polymer chains $[(NVCL)_n + H]^+$ are observed (Figure 6.4d). However, the detection of a non-negligible quantity of protons terminated polymer chains $[H(NVCL)_nH + H]^+$ (Figure 6.4d), points to a partial opening of the lactam ring. Consistently, the ring fragmentation increases as the duty cycle increases, together with side-species appearing and the overall distribution being shifted to lower masses. Indeed, the lactam ring have intrinsically weaker bond dissociation energy than the rest of the rest of the molecule, hence acting as a sacrificial function offering seven different opening pathways (Figure 6.4b). Each of the ring's possible fragmentation is likely to locally cross-link (*i.e.* via $C\bullet$ or $N\bullet$ anchor points), affecting the polymers average molecular weight, as evidenced by SEC analyses (Figure 6.2), and consequently the LCST.

Consequently, the optimal discharge frequency was fixed to 10 Hz for the growth of thermoresponsive PNVCL water-soluble homopolymer layer below its LCST and its thermal response investigated by UV−vis spectrophotometry. The thermoresponsive PNVCL homopolymer dissolved in Milli-Q displayed a sharp transition around 40°C, from hydrophilic (*i.e.* dissolved) and completely transparent at room temperature to hydrophobic (*i.e.* precipitated) milky at 60°C (Figure 6.5), exhibiting an excellent repeatability between both heating-and cooling cycles. The higher than usually reported LCST (*ca*. 33°C) is consistent with the Flory−Huggins behavior of the PNVCL TRP, since our PNVCL layer is composed of rather short homopolymer chains (Figure 6.2a), shifting the LCST to higher temperatures.[1–4] While the use of higher frequencies undoubtedly displayed a strong influence on the molecular structure (Figure 6.2c), this effect was detrimental for the thermoresponsive properties − due to very short and cross-linked chains − and negligible on the water-stability (Figure 6.3).

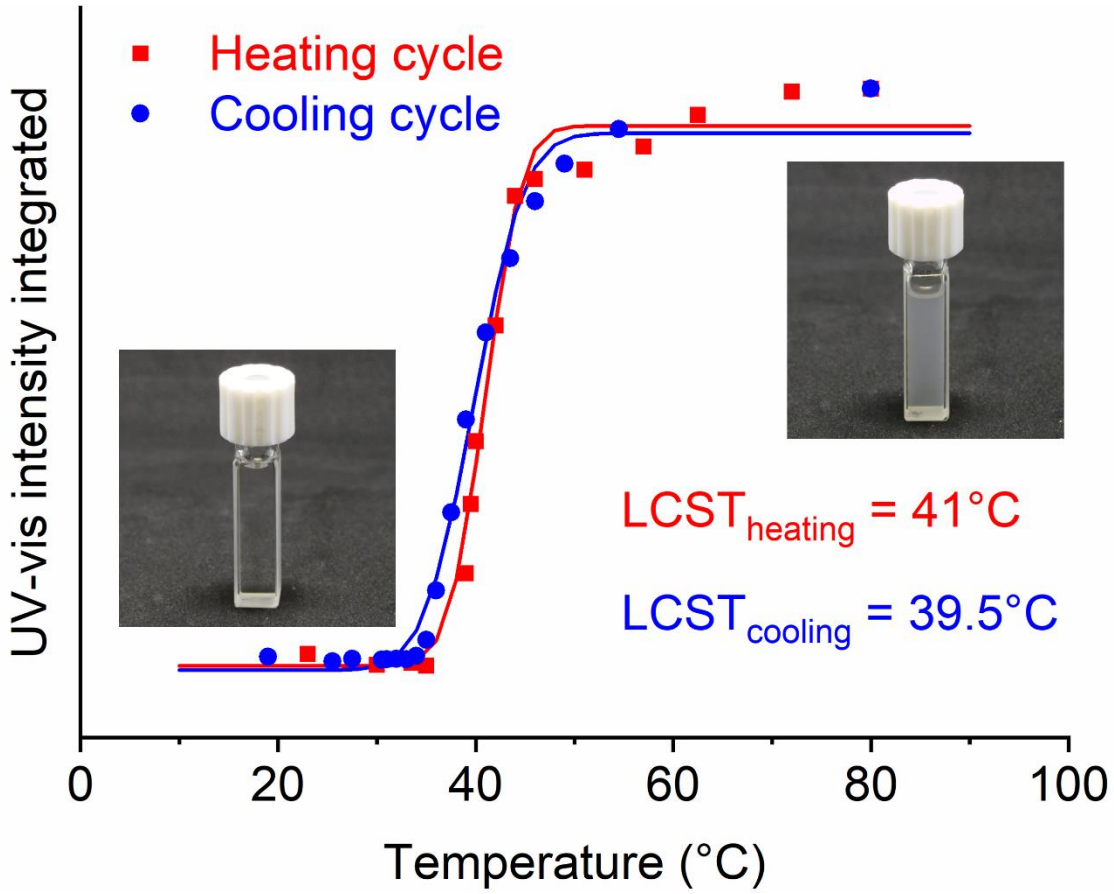

Figure 6.5. Integrations of UV−vis absorbance spectra over the visible range (300−800 nm) performed at different temperatures for pNVCL homopolymer layers grown by AP-PiCVD at 10 Hz. The presented thermal transitions were determined by an integral Gaussian fitting and the pictures of the UV-cuvettes below and above the LCSTs are displayed.

2.2. AP-PiCVD of water-stable TRP layers

To compensate for the inherent solubility of PNVCL in water, the AP-PiCVD copolymerization of NVCL with a cross-linking monomer to yield water-stable thermoresponsive thin films was investigated. Ethylene glycol dimethacrylate (EGDMA) was selected for its biocompatibility and its known efficiency as a plasma-activated cross-linker for copolymerization.[8–11] In order to combine the functionalities of each comonomer into a water-stable thermoresponsive copolymer layer, one must determine the optimal ratio of the two monomers. Indeed, the thermoresponsive and cross-linking monomers have opposite behaviors, since NVCL coil and uncoil together with the temperature while EGDMA will promote the formation of a rigid structure.

Consequently, keeping NVCL's input constant (*i.e.* 0.582 mmol·min^{-1}), different EGDMA molar flows are investigated (*i.e.* 0.056 mmol·min^{-1}, 0.174 mmol·min^{-1} and 0.285 mmol·min^{-1}) to identify the best compromise between stability and thermoresponsive properties. From the observations made during the AP-PiCVD of NVCL-based thin films, an ultrashort plasma pulses frequency of 10 Hz was selected to prepare the copolymer layers. For all the NVCL:EGDMA molar ratios investigated, smooth and defect-free thin films were formed as confirmed by AFM measurements (Figure 6.6). Notably, AFM highlighted the ultra-smooth surface of all the thin films prepared from a 10 Hz ultrashort plasma pulse frequency

with root-mean-square heights between 0.13 nm and 0.7 nm. This observation is consistent with the proposed deposition mechanisms for PiCVD of polymer layers, which relies on the successive adsorption and polymerization onto a surface.

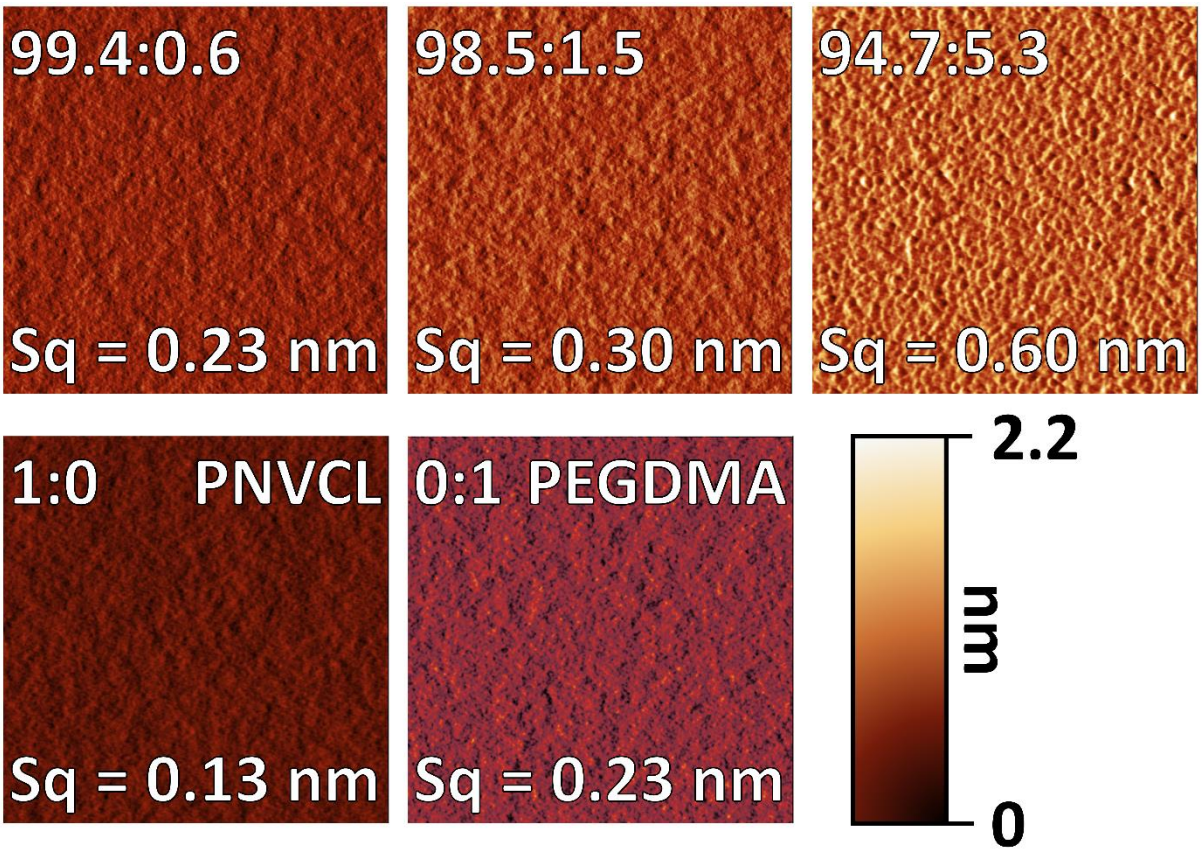

Figure 6.6. AFM pictures of pure pNVCL and pEGDMA, along with the different p(NVCL-co-EGDMA) copolymers grown by AP-PiCVD at 10 Hz. The root-mean-square height Sq is indicated.

Due to the foreseen cross-linking of the p(NVCL-co-EGDMA) copolymer layers, no MALDI-HRMS and no SEC analyses were undertaken. Yet, the copolymerization between NVCL and EGDMA was chemically monitored by FTIR spectroscopy and XPS analyses (Figure 6.7). Notably, the presence of EGDMA within the thin films was evidenced by the ester function C(O)O (1,732 cm^{-1}) and by the ether function COC contributions (1,169 cm^{-1} and 1,040 cm^{-1}).[7]

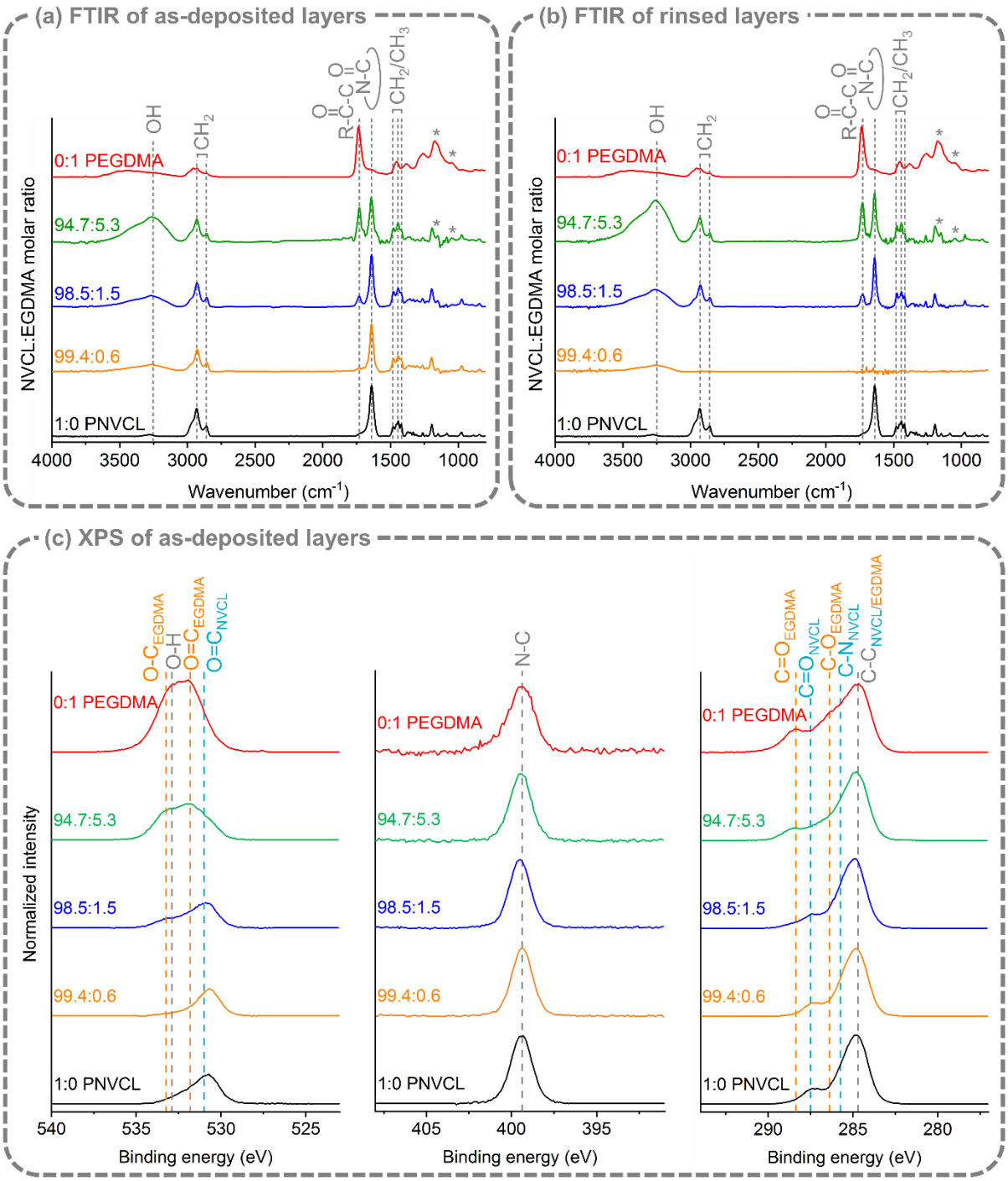

Figure 6.7. FTIR spectra of the p(NVCL-co-EGDMA) copolymer layers grown by AP-PiCVD (10 Hz) for different NVCL:EGDMA molar ratios, (a) as-deposited and (b) after being immersed for 30 min in Milli-Q water. O 1s, N 1s and C 1s XPS core levels spectra of pNVCL and pEGDMA homopolymer layers, along with the different p(NVCL-co-EGDMA) copolymer layers grown by AP-PiCVD at 10 Hz. The binding energy of the NVCL and EGDMA bonds along with hydroxyl bonds is indicated in blue, orange and grey lines, respectively.

By integrating the well-separated NVCL's caprolactam ring (1,620 cm^{-1}) and EGDMA's ester (1,732 cm^{-1}), the molar ratio of copolymerization within the thermoresponsive layers can be quantified from the equations described in Chapter 2.

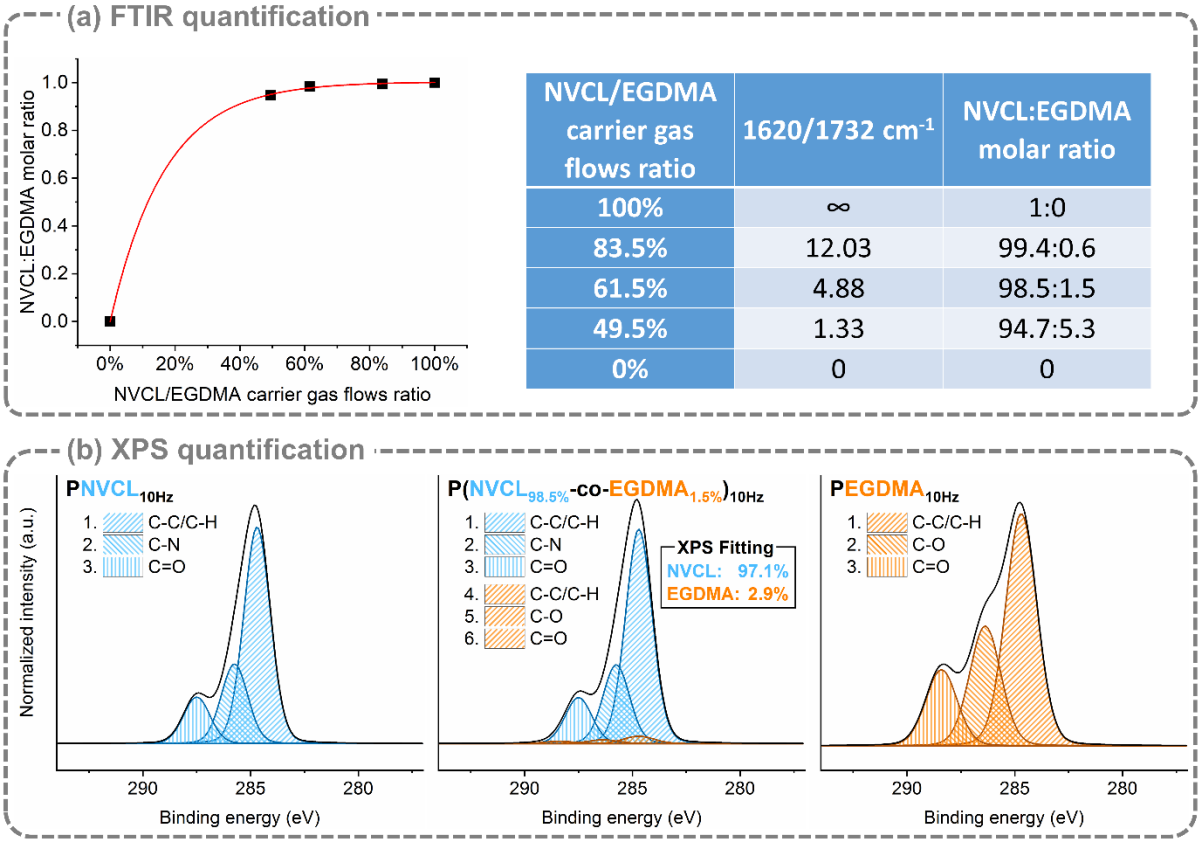

NVCL/EGDMA carrier gas flows ratio	1620/1732 cm^{-1}	NVCL:EGDMA molar ratio
100%	∞	1:0
83.5%	12.03	99.4:0.6
61.5%	4.88	98.5:1.5
49.5%	1.33	94.7:5.3
0%	0	0

Figure 6.8. (a) Chemical quantification of the NVCL:EGDMA molar ratio of the copolymer layers, using NVCL's lactam vibration at 1,620 cm^{-1} and EGDMA's ester vibration at 1,732 cm^{-1}. The films density ρ_{film} were determined based on thickness and weight measurements, yielding 0.874 kg L^{-1} and 1.490 kg L^{-1} for NVCL and EGDMA grown by AP-PiCVD, respectively. (b) C 1s XPS spectra of pNVCL and pEGDMA homopolymer layers and the p(NVCL-co-EGDMA) copolymer layer with a composition of 98.5%:1.5%, as determined by FTIR quantification. The binding energies of the C 1s core shell were fixed based on the monomers' fits: EGDMA's C-C/C-H:284.7 eV, C-O:286.365 eV, C=O:288.381 eV and NVCL's C-C/C-H:284.7 eV, C-N:285.75 eV, C=O:287.5 eV. The details of the FTIR and XPS quantifications are available in Chapter 2.

The determined NVCL:EGDMA molar ratios of the copolymer layers are equated to the monomers molar flows, yielding 99.4%:0.6% for 0.582 mmol·min^{-1}/0.056 mmol·min^{-1}, 98.5%:1.5% for 0.582 mmol·min^{-1}/0.174 mmol·min^{-1}, and 94.7%:5.3% for 0.582 mmol·min^{-1}/0.285 mmol·min^{-1}, in accordance with the EGDMA chains acting as isolated bridges to retain the NVCL chains flexibility. The low input/output ratio of EGDMA was confirmed through the fitting of the XPS C 1s core level peak of the 98.5%:1.5% p(NVCL-co-EGDMA) layer, which yield a molar ratio (97.1%:2.9%) in accordance to the one estimated by FTIR (Figure 6.8b). Since the FTIR quantifications were performed from the integration of the whole thin film thickness, in contrast to the very low depth analysis of XPS, the FTIR molar ratios will be used to further describe and identify the copolymer layers in the manuscript. Moreover, XPS fitting may artificially lead to an overestimation of the EGDMA content due to charge effects increasing its C=O contribution.

Such a nonlinear discrepancy between the monomers' molar flows and the actual copolymer layers compositions is certainly related to the comonomers' reactivity.[12] Indeed, a poor reactivity of acetates with vinyl lactams has been reported on several occasions.[13–15]

Notably, Kahn *et al.* determined the copolymerization reactivity ratios between vinyl acetate (*i.e.* r_{VAc} = 0.237) and N-vinyl pyrrolidone (*i.e.* r_{NVP} = 2.28), which bear a chemistry close to a methacrylate and the N-vinyl caprolactam, respectively.[15] The high N-vinyl pyrrolidone ratio indicates that it is able to homopropagate easily (*i.e.* forming long chains of homopolymer), while the low vinyl acetate ratio shows that it would tend to crosspropagate (*i.e.* reacting mostly with the N-vinyl pyrrolidone chains).[16] This behavior matches with a reduced incorporation of EGDMA in the p(NVCL-co-EGDMA) copolymer as previously reported in Figure 6.8.

Interestingly, NVCL's characteristic functions such as the lactam function $(N{-}C{=}O)_{ring}$ (1620 cm^{-1}) and the conservation of the CH_2 vibrational bands (2927, 2859, 1479, 1445, and 1424 cm^{-1}), highlight a very high chemical retention, irrespective of the amount of cross-linker introduced in the structure.[7] Finally, a higher integration of water is observed with higher EGDMA content into the NVCL-based thin films, such as expressed by the increasing intensity related to the hydroxyl OH band (3250 cm^{-1}).[7,17]

Such as for the NVCL-based thin films reported above, the water-stability of the p(NVCL-co-EGDMA) copolymer layers were determined by immersion in Milli-Q water for 30 min and subsequent FTIR analyses of the remaining layers (Figure 6.7b). Instantly, the 99.4%:0.6% copolymer layer appears completely rinsed indicating a lack of cross-linking between the polymer chains themselves and interactions with the substrate, while the chemical stability of the 98.5%:1.5% and 94.7%:5.3% copolymers was confirmed as their spectra are almost unaltered after the immersion. This is in accordance with previous literature works that report a cross-linker molar concentration around 1 mol % to stabilize the PNVCL chains.45 The layers' stability was further confirmed by SEM/EDX (Figure 6.9), also highlighting the conservation of the surface smoothness for the 98.5%:1.5% copolymer layer, the 94.7%:5.3% copolymer displaying some scythe-like surface alterations from the water immersion.

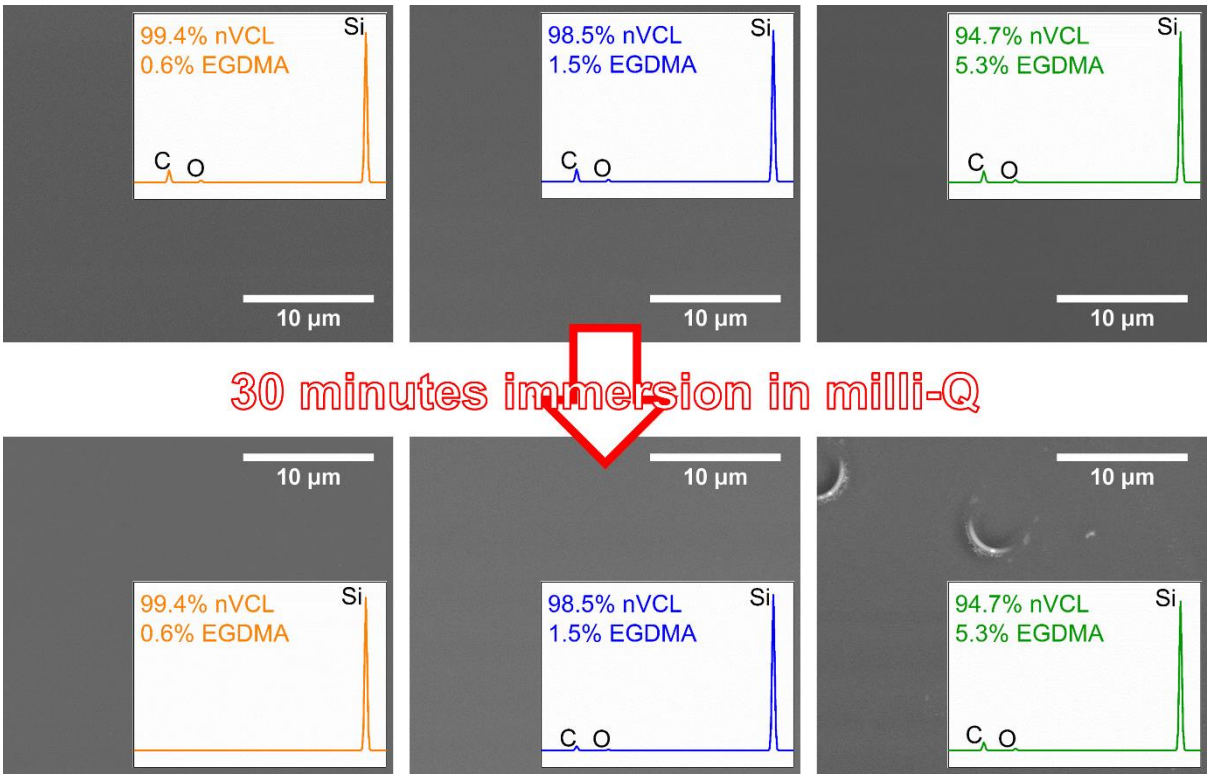

Figure 6.9. Secondary electron microscopy (SEM) images and energy-dispersive X-ray spectroscopy (EDX) spectra of p(NVCL-co-EGDMA) copolymers, grown with a plasma pulses frequency of 10 Hz, before and after being immersed in milliQ water for 30 min.

The thermoresponsive properties of the different p(NVCL-co-EGDMA) as-deposited copolymer layers were assessed from the WCA measurement at 22°C and 60°C (Figure 6.10). Interestingly, the thermoresponsive behavior of the p(NVCL-co-EGDMA) copolymer layers increases with the amount of EGDMA cross-linker up to a maximum of 52° (from 19° to 71°) for the 98.5%:1.5% molar ratio P(NVCL-co-EGDMA) layer. Such an increase of the ΔWCA from 20° for the pNVCL layer to 52° for the best P(NVCL-co-EGDMA) copolymer layer correlates with the increased water uptake observed by FTIR for higher EGDMA content (Figure 6.7). Indeed, copolymerization of NCVL with a cross-linker affects the stability of the formed hydrogel and those with a higher water uptake consistently display a better swelling capacity, and therefore a better thermoresponsive performance.[5] Unsurprisingly, lower content of EGDMA cross-linker (*i.e.* 99.4%:0.6% molar ratio) is not sufficient to confer the EGDMA's contribution to the P(NVCL-co-EGDMA) copolymer layers, and both the thermal response and the water-solubility are very close to PNVCL homopolymer layers due to a lack of polymer/polymer and polymer/substrate interactions. By the same token, a high amount of cross-linker (*i.e.* 94.7%:5.3% molar ratio) yields properties comparable to pure EGDMA, with strong water stability and no thermoresponsive behavior resulting that the PNVCL films are completely bound by 3D network and unable to coil/uncoil with the temperature.

As such, the NVCL:EGDMA molar ratio of 98.5%:1.5% appears as the best compromise between film stability and polymer chains flexibility, allowing the growth of adherent and water-stable thermoresponsive p(NVCL-co-EGDMA) copolymer layers. Finally, the total immersion of the p(NVCL-co-EGDMA) copolymer layers in Milli-Q during 30 min induced a partial washing of the surface, together with a drop in the water contact angle variation − from $\Delta WCA \approx 52°$ down to $\Delta WCA \approx 10°$ − indicating a retention of the thermoresponsive properties. This decrease of the thermoresponsivity might arise from the dissolution of the most flexible thermoresponsive chain (*i.e.* less cross-linked), leaving the ones with the strongest polymer−substrate and polymer−polymer interactions. Moreover, as evidenced by the increase of hydroxyl vibrations (3250 cm^{-1}) measured by FTIR, the introduction of water generating hydrogen bonding within the thin film might stiffen the TRP chains, hindering the chains uncoiling at low temperature.

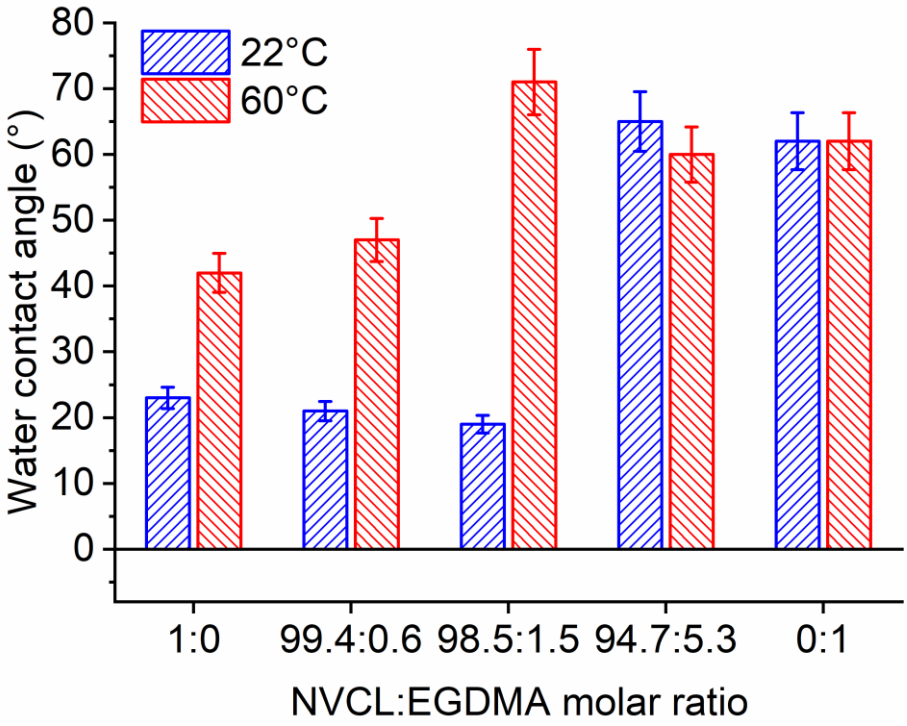

Figure 6.10. Water contact angle measurements performed at 22 and 60 °C of different molar ratios of p(NVCL-co-EGDMA) as-deposited copolymer layers grown by AP-PiCVD at 10 Hz.

To ascertain the degree of liberty of the pNVCL chains cross-linked by EGDMA units (Figure 6.11a), surface free energy (SFE) measurements were performed on the 98.5%:1.5% molar ratio p(NVCL-co-EGDMA) layer at 22°C and 60°C using the extended Fowkes equations described in Chapter 2. Both analyses were conducted using Milli-Q water, ethylene glycol and diiodomethane, allowing to extract the copolymer thin film surface free energies as well as their respective dispersive (*i.e.* non-polarized environment) and polar components (*i.e.* polarized environment) (Figure 6.11b). In a very intuitive manner, the polar component (33.4 mJ m^{-2}) of the SFE is slightly higher than the dispersive one (26.9 mJ m^{-2}) at low temperature (*i.e.* 22°C), indicating that the most polarized C═O bonds are evenly distributed on the surface of the p(NVCL-co-EGDMA) copolymer layer. When the temperature is raised and cross over the LCST, the dispersive component increases to 40.9 mJ m^{-2}, while the polar component drops considerably to 8.1 mJ m^{-2}, implying that most of the C═O bonds previously available at the surface of the p(NVCL-co-EGDMA) copolymer layer at 22°C are involved in the coiling the pNVCL chains through hydrogen bonding at 60°C. Consequently, the SFE measurements point to an optimal flexibility from the pNVCL chains adequately coupled to the rigidity brought by the EGDMA units.

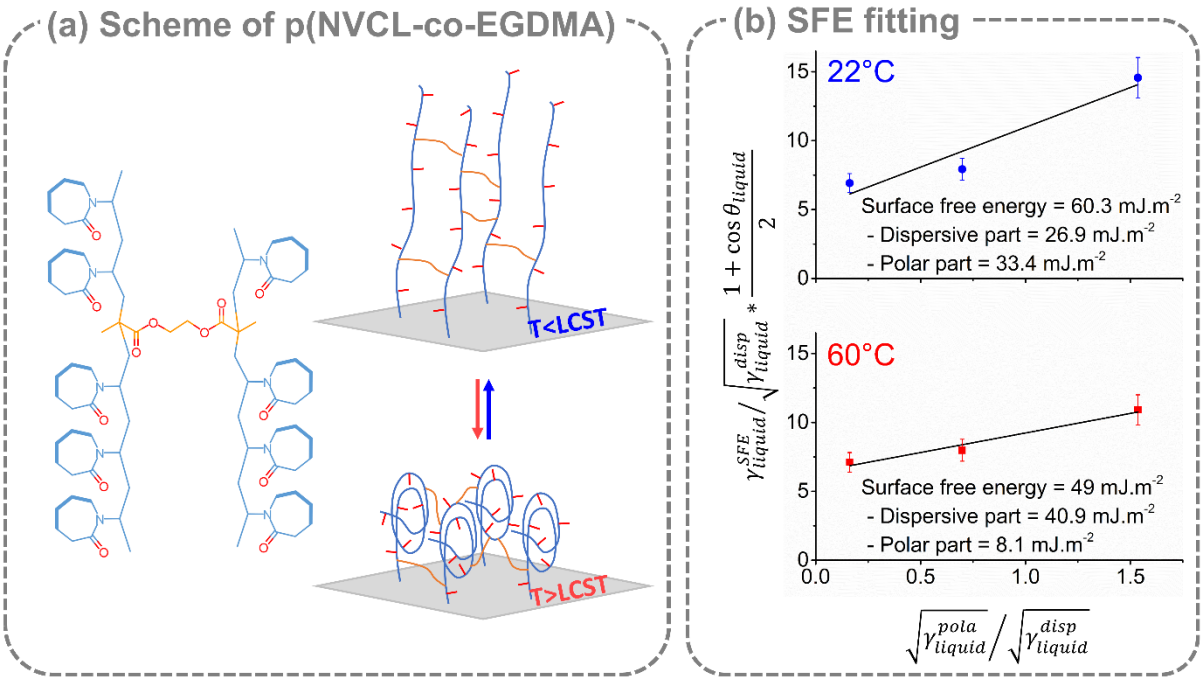

Figure 6.11. (a) Scheme of the p(NVCL-co-EGDMA) copolymer conformation together with uncoiled and coiled form of the chains depending on the temperature. (b) Fit of the extended Fowkes equations at 22 and 60°C with the corresponding surface free energies and their dispersive and polar components for the as-deposited P(NVCL-co-EGDMA) layer with a 98.5%:1.5% NVCL:EGDMA molar ratio.

Finally, the lower critical solution temperature (LCST) of the p(NVCL-co-EGDMA) copolymer layer grown from a 98.5%:1.5% NVCL:EGDMA molar ratio was determined by WCA measurements (Figure 6.12). The thermoresponsive p(NVCL-co-EGDMA) copolymer layer displayed a very long thermal transition between 15°C and 45°C with its LCST at 27.6 °C, several degrees lower than conventional pNVCL homopolymer layers, possibly due to changes in the polymeric molar mass distribution. This highlights the influence of a comonomer (cross-linker in the present case) on the thermal response of NVCL-based thin films. Considering the narrow window of processing for the copolymer ratio, the tuning of LCST of thermoresponsive p(NVCL-co-EGDMA) copolymer layer will require the use of different comonomers with different surface free energy. As an example, one may copolymerize NVCL with N-vinylacetamides or vinylesters to tune up or down the LCST of the NVCL-based thin films.[5] Aside from the chemical composition affecting the PNVCL-based copolymer layers' thermoresponsivity, one may also take advantage of the reported conformality of the thin films deposited by AP-PiCVD. Indeed, the conformal deposition of p(NVCL-co-EGDMA) copolymer layers on patterned or rough substrates should allow a tuning of the thermal transition from hydrophilic to hydrophobic.

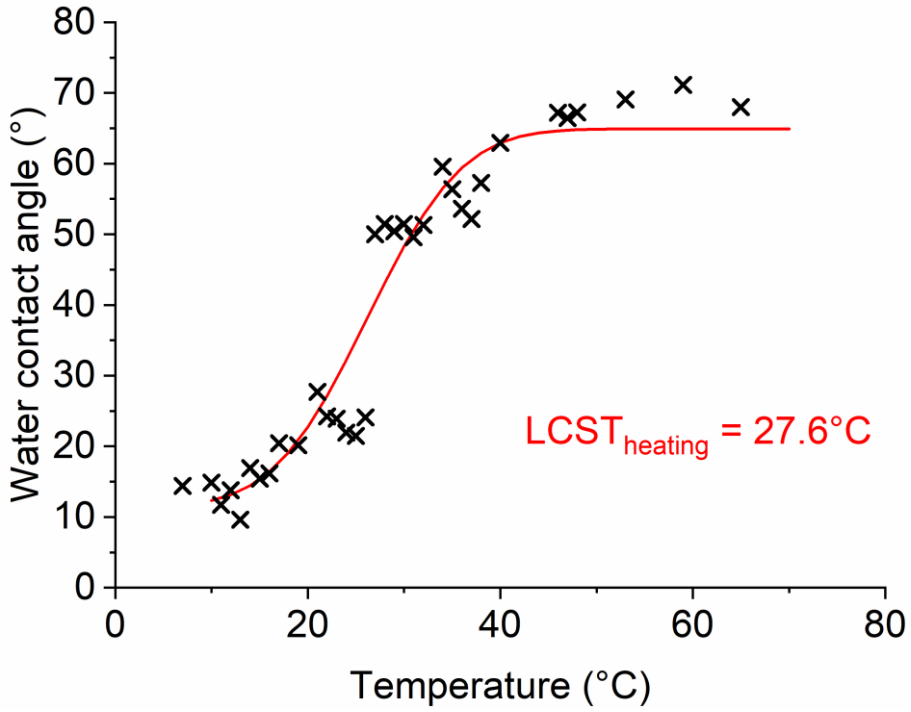

Figure 6.12. Water contact angle measurements from 7°C to 65°C for the as-deposited p(NVCL-co-EGDMA) layer with a 98.5%:1.5% NVCL:EGDMA molar ratio. The presented thermal transitions were determined by an integral Gaussian fitting.

3. Outlines

Using extremely soft conditions (f = 10 Hz), pNVCL layers with thermoresponsive properties comparable to conventional polymers were grown. Notably, the high thermal response of the grown polymer layers highlights the high retention of the particularly sensitive lactam ring at a sufficiently long-range order. Unfortunately, the pNVCL layers synthesised by AP-PiCVD shared the same drawbacks as conventional pNVCL: a strong solubility in all solvents including water.

The growth of ultra-smooth, water-stable and thermoresponsive p(NVCL$_{98.5\%}$-co-EGDMA$_{1.5\%}$) copolymer layers by AP-PiCVD demonstrates the ability of the process to efficiently retain the sensitive functional properties and combine the properties of two comonomers. The thermoresponsive copolymer thin films displayed strong changes of their surface-free energy's polar component upon temperature variation and a good stability towards water, confirming the successful copolymerisation of the selected monomers.

Furthermore, the difference in the kinetic of deposition between NVCL and EGDMA matches the reported one for solution-based copolymerization approaches. This highlights the ability of AP-PiCVD to promote not only the growth of conventional polymer layers but also conventional copolymerization pathways.

These observations extend further the range of functional thin films available by AP-PiCVD to monomer with highly sensitive chemical functions and to the use of copolymers.

4. References

1. Maeda, Y., Nakamura, T., and Ikeda, I. (2002) Hydration and Phase Behavior of Poly (N -vinylcaprolactam) and Poly (N -vinylpyrrolidone) in Water. *Macromolecules*, **35** (1), 217–222.

2. Ramos, J., Imaz, A., and Forcada, J. (2012) Temperature-sensitive nanogels: Poly(N-vinylcaprolactam) versus poly(N-isopropylacrylamide). *Polym. Chem.*, **3** (4), 852–856.

3. Beija, M., Marty, J.D., and Destarac, M. (2011) Thermoresponsive poly(N-vinyl caprolactam)-coated gold nanoparticles: Sharp reversible response and easy tunability. *Chem. Commun.*, **47** (10), 2826–2828.

4. Meeussen, F., Nies, E., Berghmans, H., Verbrugghe, S., Goethals, E., and Du Prez, F. (2000) Phase behaviour of poly(N-vinyl caprolactam) in water. *Polymer (Guildf).*, **41** (24), 8597–8602.

5. Cortez-Lemus, N.A., and Licea-Claverie, A. (2016) Poly(N-vinylcaprolactam), a comprehensive review on a thermoresponsive polymer becoming popular. *Prog. Polym. Sci.*, **53**, 1–51.

6. Lee, B., Jiao, A., Yu, S., You, J.B., Kim, D.H., and Im, S.G. (2013) Initiated chemical vapor deposition of thermoresponsive poly (N-vinylcaprolactam) thin films for cell sheet engineering. *Acta Biomater.*, **9** (8), 7691–7698.

7. Socrates, G. (2004) *Infrared and Raman characteristic group frequencies*, Wiley-VCH.

8. Adali, T., and Yilmaz, E. (2009) Synthesis, characterization and biocompatibility studies on chitosan-graft-poly(EGDMA). *Carbohydr. Polym.*, **77** (1), 136–141.

9. Czuba, U., Quintana, R., De Pauw-Gillet, M.C., Bourguignon, M., Moreno-Couranjou, M., Alexandre, M., Detrembleur, C., and Choquet, P. (2018) Atmospheric Plasma Deposition of Methacrylate Layers Containing Catechol/Quinone Groups: An Alternative to Polydopamine Bioconjugation for Biomedical Applications. *Adv. Healthc. Mater.*, **7** (11), 1–11.

10. Patra, P., Rameshbabu, A.P., Das, D., Dhara, S., Panda, A.B., and Pal, S. (2016) Stimuli-responsive, biocompatible hydrogel derived from glycogen and poly(: N -isopropylacrylamide) for colon targeted delivery of ornidazole and 5-amino salicylic acid. *Polym. Chem.*, **7** (34), 5426–5435.

11. Gonzalez-Ayon, M.A., Cortez-Lemus, N.A., Zizumbo-Lopez, A., and Licea-Claverie, A. (2014) Nanogels of poly(N-vinylcaprolactam) core and polyethyleneglycol shell by surfactant free emulsion polymerization. *Soft Mater.*, **12** (3), 315–325.

12. Mayo, F.R., and Lewis, F.M. (1944) Copolymerization. I. A Basis for Comparing the Behavior of Monomers in Copolymerization; The Copolymerization of Styrene and Methyl Methacrylate. *J. Am. Chem. Soc.*, **66** (9), 1594–1601.

13. Haaf, F., Sanner, A., and Straub, F. (1985) Polymers of N-Vinylpyrrolidone: Synthesis, Characterization and Uses. *Polym. J.*, **17** (1), 143–152.

14. Greenley, R.Z. (1980) Recalculation of Some Reactivity Ratios. *J. Macromol. Sci.,*

Chem., **14**, 445–515.

15. Kahn, D.J., and Horowitz, H.H. (1961) Evaluation of the terpolymer composition equation. *J. Polym. Sci.*, **54**, 363–374.

16. Parthiban, A. (2014) *Synthesis and Applications of Copolymers*, Wiley-VCH.

17. Wu, Y., Joseph, S., and Aluru, N.R. (2009) Effect of Cross-Linking on the Diffusion of Water, Ions, and Small Molecules in Hydrogels. *J. Phys. Chem. B*, **113** (11), 3512–3520.

CHAPTER VII – Conclusion

The present PhD dissertation provides an in-depth study of the mechanisms driving the chemical vapor polymerization and deposition of vinylic monomers using nanosecond pulsed plasma discharges. Although, the growth of functional organic layers by plasma-polymerization has already been widely studied, the fragmentation and recombination mechanisms intrinsic to plasma processes prevented the formation of true polymer layers. Nanosecond pulsed plasmas are attractive alternatives as they allow to drastically reduce the negative impact of plasma (use of ultrashort on-times) and promote conventional polymerization pathways to grow conventional polymers (using long off-times in accordance to the free-radical polymerization lifetime). Specifically, the current work focused on the understanding of the growth mechanisms in atmospheric nanosecond pulsed plasma-enhanced chemical vapor deposition (AP-PECVD) reaction of vinylic monomers.

When employing low frequency nanosecond pulsed plasma discharges (long off-times), surface reaction mechanisms (adsorption and subsequent free-radical polymerization) are predominant, leading to an unprecedented degree of polymerization compared to both PECVD processes and atmospheric-pressure CVD processes. In particular, glycidyl methacrylate exhibits an exceptionally high average molecular mass in weight up to 95,000 $g \cdot mol^{-1}$. The preponderance of surface reaction mechanisms (adsorption and subsequent free-radical polymerization) when employing low frequency nanosecond pulsed plasma discharges also yields the formation of smooth and thickness-controlled thin films with a high level of conformality. The lack of control for low thicknesses and non-conformality is one of the major drawbacks of solution-based approaches.

Unsurprisingly, the thin films' properties displayed a strong dependence on the plasma off-time. Indeed, a significant relationship between the growth mechanisms and the nanosecond plasma pulses repetition frequency was observed through specific transitions from the preponderance of conventional surface mechanisms for long off-times to the preponderance of gas phase mechanisms for short off-times. Beside the predominant free-radical polymerization pathway when employing vinylic monomers and long off-times, the in-depth high-resolution mass spectrometry study allowed to determine side mechanisms. The identification of the loss and addition patterns provided information on the fragmentation and recombination mechanisms, but also on the initiation of the free-radical polymerization of the methacrylate compounds from nanosecond pulsed plasmas.

If for all the investigated monomers, free-radical polymerization mechanisms are highly preponderant for long off-times, yielding conventional and linear polymer chains, important variations in the behavior of monomers from the same family (methacrylates) were evidenced by SEC and HRMS analyses. The strong influence of the monomers' chemical functionalities on the growth mechanisms is expressed through the occurrence of the side mechanisms, leading to termination mechanisms and shorter molecular weights for methyl and butyl methacrylates while glycidyl methacrylate produces high molecular weight layers. DFT calculations of the bond dissociation energies gave insight on the differences in fragmentation mechanisms between the methacrylate monomers by highlighting the role of the epoxy function in the glycidyl methacrylate molecule, which acted as a sacrificial function protecting the rest of the monomer's pattern.

In order to collect more information on the various growth mechanisms during (*i.e.* fragmentation) and following (*i.e.* propagation, chain transfer and termination) the discharge, a kinetic model was developed. The equations from the rotating sector method were adapted for nanosecond pulsed plasmas, allowing the extraction of the theoretical percentage of conversion to free radical species initiated by the pulse and remaining after the plasma off-

time. Those concentrations allowed the calculation of theoretical deposition rate per pulse, which could be fitted with experimental data to obtain the kinetic constants, hence the kinetic rates during a single pulse, of the different growth mechanisms.

The evolution of the kinetic rates showed very strong differences between glycidyl methacrylate and the other studied methacrylate compounds. Notably higher propagation and conventional termination rates hinting on a predominant conventional growth were identified in the case of glycidyl methacrylate. On the other hand, methyl methacrylate displays an important degree of chain-transfer mechanisms, which are indicators of the reactivity of the fragmented species, hence giving information on the degree of fragmentation of the monomer. This observation showed that the initial fragmentation of methyl methacrylate, which is not protected by a sacrificial function, leads to an excess of reactive species, fostering fast chain terminations and a larger amount of variations in the formed polymer chains, correlating with SEC and HRMS analyses. Interestingly, the theoretical and experimental data allowed the calculation of the free radical concentration in the gas phase (i.e. initiated) and on the surface (i.e. reacted). Plotting the ratio between the 2 concentrations highlighted the percentage of initiated species participating in the growth, which perfectly correlated with the transition from surface to gas phase mechanisms experimentally observed by SEM imaging and hinted on a surface saturation as a limiting mechanism when the off-time is not long enough. Moreover, the reactive volume of initiated species able to participate in the deposition could be extracted for each of the studied methacrylate monomers, which allowed the calculation of the number of discharges seen per monomer by correlating of the monomers' travelling time and the discharge frequency. Interestingly, the transition from conventional to plasma-polymerization mechanisms observed by SEC analyses matched with an increased number of monomers being subjected to more than one discharge, confirming the importance of nanosecond pulsed discharge and long off-times to preserve the desired chemistry.

Taking into account the understanding gained from model monomers, an optimal experimental procedure was considered to grow functional thermoresponsive polymer layers of n-vinyl caprolactam by AP-PiCVD. Thermoresponsive thin film are particularly difficult to grow by plasma processes as they require a high retention of the monomer's chemistry – in this case the lactam ring – at long range order to keep their properties and are intrinsically water-soluble. Therefore, an innovative approach using long pulses (*i.e.* $t_{pulse} = t_{on}$) was applied to further reduce the number of discharges seen per molecule. Thermoresponsive polymer layers of n-vinyl caprolactam were grown using the long pulse method and 100 ms off-time. To compensate for the detrimental solubility of poly-n-vinyl caprolactam, it was copolymerized with ethylene glycol dimethacrylate, a monomer able to induce crosslinking and improve the stability of the thin films. An optimal ratio between the comonomers, combining the n-vinyl caprolactam's flexibility and the ethylene glycol dimethacrylate's rigidity, was obtained to yield water-stable thermoresponsive copolymer thin films.

The knowledge developed during this work open many possibilities for the simultaneous synthesis and deposition of new polymer layers, which are unattainable using traditional plasma-polymerization processes. Indeed, the combination of ultrashort plasma pulses with long off-times in the range of the free-radical polymerization lifetime, called plasma-initiated chemical vapor deposition (PiCVD), is currently applied for the atmospheric-pressure and dry synthesis of conformal and defect-free dielectric polymer layers with extremely low-k for microelectronic applications. Moreover, the AP-PiCVD of a fire-retardant monomer have also been successfully carried out on cotton fabrics. In a simpler way, the ability to grow polymer thin films with high density of chemical functionalities offers the possibility to improve existing

applications, which was demonstrated by growing epoxy-rich layers for enzyme immobilization. Overall, the current research on the growth mechanisms and the application of the AP-PiCVD process for the deposition of conventional polymer layers pave the way towards more advanced applications such as proton exchange membranes, icephobic layers, conductive antifouling zwitterionic membranes …

Yet, the complex and numerous mechanisms in plasma-processes remain to be fully understood, especially since the monomers demonstrate a strong influence on the growth mechanisms. Indeed, sacrificial function notably showed a very high potential to further lower the plasma-polymerization side-mechanisms and promote the deposition of high molecular weight polymer layers, especially using soft method such as AP-PiCVD. The parameters controlling the adsorption mechanisms also require to be investigated, considering their prevalence in the growth mechanisms in AP-PiCVD. Notably, the influence of the P_M/P_{sat} ratio and of the substrate temperature on the polymerization kinetic and the surface reactivity would allow more advanced control over the properties of polymer thin films grown by AP-PiCVD.